The role of ANG and tRNA-derived fragments in aging, neurodegeneration and the pathophysiology of Alzheimer's Disease.

Dissertation

to obtain the degree

"Doctor of the natural sciences (Dr. rer. nat.)"

in Pharmacology and Toxicology

submitted to the faculty of Chemistry, Pharmaceutical Sciences, Geography and Geosciences of the Johannes Gutenberg University Mainz

by

Marko Jörg

born in Mainz

Mainz, April 2022

Dean: [redacted]

Name of 1st reviewer: [redacted]

Name of 2nd reviewer: [redacted]

Name of 3rd reviewer: [redacted]

Date of doctoral examination: 24.06.2022

D77 (Dissertation Universität Mainz)

Declaration of Authorship

"I, Marko Jörg, herewith declare that the presented work and thesis titled "*The role of ANG and tRNA-derived fragments in aging, neurodegeneration and the pathophysiology of Alzheimer's Disease*" are composed myself and without use of any other than the cited sources and aids.

I confirm that:

- This work was done wholly in candidature for a research degree at the Johannes Gutenberg University, Mainz
- Sentences or parts of sentences quoted literally are marked as such; other references with regard to the statement and scope are indicated by full details of the publications concerned.
- The thesis in the same or similar form has not been submitted to any examination body and has not been published.
- Where the thesis is based on work done by myself jointly with others, I have clarified exactly what others did and what I have contributed to myself.

Date:_____

Sign:_____

"Gravity explains the motions of the planets, but it cannot explain who set the planets in motion."

Isaac Newton

Johannes Gutenberg University Mainz

Abstract

Department of Pharmacology and Toxicology at the Institute of Pharmaceutical and Biomedical Sciences

Dr. rer. nat.

The role of ANG and tRNA-derived fragments in aging, neurodegeneration and the pathophysiology of Alzheimer's Disease.

Marko Jörg

Alzheimer's disease (AD) is the most common neurodegenerative disease, characterized by gradual cognitive decline and later dementia. About 15% of the over-65s and over 50% of the over-80s are affected by AD worldwide. Despite intensive basic research, the pathogenesis of AD is only partially understood. This project focused on the expression of the ribonuclease angiogenin (ANG) and RNA modifications in aging, neurodegeneration, and AD development. Cellular functions and important signal pathways depend on numerous protein-coding and non-coding RNAs. In particular, tRNA is of major importance for this project due to its regulatory role in various cellular processes, such as the inhibition of apoptosis. Due to stress response, tRNA must be cleaved by ANG to induce this mechanism. This cleavage results in tRNA-derived fragments such as tiRNAs and tRFs. tiRNAs can inhibit the proapoptotic pathway. Western Blotting was used to determine ANG expression in different cell, animal, and human aging and AD models. In addition to that, tRNA modifications play a crucial role in RNA function and stability. So far, 150 different RNA modifications have been discovered, such as adenosine, cytosine, ribose methylation, or pseudouridine incooperation. The role of tRNA modifications in pathological aging and AD is unknown. Therefore, we used Liquid Chromatography with tandem mass spectrometry (LC-MS/MS) to determine whether tRNA modifications in cell and animal models contribute to mitochondrial defects following the dynamic changes in tRNA modifications pathological process of AD. The results of this thesis revealed age- and gender-dependent dysregulation of ANG and various changes in tRNA modifications in pathological aging and AD.

Johannes Gutenberg Universität Mainz

Zusammenfassung

Department Pharmakologie und Toxikologie am Institut für Pharmazeutische und Biomedizinische Wissenschaften

Dr. rer. nat.

Die Rolle von ANG und tRNA-abhängigen Fragmenten während des Alterns, der Neurodegeneration und der Pathophysiologie von Alzheimer.

Marko Jörg

Alzheimer Demenz (AD) ist die häufigste neurodegenerative Erkrankung, die durch einen Abbau der kognitiven Fähigkeiten gekennzeichnet ist und in einer späteren Demenz endet. Derzeit sind weltweit ca. 15 % der über 65-Jährigen und mehr als 50 % der über 80-Jährigen betroffen. Die Pathogenese von AD ist jedoch nur teilweise verstanden. In diesem Projekt liegt der Schwerpunkt auf der Expression der Ribonuklease Angiogenin (ANG) und RNA Modifikationen bei Prozessen der Alterung, Neurodegeneration und AD. Zelluläre Funktionen und wichtige Signalwege hängen von zahlreichen proteincodierenden und nichtcodierenden RNAs ab. Insbesondere die tRNA ist aufgrund ihrer regulatorischen Rolle, wie z. B. der Hemmung der Apoptose, von großer Bedeutung. Die tRNA wird als Folge einer Stressreaktion von ANG gespalten, was zu einer Bildung von tRNA Fragmenten wie tiRNAs und tRFs führt. tiRNAs sind in der Lage, den proapoptotischen Weg zu hemmen. Mittels der Methode des Western Blotting wurde die Expression von ANG bestimmt. Darüber hinaus spielen tRNA-Modifikationen eine entscheidende Rolle für die Funktion und Stabilität der RNA. Bisher wurden 150 verschiedene RNA-Modifikationen entdeckt, die Rolle bei der Alterung und AD ist noch nicht bekannt. Daher wurde die Flüssigchromatographie mit Tandem-Massenspektrometrie (LC-MS/MS) eingesetzt, um tRNA-Modifikationen in Zell- und Tiermodellen zu bestimmen und festzustellen, ob Veränderungen dieser zu mitochondrialen Defekten beitragen, um den dynamischen pathologischen Prozess von AD zu verfolgen. Die Ergebnisse dieser Arbeit zeigen eine alters- und geschlechtsabhängige Dysregulation von ANG sowie verschiedene Veränderungen von tRNA-Modifikationen im Alterungsprozess und bei AD.

Acknowledgments

During my years as a PhD student, I got the opportunity to work with many great people and extraordinary scientists, whom I would like to thank in the following for their support and sharing of their knowledge.

- [redacted]
- [redacted]
- [redacted]
- [redacted]

- [redacted]
- [redacted]
- [redacted]
- [redacted]
- [redacted]

- [redacted]

- [redacted]

Abbreviations

3D-DS	three-dimensional domain swapping
Abbr.	Abbreviations
ACT	Adult Changes in Thought
AD	Alzheimers Disease
AGO	Argonaute protein
AICD	APP intracellular domain
ALS	Amyotrophic lateral sclerosis
ANG	Angiogenin
AP	Alcalic phosphatase
APAF1	Apoptotic protease-activating factor 1
ApoE	ApolipoproteinE
APP	Amyloid precursor protein
Aβ	Amyloid beta
ATCC	American Type Culture Collection
ATP	Adenosintriphosphate
ATXN2	Ataxin-2
AUC	Area Under the Curve
AWMF	Arbeitsgemeinschaft der Wissenschaftlichen Medizinischen Fachgesellschaften e.V.
BACE1	ß-secretase ß-site cleaving enzyme 1
BAK1	BCL2 Antagonist/Killer 1
BAX	BCL2 Associated X
BCL-2	B-cell lymphoma 2
BH3	Bcl-2 homology 3
CAN	Containing acetonitrile
Cas	Caspase
CDK5RAP1	CDK5 Regulatory Subunit Associated Protein 1
CMF	5-(Chloromethyl)furfural
CNS	Central nervous system
CO2	Carbon dioxide

CoA	Coenzym A
COVID-19	Coronavirus disease 2019
CTD	Carboxy-terminal domain
CTF	CCAAT box-binding transcription factor
DIABLO	Direct IAP binding protein with low pI
Dicer	Ribonuclease III
DMSO	Dimethyl sulfoxide
DNA	Deoxyribonucleic acid
DRP1	Dynamin-related protein 1
DYN2	Dynamin 2
eIF2B	Eukaryotic translation initiation factor 2B
eIF4F	Eukaryotic initiation factor 4F
ELAC2	ElaC Ribonuclease Z 2
EMA	European Medicines Agency
EOAD	Early-onset Alzheimer's disease
ER	Endoplasmatic reticulum
ETC	Electron transport chain
EU	European Union
f	Female
$FADH_2$	Flavin adenine dinucleotide
FAS	FAS cell surface death receptor
FDA	Food and Drug Administration
Fig.	Figure
FIS1	Fission 1 protein
FUS	Fused In Sarcoma
G3BP1	GTPase Activating Protein (SH3 Domain) Binding Protein 1
G4	G-quadruplex
G-418	Geneticin
GABA	gamma-Aminobutyric acid
GAPDH	Glycerinaldehyd-3-phosphat-Dehydrogenase
GCN2	General control nonderepressible 2

Gly	Glycine
GTP	guanosintriphosphate
GWAS	Genome-wide association study
H_2O	Water
HEK	Human embryonic kidney
HOAc	Acetic acid
HRI	Heme-regulated eIF2α kinase
ICD	International Statistical Classification of Diseases
IMM	Inner membrane
IMS	Inter membrane space
IQWiG	Institut für Qualität und Wirtschaftlichkeit im Gesundheitswesen
ISTD	Internal standard dilution
LBD	Lewy body disease
LC	Liquid chromatography
LLPS	Liquid–liquid phase separation
lncRNA	Long non-coding RNA
LOAD	Late-onset Alzheimer's Disease
LTP	Long term potentation
m	Male
MCI	Mild cognitive impairment
MEM	Minimum Essential Medium
MFF	Mitochondrial fission factor
MFN 1	Mitofusin-1
MFN 2	Mitofusin-2
MiD	Mitochondrial dynamics proteins
miRNA	microRNA
MMP	Mitochondrial membrane potential
MOMP	Mitochondrial outer membrane permeabilization
MRI	Magnetic resonance imaging
MRM	Multiple reaction monitoring
mRNA	messengerRNA

MS	Mass spectrometry
mtDNA	Mitochondrial DNA
mTOR	Mammalian target of rapamycin
mtROS	Mitochondrial reactive oxygen species
MWD	Multiple wavelength detector
NAD+/NADH	Nicotinamide adenine dinucleotide
NBB	Netherland Brain Bank
NFT	Neurofibrillary tangles
NMDA	N-methyl-D-aspartate
nt	Nucleotides
OMM	Outer membrane
OPA1	Optic atrophy protein 1
oTG	old transgenic
oWT	old wildtype
OXPHOS	Oxidative phosphorylation
PABP	Poly(A) binding protein
PD	Parkinson's Disease
PERK	Protein kinase R-like endoplasmic reticulum kinase
PKR	Protein kinase R
PMD	Post mortem delay
PMS	Methylphenazonium methosulphate
PSEN1	Presenilin-1
PSEN2	Presenilin-2
RBP	RNA-binding protein
RMP	RNA-modyfiing proteins
RNA	Ribonucleic acid
RNAP	RNA polymerase
RNase	Ribonuclease
RNHI	Ribonuclease/angiogenin inhibitor 1
RNP	Ribonucleoprotein
ROS	Reactive oxygen species

Rot	Rotenone
rRNA	ribosomal RNA
sAPP	soluble APP
SEM	Standard error of the mean
SG	Stress granule
siRNA	Small interfering RNA
SMAC	Second mitochondria-derived activator of caspas
sncRNA	Small non-coding RNA
snoRNA	Small nucleolar RNA
snRNA	Small nuclear RNA
TARC	Translational animal research center
TBI	Traumatic brain injury
TBP	TATA-binding protein
TBST	Tris-buffered saline with Tween20
TDP-43	TAR DNA binding protein 43
TFIIA	Transcription factor II A
TFIID	Transcription factor II D
TFIIH	Transcription factor II H
TG	Transgene
TIA1	Cytotoxic Granule Associated RNA Binding Protein
TIM	Translocase of the inner membrane
tiRNA	Stress-induced tRNA halves
TNF	Tumor necrosis factor
TOG	Terminal oligoguanine
TOM	Translocase of the outer membrane
tRF	Small tRNA fragment
tRNA	transfer RNA
tsRNA	tRNA-derived fragments
USA	United States of America
UV	Ultraviolet
VDAC	Voltage-dependent anion channel

WB	Western Blot
WHO	World health organization
WT	Wildtype
XIAP	X-Linked Inhibitor Of Apoptosis
YBX-1	Y-Box binding protein-1
yTG	young transgenic

Contents

Chapter 1

1. Introduction

1.1. Aging and Alzheimers Disease

1.1.1. Epidemiology

Compared to earlier times, the population's average age continues to rise due to better medical care in many countries worldwide. The World Health Organization (WHO) has listed that more than 1 trillion people will be 60 years old or older in 2019 [1]. According to forecasts, this number will increase to 1.4 billion people in 2030 and 2.1 trillion in 2050 [1]. The global average age has also increased significantly within the last 6 years, from 66.8 years in 2000 to 73.4 years in 2019, when the last major WHO reports on aging was released [2]. If we look at Germany, life expectancy has also risen by around 2 years within 19 years. In 2000, the average age in Germany was 78.09 years, while in 2019, it was 81.72 years [2]. However, this medical progress also brings various problems, such as diseases in the elderly. Above all, the number of age-related dementia diseases will increase significantly.

The term dementia includes various forms of the disease and generally stands for different diseases that progressively affect memory function and behavior [3]. Currently, about 50 million people worldwide are living with dementia. According to predictions, this number will triple to around 152 million by 2050 [4]. Approximately US $1 trillion is spent annually on dementia-related funding worldwide [4]. This number is expected to rise to about $2.8 trillion annually in the coming years through 2030 as the cost of treating and caring for patients becomes more expensive compared to previous times. Also, the number of worldwide dementia cases will increase [4,5]. Alzheimer's Disease (AD) is the most common neurodegenerative disease, characterized by gradual cognitive decline and later dementia. About 15% of the over-65s and over 50% of the over-80s are affected by AD worldwide. According to estimates, around 36 million people worldwide currently suffer from having AD or another type of dementia.

This number will rise to about 65 million by 2030 and by 2050 to around 115 million patients worldwide [5,6].

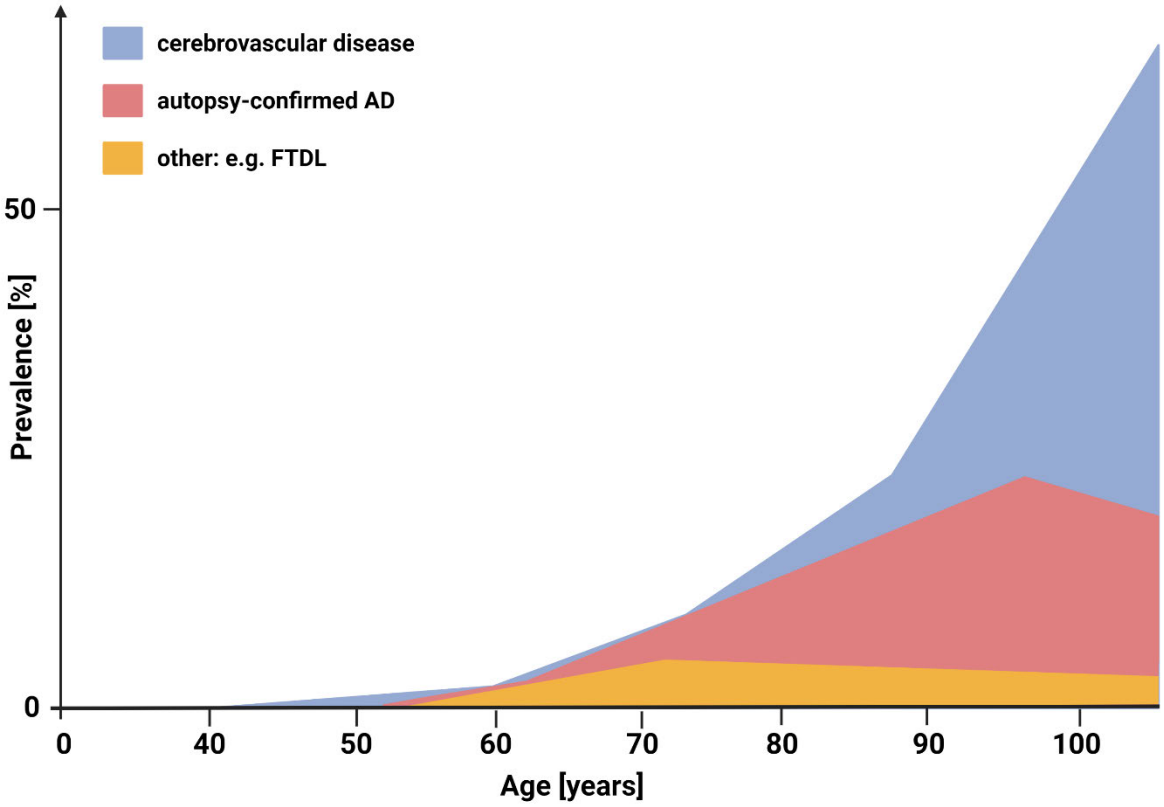

Figure 1. Neuropathological diagnoses causing cognitive impairment across the age spectrum. Modified from *Knopman, D.S., Amieva, H., Petersen, R.C. et al.* [7].

In 2017, the prevalence of developing AD in the European Union (EU) was at about 5.05%. However, the trend shows a significant increase in the cohort of the elderly [4,6]. Dementia is also the most common cause of disability and need for long-term care in advanced age. Although it is difficult to diagnose dementia as a cause of death, many patients die four to six years after the diagnosis is announced, but it is often declared as a result of aspiration pneumonia [8]. In addition to the burden on patients, dementia naturally also poses an enormous challenge for family members, the healthcare system, and the affected individuals' care [3]. Despite intensive basic research, the pathogenesis of AD is only partially understood, and because of that, there is a lack of adequate diagnostics and treatment options. Due to the drastic predictions of the increase of AD cases in the coming years, WHO launched the "*Global action plan on the public health response to dementia 2017-2025*" in May 2017 to improve the lives

of patients and their families and to reduce the impact of dementia on society and countries [9].

1.1.2. Forms of Dementia

The International Statistical Classification of Diseases and Related Health Problems is the world's most important classification system for all diseases for medical diagnosis and enjoys a high reputation published by the WHO. In May 2019, the 11th revision (ICD-11) was approved and thus replaced the old ICD-10 as of January 1st, 2022. According to the ICD-11 definition of dementia, dementia is an "[…] *acquired brain syndrome characterized by a decline from a previous level of cognitive functioning. Memory impairment is present in most forms of dementia, but cognitive impairment is not restricted to memory (i.e., there is impairment in other areas such as executive functions, attention, language, social cognition, and judgment, psychomotor speed, visuoperceptual or visuospatial abilities). The cognitive impairment is not attributable to normal aging and significantly interferes with independence in the person's performance of activities of daily living. The symptoms are not better accounted for by disturbance of consciousness, altered mental status, Delirium, Substance Intoxication, Substance Withdrawal, or another Mental, Behavioral, or Neurodevelopmental Disorder (e.g., Schizophrenia or Other Primary Psychotic Disorder, a Depressive Disorder). Based on available evidence, the cognitive impairment is attributed or assumed to be attributable to a neurological or medical condition that affects the brain, trauma, nutritional deficiency, chronic use of specific substances or medications, or exposure to heavy metals or other toxins*" [10]. The currently valid guideline for treating dementia is the S3 guideline from 2016, which still refers to the ICD-10. It is described that dementia exists if the related symptoms are present for at least 6 months or more [11]. Diagnosis is further complicated by the presence of many different forms of dementia. The two most common forms are AD and vascular dementia.

AD is the most common form of dementia as it accounts for 60-70% of all dementia cases. AD is characterized by gradual cognitive decline and leads to later dementia. Currently, about 15% of the over 65s and over 50% of the over 80s are affected by AD worldwide [5,6]. There are characteristic neuropathological and neurochemical changes

of the brain tissue, e.g., the formation of tau tangles in neurons and the deposition of amyloid-β (Aβ) plaques in and out of the neurons. However, whether these toxic deposits cause AD is highly controversial. The biggest risk factor for developing AD is aging itself [3–5]. AD can be classified into early-onset or familial AD (EOAD) and late-onset or sporadic AD (LOAD). LOAD accounts for more than 95%, whereas EOAD accounts for only 1-5% of all cases [12]. In contrast to LOAD, EOAD occurs before the age of 65. In some patients, EOAD develops in the early 30s and 40s and often results in early death [13–17]. EOAD results from three mutations involved in Aβ metabolism that have been identified as causative factors for the development of AD [13]. The mutated genes include amyloid precursor protein (APP), presenilin 1 (PSEN1), and presenilin 2 (PSEN2) [14,18–20]. However, a large pedigree remains genetically unexplained [13,21–23]. In contrast to EOAD, the most common form of AD is LOAD, which typically develops after the age of 65 years [24,25]. Large-scale genome-wide association studies (GWAS) have associated more than 20 genetic loci with increased susceptibility to LOAD, which may be involved in the pathway of Aβ production and degradation. These include the gene apolipoprotein E4 (ApoE4) [13,26,27]. In addition to Apo4, the biggest risk factor for developing LOAD is aging. The aging process is characterized by various dysfunctions, such as an increase in reactive oxygen species (ROS) or a decrease in synapse number. These changes are likely triggered by mitochondrial dysfunction and various other factors [13,26–28].

The second most common form of dementia is vascular dementia [29]. Vascular dementia ranges from cognitive impairment to dementia [29]. Typical symptoms include mental slowness and problems with executive function and memory impairment, behavioral symptoms, and psychological symptoms such as anxiety and depression [29–32]. The symptoms or signs of vascular dementia that occur during the progression of the disease depend on the extent and location of the underlying cerebrovascular pathophysiology in each patient [29–32]. Overall, vascular dementias account for only 5-10% of all dementias [29–32].

Secondary dementia is also defined in the ICD-11. This disease often refers to nutritional deficiencies, chronic dependence on various substances or medications, or exposure to heavy metals and other toxins [10].

1.1.3. Diagnostic of AD

As defined in the ICD-11 and the S-3 guideline, dementia is present when the affected patients have related symptoms for longer than 6 months [10,11]. There are several options available for diagnosis. First and foremost, the Mini-Mental status test, the DemTect, the test for early detection of dementia with depression distinction, and the Montreal cognitive assessment test are considered the most appropriate cognitive tests [11]. The accurate diagnosis of the disease dementia is essential for the therapy of dementia and the adjustment of the progression of the disease. The Mini-Mental-status test can be performed to get a first impression of the severity of dementia. Based on the score obtained there, a classification of dementia can be made. As soon as the cognitive tests have been evaluated and a performed anamnesis has additionally confirmed dementia, a differential diagnosis must be carried out in order to be able to determine the exact type of dementia [4,11,33]. Specific biomarkers can also be used to classify a present AD. These biomarkers are Aβ, tau, and hyperphosphorylated tau and can be detected in cerebrospinal fluid and blood. However, these biomarkers can be used to classify AD and monitor the therapeutic success during AD treatment [4,11,33]. It has been observed that during the progression of AD, the levels of the respective biomarkers change. Thus, as the disease progresses, the levels of Aβ in the cerebrospinal fluid decrease, while the levels of tau and hyperphosphorylated tau increase [4,11,33]. These pathophysiological changes occur at an early stage, where no cognitive changes can yet be detected [4,11,33]. This circumstance could be used to diagnose an incipient disease before the first symptoms appear and to start therapy as early as possible. In addition to laboratory diagnostic history, imaging may also be used. Specific Aβ or tau tracers can be imaged using positron emission tomography (PET) to diagnose or monitor AD progression in the brains of affected patients. In addition, SV2A radioligands are used to assess the density of neurons to analyze the progression of dementia. Magnetic resonance imaging (MRI) can also be used to determine the atrophy of both the whole brain and the hippocampus. However, the disadvantage of this method is that MRI can only be used to determine the success of therapy or the progression of the disease, not its shape. This problem results in up to 30% of dementia cases being misdiagnosed. This fact represents a significant disadvantage for the therapeutic success of the treatment option used. For this reason, it is important to invest in new approaches to improve diagnosis [4,11,33].

1.1.4. Mitochondria

Based on the endosymbiont theory, our mitochondria are derived from archaebacteria, which prokaryotic cell precursors ingested over 2 billion years ago. In addition to their best-known function of ATP production and subsequent oxidative phosphorylation (OXPHOS), mitochondria also regulate Ca^{2+} homeostasis and are crucial in initiating apoptosis.

1.1.4.1. Structure

The mitochondrion is separated from the cytosol by two membranes, the outer (OMM) and the inner membrane (IMM), classified as double-membrane organelles, which have the intermembrane space (IMS) in between [34]. This IMM surrounds the mitochondrial matrix and forms cristae. Cristae are small invaginations in which the OXPHOS system is located. The composition of phospholipids, as well as the protein-lipid ratio, differ significantly between OMM and IMM. In OMM, the protein-lipid ratio is approx. 50:50 [35], as OMM mainly consists of phosphatidylcholine, phosphatidylethanolamine, and pore-forming membrane proteins (porins). In addition, the OMM has a voltage-dependent anion channel (VDAC), which makes it permeable to ions and small molecules [35]. Larger proteins are imported into the mitochondrion by the translocase of the outer membrane (TOM) complex. No mitochondrial membrane potential (MMP) is built up at the OMM due to the porosity of the latter. In contrast to the OMM, the IMM has a protein-lipid ratio of about 75:25 [35]. Ions or other molecules can only pass through the IMM by membrane transport proteins selective for the ion or molecule. As a result of this ion selectivity, an MMP is built up at the IMM [36]. The IMM forms cristae as well. At this locus, oxidative phosphorylation takes place. Finally, the ion gradient formed at the IMM by various membrane protein complexes synthesizes ATP. As the only eukaryotic cell membrane, the IMM contains cardiolipin, a phospholipid synthesized in the mitochondria, which maintains the MMP and the function of several proteins in the mitochondrial respiratory chain [37]. Furthermore, mitochondria possess double-stranded circular DNA (mtDNA), which is maternally inherited. In contrast to nuclear DNA, mtDNA is not wrapped around histones [38,39]. Since mitochondria synthesize only a part of their required proteins themselves, they depend on the import of nuclear-encoded proteins by TOM and Translocase of the Inner Membrane (TIM) complexes [38,39].

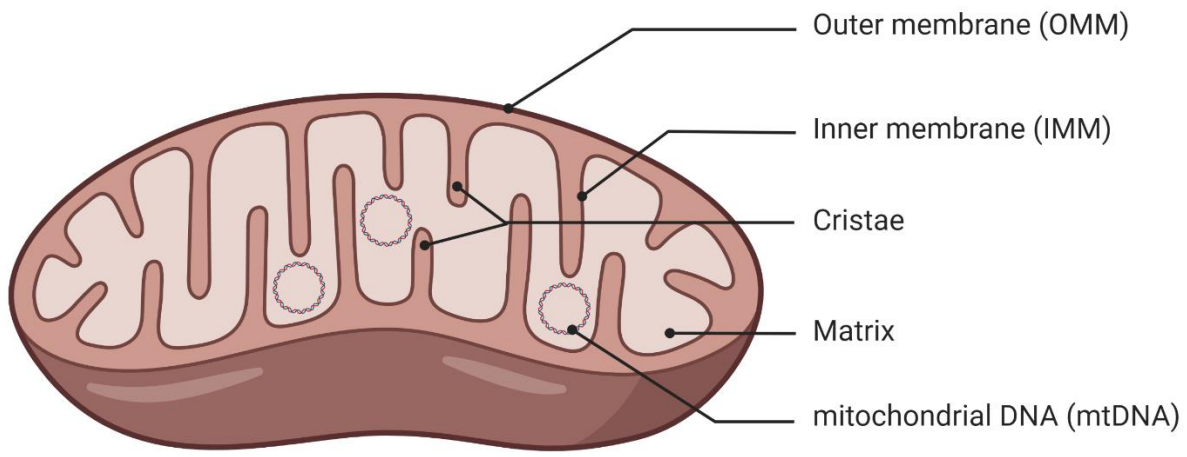

Figure 2. Structure of a mitochondrion.

1.1.4.2. Function

Mitochondria play a crucial role in different cellular mechanisms and regulatory pathways. The most important function of mitochondria is the cellular energy metabolism by generating ATP, as they are responsible for fatty acid oxidation, the Krebs cycle, and oxidative phosphorylation. Furthermore, they play an important role in inducing and regulating apoptosis.

1.1.4.3. Oxidative Phosphorylation System (OXPHOS)

As mentioned above, one of the major functions of the mitochondria is oxidative phosphorylation via the OXPHOS. This mechanism is unique by involving an interplay between mitochondrial and nuclear genome as a dual genetic control. Only a small fraction of polypeptides involved in the electron transport chain (ETC) are encoded b mtDNA. The majority of the subunits involved in ETC are encoded by the nuclear genome [40]. The ETC consists of four different transmembrane protein complexes (complex I-IV) and the mobile electron transport carriers ubiquinone and cytochrome c [41,42]. During ETC, the majority of a cell's ATP supply is generated. By comparison, another ATP-supplying mechanism is glycolysis in the cytosol of cells. This mechanism yields only two ATP per glucose molecule while the citrate cycle and oxidative phosphorylation are 36 molecules of ATP, 18 times higher ETC. The two molecules of pyruvate obtained from glycolysis are cleaved during oxidative decarboxylation to acetyl CoA and CO_2. In this reaction, two electrons are bound to two molecules of NADH, which function as reduction equivalents. In the Krebs cycle, the oxidation of the

two molecules of acetyl CoA to CO_2 then takes place step by step. Per acetyl CoA, one molecule of GTP (equivalent to one ATP) and five electrons bound to three NADH and one $FADH_2$ are formed. With the help of the electrons from the NADH and the $FADH_2$, the stepwise reduction of molecular oxygen to water occurs in the oxidative phosphorylation, whereby a proton gradient is built up at the IMM [42–44].

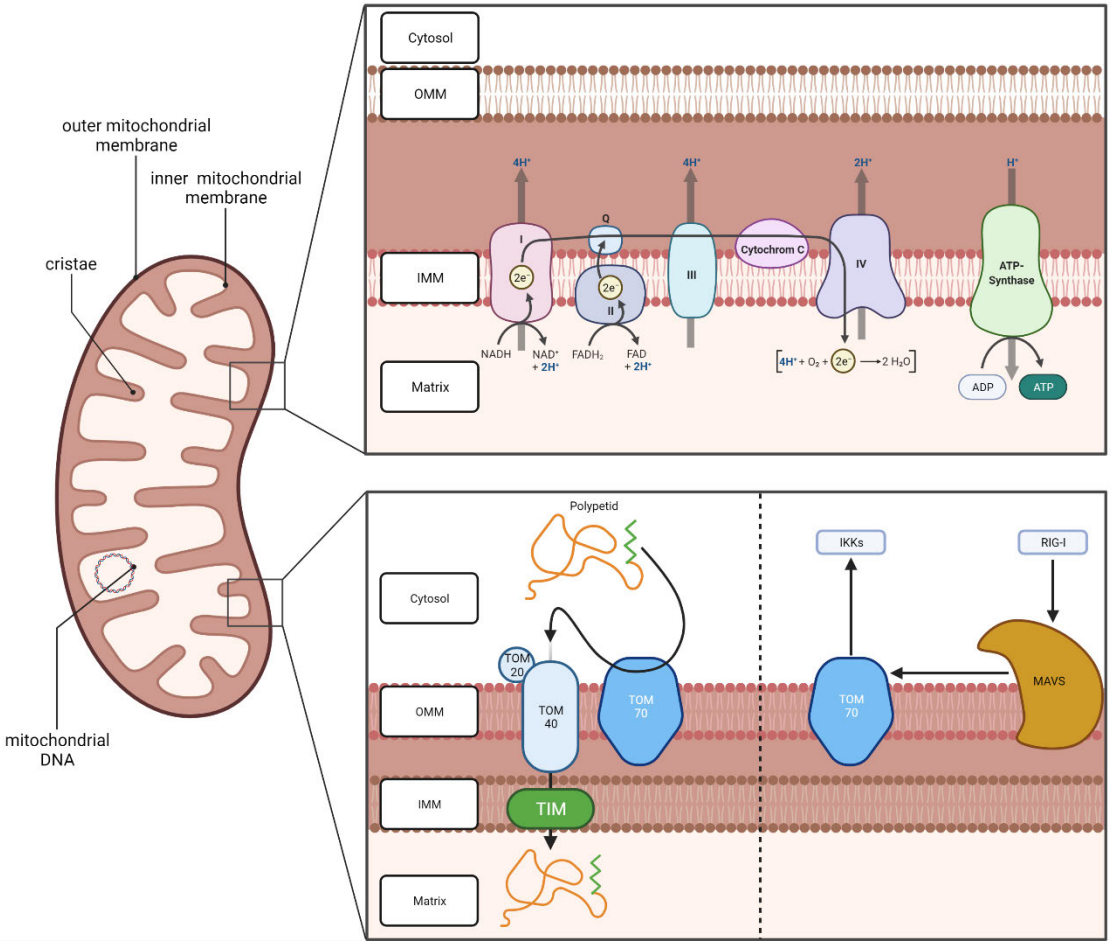

Figure 3. Schematic representation of the respiratory chain, which builds up the membrane potential. Multiple redox reactions at complexes I-IV generate a proton gradient that drives ATP synthase. In the lower part of the Image schematic representation of the role of TOMs and TIMs in mitochondrial membranes. Involvement in protein import is shown on the left, and their involvement in signal transduction along the OMM is shown on the right.

Redox complexes I, III, and IV are responsible for this reaction: complex represents NADH dehydrogenase, complex III represents cytochrome c oxidoreductase, and complex IV represents cytochrome c oxidase. In contrast to complexes I, III, and IV, succinate dehydrogenase (complex II) does not pump protons into the IMS but is

directly linked to the Krebs cycle and can use $FADH_2$ as reduction equivalents. Electrons are transported between the individual complexes using mobile electron transport carriers ubiquinone and cytochrome c [41–43]. Transport of protons and electrons along the ETC results in a charge difference and a concentration difference at the IMM. The resulting charge difference of approx. 150 mV is expressed by the MMP $\Delta\Psi m$. In contrast, the proton gradient $\Delta\Psi p$ generates a potential of about 30 mV. Together, the charge and concentration difference form a promotive force ΔP of 180 mV, which is used to synthesize ATP with the aid of the ATPase (complex V) [45].

1.1.4.4. Mitochondrial Dynamics

Mitochondria are highly dynamic cellular organelles that adapt to their environment while constantly changing. The proportion of mitochondrial mass in cells is crucial for energy balance and producing certain metabolic products such as succinate and lactate [46,47]. Depending on different situations such as stress or metabolic state, mitochondria can undergo fission and fusion events triggered by various fluids [48,49]. Fusion events of two mitochondria by their OMM are mainly controlled by GTPases mitofusin-1 and -2 (MFN 1 and MFN 2) proteins, whereas fusion of IMMs is regulated by optic atrophy protein 1 (OPA1). OPA1 also regulates the formation and structure of Christae and ETC. The fusion of two or more mitochondria enables the exchange of metabolites and mtDNA and increases the energy efficiency of the cell. Mitochondrial fusion occurs primarily when resources within the cell are scarce. In contrast, mitochondrial fission events increase the storage capacity of the cell and occur during times of increased resource supply. The process of Fission is controlled by dynamin-related protein 1 (DRP1), dynamin 2 (DYN2), and DRP1 receptor proteins mitochondrial fission 1 protein (FIS1), mitochondrial fission factor (MFF), and mitochondrial dynamics proteins (MiD) 49 and MiD51. The event of fission results in an increase in mitochondrial number leading to increasing levels of mitochondrial-derived ROS (mtROS). Damaged mitochondria are digested via autophagosome to prevent the uncontrolled formation and toxic effects of mtROS [46,50].

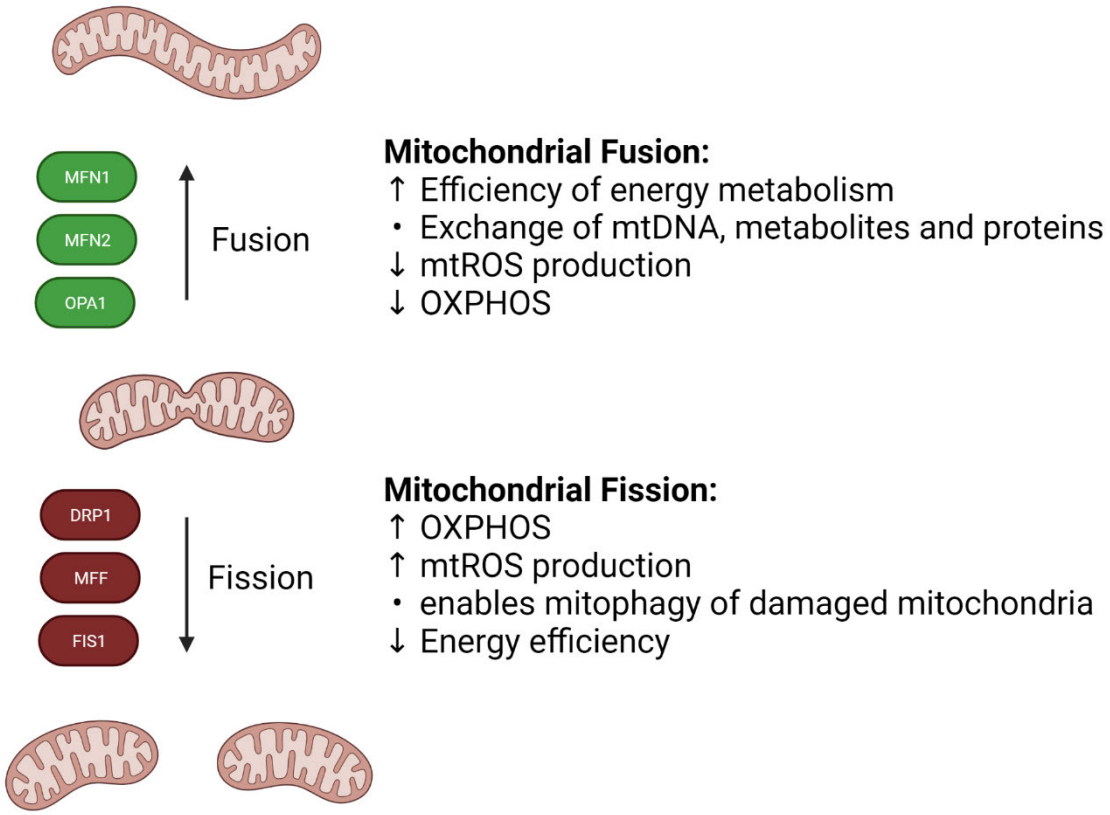

Figure 4. Schematic representation of fusion and fission and degradation of damaged fragments by an autophagosome.

1.1.4.5. Apoptosis and cell death

In addition to the already mentioned functions of ATP generation, mitochondria also play a crucial role in regulating cell survival and cell death. Apoptosis, the programmed cell death, is a physiological feature and occurs during development, as a defense mechanism, or as a result of aging. Intrinsic and extrinsic stimuli can activate apoptosis. Based on these stimuli, the activation of apoptosis can be separated into the intrinsic pathway and the extrinsic pathway. The intrinsic pathway is controlled by members of the BCL-2 protein family and the release of mitochondrial proteins [51,52]. Intrinsic apoptotic stimuli are ROS, DNA damage, growth factor withdrawal, and many more stressors. In response to these intrinsic stimuli, BCL-2 associated X, apoptosis regulator (BAX), and BCL-2 homologous antagonist/killer (BAK1) are activated by pro-apoptotic BH3 only proteins. BAX and BAK1 oligomerize during the activation inducing outer mitochondrial membrane permeabilization (MOMP). MOMP is considered as the point of no return for the induction process of apoptosis. MOMP leads to the release of IMS proteins cytochrome c and second mitochondria-derived caspase activator

(SMAC or DIABLO). The release of cytochrome c leads to the formation of the apoptosome complex. This complex is formed by cytochrome c, apoptotic protease-activating factor 1 (APAF1), ATP, and procaspase-9 resulting in the activation of caspase-9 (Cas-9). Subsequently, Cas-9 activates caspases 3 and 7, which finally initiates apoptosis [51,52]. The extrinsic pathway is activated by external stimuli leading to the activation of the cell death receptor, finally causing apoptosis [51,52].

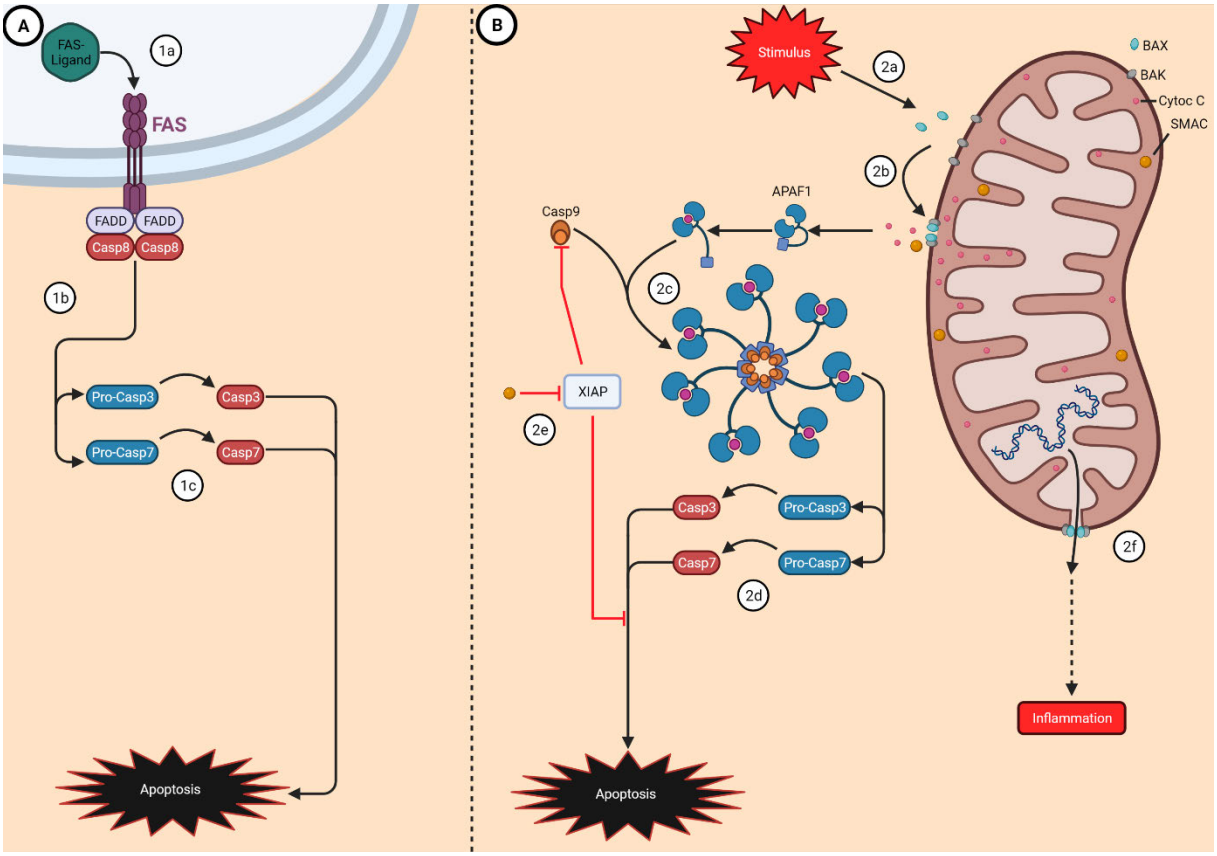

Figure 5. (A) Representation of the extrinsic pathway via the death receptor FAS. (1a) Binding the ligand to FAS leads to activation (1b) and cutting of pro-caspases 3 and 7 activating them (1c). **(B)** Representation of intrinsic pathway. (2a) A cellular stimulus ensures the binding of BAX to the outer membrane. This stimulus is followed by oligomerization of BAX and BAK to form pores in the outer membrane (2b), cytochrome c, and pro-apoptotic factors diffuse through these from the intermembrane space into the cytosol resulting in a drop of the membrane potential. (2c) The assembly of APAF1, Casp-9, and cytochrome c leads to apoptosome formation. This proteolytically activates Casp-3 and Casp-7, which start apoptosis inside the cell. (2d) XIAP and other anti-apoptotic factors are blocked by SMAC and other factors (2e). The breakdown and destabilization of the double membrane structure allow mitochondrial DNA and other matrix components to enter the cytosol. As DAMPs, they initiate different cellular pro-inflammatory signaling cascades (2f).

1.1.4.6. Mitochondrial motility

One of the key features of mitochondria is the so-called mitochondrial motility which ensures the meeting of mitochondria to fuse and the transporting to sites of high energy demand. As a result, mitochondrial locomotion is critical for the quality control of mitochondria. Mitochondria uses microtubules to carry through the cells transported by motor proteins kinesin 1 and dynein. Kinesin 1 transports mitochondria anterograde (away from the soma), and dynein transports them retrograde (towards the soma) [53–55]. They also move to a limited extent bound to myosin on actin filaments, where myosin transports both anterograde and retrograde in contrast to kinesin and dynein. The microtubule or actin filament transport requires energy generated by ATP hydrolysis of motor proteins [53–55].

1.1.5. Process of Aging and its role in neurodegeneration

The aging process is one of the most critical factors in the pathogenesis of AD and is characterized by various dysfunctions, such as an increase in ROS or a decrease in synapse number. These changes are likely triggered by mitochondrial dysfunction and various other factors [13,26–28]. These changes mainly lead to loss of memory, loss of neuronal plasticity, altered gene expression, altered DNA repair, and mitochondrial dysfunction and mainly affect the prefrontal cortex and the hippocampus, which also play an important role in AD [56].

1.1.5.1. Loss of Memory and cognitive decline

Starting with memory loss, it is striking that in adult life, working memory, short-term recall, and in general, the speed of processing information continues to decrease [56–60]. In these age-related changes, activation of the prefrontal cortex and the hippocampus plays an important role. After a task, it was shown that areas that typically showed particularly high activity in young adults showed significantly reduced activity as they aged, using magnetic resonance imaging and positron emission tomography studies [56,61,62]. When performing memory tasks, hippocampal activation is also significantly reduced in aged adults compared to young adults [56,63]. To some degree, this age-related memory loss is normal, but it transitions to a pathological state at a certain point. Here, the degree of impairment and the speed of cognitive decline is

crucial. Structurally, memory loss can also be evidenced by a loss of volume in the affected area, which can occur to a certain degree due to age but can develop into severe atrophy in AD [56,63,64].

1.1.5.2. Loss of neuronal Plasticity and long-term potentiation (LTP)/long-term depression (LTB)

In addition to these cognitive impairments, a loss of neurons and synaptic plasticity occurs. In this process, the cortex and the hippocampus are again mainly affected [56,65], but a reduction in white matter density can also be measured [56,64,66]. Precisely this reduction in density correlates with changes in executive function, short-term recall, and the general speed of processing information [56,64]. The density of synapses also decreases with aging, especially in the frontal cortex and the hippocampus [56,67,68]. Another important aspect is the influence of these changes on long-term potentiation (LTP) and long-term depression (LTB). Impaired induction and maintenance of LTP have been observed in many studies [56,69–72]. This synaptic plasticity is mainly dependent on the regulation of neuronal calcium fluxes and the calcium-mediated signaling pathway. Altered calcium homeostasis in the aged brain also contributes to altered synaptic plasticity [56,73]. One study showed an increase in voltage-activated calcium influx in rat hippocampal CA1 neurons. This change is associated with increased L-type calcium channels [56,73]. In addition to this, calcium buffering capacity may be affected in aged brains, increasing intraneuronal calcium levels [74]. This is likely due to decreased immunoreactivity of the neuronal calcium buffer protein calbindin 1 in cholinergic and cortical neurons and decreased mRNA expression of calbindin 1, various calcium channel subtypes, and the crucial signaling protein calmodulin 1. Therefore, these changes may contribute to altered calcium homeostasis and synaptic plasticity during aging [56,74,75]. It also increases the vulnerability of neurons to a variety of other toxic influences. However, gene expression of various other proteins may also change during aging.

1.1.5.3. Defective DNA repair system

Another important aspect is the altered DNA repair, which constantly decreases during aging. This results mainly in oxidative DNA damage such as 8-oxoguanines, which can be increasingly detected in aged brains [56,75–78]. These arise mainly from

ROS generated by aged mitochondria. The DNA repair complex immediately repairs these changes in young brains, whereas these persist in the aged brain [56,75–78]. This process can lead to the silencing of genes responsible for processes such as synaptic plasticity and mitochondrial function in the aged brain. These processes can also progress to cognitive decline and even neurodegenerative disease [56,75–78].

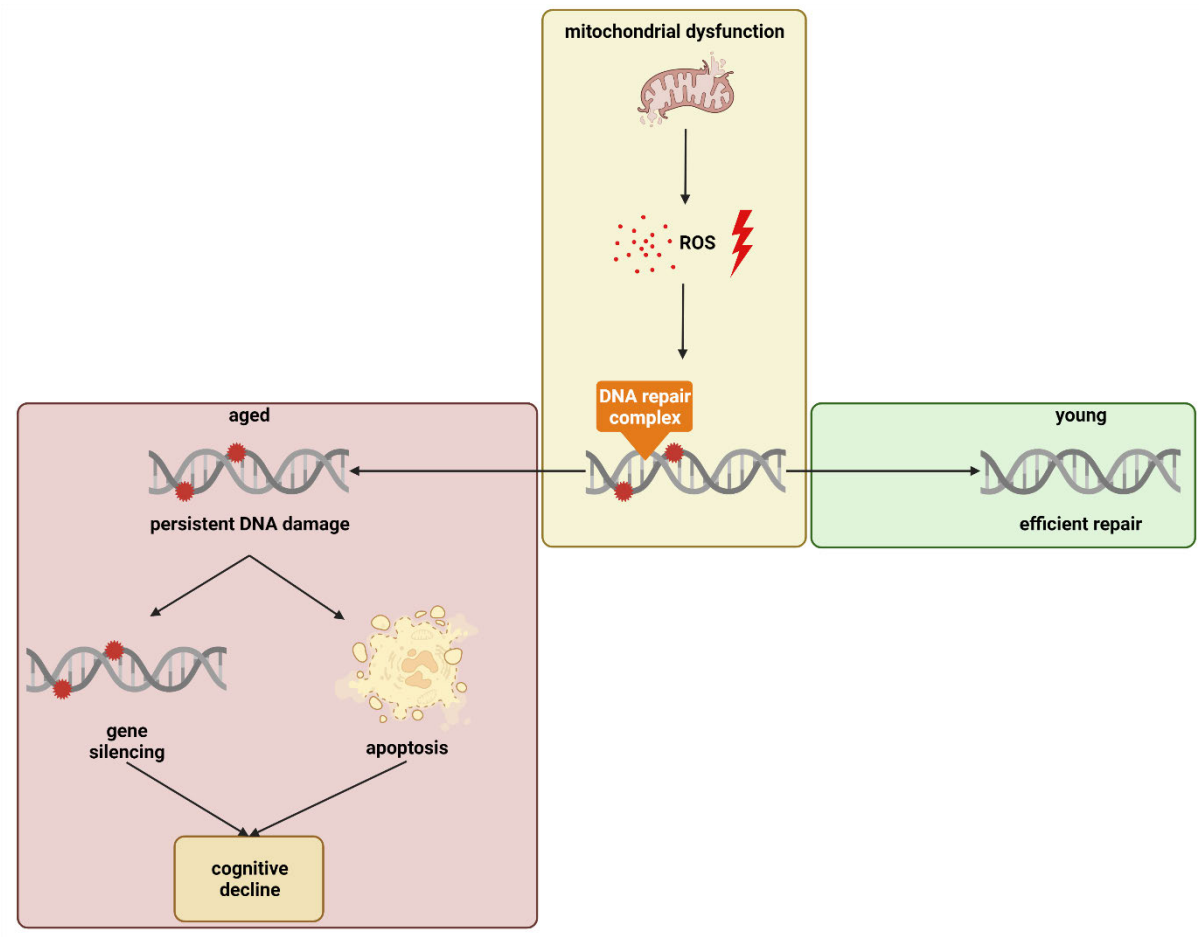

Figure 6. Oxidative DNA damage in brain aging.

1.1.5.4. Mitochondrial dysfunction

Probably the most important factor in aging is the development of mitochondrial dysfunction, which contributes significantly to the progression of the aging process. This is particularly affected by postmitotic tissues such as the brain and muscle [56,79]. Due to insufficient ETC, there is decreased ATP synthesis and thus the generation of mtROS as a byproduct. The healthy mitochondrion is normally protected against

endogenous ROS by antioxidant defense mechanisms such as cytochrome oxidase and manganese superoxide dismutase [56].

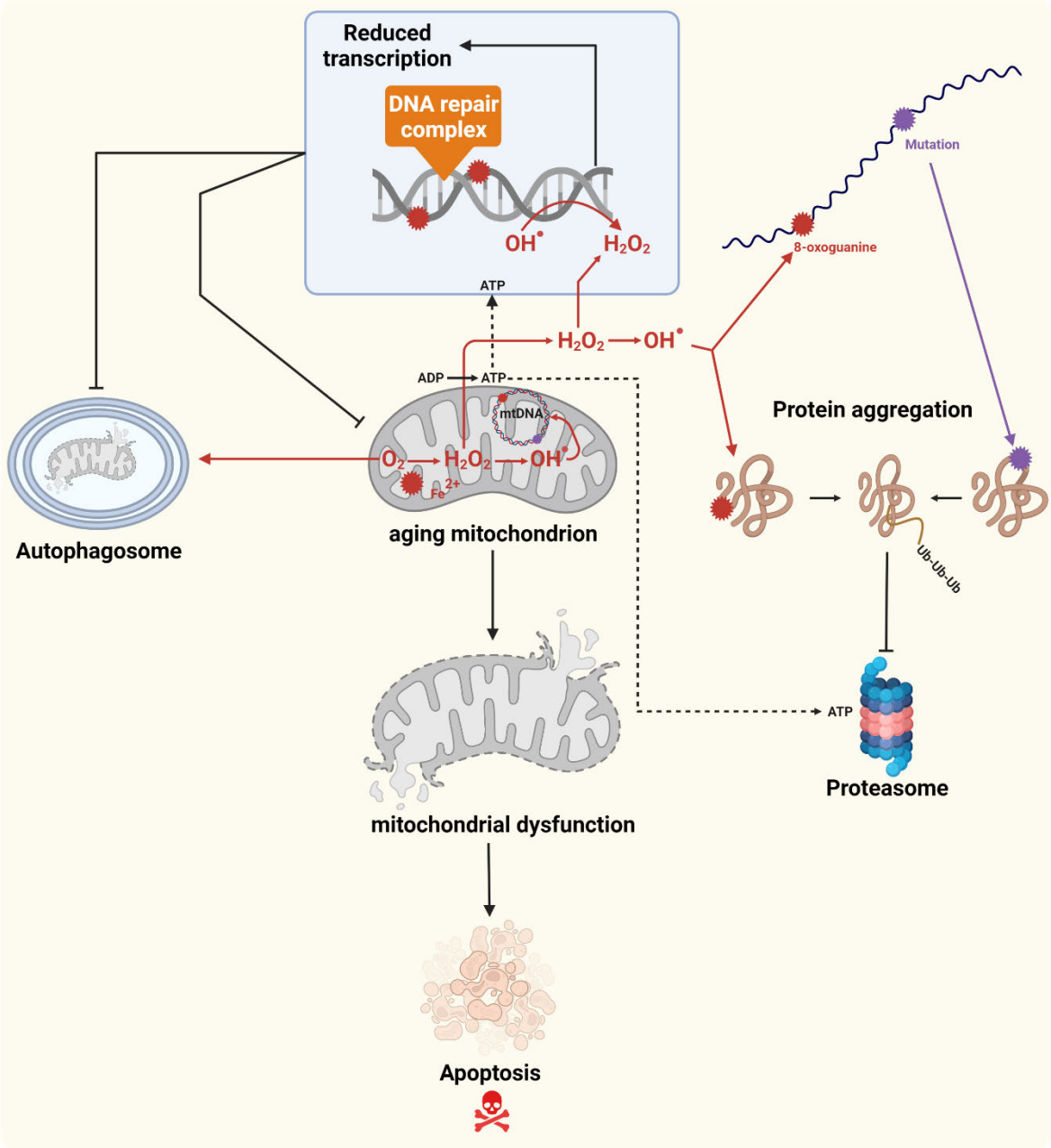

Figure 7. Impact of mitochondrial aging in cellular functions [56].

However, these mechanisms undergo alteration during aging, making them less effective and thus making mitochondria more vulnerable. This results in greater damage to the mitochondria, which leads to the production of mtROS, triggering a

circulus vitiosus. This ultimately ends in the development of mitochondrial dysfunction. Mitochondrial DNA is also increasingly damaged when triggered by the resulting increased ROS levels [56,80–84]. These mutations may contribute to altered transcription and replication of mitochondrial DNA, which also reduces the activity of respiratory chain enzymes, resulting in dysfunction of these [56,83–85]. This damage, in turn, generates ROS, extending the damage. Another consequence of mutations mtDNA is the formation of misfolding and aggregated proteins, which can accumulate in the brain over a prolonged period of time, as autophagy and ubiquitin-proteasome pathways may also be disrupted in old age [56]. This can lead to toxic deposits, leading to the development of neurodegenerative diseases [56].

1.1.6. Pathophysiology of AD

AD is a neurodegenerative disease characterized by the loss of neurons, especially in the brain areas of the hippocampus and the cortex, and a loss of memory function, behavioral changes, and personality changes. The disease has been known for over 120 years, but a cause has still not been found, with only theories and explanations circulating. So far, it is known that misfolded proteins accumulate in the brain of affected patients and, as a consequence, lead to inflammation, oxidative damage, and finally to neuronal loss [4,33,86]. August Alzheimer already discovered such changes in the brain of Auguste Deter, the first Alzheimer's patient [4,33,86]. Both there and in further histological examinations of postmortem brain tissue from patients diagnosed with AD, senile plaques consisting of Aβ and neurofibrillary tangles of hyperphosphorylated tau could be found [4,33,86]. These changes are mainly found in the brain regions of the hippocampus and the cerebral cortex, which are particularly affected by AD [4,33,86]. How these two histopathological hallmarks play a role as a causative factor in the pathogenesis of AD remains unclear. In EOAD, homozygotic risk genes (APP, PSEN1, PSEN2) have already been identified, enhancing the production of Aβ and, therefore, levels of Aβ [87–89]. Therefore, one of the first theories trying to explain the cause of AD was the amyloid cascade hypothesis. The generation of Aβ results from the cleavage of the APP. APP is a Type I transmembrane protein frequently expressed in the mammalian brain, and it is typically cleaved by α-, β-, and γ-secretases resulting in different cleavage products.

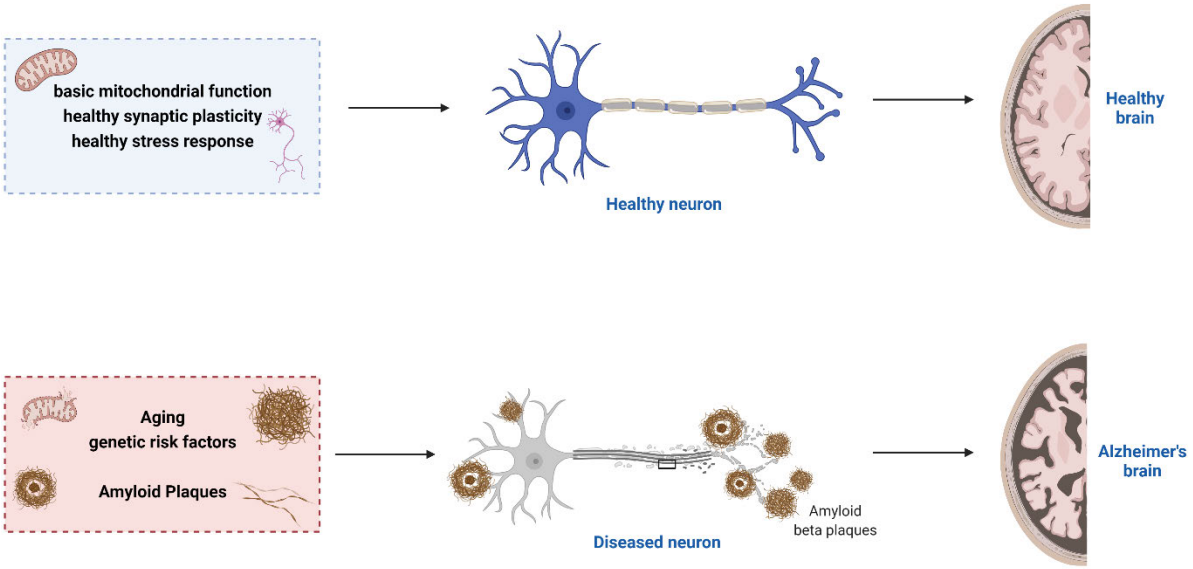

Figure 8. Amyloid cascade hypothesis.

The cleavage can be distinguished into two major pathways: amyloidogenic and anti-amyloidogenic [87–89]. The amyloidogenic pathway leads to the synthesis of the peptide Aβ; meanwhile, the anti-amyloidogenic pathway processes APP without synthesizing Aβ [87–89]. In the anti-amyloidogenic pathway, Aβ formation is already avoided during the first steps. This circumstance is because the α-secretase cuts APP directly within the corresponding Aβ sequence, thus preventing its formation. The degradation products of α-secretase are extracellular soluble APP (sAPP) α and the transmembrane carboxy-terminal fragment (CTF) α. Subsequently, the resulting CFTα fragment is cleaved by γ-secretase, resulting in the two degradation products p3 and the APP intracellular domain (AICD) [87–89]. In the amyloidogenic pathway, however, cleavage of APP occurs by β-secretase. The most abundant secretase in neurons is β-secretase β-site cleaving enzyme 1 (BACE1). This β-secretase cuts above the Aβ sequence, giving rise to sAPPβ and the transmembrane CFTβ. The latter still contains the complete sequence of Aβ and is therefore important for further processing. For continued degradation, the enzyme γ-secretase is required.

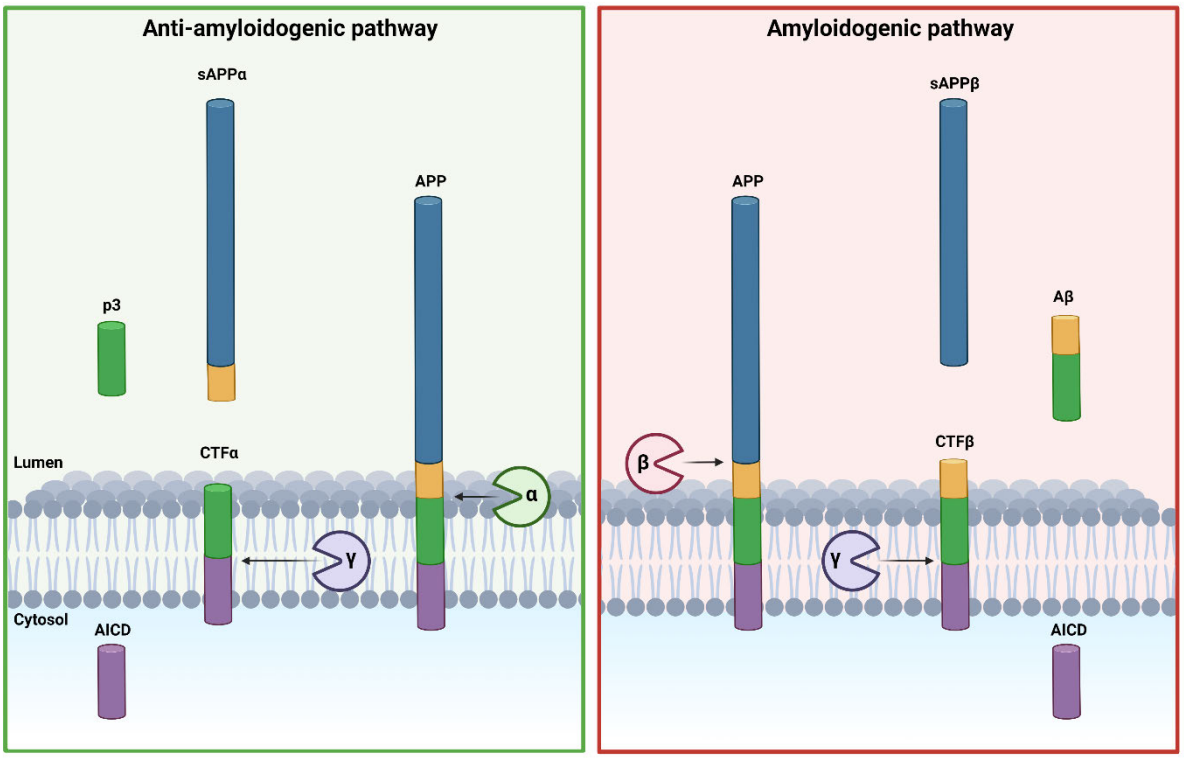

Figure 9. APP processing in human neuronal cells.

This enzyme is a larger protease complex consisting of four subunits, which contain PSEN1 and PSEN2 in their active catalytic domain. This domain is crucial for the enzyme's function and, therefore, explains why mutations in one of the two genes increase γ-secretase activity and thus result in increased Aβ production, promoting the formation of EOAD. In the following process, CFTβ is now degraded by γ-secretase into extracellular Aβ and intracellular AICD. The Aβ formed is between 36 and 43 amino acids long, depending on where the γ-secretase cut CFTβ [87–89]. Depending on the length, mainly two forms of Aβ are relevant for AD development: Aβ1-40 and Aβ1-42. Especially soluble oligomers of Aβ1-42 have particularly harmful and AD-promoting effects [87–89]. Moreover, these soluble oligomers of Aβ1-42 are particularly prone to aggregation because they contain hydrophobic domains, which can bind monomers to form plaques [87–89]. These intracellular Aβ oligomers can trigger several other neurotoxic cascades, ranging from synaptic dysfunction, the induction of oxidative stress, the development of mitochondrial dysfunction, hyperphosphorylation of tau, and neuroinflammation [90]. Aβ additionally impairs synaptic plasticity over time, triggered by suppression of long-term potentiation (LTP) and promotion of long-term depression (LTD). These changes lead to significant impairment of learning and memory function

in affected patients [91,92]. Moreover, the major pathway of neuronal oxidative stress is the Aβ-mediated impairment of the mitochondrial OXPHOS system, leading to increased ROS formation [93,94]. In addition, senile Aβ plaques contain various metal ions such as copper, iron, and zinc, which, when bound to Aβ, induce the formation of further ROS [94,95]. Aβ itself also triggers an increase in intracellular ROS levels, promoting oxidative stress and activation of microglia, e.g., macrophages in the CNS [94,96]. Moreover, Aβ increases the toxicity of its partner tau by promoting the conversion of tau to its toxic product, hyperphosphorylated tau. It also promotes the proliferation of neurofibrillary tangles (NFTs). These NFTs cause neuronal lesions, which promote the toxicity of Aβ, thus initiating a circulus vitiosus [97–99]. Furthermore, because Aβ and APP are localized to the mitochondrial membrane, they impair mitochondrial function by interfering with the import of nuclear-encoded mitochondrial proteins. This effect leads to membrane depolarization, a decrease in ATP concentration, increased ROS concentration due to impairment of OXPHOS, and altered mitochondrial morphology and motility [93,94,100]. The activation, as mentioned earlier, of microglia by Aβ causes them to migrate to and phagocytose Aβ plaques in the brain. Aβ promotes the development of a neurotoxic subtype of microglia that increases the release of proinflammatory cytokines, causing further tissue damage and promoting disease progression [101–103]. In summary, these Aβ-related mechanisms contribute to the loss of neurons and thus to the progression of AD. Another important fact is that the gene for APP is located on chromosome 21, resulting in a tendency to form higher levels of APP in patients with down syndrome trisomy 21 [104]. Also, several other genes relevant for oxidative stress and mitochondrial dysfunction are located on the same chromosome, leading to typical age-related mitochondrial deficits but at a much younger age in down syndrome patients [104–106]. These findings lead to the Aβ cascade hypothesis suggesting slow accumulation of Aβ containing plaques and soluble highly toxic low molecular weight Aβ as a major causative pathomechanism of AD for the development of EOAD and LOAD. The described amyloid cascade hypothesis resulted from preclinical data from transgenic cell and animal models [105,107]. The simple conclusion of science was that removing Aβ oligomers, fibrils, and plaques was considered the first option for treating AD. However, this hypothesis was very quickly invalidated, as no correlation could be found between plaque density in the brain and the presence and severity of clinical symptoms [105,108,109]. In this model, aging was neglected as an important factor for LOAD [105,108,109]. Based on the amyloid

cascade hypothesis, many drugs were developed (e.g., aggregation inhibitors, inhibitors of secretases that produce Aβ from its precursor protein APP, antibodies to eliminate Aβ, or enhanced production of antibodies by vaccination), all of which failed because they neither improved symptoms nor addressed the cause. In some cases, they even exacerbated the predominant symptoms [105,110,111]. In fact, some very older adults have been shown to have significantly elevated Aβ levels in the brain but have not shown symptoms of dementia [105,112,113]. In contrast, a group of patients showed typical signs of neurodegeneration with or without the typical symptoms of dementia long before Aβ plaques could be detected. Vaccination against Aβ also largely eliminated the Aβ oligomers but failed to halt the progression of the disease [105,114,115]. Based on these findings, the relatively simple amyloid cascade hypothesis was considered to have failed, especially concerning the development of new drugs to treat AD. For this reason, other aspects related to clinical symptoms as well as progressive neurodegeneration were included. One important aspect was the connection with mitochondrial dysfunction, which will be discussed later [105,116–121].

Since the simple amyloid cascade hypothesis had failed and was quickly rejected as the only explanation, the presence of hyperphosphorylated tau fibrils was discussed. Tau is an important protein mainly associated with microtubules and is mainly found in the axons of neurons in the CNS. The primary role of tau is usually to ensure the assembly and stability of microtubules [122–124]. In addition, tau is essential for neuronal morphology and the transport of organelles, vesicles, and proteins. Phosphorylation of tau is a central feature of this function and the decay process in tauopathies. When tau is additionally phosphorylated at residues Ser262 and Ser214, hyperphosphorylated tau leads to detachment from microtubules and aggregation into NFTs [122–124]. The phosphorylation of tau leads to a loss of physiological function of tau, disruption of axonal morphology, impaired axonal transport, and, in addition, neuronal decline. These changes could be observed in AD patients and other tauopathies. The lack of microtubule stabilization additionally leads to synaptic dysfunction characterized by a loss of synaptic plasticity. Furthermore, impairment of mitochondria by disruption of tau-triggered OXPHOS has been demonstrated, leading to altered mitochondrial dynamics as well as mitophagy [125–128]. The resulting mitochondrial dysfunction enhances the neurotoxicity of hyperphosphorylated tau and thus also contributes significantly to the development and progression of AD.

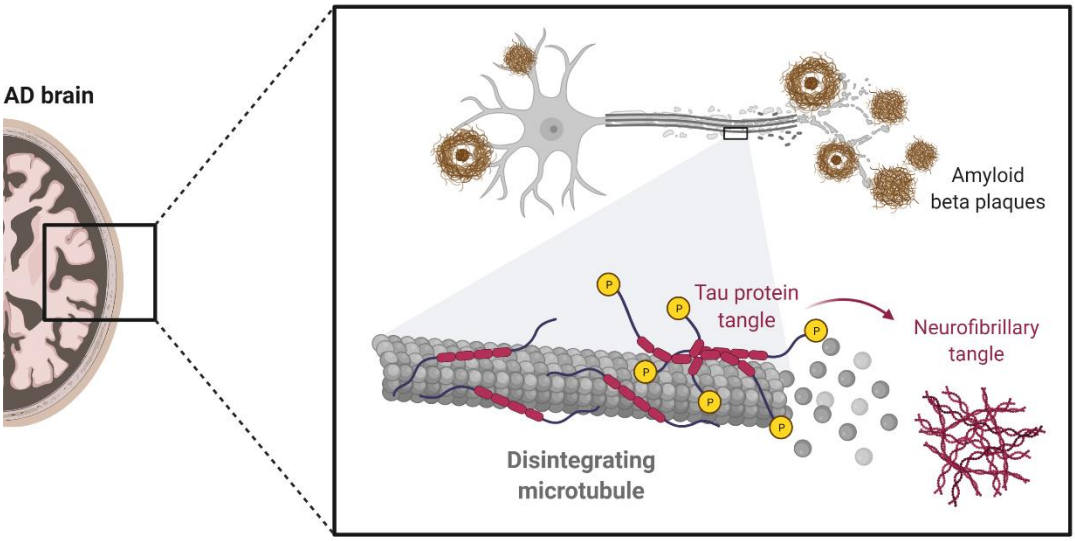

Figure 10. Tau pathophysiology.

However, whether these toxic deposits cause AD is highly controversial. The biggest risk factor to develop AD is aging itself. The aging process is characterized by various dysfunctions, such as increased ROS or decreased synapse number. These changes are likely all triggered by mitochondrial dysfunction. For this reason, the mitochondrial cascade hypothesis was proposed about 20 years ago by *Swerdlow et al.* as an alternative to the failed amyloid cascade hypothesis [105,110,129,130]. The CNS is profoundly affected during aging by a decline of several physiological abilities, including sensory, motor, emotional, or cognitive functions [105,131]. Aging brain cells also experience increasing amounts of oxidative stress, perturbed energy metabolism and homeostasis, accumulation of different damaged proteins, lesions in their nucleic acids leading to an impaired function of signaling mechanisms, and altered gene expression in the cell - all of these aspects of aging that cannot be stopped cause mitochondrial perturbations. During aging, mitochondria become less efficient because of decreased activity of complex I and III, leading to enhanced mitochondrial production of ROS, impaired mitochondrial fission, and fusion, altered mitophagy, reduced Ca^{2+} buffering capacity, and an increased accumulation of mitochondrial DNA (mtDNA) mutations [105,131,132].

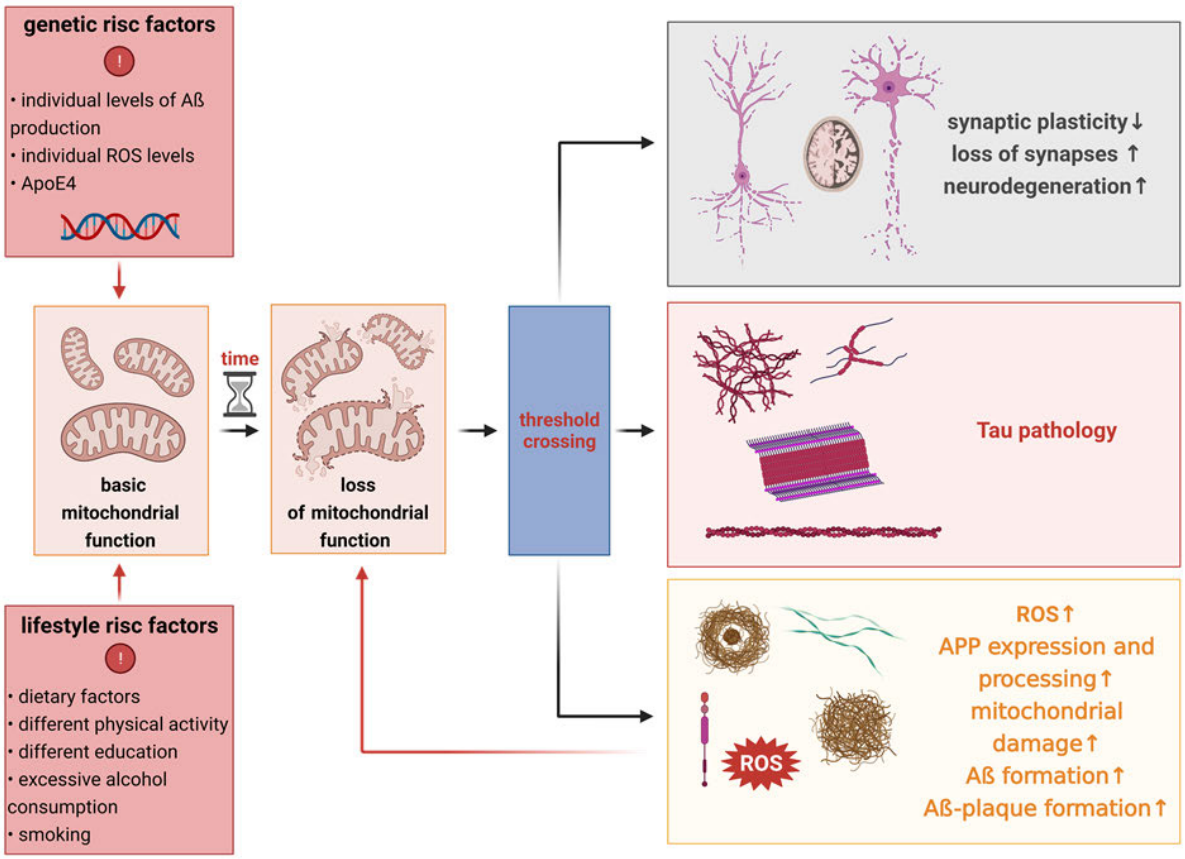

Figure 11. The Mitochondrial cascade hypothesis of aging and AD. The hypothesis is driven by genetic, environmental, and individual factors, mitochondrial dysfunction associated with elevated free radical (ROS) production cumulates in susceptible patients over many years, regulated by the individual balance between ROS production and the activity of the antioxidant defense system, including the activities of antioxidant enzymes. The biological aging process, which begins in animals and men around midlife, leads to an imbalance between ROS production and ROS detoxification and elevated levels of ROS and oxidative damage. Gender, ApoE4 state, and lifestyle are important other individual factors. This process is self-accelerating as ROS will further damage mitochondria, which will respond with a further elevation of ROS. Elevated ROS production reaches a critical level where Aβ (soluble, oligomers) production increases due to ROS-mediated β-secretase and γ-secretase activation. Aβ, in turn, will further increasingly impair mitochondrial function leading to synaptic dysfunction, the first sign of neurodegeneration as neurons are most sensitive to a deficit of energy (ATP) supply. At a critical concentration, Aβ itself will aggregate to fibrils and finally to plaques which are rather extracellular trash than disease-relevant histopathological alterations. This scenario suggests that Aβ still has a causative role in the pathophysiological cascade of AD but is probably not the only major player. This can easily explain that Aβ deposits do not correlate with early signs of neurodegeneration or impaired cognition [105,107–109,133].

These alterations in mitochondrial functions reveal mitochondria's role as critical regulators of programmed cell death in the aging brain. Therefore, abnormalities in mitochondrial function and oxidative stress are also important in the pathogenesis of AD, according to the consensus in the scientific community [105,121,134]. Mitochondrial dysfunction caused by increased ROS concentrations enhances the production of neurotoxic Aβ, setting in motion a circulus vitiosus that accounts not only for mitochondrial dysfunction per se but also for the toxic effects of Aβ and the resulting aggregation of Aβ into extracellular plaques [105,135,136]. Importantly, it was found in postmortem brains of AD patients that mitochondrial dysfunction and reduced bioenergetics occur early in pathogenesis preceding the development of plaque formation and thus repeatedly reinforcing the progression of AD. The mitochondrial cascade hypothesis by *Swerdlow et al.* assumes mitochondrial dysfunction as one of the major pathomechanisms in AD development, which slowly occurs during aging [105,110,129,130]. The most important aspects of the mitochondrial cascade hypothesis relate to the early stages of mitochondrial dysfunction triggered by the combined effects of oxidative stress due to aging and mildly elevated oligomeric intracellular Aβ levels caused by genetic and individual risk factors. Thus, the hypothesis starts long before pronounced Aβ deposits begin to form [105]. It can be said that the scientific evidence for the mitochondrial cascade hypothesis in dementia, especially in LOAD, is much better supported by numerous data from cell models, animal studies, and various tissues of AD patients while comparing the amyloid cascade hypothesis established at the beginning of AD research. The hypothesis could be further supported if drug treatment reduced mitochondrial dysfunction, thereby significantly improving cognitive impairment starting from the normal process of aging, through Mild Cognitive Impairment (MCI), to far advanced AD disease [105,137].

In addition to this hypothesis, other risk factors for AD development are present. Besides aging, and gender, genetic disposition also plays an important role. In the female brain, decreased production of neuroprotective estrogens leads to an increased impact of aging and thus to severe mitochondrial deficits and earlier onset of neurodegeneration compared with male individuals [105,138]. This increases the prevalence to develop AD in the aged female population. Besides aging and mutations in APP, PSEN1, and PSEN2 genes, the apolipoprotein E (Apo E) genotype is also one of the most important risk factors for the development of sporadic AD. In humans, three

major isoforms of the Apo E genes occur (E2, E3, and E4). The Isoform Apo E4 is suggested to impair the antioxidative defense system, resulting in increased ROS levels, altered expression of the respiratory chain complexes, reduced mitochondrial respiration, and early signs of neurodegeneration [105,139–142]. These effects of Apo E4 are associated with an increased risk of developing AD [105,139–142].

The previously discussed hypotheses highlight the complexity of AD's pathophysiology and the resulting difficulty in developing appropriate treatment strategies. Not without reason, more than 120 years after the disease became known, there is still no effective therapy, and final clarification of the development of the disease found, and it requires further intensive scientific research to close this knowledge gap as soon as possible to be able to treat AD soon.

1.2. The Ribonuclease Angiogenin

1.2.1. Structure, localization, and function of human Angiogenin

Human angiogenin belongs to the major gene superfamily, which exclusively expresses secreted ribonuclease (RNase) in vertebrates. Previously, the family was named pancreatic RNase superfamily because the prototype of this family was the bovine pancreatic RNase A [143,144]. Other members of this RNase superfamily are RNase 1 (pancreatic ribonuclease), RNase 2 (eosinophil-derived neurotoxin), RNase 3 (eosinophil cationic protein), RNase 4, RNase 6 (k6), RNase 7 and RNase 8 [145,146]. As part of the RNase A superfamily, human ANG is a 14kDa large monomeric nuclear protein consisting of 123 amino acid residues that can induce neovascularization [147,148]. ANG was originally discovered as a tumor-derived angiogenic factor in human colon adenocarcinoma cells [147]. ANG stimulates endothelial cell proliferation and is furthermore required for the angiogenic activity of vascular endothelial growth factor (VEGF) and fibroblast growth factor-2 (FGF-2) [146,149]. In this process, ANG stimulates ribosomal RNA (rRNA) transcription in the nucleus of the cells and thus acts synergistically with VEGF and FGF-2 to increase protein synthesis for the formation of new blood vessels [146,150]. Another effect associated with cancer is the indirect activation of PI3-kinase and Akt kinase pathways in endothelial and bladder cancer

cells [146,151–153]. In addition to these effects, ANG has the same catalytic properties as RNase A and predominantly cuts at the 3' end of pyrimidine. The cutting mechanism is based on transphosphorylation or hydrolysis [154–156]. Also known as RNase 5, ANG is the 5th member of the RNase A superfamily group [148]. The crystal structure of human ANG reveals that it has a catalytic triad in the active site (residues H13, K40, and H114) and three distinct functional sites [156,157]. The specific functional sites can be divided into a receptor-binding domain, a nuclear localization sequence (NLS), and the described catalytic site. The receptor-binding site is located in the region from K60 to N68. However, this domain interacts with a receptor still unknown today [144,158]. Under normal circumstances, ANG binds to its cell surface receptor and is internalized and translocated to the nucleus. The process is mediated by the NLS domain located between residues M30 and G34 [144,159,160]. The actual ribonuclease activity originates from the active site where the catalytic triad is located (H13, K40, and H114) [8]. All three sites are required for the functions of ANG. Compared to other ribonucleases, ANG has a relatively weak ribonuclease activity, which is of great importance for the process of angiogenesis [154,161].

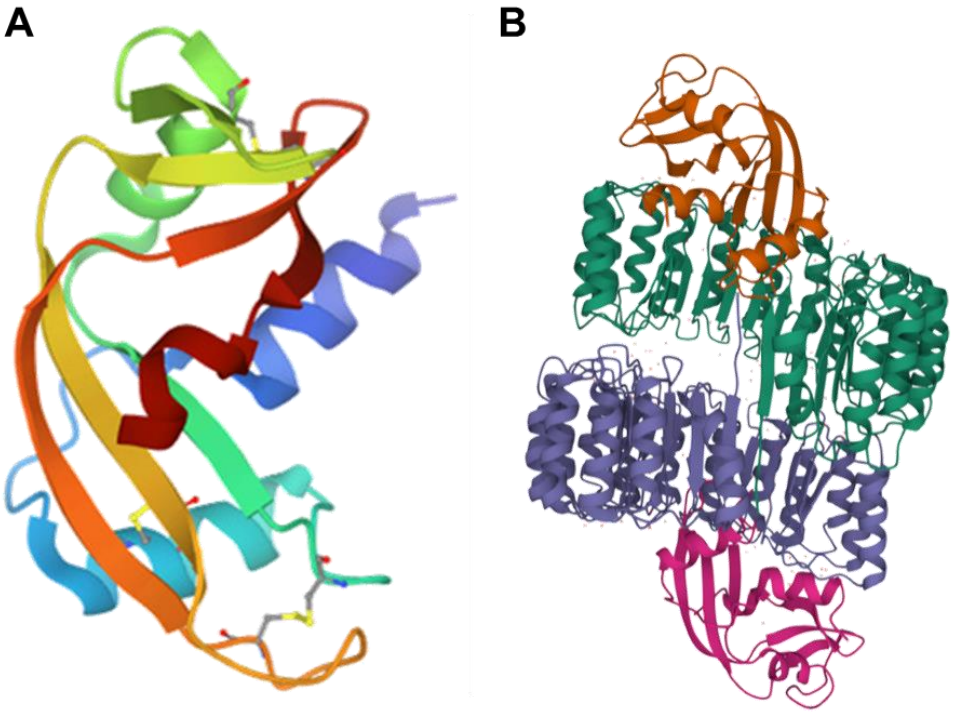

Figure 12. (A) Crystal structure of human Angiogenin at 1.35 Å resolution [162]. **(B)** Crystal structure of ANG in complex with its physiological inhibitor RNH1 [163].

In the state of rest, ANG is present in the nucleus bound to its natural inhibitor ribonuclease/angiogenin inhibitor 1 (RNH1) [164]. RNH1 usually binds to all pancreatic RNase A superfamily members to inhibit them. RNH1 has been shown to bind especially strongly to ANG, thereby inhibiting its RNase activity [165]. This strong binding is caused by forming a salt bridge between Asp435 of RNH1 and Lys40 in the active site of ANG [163]. The resulting ANG-RNH1 complex has a dissociation constant of ~1 fM, making it one of the strongest known noncovalent bonds observed in biochemistry [166]. In addition to its inhibitory function on ANG, RNH1 also has functions independent of ANG, such as acting as an oxidation sensor in human cells [166,167].

Besides its function in neovascularization, ANG also plays a crucial role in stress response and protecting cells. As a result of stress, ANG translocates from the nucleus to the cytoplasm and dissociates from RNH1 resulting in the cleavage of cytoplasmic tRNAs into tRNA halves (tiRNAs). These then bind to mitochondrially released cytochrome c inhibiting the pro-apoptotic signal pathway and the caspase 3 activity [168]. ANG primarily cuts the tRNA in the anticodon loop region to generate two tiRNAs (3'-tiRNA and 5'-tiRNA). This process is strongly dependent on RNA modifications, as these regulate the degradation of the tRNA by ANG. One example is the RNA modification 5-methylcytosine (m^5C) located in the variable loop region at positions 48/49/50, which plays an important role in regulating the cleavage of tRNAs [169] and will be discussed in detail in section *1.3.6. RNA modifications*. ANG can also initiate the formation of stress granules (SGs), which have protective properties in the case of acute damage, but neurotoxic effects in the case of chronic damage.

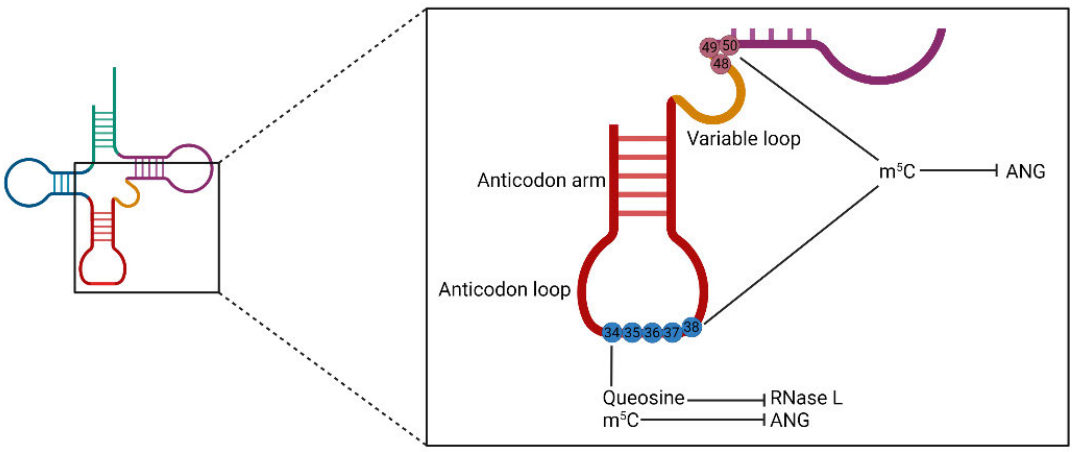

Figure 13. Role of RNA modifications in the regulation of tRNA cleavage.

A sequence similarity network (SSN) generation reveals that human ANG, rat ANG, and mouse ANG cluster together (Fig. 14). A SSN allows visualization of protein sequences grouping most related proteins together in clusters [170]. This considers a relation between these three proteins because of sequence similarity. It can be concluded that the function of ANG is similar in all three organisms. This information is of particular importance as it ensures the comparability of the function of ANG and thus the results obtained in this work.

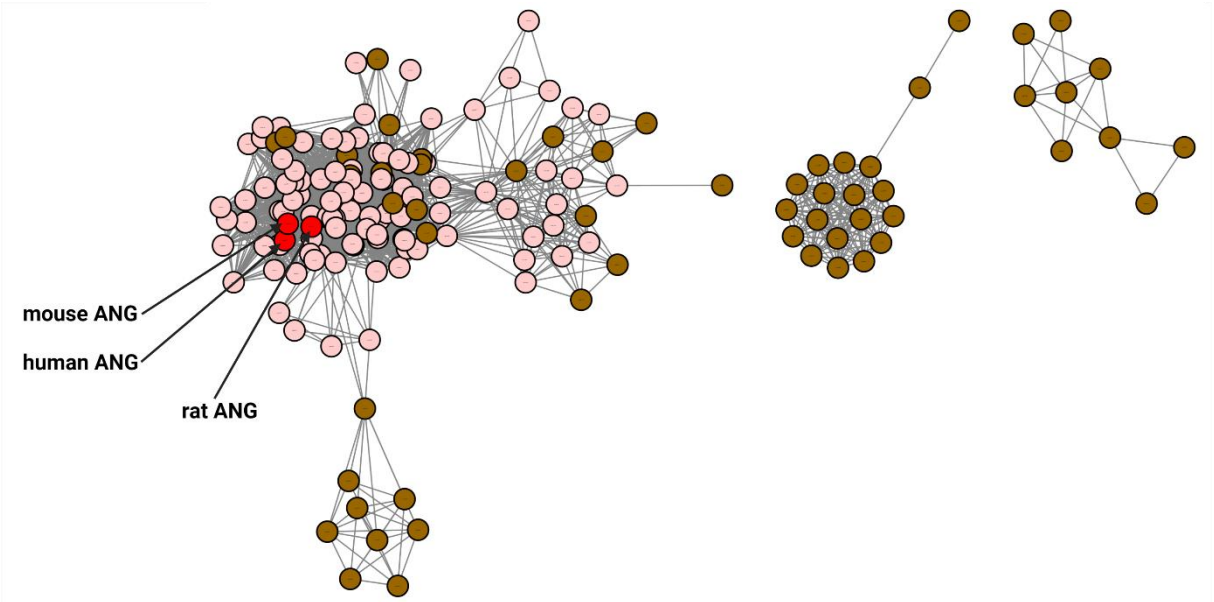

Figure 14. Sequence similarity network of ANG in various organisms. Clusters show similarities resulting in the same predicted function. Light red color implicates ANG in various organisms. Red color implicates human, mouse, and rat ANG labeled with arrows. Brown color indicates several other proteins.

Under normal circumstances, ANG is present as a monomer in the cell. However, some pancreatic RNase A superfamily members are also known to form domain-swapped dimers or larger oligomers [171–174]. This process results from a three-dimensional domain swapping (3D-DS) mechanism [175]. These dimers or oligomers have additional functions apart from the monomer [176]. However, the enzymatic function of ANG remains still active even with the dimer [174].

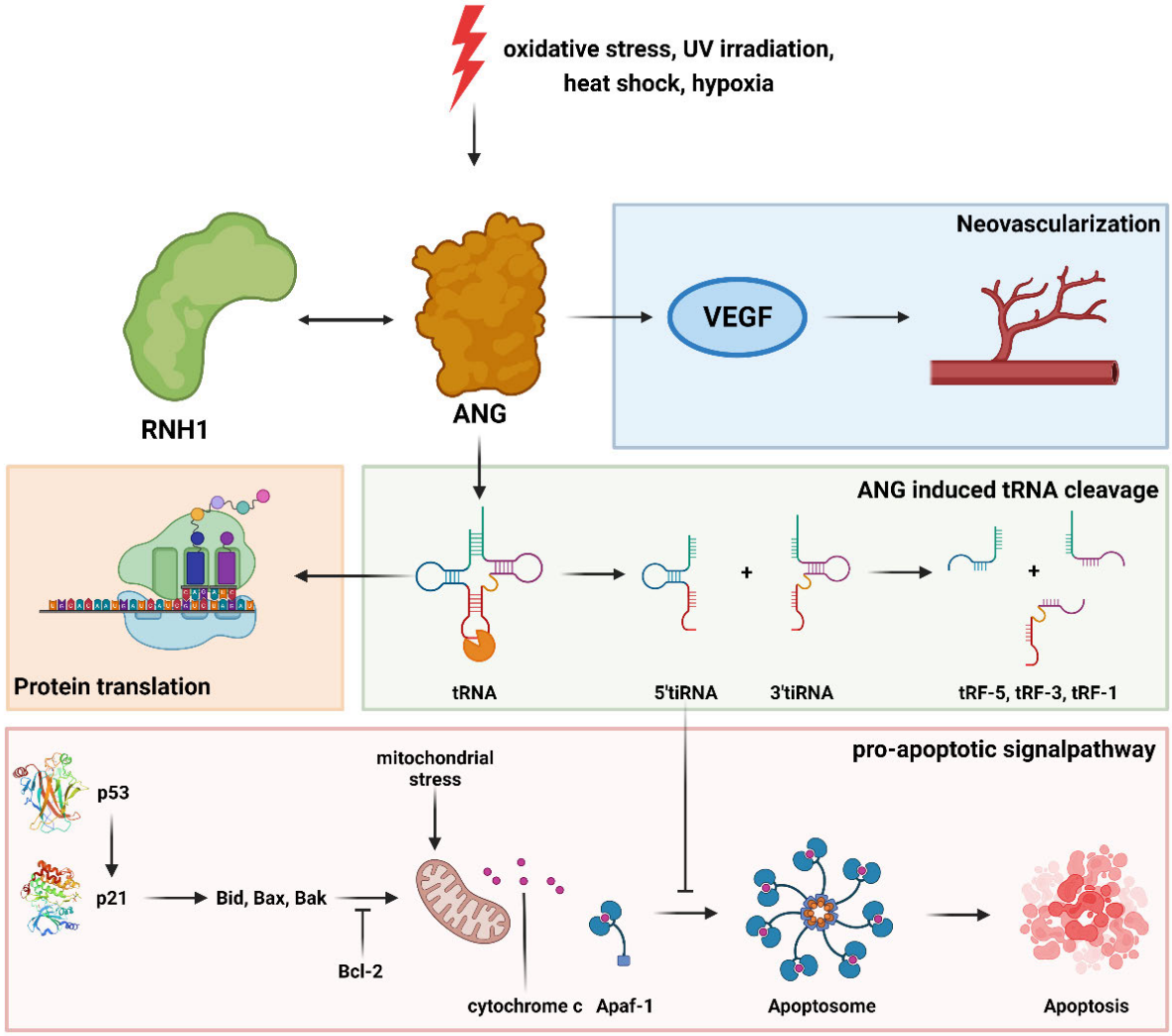

Figure 15. Cellular functions of human ANG.

In 2006, the Greenway group was able to identify seven different ANG variants that are directly related to the disease ALS, which leads to a loss of ribonuclease activity [177,178]. Subsequently, in a US study, additional ANG mutations were found to also lead to loss of function [179]. In 2011, ANG variants similar to those in ALS were also discovered in the neurodegenerative disease Parkinson's disease (PD) [180]. PD is characterized by progressive loss of dopaminergic neurons, mainly in the substantia nigra pars compacta [146]. Since PD is also a progressive neurodegenerative disease, it is reasonable to assume that there is also an alteration in the function or mutation of ANG in AD. Another change described in the studies was that some ANG variants inhibit the transport of ANG and the nucleus and destabilize the protein itself [146,178,179]. However, the ANG variants mainly showed an insufficient neuroprotective effect in many of these studies. Considering this finding, it is obvious that neurodegeneration

itself is enhanced in all neurodegenerative diseases due to the absence of this effect. A recent study has already detected ANG mutations in familial cases of AD [181]. Interestingly, ang1 knock-out mice do not develop neurodegeneration, demonstrating a link between ANG and neurodegeneration [182]. In summary, the data suggest that ANG has an important neuroprotective role in the CNS but is also critical in developing neurodegenerative diseases such as ALS, PD, or AD [146].

1.3. RNA and small non-coding RNAs (sncRNA) as novel and unique regulators of stress responses

1.3.1. General about RNA

Ribonucleic acids are small chains of nucleotides, similar to DNA but mostly single-stranded, which usually form polynucleotides, but there are exceptions in which short regions of complementary base pairs can form a so-called refold. Both have in common that the respective nucleobases are linked with ribose and phosphate residues. The individual organic bases of RNA are cytosine, guanine, adenine, and uracil, which replace thymine in DNA complementary to adenine. As already mentioned, ribose forms a nucleotide with a phosphate residue and the respective organic base. Ribose differs from DNA in that instead of a hydrogen atom, a hydroxyl group is present at the 2' position. This difference results in RNA being significantly more unstable than DNA since the hydroxyl group is more sensitive to hydrolysis [183,184]. Both secondary and tertiary structures can also occur in RNA. The most common secondary structures are hairpin and stem-loop structures. These loop structures are formed by intramolecular base pairing within the RNA. The presence of a tertiary structure is also possible, which is particularly important for tRNA since it can only fulfill its function through this structure [183,184]. The synthesis of RNA occurs during transcription by RNA polymerase (RNAP).

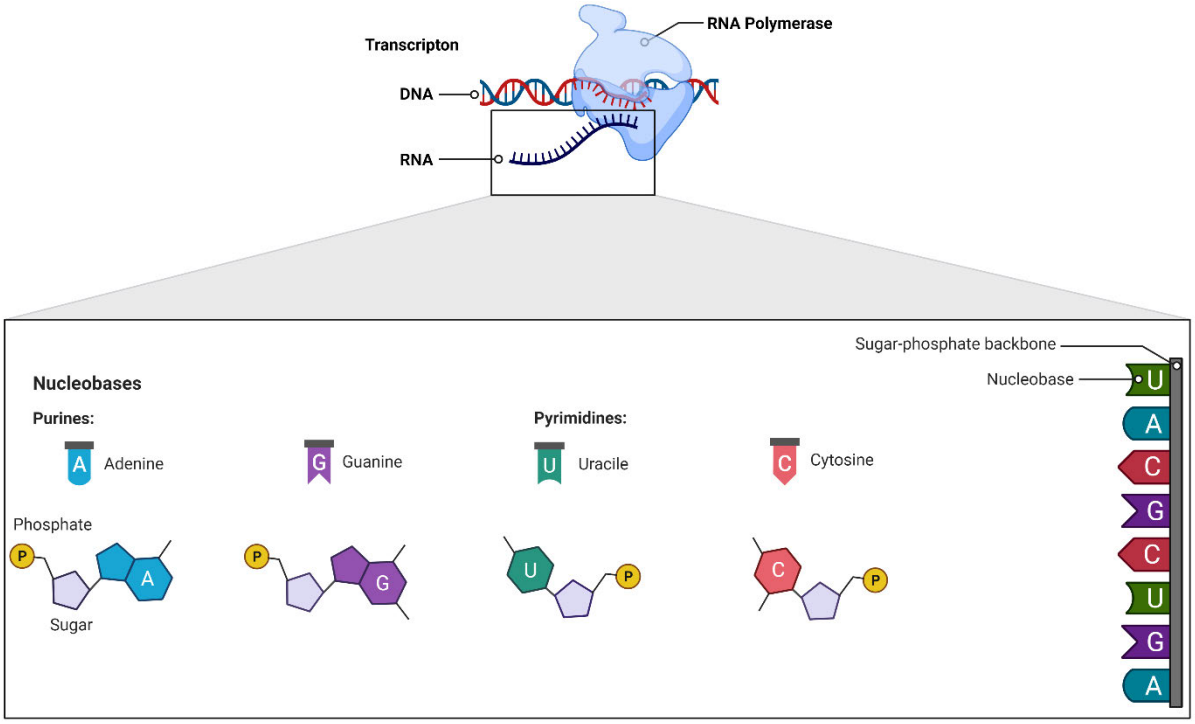

Figure 16. The general structure of RNA.

However, a preinitiation complex must first form, consisting of transcription factor IID (TFIID). TFIID is composed of TATA-binding protein (TBP) and TBP-associated factors (TAFs). TBP recognizes and binds to the TATA-binding box, whereas TAFs bind to promoters lacking the TATA-binding box [185]. Subsequently, TFIID is stabilized by another factor (TFIIA) at the promoter. To bind RNAP, TFIIB is now associated with the previously formed complex. Together with TFIIF, RNAP binds to the promoter sequence, and subsequently, TFIIE allows docking of TFIIH, which has helicase and protein kinase activity, so that the helicase can now unwind the DNA strand. The protein kinase activity of TFIIH phosphorylates specific regions, the carboxy-terminal domain (CTD), which leads to the disruption of the connection between the promoter and the preinitiation complex after synthesizing the mRNA [185,186]. Following this process, initiation begins by binding the DNA to the catalytically active site of RNAP. Now, nucleotides are successively incorporated with the cleavage of pyrophosphate, and the mRNA strand complementary to the DNA is synthesized [185–188]. After the insertion of four nucleotides, the complex detaches from the promoter due to ATP deficiency in the TFIIH subunit, and a 5' cap sequence is inserted to protect the RNA from degradation and mark it for splicing. From the eleventh nucleotide inserted, the elongation phase begins, during which RNAP synthesizes the mRNA strand

complementary to the DNA [185,186,189]. The RNA synthesis always takes place in the 5'→3' direction. A transcription terminator completes the synthesis.

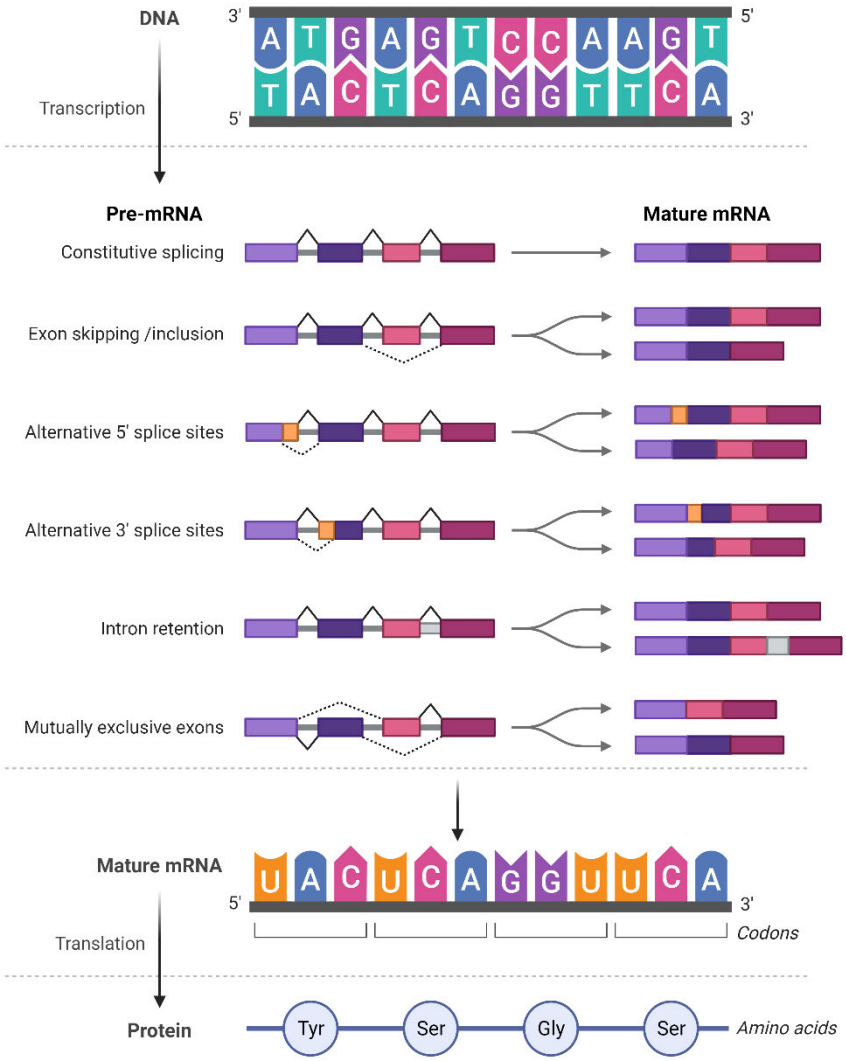

Figure 17. Processing of RNA.

In eukaryotes, this consists of an interplay between specific nucleotide sequences and various termination factors, although this mechanism is not yet fully understood [185]. The product resulting from transcription is a pre-mRNA containing non-coding regions (introns) and coding regions (exon). The splicing process removes the introns from the pre-mRNA, resulting in the final mRNA. Splicing can occur at the spliceosome, a large complex composed of RNA and proteins. Splicing also involves other important processes such as capping and tailing. Capping involves the addition of a 7-methylguanosine (m^7G) to the 5' end of the RNA strand, which stabilizes the RNA

during translation. During tailing, a 150-200 nucleotide long poly-A tail is inserted [190]. Another possibility of splicing is self-splicing and alternative splicing. In 1989, the Nobel Prize was awarded for discovering self-splicing, as it was seen that some RNA molecules could splice themselves. Accordingly, a distinction is made between group I and group II introns. Group I introns form a complex secondary structure consisting of 9 loops [190]. In contrast to group I introns, group II introns are located in mitochondrial genes. The splicing mechanism is strongly reminiscent of classical splicing of pre-mRNA, leading to the assumption that classical splicing evolved from it [190,191]. Alternative splicing was also discovered very early in an IgM gene [192]. In some cases, certain exons are skipped (exon skipping), or other splice sites are used [190–192]. This mechanism allows the synthesis of many proteins from just a single gene, thereby greatly increasing the variability of protein formation. Depending on the RNA's function, different RNA classes can be distinguished. The best known is the already mentioned mRNA, which is responsible for protein biosynthesis. In the following, some RNA types with their function are listed in tabular form:

Table 1. Classification of different RNA types with their respective function.

RNA	Abbreviation	Function
antisense-RNA	asRNA	Regulation of genexpression [193]
circular RNA	circRNA	Regulation of miRNA pathway [194]
heterogeneous nuclear RNA	hnRNA	precursor of mRNA (also called pre-mRNA) [195]
micro RNA	miRNA	Regulation of cellular processes, e.g., apoptosis [196]
ribosomal RNA	rRNA	Involved in ribosome assembly and catalytic effect in peptide bond formation [197]
small interfering RNA	siRNA	RNA interference [191]
small nuclear RNA	snRNA	Splicing activity [191]
long noncoding RNA	lncRNA	>200 nucleotides without regulatory function [198]
transfer RNA	tRNA	Translation [199]

Since new RNA is constantly being synthesized, RNases are used to degrade old RNA. The cleaved monomers can then be used for the synthesis of new RNA. The length of the poly-A tail at the 3' end is crucial here, as it is degraded further and further until the RNA is finally degraded [200].

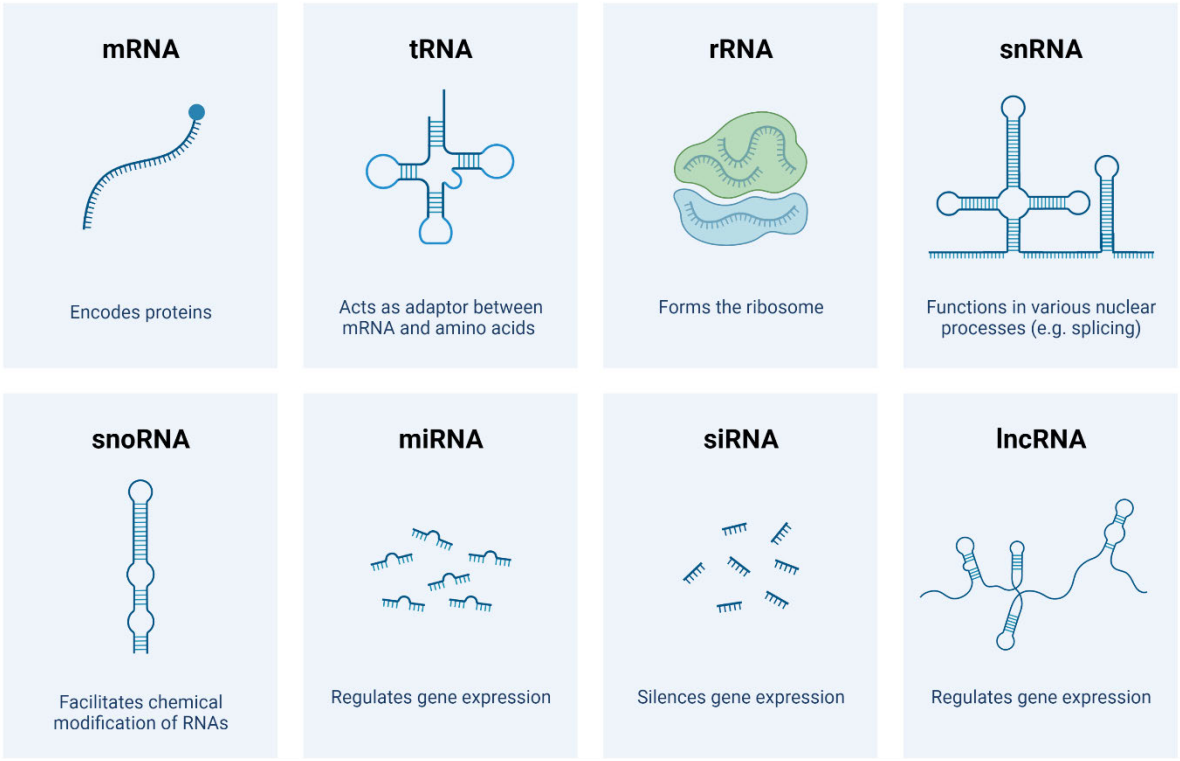

Figure 18. Various types of RNA synthesized in cells.

The development of new mRNA-based COVID-19 vaccines has given another enormous boost to the importance of RNA, especially in the media. This again highlights the importance of RNA research in understanding the pathogenesis as well as developing new therapies for the treatment of various diseases.

1.3.2. tRNA

Cellular functions and important signal pathways depend on numerous protein-coding and non-coding RNAs. Especially tRNAs are very important in different mechanisms in the human body. Mature tRNAs are noncoding RNAs consisting of 73-90 nucleotides (nt). They form a characteristic cloverleaf secondary structure, and “L” shaped tertiary structure [201,202]. The first structure was published in 1695 by Robert

Holley's research group at Cornell University in Ithaca, NY (USA). It was the structure of yeast tRNA, more precisely $tRNA^{ALA}$, which already contained modified nucleosides [202].

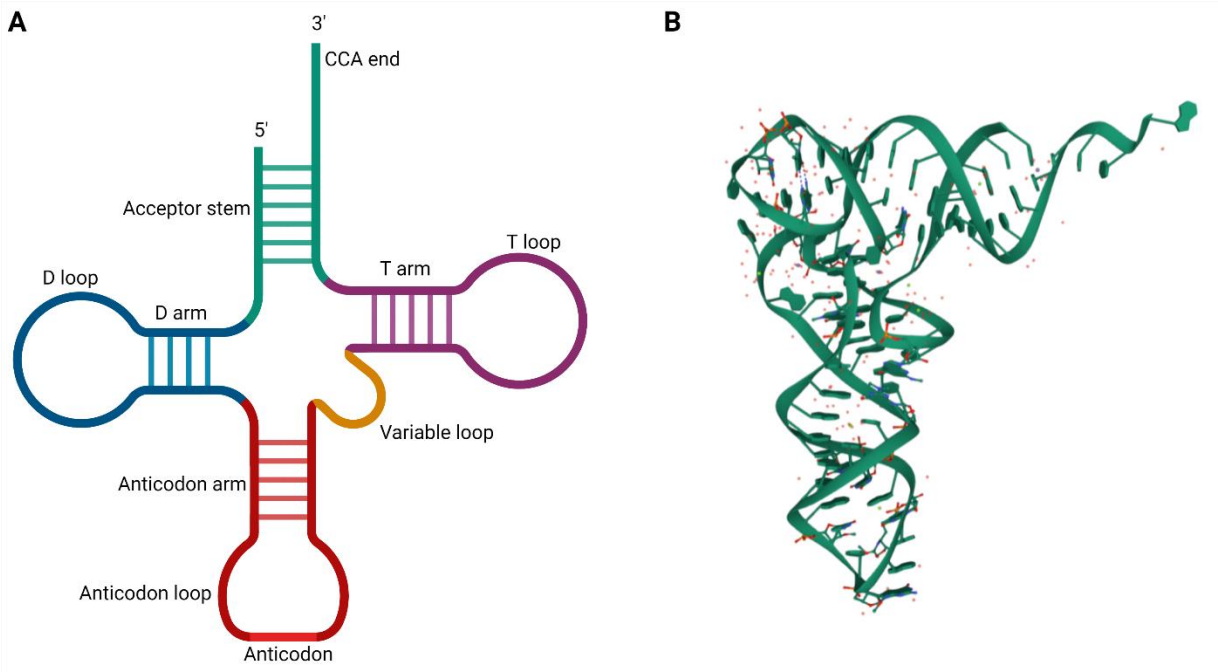

Figure 19. (A) The basic structure of tRNA. **(B)** Crystal structure of yeast phenylalanine tRNA at 1.93 Å resolution [203].

The characteristic cloverleaf secondary structure consists of an acceptor stem (includes 3' CCA tail), a thymidine (T) domain consisting of the T arm and the T loop, the variable (V) loop, the anticodon (AC) domain consisting of the AC arm and the AC loop, and a dihydrouridine (D) domain consisting of the D arm and the D loop [201]. Besides ribosomal RNA (rRNA), the most common non-coding RNA group is tRNA. The ratio here is ~80% to 4% [204,205].

The well-known function of tRNA is to transmit the correct amino acid to the corresponding codon of the mRNA during translation via the base triplet of its anticodon. Thus, they form an important interface between nucleic acids and proteins during ribosomal protein biosynthesis, e.g., they act as a type of adapter [206,207]. Each tRNA is loaded with an amino acid at its 3' end to fulfill this function. The related

aminoacyl-tRNA synthetase mediates this reaction. These enzymes represent a class that is further subdivided into two classes based on the different origins of the catalytic center [208]. Each tRNA has a so-called anticodon loop with the corresponding anticodon to bind to the mRNA. The anticodon consists of a trinucleotide sequence located at positions 34, 35, and 36. There is a complementary codon on the mRNA. The codon consists of 3 nucleobases complementary to an anticodon of the tRNA. As a result, the tRNA loaded with the corresponding amino acid binds precisely at a specific position on the mRNA, allowing specific proteins to be synthesized.

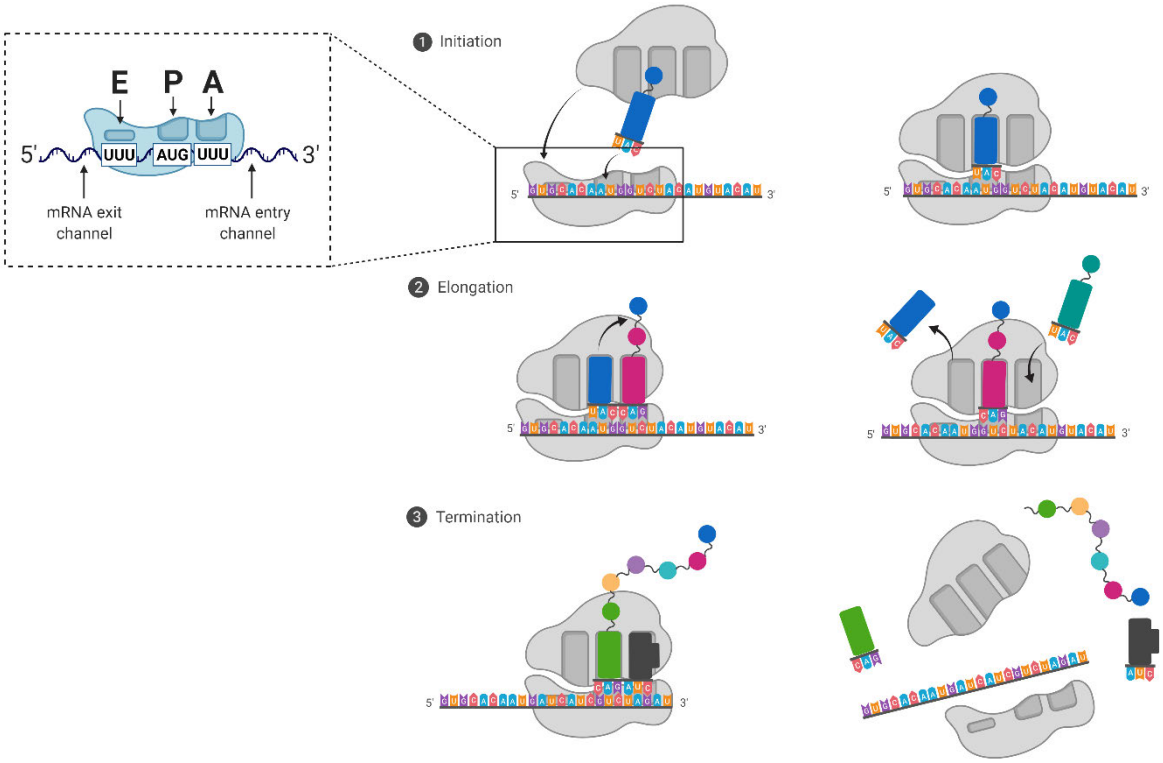

Figure 20. Process of translation at ribosomal complex regulated by tRNA.

The genetic triplet code provides for a total of 64 permutations for 20 amino acids plus stop codons. As a result of redundancy, several codon boxes correspond to identical amino acids [204]. In this case, a so-called isoacceptor tRNA decodes the codons in one box, while other isoacceptors are needed to decode the same amino acid in other boxes. Isoacceptor tRNAs are thus tRNAs that are chemically different but are acylated by the same amino acid. Due to the degeneracy of the genetic code, isoacceptor tRNAs are required [209,210]. The number of aminoacylated isoacceptor tRNA may

influence the rate of translation, which may influence protein folding [204,211,212]. If the isoacceptor tRNAs are subdivided once again, isodecoders are obtained. Isodecoder tRNAs have the same anticodon sequence but originate from different genes. The sequence outside the anticodon can also be altered, e.g., by point mutations [204,213]. This specificity depends primarily on aminoacyl-tRNA synthetase, e.g., on this enzyme loading the correct amino acid onto the 3' end of the tRNA. If this is not the case, an incorrect amino acid can be incorporated, which in turn can lead to misfolded or functionless proteins. In addition, the function of the proteins can change so that diseases such as cancer can develop [206,208].

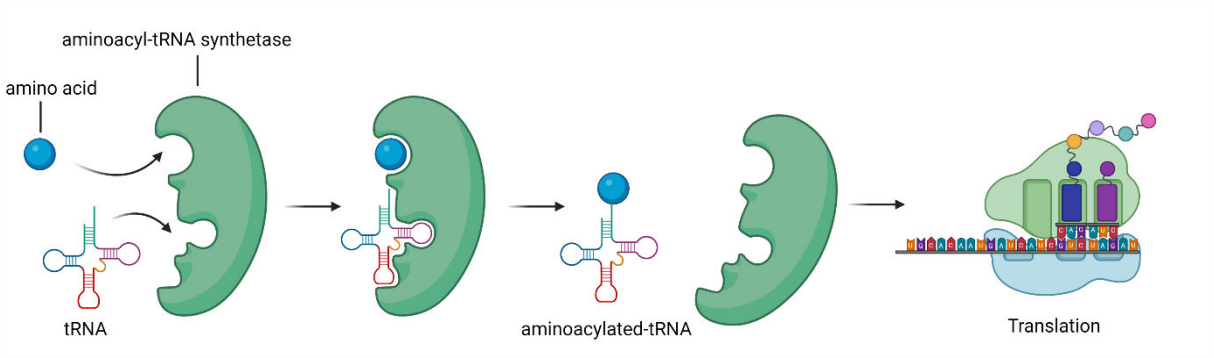

Figure 21. Aminoacylation of tRNA.

However, tRNAs are also important in some other processes, such as cellular signaling pathways, stress response, or regulation of apoptosis. In order to fulfill its functions, a tRNA must first undergo various aging processes. The tRNA and other non-coding RNAs genes are transcribed in eukaryotes by polymerase III. This produces a polycistronic transcript further processed by various nucleases [204,214,215]. Polycistronic transcriptome refers to mRNA segments encoded by multiple consecutive genes on the DNA [216]. In the first step of tRNA maturation, the 5'-leader sequence of the precursor tRNA is removed by the endonuclease RNase P. The 5'-leader sequence of the precursor tRNA is removed by the RNase Z enzyme. In parallel, removing the 3'-pendant sequence by the enzyme RNase Z matures the 3'-end. In addition, a non-templated CCA tail is removed by the nucleotidyltransferase CCase [215,217–219]. Some eukaryotic and archeal tRNA precursors contain introns spliced during aging by specific tRNA splicing enzymes. There is no correlation between tRNA splicing and mRNA splicing [204,220].

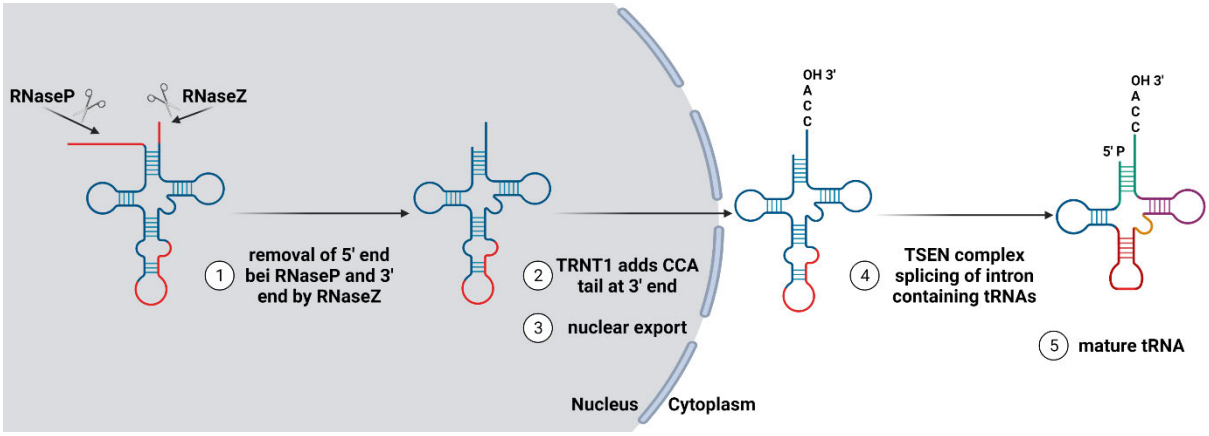

Figure 22. The maturation process of tRNA.

There are about 500 tRNA genes in the human genome, decoding 61 codons. About 50% of the human tRNA genes contribute to less than 1% of their respective isodecor pools [204,221]. Variations in isodecoder tRNA gene expression have little effect on mature tRNA content but are involved in regulating tRNA-derived fragments [222].

1.3.3. tRNA derived fragments in stress response and neurodegeneration

Research efforts have largely focused on microRNA (miRNA), a unique class of small, non-coding RNA (sncRNA) that post-transcriptionally regulate gene expression. They do this by binding to their target mRNAs' untranslated region (3'-UTR). Interestingly, more recently, it emerged that fragments derived from transfer RNAs (tsRNA) constitute a new class of small, non-coding RNA that play a crucial role in the regulation and resolution of cellular stress responses. The tsRNA can be divided into two subgroups: on the one hand, tRNA-derived stress-induced RNA halves (tiRNA) and, on the other hand, even smaller fragments, named tRFs [204,223]. tRNA can inhibit apoptosis by binding to released, cytotoxic mitochondrial protein cytochrome c. This binding suppresses downstream signal transduction cascades and cell death [168,204]. Furthermore, oxidative stress, heat shock, UV radiation, hypoxia, and starvation trigger the formation of tiRNAs or tRFs [168,204,224–228]. tiRNAs are formed by ANG-induced cleavage of mature tRNA. ANG cleaves in the region of the anticodon loop, resulting in two halves of the tRNA, each 31-40 nt long [229]. The resulting halves are further divided into 5'- and 3'-tiRNAs, depending on whether the anticodon loop has a 3'- or 5'-end [204]. The difference between normal tRNAs and tiRNAs is, first, the size of the molecules, and second, the different binding capacity to mitochondrial released

cytochrome c. tiRNAs bind to cytochrome c more strongly than normal tRNAs. The cleavage of the tRNAs is induced by ribonuclease ANG, which is released due to oxidative stress. As a result of stress, ANG translocates from the nucleus to the cytoplasm and dissociates from RNH1 resulting in the cleavage of cytoplasmic tRNAs into tiRNAs. These then bind to mitochondrially released cytochrome c, inhibiting apoptosis [204,229]. However, by inhibiting the translation initiation factor eIF4F, tiRNAs inhibit protein translation and regulate stem cell differentiation. Under physiological conditions, tiRNAs protect cells against stress-induced apoptosis and thus may have an important role in the response of cells to stress conditions [204]. tRFs have a length of 14-30 nt and are thus significantly smaller than tiRNAs. Depending on the site where the tRNA or tiRNA is cut, different tRFs with different lengths are produced. A first rough subdivision results in a total of three subclasses: 3'U tRFs (tRF-1), 3' CCA tRFs (tRF-3) and 5' tRFs (tRF-5) [204,230,231]. These much smaller fragments are formed by the further degradation of tRNA or tiRNA by the enzymes ANG, Dicer, or others in the RNase superfamily. Dicer is an RNase III family enzyme whose best-known function is to initiate the RNA interference (RNAi) pathway and degrade long double-stranded RNA (dsRNA) into short dsRNA molecules. In addition, Dicer can also degrade various other RNAs, including tRNAs. Typical of Dicer-induced degradation is that the size of the resulting products is in the range of ~20-30 nt [230]. tRF-1 is initially formed by another enzyme, RNase Z, also known as tRNA-3' endonuclease ELAC2. tRF-5 are formed by degradation in the D-loop region by RNaseP. tRF-3 are formed by degradation in the T-loop region [204,230,231Both tRF-5 and tRF-3 have a 5'-phosphate and a 3'-hydroxyl end and can both be cleaved by the Dicer protein complex [228,230,232–235]. In particular, tRF-3, produced by the cleavage of $tRNA^{(Gln)}$, depends on Dicer [230,232,233]. Recent studies have shown that tRF, which derives from $tRNA^{(Gln)}$, performs functions similar to miRNA [228]. According to current scientific knowledge, tRFs are involved in regulating gene expression and protein translation and therefore play an important role, especially in the development of disease. Recent studies show an important involvement of tRFs in cancer development [204,228,236–238].

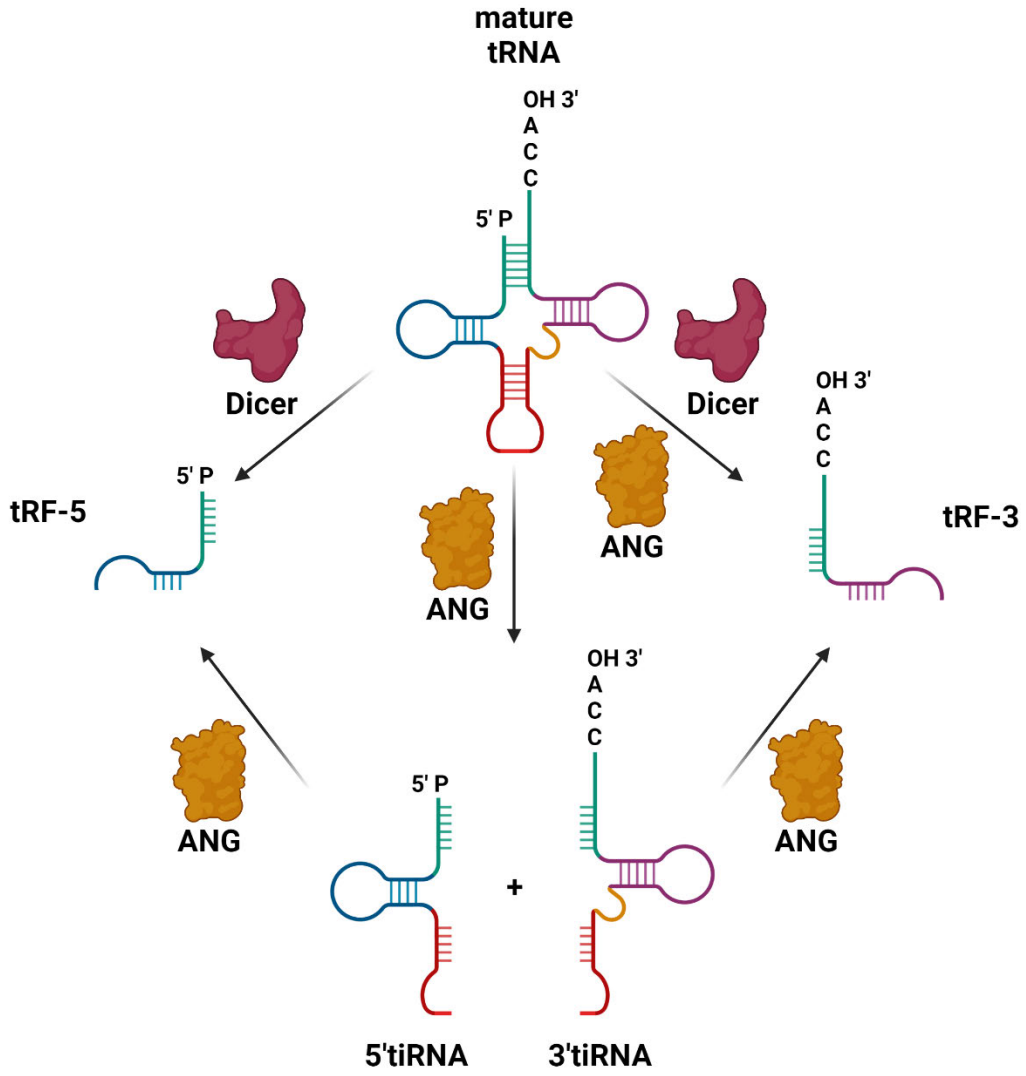

Figure 23. ANG induced cleavage of tRNA.

There is strong evidence that tsRNA production is an important component in healthy and diseased nervous systems [239]. Some studies show that tsRNA is actively secreted by neurons and other cell types [204,240,241]. In a study by *Hogg et al. 2020*, basal release of tiRNAs in human SH-SY5Y neuroblastoma cells was shown to be dependent on secretion into extracellular vesicles [242]. However, the final mechanism of the release of tsRNAs has not been precisely elucidated. The individual functions of tsRNAs are also extremely diverse. In addition to the already explained inhibition of apoptosis, they range from the regulation of translation and gene expression to the control of inflammatory processes [204]. It is also known that tsRNA can inhibit protein translation. Specific tiRNAs resulting from stress-induced ANG degradation have been shown to inhibit protein translation independently of phosphorylation of eukaryotic

translation initiation factor 2a (eIF2a) [229]. Specific 5'-tiRNAs containing a terminal oligoguanine (TOG) are required, e.g., 5'tiRNA^{Ala} or 5'-tiRNA^{Cys}. These tiRNAs can form a G-quadruplex (G4). This complex then binds to the HEAT domain of eIF4G and impairs scanning of the 40S ribosome. This mechanism triggers a translational arrest, and the formation of SGs immediately follows [204,227,243–246]. This mechanism is thought to protect the integrity of the polyribosome complex and thus also promote neuron survival [243,246,247]. Another role is attributed to tsRNA in the regulation of gene expression. Certain tRFs have been shown to interact with human Argonaute proteins (AGO1-4). AGOs are involved in many critical cellular processes and may also mediate gene silencing [248]. In addition, they are important proteins of the RNA-induced silencing complex [204,228]. Human AGO1-4 are structurally very similar. The best described of these proteins is Ago2, as it is the only protein in its family with mRNA slicing activity [249,250]. However, tsRNAs can regulate gene expression even without interaction with AGO. One study showed that inhibition of tRF-5c by Gly-GCC leads to a significant change in gene regulation in embryonic stem cells [204,238]. One of the most important roles is the control mentioned above of the apoptotic cascade by tiRNAs. tiRNAs can inhibit the pro-apoptotic signaling cascade [204]. A stress stimulus, such as oxidative stress or heat shock, leads to increased expression of ANG. This cleaves tRNAs at the anticodon site (positions 34-37), resulting in 5'- and 3'-tiRNAs. 5'-tiRNAs can interact with cytochrome c by forming a ribonucleoprotein complex [168,229]. This inhibits the formation of apoptosis and the subsequently connected caspase 3 and thus protects the cell. The protective effect thus mediated by ANG has also been observed in several studies [245,251,252]. It is suggested that tsRNAs are also involved in inflammatory responses, as the concentration of tRF-5 in human monocytes was significantly increased after inflammation [253]. Initial studies have shown that certain tsRNAs can interact with Toll-like receptors, which are important for antigen recognition. This interaction triggers a powerful inflammatory response from T helper cells and cytotoxic T cells [204,254].

1.3.4. Role of tiRNA in the generation of stress granules

Another important function is the impact of tiRNAs on SG formation. SGs belong to the family of RNA granules and play a crucial role in processes such as mRNA metabolism and the control of translation. They are also associated with many diseases such as cancer and neurodegeneration [255–259]. SGs average 200-400 nm in

size but range from 100 nm to 1,000 nm depending on stress conditions. Typically, SGs contain polyadenylated mRNAs, poly(A)-binding protein (PABP) and intracellular T cell antigen 1 (TIA1) [255,260,261]. The formation of these SGs is critically dependent on the phosphorylation of the α subunit of eIF2a. This fact allowed the first correlation between the function of SGs and mRNA translation [261]. In addition, it is now known that the main components of SGs are messenger RNP complexes (RNP), mRNAs, and associated translation initiation factors. SGs thus contain all the information required for the synthesis of proteins necessary for the cell's survival under stress conditions [255,262,263]. In SGs, there are important mRNPs that contain untranslated transcripts, which then form so-called SG nuclei to form new SG nucleators and thus further SGs [262,264]. However, the most important property of SGs is their dynamism to respond quickly to stressful conditions and regress quickly when the stress is removed [255]. There must always be an equilibrium of SGs between the cytosol and the cell nucleus to ensure this dynamic. Individual proteins then serve as a transporter to transport the SGs from the nucleus to the cytosol or back again. If this balance is no longer present, the degradation of SGs can be disturbed so that they accumulate and develop pathological effects [255]. The assembly of SGs first begins with the perception of cellular stress. Then, translational arrest is triggered, followed by phosphorylation of eIF2a [264]. However, the formation of SGs is not exclusively dependent on eIF2a, in which case 5'-tiRNA acts as a mediator for the formation of SGs [227]. 5'-tiRNA^{Ala} initiates the packing of stalled translational complexes in SGs by binding to Y-box binding protein 1 (YBX-1) [247]. The same mechanism has already been demonstrated in PC-12 cells under oxidative stress [204,225]. Another important regulator of SGs is the mammalian target of rapamycin (mTOR). mTOR has various functions, e.g., cell metabolism regulator [255,265–267]. Under stress conditions, mTOR is inactivated, leading to the formation of the eIF4E-4E-BP complex. This association leads to the formation of RBPs and ultimately to the synthesis of SGs [255,265–268]. Another important checkpoint is represented by GTP, the initiator methionine tRNA (tRNAi^{Met}), and the ternary complex with eIF2 [255,269]. Upon stress, eIF2a kinases are activated in response. These kinases play a key role in the stress response by participating in a system that monitors intracellular and extracellular signals to regulate cellular translation [270]. In total, four different eIF2a kinases can be activated by different forms of stress: general controllable non-compressible kinase 2 (GCN2), PKR-like ER kinase (PERK), protein kinase R (PKR), and heme-regulated eIF2a-kinase (HRI). GCN2 has

the main function of monitoring the level of charged tRNAs and nutrient stress; PERK is responsible for the level of unfolded proteins and ER stress; PKR monitors the presence of viral RNA, and HRI permanently checks the presence of heme [255,271–274]. As a result of activating one of the above kinases, charged $tRNAi^{Met}$ are attached to untranslated mRNAs. This attachment and accumulation of untranslated mRNA then lead to the formation of SGs [255,270,275]. In this context, the cascade via eIF4 has been considered as one of the potentially most important possible pathways for the development of SGs in neurodegenerative diseases because it is known that the RNA helicase eIF4A, the initiation factor eIF4B, and eIF4E can form protein interactions with tau and the TAR DNA-binding protein 43 (TDP43) [255,276–279].

Another important point is that the biology of SG in neurons is different from that in dividing cells. Cells respond much faster to stress than neurons do [260]. However, the life cycle of SG is also of particular importance for the development of diseases. Under normal, healthy conditions, this can be divided into 5 phases. Phase 1 represents the basal level, e.g., the initial state. In this phase, all proteins involved in SG formation (e.g., RBPs, TIA1, TDP43) perform their normal function in the nucleus or cytoplasm. In phase 2, nuclear RBPs are translocated from the nucleus to the cytoplasm subsequently disperse. Next is SG nucleation (phase 3), in which nucleated TBPS (e.g., TIA1, G3BP1) assemble to form a SG. The maturation of the SG takes place in phase 4. In this step, secondary RBPs (RBPs that are not essential for the first step of SG formation) are incorporated into the SG. An example of a secondary RBP is ataxin 2 (ATXN2). After phase 4, SGs can now fully fulfill their function. Phase 5 then initiates the degradation of the SG, including transporting soluble RBPs back into the nucleus to restore the basal stage [255,280–283]. However, SG accumulation occurs if this particular phase 5 is disturbed or altered. The SGs formed in response to an acute stress state are now no longer transported back to the nucleus, accumulating in the cytoplasm. The persistent SGs can now aggregate into larger aggregates and form pathological SGs that promote a chronic stress state. In these pathological SGs, proteins such as TDP43, which already play a role in neurodegenerative diseases, are now much more abundant. This disturbs the balance between the baseline state and the acute stress response because there is no longer any reverse transport [255,282,283]. For this reason, RBPs can also be divided into normal RBPs exclusively involved in the acute stress response (e.g., TIA1) and RBPs that play a role in both the acute and

chronic pathological stress response [255]. One approach explaining why SGs are no longer dispersed is to hypothesize TDP43 forming insoluble gels. In an acute stress situation, TDP43, like several other RBPs, translocates from the nucleus to the cytoplasm to participate in the formation of SGs. With increasing stress, the dynamics of SGs and TDP43 decrease, leading to the formation of non-liquid gels [255,284,285]. In addition, phosphorylated TDP43 can interact with other SGs and form larger SG aggregates in the cytoplasm [255,284,285]. The TDP43 aggregates formed can inhibit, e.g., splicing [286]. An interaction with tau is also very likely, as several studies have shown that tau aggregates colocalize with SG RBPs [276,287]. It is also known that tau interacts strongly with mRNA, a main component of SGs. mRNA can modulate the folding pathways of tau [288]. The detailed mechanism behind this reaction is still unclear [289,290]. Recent studies have shown that tau undergoes a process of liquid-liquid phase separation (LLPS). The same mechanism could also be observed in RBPs. Interestingly, this process is significantly enhanced and intensified in the presence of RNA [291]. Tau needs both RBPs and RNA to enter this process. Studies have shown that tau cannot interact with SGs without the presence of either component [276,292,293].

However, other signaling pathways can also lead to the development of neurodegenerative diseases associated with SGs. In particular, activation of the immune system in the form of inflammation is known to play a role in neurodegenerative diseases. It has been shown that deletion of RBP TIA1 leads to an extremely potent release of cytokines from immune cells. This particularly affects the cytokine tumor necrosis factor (TNF) [294,295]. In summary, the literature suggests an RBP cascade hypothesis [255]. This hypothesis states that the disease mechanisms leading to neurodegeneration associated with RBPs are due to a biochemical pathway divided into three levels. The first level includes all extracellular factors that have neurodegenerative properties, such as increased levels of oligomeric Aβ. The second or middle level is the intracellular toxic mediators, hyperphosphorylated tau and TDP43. Thus, these proteins mediate the effects previously induced at level 1. The third and lowest level of this central cascade comprises the RBPs. These mediate the translational stress responses triggered at the previous levels and initiate the formation of SGs. In the final stage of maturation, the involvement of a huge number of RBPs occurs. If mutations now occur in the RBP genes, this leads to neurodegenerative

diseases such as ALS. These persistent stress factors lead to a chronification and persistence of SGs, which in turn amplify the pathophysiology of neurodegenerative diseases and interact, for example, with TDP43 and tau [255,296–302].

1.3.5. tRNA fragments in aging and neurodegenerative diseases

Since aging itself is one of the most important risk factors for developing neurodegenerative diseases that cannot be circumvented, the study of the alteration of tsRNAs during this very process is an important topic. Initial studies have demonstrated an age-dependent change in the expression of 5'-tiRNA in mouse serum. Also, the respective levels of the different 5'-tiRNAs were either increased or decreased at different stages of aging [204,303,304]. There are also initial starting points for research into neurodegenerative diseases. In 2006, the Greenway group was able to identify seven different ANG variants that are directly related to the disease ALS, which leads to a loss of ribonuclease activity [177,178]. Subsequently, in a US study, additional ANG mutations were found to also lead to loss of function [179]. In 2011, ANG variants similar to those in ALS were also discovered in the neurodegenerative disease Parkinson's disease (PD) [180]. Since almost all of these mutations result in a loss of ribonuclease activity of ANG, it suggests that the resulting stress response is also impaired [204]. Thus, the absence of 5'-tiRNAs would abolish the inhibitory effect on the pro-apoptotic signaling cascade, including inhibition of caspase 3 activity and the neuroprotective function of ANG per se. Since an alteration has already been demonstrated in ALS and PD, it is evident that both ANG and tsRNA play an important role in developing neurodegenerative diseases [180,204].

1.3.6. RNA modifications

In addition, tRNA modifications play a crucial role in RNA function and stability. So far, 170 different RNA modifications have been discovered, such as adenosine and cytosine methylation such as m^1A, m^6A, m^5C, and ms^2i^6A or ribose methylation or pseudouridine incooperation. The m^1A adenosine methylation is particularly common in tRNA [305]. The majority of all RNA modifications are present on tRNAs. In general, tRNA modifications are simple chemical changes at individual bases. The most common modification is methylation [306]. These changes in tRNA are thought to improve biochemical and biophysical stability and the scaffold of tRNA [307,308]. The

absence of some essential tRNA modifications reduces structural stability, which in eukaryotes is monitored by at least two independent signaling or degradation pathways [204,309–311]. In these cases, the sum of collective stabilizing modifications has a protective effect of preventing tRNA degradation. Individual modifications can also prevent degradation by specific tRNases [312]. A unique example, which will also play a role in the other part of this work, is the methylation of cytidine, which leads to the modification m^5C. m^5C is located at positions 47, 48, 49, or 50 of matured tRNAs, preventing ANG-mediated degradation. This is possible because m^5C is located near or at the cleavage site of the tRNA for ANG [169,313]. m^5C is also an optimal example to illustrate the influence of RNA modifications on the formation of tsRNA. Other ribose methylations such as Am, Cm, Gm, and Um are also thought to play a role under stress conditions. These modifications may directly affect the catalytic mechanism of RNase and are therefore also considered as possible candidates for influencing the biogenesis of tRNA fragments [204,312]. In the context of this work, this regulatory effect of RNA modifications on tRNA cleavage is of particular importance.

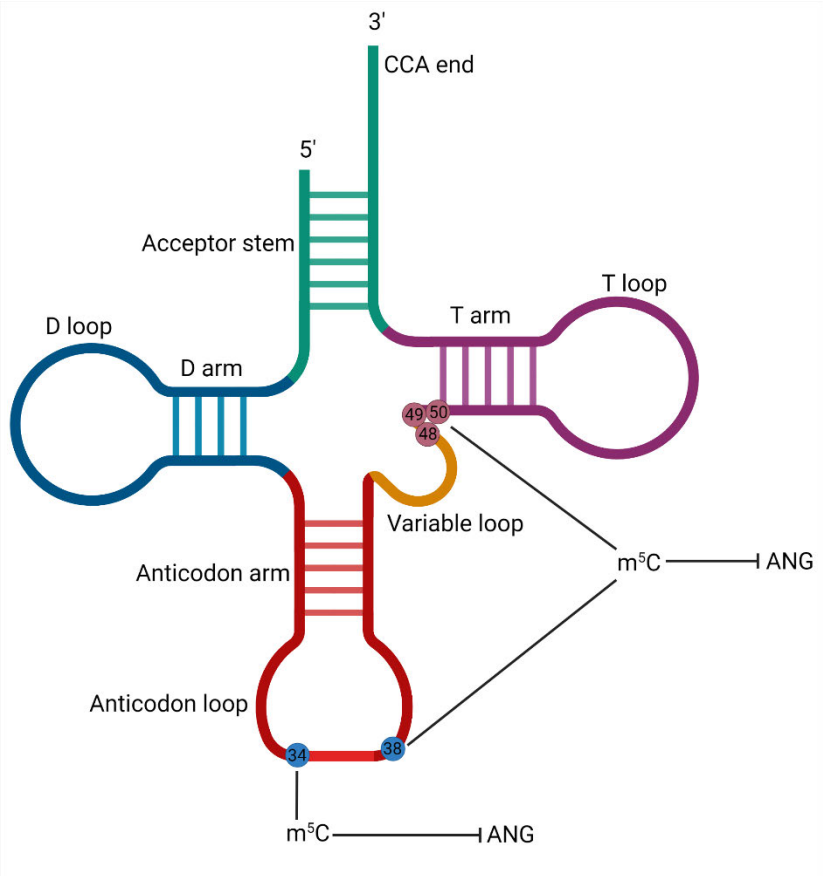

Figure 24. Position and function of m^5C in human tRNA.

Modifications can also occur in the anticodon region. These occur mainly at positions 34 and 37, which are also responsible for the accuracy and speed of mRNA decoding [169,204,313]. It has been shown that these modifications are generated by many serial enzymatic conversion steps and are usually very bulky [204,314,315]. Recent research results have shown that an increased number of mutations can be found in the genes for human tRNA-modifying enzymes. It could be shown that such mutations often lead to diseases mainly affecting the CNS [314,316–322]. In terms of the proportion of genes responsible for RNA modifications in the human genome, genes encoding enzymes for human tRNA modifications account for a total of 2% of the human genome [314]. The epitranscriptome is characterized by more than a hundred chemical marks on cellular RNA to regulate the transcripts' activities. There are molecules called readers to recognize these RNA modifications at specific transcript regions. These reactions are catalyzed by effectors that can deposit and remove these modifications. This group of proteins is collectively known as RNA-modifying proteins (RMPs) and is further subdivided into three distinct groups: “writers”, “readers”, and “erasers”. "Writers" are enzymes that chemically label RNA; “erasers” remove them again; and “readers” selectively recognize and bind to certain specific chemical RNA modifications leading to producing a cellular response. An example of this represents Cdk5 regulatory subunit-associated protein 1 (CDK5RAP1). The “writer” of ms^2i^6A is known as a tRNA-specific modification that regulates efficient mitochondrial translation and energy metabolism. CDK5RAP1 is also linked to human diseases, especially AD and breast cancer. In general, these proteins modulate RNA metabolism and functions, affecting cell fate and cell differentiation. The insertion of an RNA modification by one of these enzymes affects RNA metabolism, including RNA processing, splicing, polyadenylation, editing, structure, stability, localization, translation initiation, and gene expression [323]. RNA modifications represent a code that can be altered by stress during aging and neurodegeneration. In summary, it is clear how important RNA research is for further research into diseases and the development of new drugs to treat them.

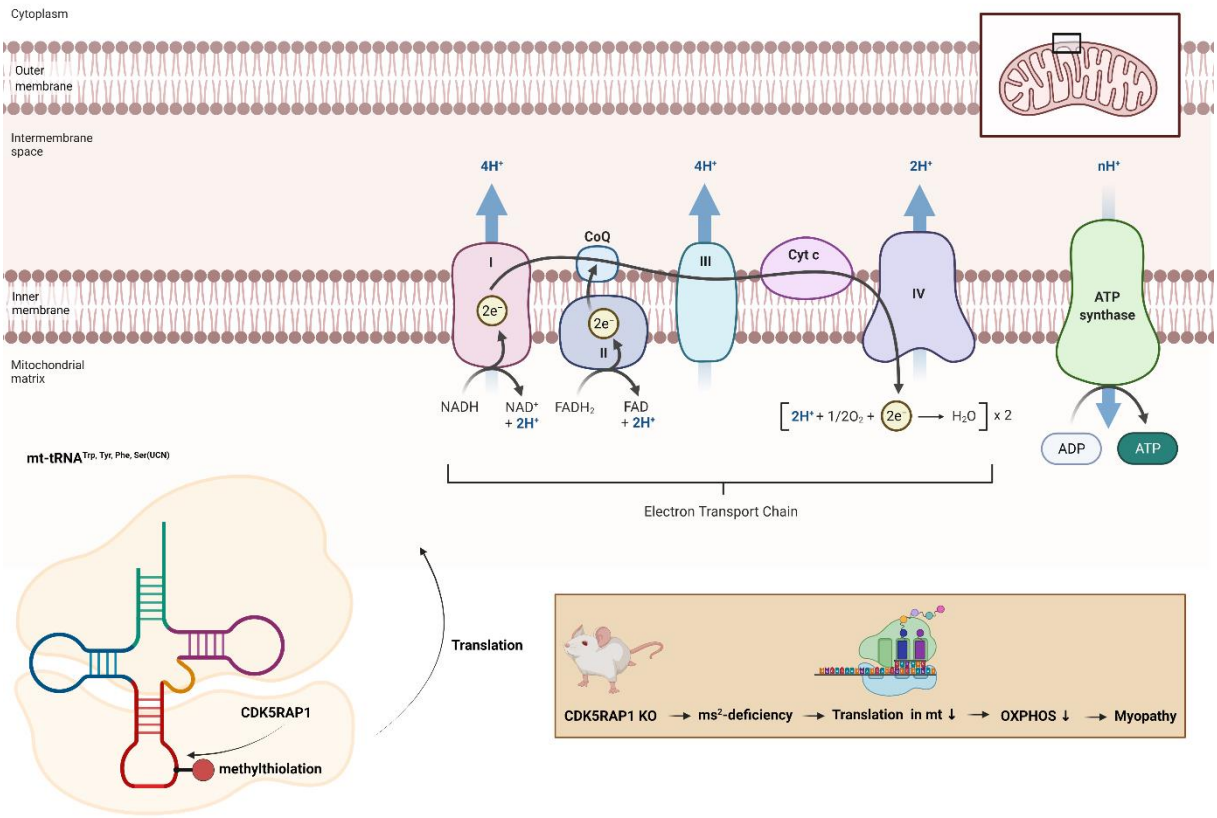

Figure 25. Effect of RNA modification writer CDK5RAP1 on cellular function.

1.4. Objectives of this scientific work

Even about 120 years after Alois Alzheimer and Auguste Deter were the starting point in the discovery and the beginning of AD treatment and research, there is still no exact pathophysiology and therapy available. As mentioned above, it was assumed that Aβ was the main cause of AD for many years. However, the ate alone hypothesis was quickly disproved by clinical trials attempting to reduce levels and plaques of toxic ate, which failed. It is, therefore, all the more surprising that the first anti-Aβ antibody, aducanumab® 2021, was approved by the FDA in the USA. However, here, there is some controversy about the study situation, which is why the EMA refused to approve the drug due to the unclear data on its efficacy [133,324,325]. Because of this failure, it quickly became clear that there must be other factors contributing to the development of AD. An important milestone was the establishment of the mitochondrial cascade hypothesis by *Swerdlow et al.* in 2004 [110,129,130]. In this hypothesis, the presence of mitochondrial dysfunction, including the generation of ROS and the resulting damaging effects on other mitochondria and neurons, was postulated for the first time. Based on this consideration, another important risk factor for the development of mitochondrial

dysfunction and thus AD came to the fore, namely aging itself. Various effects characterize the aging process, but first and foremost by a disturbed DNA repair system and the development of mitochondrial dysfunction. For this reason, the focus of research is no longer on Aβ or tau alone but rather on new approaches that can provide a further step toward effective therapy or causal research. The protein ANG provides a completely new approach in this field, as first alterations have already been discovered in other neurodegenerative diseases such as PD and ALS [146,180,245,326–329]. However, there is still no study exploring the expression of ANG during aging and AD. For this reason, this work determined the expression of ANG in central tissues such as the brain and peripheral tissues. Peripheral tissues are of particular importance, as studies have shown that central tissues and peripheral tissues show alterations in AD [330–337]. This question will be addressed in detail in this work. Due to the tRNA degradative function of ANG, the focus is also on tRNA modifications that act as regulators of ANG-induced degradation. Especially due to the development of mRNA vaccines against COVID-19, the research field of RNA has gained special attention. More and more causes of diseases can be traced back to changes in RNA. Again, little to nothing is known in the field of neurodegeneration, as studies have largely focused on PD and ALS. For this reason, this work additionally investigated tRNA modifications and RNA modifications of the resulting fragments in relation to the process of aging and the development of AD to provide a completely new approach in the study of the development of AD.

In summary, the objectives of this scientific work are as follows:

1. determination of the expression of ANG in different cell models
2. determination of the expression of ANG in different central and peripheral tissues in animal models as well as in human postmortem samples in order to investigate age-dependent and AD-specific effects
3. determination of tRNA modifications in cellular and animal models to investigate age-dependent and AD-specific effects.

Chapter 2

2. Material and Methods

2.1. Materials

2.1.1. Consumable and Instruments

Table 2. Consumables and Instruments

Name	Manufacturer
µ-Dish 35 mm, high Glass Bottom	Ibidi
10 mL Gilson-Style Graduated Macro Tip	Starlab
96-Well-Plate (black)	Greiner bio-one
96-Well-plate (white)	Corning
ACCU-Jet Pro	Brand
AG245 Analytic Balance	Mettler Toledo
Agilent 1260 Infinity	Agilent Santa Clara, CA, USA
Agilent 6460 Triple Quadrupole mass detection system	Agilent, Santa Clara, CA, USA
Autoclave	Fedegari Autoclavi
Biowave S2100 UV/Vis Diode Array Spectrophotometer	WPA
Buffer Tank and Lid	Bio-Rad Laboratories Inc.
Cell scraper 28 cm	Greiner Bio One
CELLSTAR® Cell Culture Dishes (60/15 mm, 100/20 mm)	Greiner Bio One
CELLSTAR® Tubes (15 mL, 50 mL)	Greiner Bio One
Centrifuge Function line	Heraeus Instruments
Centrifuge Mini Star silverline	VWR
Centrifuge Universal 320R	Hettich Centrifuges
Coulter Counter	Beckman Coulter
Cryo-Vial 2 mL	Thermo Fisher Scientific

Cytometer according to Neubauer Marienfeld	Lauda-Königshofen
Digital dual timer C5080	TFA Dostmann
Direct-Q® 3UV	Merck Millipore
drying chamber Hotmaker 2000	Heraeus Instruments
Duran Bottles (2 L, 1 L, 500 mL, 250 mL, 100 mL)	Schott
EZ-Vac Vacuum Manifold	Zymo Research
Falcon Tube 50 mL, 15 mL	Greiner bio-one
Fiber Pads	Bio-Rad Laboratories Inc.
FlexStation 3	Molecular Devices
Fom/B50 Autoclave	Fedegari Autoclavi SPA
Freezer FORMA 900 Series	Thermo Fisher Scientific
Freezing container Nalgene®	Thermo Fisher Scientific
Gel blotting sheets GB003	GE Healthcare
Gel Releasers	Bio-Rad Laboratories Inc.
IKAMAG™ RET	IKA-Werke GmbH
Imager FUSION Pulse TS	Vilber
Incubator Hera Cell	Heraeus Instruments
KIMTECH Science Tissues	Kimberly-Clark
Labofuge 400R Centrifuge	Heraeus Instruments
Laminar Airflow Bench HERAsafe	Heraeus Instruments
Laminar Airflow Bench Lamin Air	Heraeus Instruments
Latex gloves	VWR
Liebherr MediLine	Liebherr
Liquid nitrogen freezing container LS3000	Taylor Wharton
MaxQ™ 4000 Benchtop Orbital Shaker	Thermo Fisher Scientific
Microtube (0.5 mL, 1.5 mL, 2 mL)	Sarstedt
Miele Professional PG 8583	Miele
Millipore Direct-Q 3UV	Merck Millipore
Mini Cell Buffer Dams	Bio-Rad Laboratories Inc.
Mini Gel Holder Cassette	Bio-Rad Laboratories Inc.

Mini Star Microcentrifuge	VWR
Mini Trans-Blot©Cell	Bio-Rad Laboratories Inc.
Mini-PROTEAN Casting Stand	Bio-Rad Laboratories Inc.
Mini-PROTEAN Clamps	Bio-Rad Laboratories Inc.
Mini-PROTEAN Comb, 10-well	Bio-Rad Laboratories Inc.
Mini-PROTEAN Comb, 15-well	Bio-Rad Laboratories Inc.
Mini-PROTEAN Short Plates	Bio-Rad Laboratories Inc.
Mini-PROTEAN Spacer Plates	Bio-Rad Laboratories Inc.
Mini-PROTEAN Tetra Electrode Assembly	Bio-Rad Laboratories Inc.
Multi Pipette M4	Eppendorf
Multichannel Pipette Discovery	Abimed
Nalgene Dewar flask	Thermo Fisher Scientific
Nitril gloves	VWR
Nitrile gloves	VWR
Nunclon cell culture flask	Nunc
Nunc™ EasYFlask™ Cell Culture Flasks (25 cm^2, 75 cm^2, 175 cm^2)	Thermo Fisher Scientific
PB3002 DeltaRange	Mettler Toledo
pHenomenal® pH 1100L	VWR
PIPETMAN Classic (P20, P100, P200, P1000)	Gilson
Pipette tips 1000 µL, 200 µL, 10 µL	Sarstedt
Pipettes 1000 µL, 200 µL, 20 µL	Gilson, Middleton & Labnet International
Pipettes 1000 µL, 200 µL, 20 µL	Eppendorf
Polycarbonate Baffled Culture Flasks	Thermo Fisher Scientific
Potter S	B. Braun Biotech International
PowerPac™ HC Power Supply	Bio-Rad Laboratories
PVDF membrane	Thermo Fisher Scientific
Refrigerator	Liebherr
Rocking Platform	VWR
Roller	Bio-Rad Laboratories
SafeSeal Tips Premium 1000 µL steril	Biozym Scientific

Scale AG245	Mettler Toledo
Serological pipette (2 mL, 5 mL, 10 mL, 25 mL)	Sarstedt
Serological pipette 25 mL, 10 mL, 5 mL	Sarstedt
Shaker Orbit LS	Labnet
Sterilization tape for autoclaves	A. Hartenstein
Super PAP Pen	Daido Sangyo
SuperFrost™ Microscope Slides	Thermo Fisher Scientific
Synergie™ Fusion RP C18	Phenomenex, Torrance, USA
TC-Plate 6 Well	Sarstedt
Tetra Cooling Unit	Bio-Rad Laboratories
TipOne® Tips (20 µL, 200 µL) steril	Starlab
Tissue embedding cassetts	Kartell Spa
Transmitted light microscope Motic AE20 Motic	Wetzlar
UNIVERSAL 320R centrifuge	Andreas Hettich GmbH
Visitron Spinning Disc microscope	Visitron
Volumetric flask 100 mL	Simax
Vortexer VortexGenie 2	Bender & Hobein
Vortex-Genie 2	Scientific Industries
Water bath type 3044	Koettermann
Water Bath WNB 22	Memmert
Waterbath	Memmert
Z2 Coulter Particle Count and Size Analyzer	Beckman Coulter

2.1.2. Computer Software

Table 3. Computer Software

Name	Description
Agilent Mass Hunter 10.0	Agilent, Santa Clara, CA, USA
BioRender	Sciences Suite Inc.
Cytoscape V5	Cytoscape Consortium

FIJI 2.3.0/1.53f	Open Source
Microsoft Excel 16.57	Microsoft
Microsoft PowerPoint 16.57	Microsoft
Microsoft Word 16.57	Microsoft
Molecular Devices Flex Software	Wokingham, Berkshire, United Kingdom
Perseus 1.5.0.9.	Jürgen Cox and Mathias Mann, MPI Munich
PRISM Graph Pad 9.2.0.	Graph Pad Software

2.1.3. Chemicals, Reagents & kits

Table 4. Chemicals, reagents and kits

Productname	**Manufacturer**
0.05% Trypsin EDTA	Thermo Fisher Scientific
2-Mercaptoethanol	Sigma-Aldrich
2-Propanol ROTISOLV® HPLC	Carl Roth
30% Acrylamid Mix	Carl Roth
Acetic acid	Carl Roth
Acetonitrile	Honeywell Riedel-deHae:n
Albumin Fraction V, protease-free	Carl Roth
Amersham™ ECL™ Prime Western Blotting Detection Reagent	GE Healthcare
Ammonium persulfate	Thermo Fisher Scientific
Ammoniumacetate	Thermo Fisher Scientific
Ampicillin	Thermo Fisher Scientific
Bacto™ Agar	Becton Dickinson
Bacto™ Tryptone	Becton Dickinson
Benzonase®	Sigma Aldrich
Bio-Rad Protein Assay Dye Reagent Concentrate	Bio-Rad Laboratories Inc.
Boric acid ≥99.5%	Sigma-Aldrich

Calcium chloride dihydrate ≥ 99%, Ph. Eur., USP	Carl Roth
Chloroform ≥99.5%	Sigma-Aldrich
cOmplete Tablets, Mini EASYpack	Roche
COULTER ISOTON II Dilutent	Beckman Coulter
Dihydro Ethidium bromide (DHE)	Thermo Fisher Scientific
Dihydrorhodamine (DHR)	Thermo Fisher Scientific
di-Sodium hydrogen phosphate dihydrate ≥99.5%	Carl Roth
DMEM, high glucose, GlutaMAX™	Thermo Fisher Scientific
DMEM, high glucose, GlutaMAX™, no phenol red	Thermo Fisher Scientific
DMEM, high glucose, no glutamine	Thermo Fisher Scientific
DMEM, high glucose, no glutamine, no phenol red	Thermo Fisher Scientific
Dimethyl sulfoxide (DMSO) ≥99.8%,	Carl Roth
Effectene® Transfection Reagent	QIAGEN
Escherichia coli ISTD	Thermo Fisher Scientific
Ethanol ≥99.5%, Ph.Eur., extra pure	Carl Roth
Ethanol ≥99%	Fisher Chemical
Ethanol 99.5% Ph. Eur.	Carl Roth
Ethylenediamine tetraacetic acid (EDTA) disodium salt dihydrate ≥99%	Carl Roth
FastAP	Thermo Fisher Scientific
Fetal bovine serum (FBS)	Thermo Fisher Scientific
G-418	Roche
GenElute™ HP Plasmid Midiprep Kit	Sigma-Aldrich
GeneRuler Ultra Low Range DNA Ladder	Thermo Fisher Scientific
GlutaMAX™ Supplement (100x)	Thermo Fisher Scientific
Glycine ≥99%	Carl Roth
Glycogen, RNA grade	Thermo Scientific™
Hydrochloric acid 37%	VWR Chemicals
Hydrogen peroxide 30%	Sigma-Aldrich

Hygromycine B	Thermo Fisher Scientific
Isoflurane-Piramal	Piramal Critical Care Deutschland GmbH
Magnesium chloride hexahydrate ≥99%	Carl Roth
MEM Non-Essential Amino Acids Solution (100X)	Thermo Fisher Scientific
MEM Vitamins Solution (100X)	Thermo Fisher Scientific
Methanol ≥99.9%	Fisher Chemical
Mini Protease Inhibitor Cocktail	Roche
Sodiumdeoxycholate	Merck
Sodiumpyruvate	Thermo Fisher Scientific
Novex® TBE-Urea Sample Buffer	Invitrogen
Nuclease P1 from *Penicillium citrinum*	Thermo Fisher Scientific
Nuclease-free water	Life Sciences
Opti-MEM	Thermo Fisher Scientific
PAGERuler™ Prestained Protein Ladder	Thermo Fisher Scientific
Penicillin-Streptomycin (10,000 U/mL)	Thermo Fisher Scientific
Pentostatin ≥95%	Sigma Aldrich
Phenylmethyl sulphonyl fluoride (PMSF) ≥99%	Carl Roth
Phosphodisterase	Thermo Fisher Scientific
Polyethylene glycol alkylphenyl ether (Triton-X 100)	Carl Roth
Polysorbate 20 (TWEEN® 20)	Carl Roth
Potassium chloride ≥99.5%	Carl Roth
Potassium dihydrogen phosphate	Merck
RNase Zap™	Invitrogen
Rotenone	Thermo Fisher Scientific
ROTI® Zol RNA	Carl Roth
Roti®Load 1 (reducing) 4X	Carl Roth
Rotiphorese® Gel 30 (37,5:1)	Carl Roth
ROTIPHORESE® Sequencing Gel Diluent	Carl Roth
Saccharomyces cerevisiae ISTD	Thermo Fisher Scientific

Snake venom phosphodiesterase from *Crotalus adamanteus*	Worthington
Sodium chloride	VWR Chemicals
Sodium dihydrogen phosphate monohydrate ≥98%	Carl Roth
Sodium Dodecyl Sulfate	Thermo Fisher Scientific
Sodium hydroxide pellets	Carl Roth
Sodium Pyruvate (100 mM)	Thermo Fisher Scientific
SYBR™ Gold	Invitrogen™
TEMED ≥99%	Carl Roth
Thiazolyl Blue Tetrazolium Bromide	Sigma-Aldrich
Tris hydrochloride	SERVA Electrophoresis
Tris-(hydroxymethyl)-amino methane ≥99.9% (Tris)	Carl Roth
Urea	Carl Roth
ZR small-RNA™ PAGE Recovery Kit	Zymo Research

2.1.4. Antibodies

Table 5. Primary Antibodies

Antibody	Dilution	Catalog no.	Manufacturer
Rabbit polyclonal Anti-ANG	1:1000	ab139947	Abcam
Rabbit monoclonal Anti-GAPDH	WB: 1:10000	ab181602	Abcam

Table 6. Secundary Antibodies

Antibody	Dilution	Catalog no.	Manufacturer
Goat Anti-Mouse HRP	WB: 1:5000	31430	Thermo Fisher Scientific
Goat Anti-Rabbit–Peroxidase conjugated	WB: 1:10000	A0545	Sigma-Aldrich

2.1.5. Buffers and solutions

0.5M EDTA

EDTA x 2 H_2O	23.26 g
Purified H_2O	100 mL

Adjust pH 8.0 using NaOH.

0.1% TWEEN® 20/PBS-CMF

TWEEN® 20	50 µL
PBS-CMF	ad 50 µL

0.5% Triton X 100/PBS

Triton X	250 µL
PBS-CMF	49.750 mL

1.5M Tris pH 6.8

Tris	121.1 g
Purified H_2O	800 mL

1M Tris-HCl pH 7.4

Tris	121.1 g
Purified H_2O	800 mL
HCl 37%	adjust to pH 7.4
Purified H_2O	ad 1 L

Control pH and autoclave.

1.5M Tris pH 8.8

Tris	121.1 g
Purified H_2O	800 mL
HCl 37%	adjust to pH 8.8
Purified H_2O	ad 1 L

Control pH and autoclave.

10% Ammonium persulfate (APS) solution

APS	100 mg
2-Propanol	1 mL

10% Urea solution

Urea	20 g
Purified H_2O	200 mL

Heat until Urea is completely dissolved.

10X Running buffer pH 8.45 for Western Blotting

Tris	30.2 g
Glycine	144 g
20% SDS	50 mL
Purified H_2O	ad 1 L

10X Transfer buffer for Western Blotting

Tris	30.3 g
Glycine	144 g
Purified H_2O	ad 1 L

Autoclave.

10X Tris Borate EDTA (TBE) buffer

Tris	108 g
Boric acid	55 g
0.5M EDTA	20 mL
Purified H_2O	ad 1 L

10X Tris Buffered Saline (TBS) buffer

Tris	24.2 g
NaCl	87.8 g
Purified H_2O	ad 1 L

1M NaCl

NaCl	292 mg
Purified H_2O	5 mL

1M NaOH

NaOH	40 g
Purified H_2O	ad 1 L

1X Running buffer for Western Blotting

10X Running buffer	100 mL
Purified H_2O	900 mL

1X TBE Running buffer

10X TBE buffer	100 mL
Purified H_2O	900 mL

1X Transfer buffer for Western Blotting

10X Transfer buffer	100 mL
Methanol	200 mL
Purified H_2O	700 mL

20% SDS solution

SDS	20 g
Purified H_2O	ad 100 mL

Adjust pH 7.2 using HCl 37%.

5% Bovine serum albumin (BSA) Blocking solution for Western Blotting

BSA	25 g
0.1 TBST buffer	500 mL

5% Bovine serum albumin (BSA) antibody dilution buffer for Western Blotting

BSA	25 g
0.1 TBST buffer	500 mL

Phosphate buffered saline without Ca^{2+} and Mg^{2+} (PBS-CMF)

NaCl	8 g
KCl	0.2 g
Na_2HPO_4	1.5 g
K_2HPO_4	0.2 g
Purified H_2O	ad 1 L

Autoclave.

Phenylmethylsulfonyl fluoride (PMSF) 100 mM

PMSF	175 mg
2-Propanol	10 mL

Protease Inhibitor solution

Mini Protease Inhibitor	1 tablet
Purified H_2O	1 mL

Radioimmunoprecipitation assay (RIPA) buffer

1M Tris-HCl, pH 7.4	1.25 mL
1M NaCl	3.75 mL
Triton-X100	250 µL
Sodiumdeoxycholate	125 mg
20% SDS	125 µL
0.5M EDTA	250 µL

Stripping solution for antibody removal

20% SDS	10 mL
0.5M Tris (pH 6.8)	12.5 mL
2-Mercaptoethanol	0.8 mL
Purified H_2O	77.5 mL

TBST 0.1%

10X TBS	100 mL
TWEEN® 20	1 mL
Purified H_2O	ad 1 L

TBST 0.5%

10X TBS	100 mL
TWEEN® 20	5 mL
Purified H_2O	ad 1 L

Tris-EDTA buffer

Tris	1.21 mg
EDTA	370 mg
Purified H_2O	ad 1 L

2.1.6. Cell culture media

Full medium transfected SH-SY5Y cells

DMEM GlutaMAX®	500 mL
FBS	50 mL
Hygromycine B	3.4 mL
Penicillin / Streoptomycin	5.7 mL
MEM Vitamin Solution (100X)	5 mL
MEM Non- Essential Amino Acids (100X)	5 mL
Sodiumpyruvate	5 mL

Reduced medium transfected SH-SY5Y cells

DMEM GlutaMAX®	500 mL
FBS	10 mL
Hygromycine B	3.4 mL
Penicillin / Streoptomycin	5.7 mL
MEM Vitamin Solution (100X)	5 mL
MEM Non- Essential Amino Acids (100X)	5 mL
Sodiumpyruvate	5 mL

Reduced medium for live cell imaging of transfected SH-SY5Y cells

DMEM, high glucose, no glutamine, no phenol red	500 mL
GlutaMAX™ supplement (100x)	10 mL
FBS	10 mL
Hygromycine	3.4 mL
Penicillin / Streoptomycin	5.7 mL
MEM Vitamin Solution (100X)	5 mL
MEM Non- Essential Amino Acids (100X)	5 mL
Sodiumpyruvate	5 mL

Full medium untransfected HEK293 cells

DMEM, high glucose, no glutamine	500 mL
FBS	50 mL
Penicillin / Streoptomycin	60 U/mL (= 5.7 mL)

Full media HEK APPwt+sw

DMEM, high glucose, no glutamine	500 mL
FBS	50 mL
Penicillin / Streoptomycin	60 U/mL
G-418	

Cell freezing media

Full medium	95%
DMSO	5%

2.1.7. Cell lines

2.1.7.1. Human Embryonic Kidney 293 cells

Human Embryo Kidney 293 (HEK293) cells are immortalized cells derived from embryonic kidney cells of a female human fetus exposed to sheared fragments of adenovirus type 5 DNA [338]. For all experiments we used HEK293 untransfected (ut), HEKK APPwt, and HEK APPsw cells. HEK APPwt, and HEK APPsw stably overexpress either wildtype APP (wt) or the Swedish mutation (K640/n671L, APPsw). Cells are characterized by different Aβ1-40 loads increasing from HEK ut to HEK APPwt and sw. While HEK APPwt represents a model for sporadic AD and HEK APPsw serves as a model for late sporadic AD, HEK ut were used as control cells [94,100,339]. HEK293 cells (HEK ut, HEK APPwt, HEK APPsw) were kindly provided by the research group of Prof. Dr. rer. nat. Walter. E. Müller (Goethe University, Frankfurt).

2.1.7.2. SH-SY5Y cells

SH-SY5Y cells are human neuroblastoma cells. SH-SY5Y cells are thrice cloned human neuroblastoma cells, a subline of SK-N-SH. It was originally isolated in 1970 from a metastatic bone tumor of a 4-year-old girl. SH-SY5Y cells were stably transfected with the human APP695 gene on a pCEP4 vector to design a model for the disease state of an early form of LOAD. This provides mild levels of Aβ1-40. These mutants carry an additional copy of human wt APP695 gene. Therefore they are called SH-SY5Y APPwt cells. To develop a comparable corresponding control cell line, SH-SY5Yut was stably transfected with an empty pCEP4 vector (SH-SY5Y Mock) [340,341]. The SH-SY5Yut cell line is from the American Type Culture Collection (ATCC) and was kindly provided by the research group of Prof. Dr. rer. nat. Christian Behl (University Medical Center, Mainz).

2.1.8. Animals

2.1.8.1. C57BL/6J

Wildtype C57BL/6J were obtained from our animal pool or purchased from the Translational Animal Research Center (TARC) in Mainz, Germany. Wildtype mice were 3 and 12 months of age. All animals were sex-mixed.

2.1.8.2. 5X FAD (B6SJL)

5X FAD mice express human APP and PSEN1 transgenes. APP and PSEN1 are expressed with different mutations, Swedish (K670N/M671L), Florida (I716V), and London (V717I) mutations for APP and M146L and L286V for PSEN1. First, amyloid plaques occur at about 3 months of age, leading to a range of cognitive and motor deficits. Transgenic mice were about 3 to 12 months old. All animals were sex-matched [342]. 5X FAD mice were kindly provided by the research group of Prof. Dr. rer. nat. Christina Endres (University Medical Center, Mainz).

2.1.8.3. Overview of all animals used during this work

Table 7. List of all animals used during this study.

Mouse ID	Sex	Age [weeks]	genetics
615.1	f	43	wt
615.2	f	43	wt
616.1	m	43	tg
616.2	m	43	tg
617.1	m	43	wt
618.1	m	43	wt
618.2	m	43	tg
619.2	f	43	tg
620.1	m	43	wt
621.2	f	43	tg
634.1	m	24	tg
635.2	f	17	tg

638.1	m	17	wt
638.2	m	20	tg
638.3	m	20	tg
642.1	f	17	tg
642.2	f	17	tg
643.4	m	16	tg
644.3	f	16	tg
644.4	f	16	tg
644.5	f	16	tg
645.1	m	19	wt
645.1*	m	19	wt
647.1	m	17	wt
647.4	m	17	wt
AP1.392	m	63	tg
AP1.418	m	52	wt
AP1.422	m	51	tg
AP1.422*	m	51	tg
AP1.424	m	46	tg
AP1.425	f	46	wt
AP1.426	f	42	wt
AP1.428	f	42	wt
FRI-0031	m	52	wt
FRI-0032	m	52	wt
FRI-0034	m	52	wt
FRI-0035	f	52	wt
FRI-0036	f	52	wt
FRI-0041	m	52	wt
FRI-0049	f	48	wt
FRI-0050	f	48	wt
LUT-DCV8	f	13	wt
LUT-DCV9	f	13	wt
LUT-DCW0	f	13	wt
LUT-DCW1	f	13	wt
TAR-V190	f	48	wt
TRC1	f	47	wt
TRC2	f	47	wt

TRC3	m	22	wt
TRC4	m	22	wt
TRC5	m	22	wt
TRC6	m	22	wt
TRC7	m	22	wt
TRC8	f	22	wt
TRC9	f	22	wt
X817	f	10	wt
Y131	m	12	wt
Y132	m	9	wt
Y215	F	9	wt

2.1.8.4. Euthanization of mice

All mice were euthanized using cervical dislocation or inhalation of narcotic isoflurane. After euthanization, appropriate tissue was dissected and stored in liquid nitrogen briefly.

2.1.8.5. TgF344 rats

The rats used in this study were TgF344-AD animals. These animals express human APP with the Swedish mutation and human PSEN1 with the d-exon 9 mutation, resulting in 2.6 times more human APP and 6.2 times more human PSEN1 being expressed in the brain compared to total protein levels [343]. The rats show an age-dependent increase in detergent-soluble and detergent-insoluble Aβ 40 and Aβ 42 levels at 6-26 months of age. The Aβ 40/Aβ 42 ratio also increases with age in the soluble fraction, whereas it decreases in the insoluble fraction. Aβ plaques occur primarily in the hippocampus and cortex, but to some extent also in the striatum and cerebellum of animals. In addition, plaque-associated neurotic dystrophies can be observed. Tau pathology has also been observed in TgF344-AD rats. An advantage of the model is that the number of neurons in the hippocampus and cortex is comparable to the number of neurons in wt rats at the same age between 6-26 months [343]. Rats were kindly provided by the research group of Prof. Dr. rer. nat. Jochen Klein (Goethe University, Frankfurt).

Table 8. Rats used in this study.

sex	genetic	Age [months]
m	wt	6
m	wt	6
m	tg	6
m	tg	6
f	wt	6
f	wt	6
f	tg	6
f	tg	6
m	wt	15
m	wt	15
m	tg	15
m	tg	15
f	wt	15
f	wt	15
f	tg	15
f	tg	15

2.1.9. Human brain samples

In order to receive the samples, a detailed application had to be submitted to the Netherland Brain Bank (NBB) based in Amsterdam. This application was approved, and our project was given project number 1341. In total, we received 32 human cerebral cortex samples, some of which were supplied as cryo bags or cryovials. All samples were from the superior frontal gyrus (gfs and 4). This part of the cerebral cortex is also associated with AD [344,345].

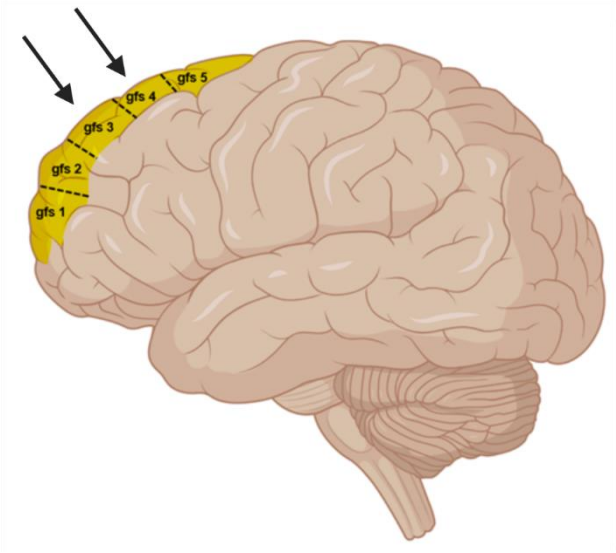

Figure 26. Human brain. Dissected areas were gfs3 and gfs4 (arrows). Yellow color indicates superior frontal gyrus.

We obtained 14 female and 6 male AD cortexes and 6 female and 6 male non-demented control subjects. In this way, we covered a broad cohort of different individuals. The age of all patients ranged from 71 to 102 years, which leads to an average of 83.5 years. BRAAK stage was between 3 and 6 in all subjects. Care was also taken to keep postmortem delay (PMD) as low as possible. A PMD of 4-7 h could be maintained in our case. All values can be found for each individual in Tab 16.

Table 9. Characterization of Human brain samples.

NBB No.	sex	age	braak	amyloid	pmd	weight	diagnosis	region
2009-009	f	88	5	C	06:45	1148	Alzheimer's disease	superior frontal gyrus
2009-009	f	88	5	C	06:45	1148	Alzheimer's disease	superior frontal gyrus
2017-042	f	86	5		05:50	1090	Alzheimer's disease	superior frontal gyrus
2017-062	f	81	6		05:30	1015	Alzheimer's disease	superior frontal gyrus
2017-062	f	81	6		05:30	1015	Alzheimer's disease	superior frontal gyrus

2017-078	f	88	4		10:00	1052	Alzheimer's disease	superior frontal gyrus
2017-092	f	72	5		06:10	1035	Alzheimer's disease	superior frontal gyrus
2017-092	f	72	5		06:10	1035	Alzheimer's disease	superior frontal gyrus
2017-102	f	98	5	C	06:05	1090	Alzheimer's disease	superior frontal gyrus
2017-156	f	87	4		03:25	1193	Alzheimer's disease	superior frontal gyrus
2017-156	f	87	4		03:25	1193	Alzheimer's disease	superior frontal gyrus
2019-085	f	76	4		05:00	1120	Alzheimer's disease	superior frontal gyrus
2019-085	f	76	4		05:00	1120	Alzheimer's disease	superior frontal gyrus
2019-085	f	76	4		05:00	1120	Alzheimer's disease	superior frontal gyrus
2010-011	m	80	4	C	04:00	1288	Alzheimer's disease	superior frontal gyrus
2010-011	m	80	4	C	04:00	1288	Alzheimer's disease	superior frontal gyrus
2014-010	m	78	5	C	05:55	1275	Alzheimer's disease	superior frontal gyrus
2017-157	m	86	4		04:50	1295	Alzheimer's disease	superior frontal gyrus
2018-090	m	97	5		05:10	1120	Alzheimer's disease	superior frontal gyrus
2019-059	m	74	5		13:00	1555	Alzheimer's disease	superior frontal gyrus
2012-042	f	83	2	B	06:03	1030	Non-demented control	superior frontal gyrus
2014-014	f	90	3	B	06:05	1255	Non-demented control	superior frontal gyrus
2015-027	f	76	2		04:45	1140	Non-demented control	superior frontal gyrus

2017-131	f	71	2		06:15	1175	Non-demented control	superior frontal gyrus
2019-036	f	85	3		06:50	1190	Non-demented control	superior frontal gyrus
2019-079	f	84	3		07:50	1345	Non-demented control	superior frontal gyrus
2009-096	m	92	4	C	08:25	1117	Non-demented control	superior frontal gyrus
2012-067	m	102	3	A	05:00	1124	Non-demented control	superior frontal gyrus
2015-033	m	93	0	A	07:40	1155	Non-demented control	superior frontal gyrus
2017-016	m	72	2		04:20	1385	Non-demented control	superior frontal gyrus
2018-105	m	86	3		06:45	1340	Non-demented control	superior frontal gyrus
2019-029	m	87	3		06:20	1275	Non-demented control	superior frontal gyrus

2.1.10. Adult Changes in Cohort (ACT) study

The *Adult Changes in Thought (ACT) study* was initiated in 1994 and conducted as a prospective longitudinal cohort study. Individuals of 65 years or older were selected for this study. At baseline, patients were asymptomatic, meaning they had no cognitive impairment and were therefore classified as not having dementia. Other criteria for dementia included microvascular brain injury (mVBI) and Lewy body disease (LBD). Over time, individual patients were then classified into the dementia group or, if a diagnosis of AD was present, into that group. A total of 4690 subjects were recorded [346]. As part of this study, RNA sequencing datasets from 107 brains, including 377 samples from cortical grey (parietal and temporal) and white matter (parietal) and hippocampus was collected to perform another study named *Aging, Dementia and TBI study*. This study was used to determine the alteration and expression of ANG in clinical patient datasets. This study is a detailed neuropathologic, molecular, and transcriptomic characterization of brains of control and TBI exposure cases from a unique aged population-based cohort from the *Adult Changes in Thought (ACT) study* and is available for the public on the web.

2.2. Methods

2.2.1. Cell culture

2.2.1.1. Splitting and seeding cells

When splitting the cells, the old medium was first discarded. HEK293 cells could be rinsed directly with fresh medium from the surface, whereas the more adherent SH-SY5Y cells had to be washed with ice-cold PMS-CMF to remove excess FBS. Subsequently, 0.05% trypsin was added, and the cell culture flask was incubated at 37°C for 5 min in the incubator. As soon as the SH-SY5Y cells detached from the surface, they were rinsed off with fresh medium and resuspended. Both cell lines were then centrifuged at 1,000 g for 5 min at room temperature. The supernatant was discarded, and the resulting pellet was resuspended in fresh medium. Then, 200 µL of each cell solution was diluted in 9.8 mL of Coulter isotone, and the cell number was determined using the Beckman Coulter Counter. The result was indicated in cells per mL. $2.5x10^6$ SH-SY5Y Mock cells, SH-SY5Y APPwt cells, HEK293 ut, HEK APPwt, and HEK APPsw cells were seeded for regular weekly maintenance into a 175 cm^2 cell culture flask. HEK293 cells were grown in modified Dulbecco-Eagle medium , supplemented with 10% heat-inactivated FBS, 50 units/mL penicillin/streptomycin solution, and 400 lg/mL G-418, SH-SY5Y cells were grown in modified Dulbecco-Eagle medium (modified with GlutaMAX®), supplemented with 10% heat-inactivated FBS, 50 units/mL hygromycin B, 60 units/mL penicillin/streptomycin, 5 mL MEM vitamin solution (100X), 5 mL nonessential amino acids (100X), and 5 mL sodium pyruvate. All cell lines were grown at 37°C in a humidified incubator containing 5% CO_2 until 80% confluency was reached.

2.2.1.2. Freezing cells

Two days before freezing, $1x10^6$ HEK293 and SH-SY5Y cells were grown in a 100 mm cell culture dish to 80-90% confluency. After 48h, cells were washed and resuspended with 4 mL of appropriate media. 2 mL of the cell suspension were put into a 2 mL cryovial containing 20 µL DMSO to protect the cells from the fast freezing process. 2 days after storage at -80°C cells were transferred to liquid nitrogen tank for long term storage.

2.2.1.3. Thawing cells

The cryotube with the desired cells was taken out from the liquid nitrogen tank and smoothly thawed in hands. Once the cell suspension began to thaw, the whole suspension was transferred to 9 mL of appropriate cold full medium. After centrifugation (1,000 g, 5 min, room temperature), the cell pellet was resuspended in prewarmed (37°C) full medium and seeded into a fresh cell culture flask. The next day, old medium was replaced by new prewarmed (37°C) medium to remove dead cells for further growth.

2.2.2. Bioinformatic analysis of ACT study

We received an introduction from the Core Facility Bioinformatics of the Institute of Molecular Biology (IMB) Mainz for the bioinformatics analysis. The RNAseq data was downloaded for ANG, and the ZIP file was unpacked. The age, etc., could then be assigned to each patient and the data set analyzed. The datasets were divided into the following age groups: 75-80, 81-85, 86-89, 90-94, and 95-99. On this basis, the age dependence of ANG expression can be re-examined. In this study, samples were taken from the cortex and hippocampus. Samples from the cerebellum were not taken. Because the cohorts were too small to separate male and female individuals, they were analyzed together in the subsequent analysis.

2.2.3. Generation of sequence similarity network

The SSN was created using the Cytoscape V5 program. The Pfam pathway PF00074 was used as the protein family. The cut-off of the alignment score was adjusted to 60 to obtain better separation of the individual clusters. The color design was selected based on the function of the proteins. All ANG proteins in various organisms were stained in light red, human ANG, mouse ANG, and rat ANG were stained in red, and all other proteins were stained in brown. Finally, the SSN was exported as an image.

2.2.4. Western Blotting

2.2.4.1. Protein extraction

48h before extraction, $1x10^6$ cells were seeded in 100 mm cell culture dish. On the day of extraction, cells were placed on ice for a short time. The medium was then removed, and the cells were washed with ice-cold PBS-CMF. Subsequently, 200 µL of a RIPA-PMSF mixture (100:1) was added dropwise to the cells. Tissue was handled equally, except for the amount of RIPA buffer. After cervical dislocation, cerebellum, prefrontal cortex, and hippocampus were briefly dissected from each mouse, frozen directly in liquid nitrogen, and stored at -80°C. Depending on the tissue size, 200-1000 µL of RIPA was used. After incubation for 15 min on ice, the cells were scraped off with a cell scraper, and the lysate was transferred to a pre-cooled Eppendorf tube. Tissue was still placed on ice. After additional incubation of 30 min on ice, tubes were centrifuged (10,000 g, 10 min. at 4°C) and the supernatant was withdrawn, and the pellet was discarded. From this supernatant, 20 µL were collected for the Bradford assay, and the remainder was mixed with protease inhibitor at a ratio of 10:1.1 and aliquoted for later use.

2.2.4.2. Bradford Protein Assay

The Bradford assay was used to quantify unknown protein concentrations from protein extracts. Coomassie G-250 is the dye used for this assay. Through binding to proteins, a color shift of Coomassie G-250 was detected. Unbound Coomassie G-250 has an absorbance maximum of 470 nm, while the absorbance of bound Coomassie G-250 shifts to a maximum of 595 nm. This change in absorbance is determined photometrically. Since the amount of Coomassie G-250 is proportional to that of proteins, the exact concentration can be calculated from this. According to Bradford, a calibration grade was first performed using 1000 µg/mL BSA solution to determine standard protein concentration. For this purpose, 125 mg BSA was dissolved in 100 mL purified H_2O and diluted in a series of dilutions. This is shown in the following table.

Table 10. Preperation for Bradford calibration curve.

Stock	Composition	Concentration [µg/mL]
0	125 mg BSA ad 100 mL H_2O	1000
A	32 µL stock 0 + 1598 µL H_2O	20
B	800 µL stock A + 800 µL H_2O	10
C	800 µL stock B + 800 µL H_2O	5
D	800 µL stock C + 800 µL H_2O	2.5
E	800 µL stock D + 800 µL H_2O	1.25

Protein extracts were prepared as follows: 20 µL of protein extract was collected from the supernatant of samples, and 1980 µL of H_2O was added to each preparation (1:100). 80 µL of 1:100 solution was added to 720 µL into a new Eppendorf tube (1:1000). Finally, 200 µL of Biorad dye was added to each solution and incubated for 5 minutes in the dark. In addition, a blank (1000 µL H_2O) and a zero reference (800 µL H_2O + 200 µL Biorad dye) were prepared. The absorbance was determined photometrically at 595 nm and 470 nm.

2.2.4.3. SDS Page and Western Blotting

Whole cell extracts were fractionated by 12% SDS-Polyacrylamide gel electrophoresis. The gel consisted of a running and a stacking gel.

Running gel

H_2O	1625 µL
30% acrylamide mix	2000 µL
1.5M Tris (pH 8.8)	1300 µL
20% SDS solution	25 µL
10% APS soluition	50 µL
TEMED	2 µL

Stacking gel

H_2O	1370 µL
30% acrylamide mix	340 µL
1.5M Tris (pH 8.8)	260 µL
20% SDS solution	10 µL
10% APS soluition	20 µL
TEMED	2 µL

Before casting the gels, the glass plates first had to be cleaned with ethanol to remove any troublesome fatty stains. They were then assembled in a special apparatus. First, the running gel was prepared. For this purpose, 4 mL of the corresponding mixture was pipetted between each glass plate and covered with approximately 1 mL of isopropanol. This served to remove excessive air bubbles. After polymerizing the gel, the isopropanol was discarded and rewashed with purified H_2O. The components of the stacking gel were then pipetted together, 2 mL of each was poured over the existing running gel, and the comb was inserted. After about 30 min, the gel was polymerized and wrapped in wet wipes for storage at 4°C. The samples were prepared by thawing and vortexing them shortly. Extracted proteins were dissolved in 18 µL of water and 6 µL of 4X Roti®Load 1. Incubation was performed for 5 min at 85°C. Meanwhile, the running chamber was prepared, and the gel comb was removed. 20 µL of the protein solution was added to each gel pocket. 6 µL PageRuler^{TM} prestained protein ladder was used as a marker. Electrophoresis was performed at 80V until proteins reached the end of the separating gel. The voltage was then increased to 120V. Electrophoresis was stopped before the PageRuler^{TM} prestained protein ladder reached the running gel's end. After protein extracts were fractionated by 12% SDS-Page, they were transferred to a polyvinylidene difluoride (PVDF) membrane at 4°C for 1h using a transfer apparatus. For this, the PVDF membrane was first activated in methanol and then rehydrated in H_2O. The transfer sandwich was assembled in a special holder consisting of (in order from bottom to top): fiber pad, filter paper, membrane, gel, filter paper, fiber pad. The transfer was performed at 4°C for 1h at 100 V. Membranes were incubated for 1h at room temperature with 5% BSA to block non-specific binding.

Afterward, membranes were washed three times with 0.5% TBST (1st 15 min., 2nd 10 min., 3rd 5 min.). This was followed by overnight incubation at 4°C with a primary antibody that binds specifically to a sequence at the target protein. Antibodies are listed in section *2.1.4. Antibodies*. The primary antibody was diluted to desired concentration in 5% BSA solution. After overnight incubation, membranes were washed thrice for 10 min using 0.5% TBST and incubated with a horseradish peroxidase-conjugated secondary anti-mouse or anti-rabbit antibody for 1h. After three additional washing steps with 0.5% TBST, membranes were developed with Amersham™ ECL™ Prime Western Blotting Detection Reagent according to the manufacturer's protocols.

2.2.4.4. Amersham™ ECL™ Prime Western Blotting Detection Reagent

Solution A and B were mixed in equal parts to develop the Western blot membranes. Depending on the size of the membranes, 200-1000 µL of the mixture was added to each membrane. After an incubation period of 5 minutes, the membranes were analyzed using the Vilber Fusion TS FX imager. The following settings were chosen as setup:

Table 11. Set up for Fusion FX Imager.

Variable	Set up
Lightning	Prime
Time	Auto
Tray	4

The amount of protein could be quantified by determining the band intensity using a peroxidase reaction with resulting luminescence.

2.2.4.5. Stripping the membrane

Stripping was performed to remove the antibodies from the membrane. The stripping solution was preheated to 50°C, and the membrane was incubated with the stripping solution at 50°C for 30 min. After incubation, the membranes were washed twice with 0.5% TBST. An image was developed using the Amersham™ ECL™ Prime

Western Blotting Detection Reagent and the Vilber Fusion TS FX Imager to determine complete antibody removal.

2.2.4.6. Analysis of the membranes

The images obtained from the Vilber Fusion TS FX imager were analyzed using Fiji ImageJ. Each individual band was marked, and the intensity of each was determined. The obtained intensity values were set to the standard GAPDH and converted to percent. The final plots were made using Graph Pad Prism 9.2.0.

2.2.5. LC-MS/MS Analysis

2.2.5.1. RNA extraction

RNA extracts were isolated using phase separation. Tissue samples for RNA extraction were mixed with 1 mL ROTI®Zol RNA, and the tissue was homogenized using a Squisher. Cells were seeded 48 h prior to extraction and should have an 80% or above confluency. Again, 1 mL of ROTI®Zol RNA was added, and cells were detached from the culture plate using a cell scraper and transferred to a new Biosphere® SafeSeal Tube 1.5 mL. The cell suspension was also homogenized using a squisher. After adding Roti®Zol, 200 µL chloroform was added and incubated for 10 min. at room temperature, followed by a centrifugation step (10,000 rpm, 15 min., 4°C). The colorless upper phase (which contains RNA) was then transferred to a new 1.5 mL Biosphere® SafeSeal Tube containing 1µL glycogen, RNA grade. 100% 2-Propanol was added to precipitate RNA, followed by 10 min. incubation at room temperature and centrifugation (10,000 rpm, 15 min., 4°C). The supernatant was carefully transferred to a new 1.5 mL Biosphere® SafeSeal tube and washed once with 70% ethanol. After centrifugation (13,000 rpm, 10 min., 4°C), the supernatant was removed, and the RNA pellet was resuspended in RNAse free H_2O. The content of RNA was determined using fluorescent spectrometry.

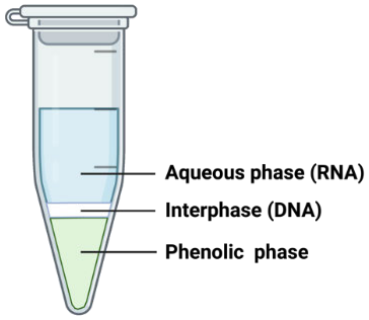

Figure 27. Phase separation at RNA extraction.

2.2.5.2. ZR small-RNA™ PAGE Recovery Kit

RNA was then separated by size using an 8M TBE-Urea gel electrophoresis, and the individual bands of tRNA, tiRNA, and tRFs were excised from the gel using a scalpel. The excised fragments were purified using the ZR small-RNA™ PAGE Recovery Kit (Zymo Research) according to the manufacturer's protocol. After the RNA was extracted from the gel pieces, the concentration of the RNA was again determined using the NanoDrop One®. Each of the brain areas was then pooled in its respective group to increase RNA concentration.

2.2.5.3. Overnight nucleoside sample digestion

400-750 ng of RNA samples were used for digestion to the nucleoside level. For digestion, 0.6 U nuclease P1 from *p. citrinum* , 0.2 U snake venom phosphodiesterase from *c. adamanteus*, 2 U FastAP (to remove remaining phosphatases), 10 U benzonase, 200 ng pentostatin in 25 mM ammonium acetate buffer (pH 7.5) was added to the purified RNA in a total volume of 50 µL and incubated overnight at 37°C protected from light.

2.2.5.4. LC-MS/MS analysis of RNA modifications

100 ng were used per injection. 50 ng of ^{13}C stable isotope-labeled nucleosides was added to digested RNA samples. The internal standard dilution (ISTD) was a long-lasting stock mixture of 50 ng/µL *Saccharomyces cerevisiae* and *Escherichia coli*. The internal standard was prepared by mixing 5 ng of *s. cerevisiae* and *e. coli*. 1.1 µL ISTD was added to 50 µL of the digested sample. All measurements were performed on an Agilent 1260 Infinity LC coupled to an Agilent 6460 Triple Quadrupole mass detection

system. The separation of the nucleosides was conducted on a Synergie™ Fusion RP C18 column (S-4 µm, 80A, column size 250x 2.0 mm I.D.) from Phenomenex. The column oven was set to 35°C. For analysis, a gradient method NUCS5 was used. This method was defined by the following conditions: Phase A containing acetonitrile (CAN) starting at 0%. After 10 min., Phase A was increased to 8% ACN and then to 40% ACN in 10 min. Equilibration time was another 10 min. Phase B contained freshly prepared 5 mM NH_4OAc buffer (pH 5.3). If needed pH value was adjusted using HOAc. The flow rate was set to 0.35 mL/min. UV trace was recorded in a multiple wavelength detector (MWD) at 254 nm at an attenuation of 1000 mAU. The sample rate was set to 2.5 Hz. All prepared samples were injected via EJS ESI source in positive ion mode to the mass spectrometer. Various parameters were defined for conduction of measurement listed below: Capillary current 5400 nA, gas temperature 350°C, sheath gas temperature 345°C, sheath gas flow 10.0 L/min, gas flow 8 L/min, Nebulizer 50.0 psi, Corona voltage 0V. A first test run was used to get correct elution times. Mass spectrometry dynamic Multiple Reaction Monitoring (MRM) was programmed to their appropriate elution time window, adding +/- 6 min for each modification. A wide range of ^{13}C-labeled and their counterparts were measured during 1 run.

2.2.5.5. Data analysis

All data were extracted and analyzed using the following programs: Extraction of UV trace area and relative quantification of ion chromatograms of the MRM was done in Agilent Mass Hunter Qualitative Analysis 10.0 for canonical nucleosides C, U, G, and A. UV-A was used for data analysis. For relative quantification integration of respective peaks, providing area under the curve (AUC) was performed. Only peaks with normal distributed peaks and a signal-to-noise ratio of 5 in at least one of several samples were further used for heatmap analysis. Signals of 12C AUC were normalized on their respective ^{13}C internal standard AUC calculating their ratio. This ratio was then normalized to the subtraction of UV-A of ^{13}C internal standard and UV-A of 12C sample signal. For heatmap creation and statistical analysis, all values were applied in Perseus 1.5.0.9. Software (Jürgen Cox and Mathias Mann, MPI Munich). Data were normalized using a normalization filter. This filter divided each row by its mean. Normalized data were then opened in Graph Pad PRISM 9.2.0 to generate cluster-driven heatmaps.

Chapter 3

3. Expression of ANG

Under normal conditions, ANG is located in the nucleus and is bound to its physiological inhibitor RNH1. Only after it is released from this does ANG enter the cytosol, where it can cleave tRNA into tRNA halves and fragments. Subsequently, the 5'-tiRNAs can inhibit the pro-apoptotic signaling pathway. This mechanism protects cells from excessive apoptosis and is therefore particularly interesting for further research on aging and neurodegenerative diseases.

Various organs and tissues were dissected to investigate the expression of ANG. These included the brain, there the areas of the cerebellum, cerebral cortex, and hippocampus to investigate the expression of ANG in central tissues. However, since some studies have found peripheral changes during aging or the development of AD, peripheral tissues such as the liver, heart, lung, and kidney were also used. This allowed us to investigate whether the expression of ANG also changes from the CNS compared to the periphery and whether this is an age-dependent or an AD-specific effect. To address this question, ANG expression was first determined in a cell model and then in mouse and rat models. Finally, human postmortem brain samples were examined again, and the expression of ANG was also determined.

3.1. Cellular levels of ANG in human cell lines

3.1.1. Expression of ANG in HEK293 cells and SH-SH5Y cells

3.1.1.1. Expression of ANG under physiological conditions

To determine the expression of ANG, we used well-characterized HEK293 cells. HEK APPwt and HEK APPsw cells were used as AD models. HEK APPwt and HEK APPsw stably overexpress either wildtype APP (wt) or the Swedish mutation (K640/n671L, APPsw). Cells are characterized by different Aβ1-40 loads increasing from HEK ut to HEK APPwt and sw. While HEK APPwt represents a model for sporadic

AD and HEK APPsw serves as a model for late sporadic AD, HEK ut were used as control cells [94,100,339]. Additionally, human SH-SY5Y cells were used as a neuronal cell model. SH-SY5Y cells stably transfected with an empty pCEP4 vector were used as control (Mock), and Aβ 1-40 producing SH-SY5Y cells (APPwt) were used as LOAD model [347–349]. Compared to the HEK293 model, the SH-SY5Y model is characterized by a lower Aβ1-40 load. The following experiments were performed to check the impact of AD, especially Aβ1-40 loads, on ANG expression. To verify this approach, the expression of ANG was first checked under physiological conditions, e.g., without treating the cells with a stressor. This allows determining the basal level of ANG in the existing cell model, which has not yet been described in the literature. If one goes by the theory, a significant increase in ANG levels in APPwt and sw cells would be expected since ANG is upregulated during stress conditions. Due to increased levels of Aβ1-40, a potent stress factor is present. The analysis was performed by WB.

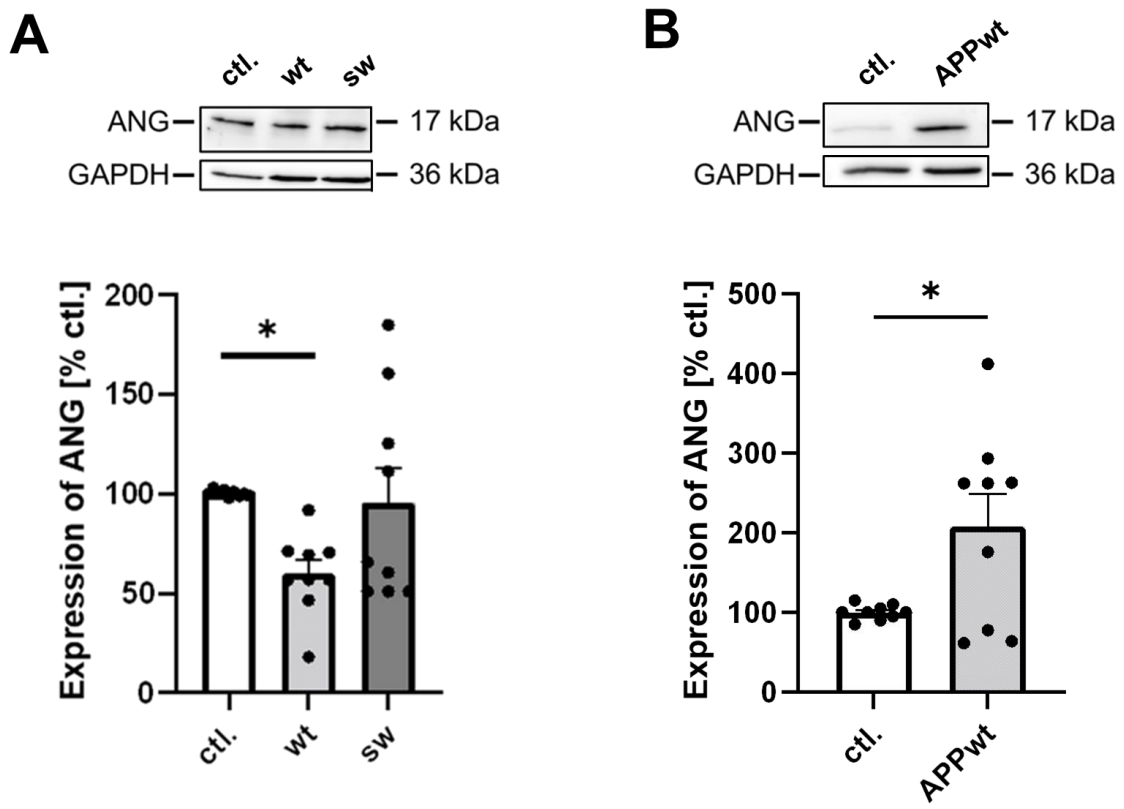

Figure 28. Expression of ANG in HEK293 cells and SH-SY5Y cells. Data are expressed as mean ± SEM; student's unpaired t-test (*p <0.05). n = 9. n = 1 is equivalent to 1 protein extraction.

Surprisingly, a significant reduction of ANG expression could be determined in the HEK293 APPwt cells. The expression was only 59.83% compared to the control HEKut. In the APPsw cells, however, only a slight trend could be detected, but no significance due to the greater scatter of the results.

In contrast, a significant increase in ANG levels was determined in SH-SY5Y APPwt compared with the control SH-SY5Y mock group. At 208.15%, the measured values were more than twice those of SH-SY5Y Mock cells.

The confluence of the 96-well plate was determined optically before both experiments to ensure a homogeneous distribution of cells and an equal number of cells in each well. In the next step, in addition to the physiological conditions, the expression levels of ANG were determined upon treatment with rotenone to verify the impact of stress factors

3.1.1.2. Expression of ANG under the treatment of complex I inhibitor rotenone

Following the results obtained previously, the question was raised as to how the expression of ANG behaves when mitochondrial dysfunction is additionally induced by the addition of a stressor such as rotenone. Rotenone belongs to the retinoid family and occurs naturally in legumes having toxic effects.

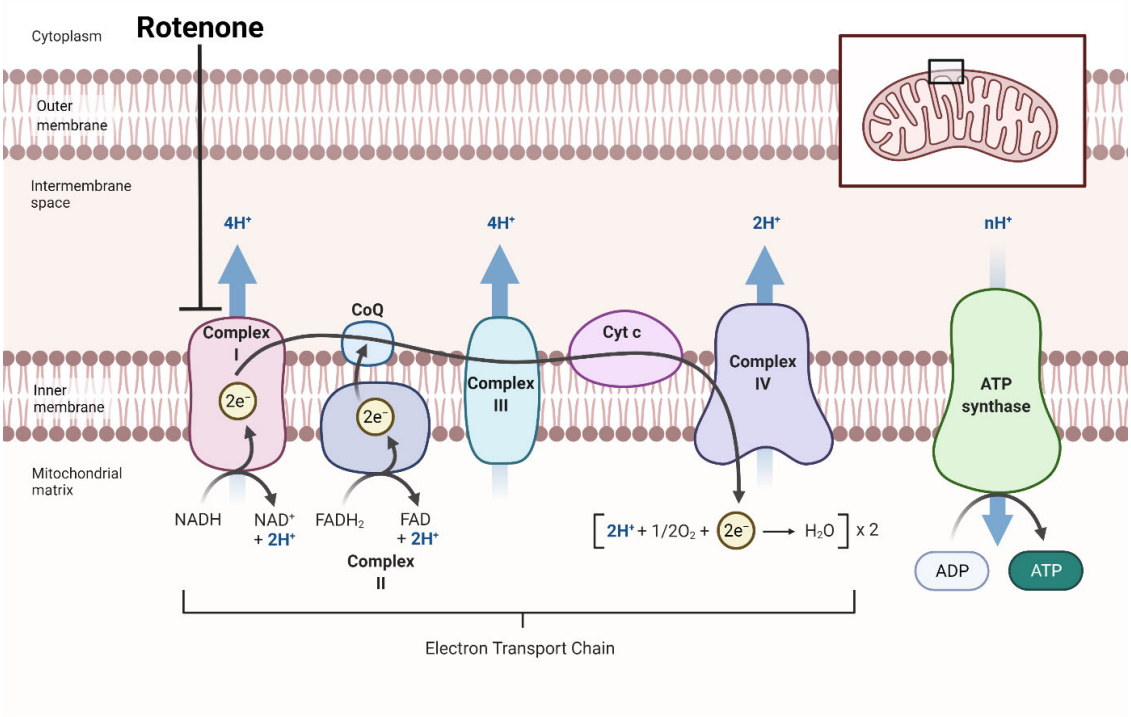

Figure 29. Mechanism of action of rotenone inhibiting complex I of ETC.

Rotenone is an inhibitor of complex I of the mitochondrial respiratory chain. It inhibits mitochondrial electron transport at nicotinamide adenine dinucleotide (NADH):ubiquinone oxidoreductase, which usually transports $4H^+$ into the intermembrane space and transfers $2e^-$ to complex II. In this process, NADH is typically reduced to NAD^+. This mechanism induces mitochondrial dysfunction. As a result of Rotenone treatment, mitochondria appear fragmented, spherical, and no longer exhibit the tubular, cohesive network seen in untreated cells [94]. Since mitochondrial dysfunction was also found in AD, this model can be used to test the impact of stress factors on ANG expression. In this experiment, the cells were incubated for 6h with 5 µM rotenone. The period of 6h was chosen because changes at the protein level can only be expected after this incubation period due to the duration of translation [350]. The concentration of 5 µM Rotenone was previously determined by cell viability assay and determined to be the best concentration to use. After the incubation period of 6h, proteins were isolated from cells, and WB analyzed expression. The intensity of ANG bands was correlated using GAPDH as an internal standard.

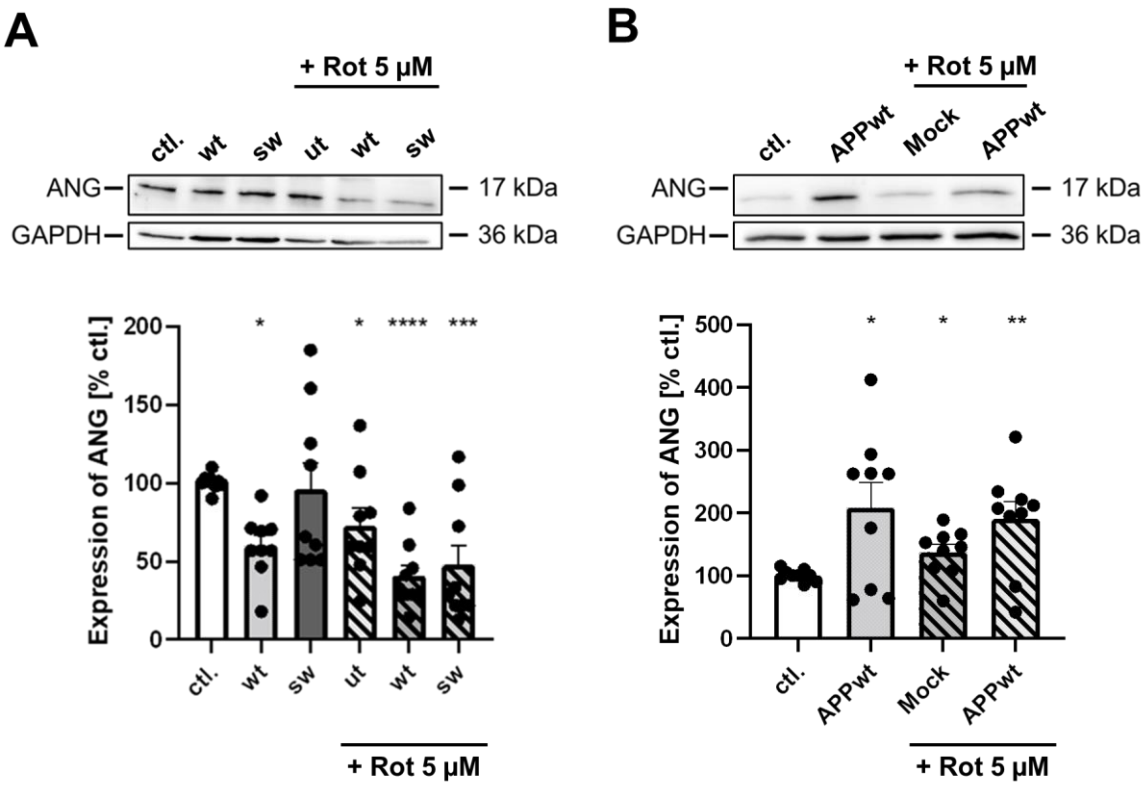

Figure 30. Expression of ANG under treatment with 5 µM rotenone. The results not treated with Rotenone have been included in the graph for completeness. Data are expressed as mean ± SEM; student's unpaired t-test (*p <0.05; **p <0.01, ***p <0.001, ****p <0.0001). n = 8-9. n = 1 is equivalent to 1 protein extraction.

After analyzing the data, a significant reduction in ANG expression was determined in all three cell lines. Compared to the control, the levels were 72.75% in HEKut, 40.58% in APPwt, and 47.68% in APPsw. Also, compared to the physiological conditions, the obtained results of the expression levels of ANG are again about 20% lower. It was ensured that the decreased expression levels were not due to a lower cell number caused by the loss of cells during washing steps.

In SH-SY5Y cells, protein levels of ANG were significantly altered compared to the control. All cell lines showed a significant increase in ANG levels. SH-SY5Y Mock cells treated with 5 µM rotenone showed an increase to 137.20% and SH-SY5Y APPwt to 190.53% compared to control. Surprisingly, treatment of cells with 5 µM rotenone at an incubation time of 6h led to an increase in ANG levels compared to the HEK293 cell model. There, the same treatment leads to a decrease in ANG expression. The confluence of the 96-well plate was determined optically before both experiments to ensure a homogeneous distribution of cells and an equal number of cells in each well.

3.1.2. Discussion

Experimental determination of ANG expression in HEK293 cells revealed a decrease in APPwt cells and no change in APPsw cells (Fig. 28). This result is initially rather surprising because ANG is normally released during a cell's stress response. The presence of Aβ induces oxidative stress in both cell models, which, following this theory, should increase the expression of ANG. Surprisingly, however, the opposite is observed, vigorously decreasing ANG levels in APPwt cells. This could be due to several reasons. On the one hand, it could be that the level of oligomeric Aβ 1-40 in the cell model is not sufficient to activate ANG sufficiently strongly. On the other hand, it could also be that there is a permanent downregulation of ANG due to the permanently present mutations and the resulting permanent chronic stress that Aβ 1-40 triggers in this model. Such downregulation is also described in the literature for other proteins, as stress can inhibit the initiation of translation and, thus, the proteins' formation [351,352]. Several proteins are downregulated at the genetic level during a stress response to allow the cell to focus on synthesizing important proteins for survival [353,354]. The observation also supports this chronic stress theory that APPsw cells, which have significantly higher Aβ 1-40 levels due to their mutation, show no change in ANG expression than controls. Therefore, the cell model APPwt represents

a model for MCI, while APPsw represents a model for early form of LOAD. This suggests that under prolonged chronic stress, such as is present upon exposure to Aβ, the cell downregulates its proper protective mechanism, and thus apoptosis may be induced to a greater extent. This suggestion is further supported by the results of the analysis of HEK293 cells treated with 5 µM rotenone for 6 hours (Fig. 30). The long incubation time ensured that changes at the mRNA level were also possible. It can be clearly seen that all cell models, HEKut and the APPwt and APPsw mutants, showed a significant decrease in ANG levels instead of an expected increase. The expression of ANG was even more significantly reduced in the mutants than in the HEK ut cells that did not exhibit Aβ loading. However, it is also evident that the sustained stress induced by the complex I inhibitor rotenone causes downregulation of ANG.

Looking now at the expression of ANG in the human SH-SY5Y mock cells and SH-SY5Y APPwt, it is evident that it is significantly increased in the mutants (Fig. 28). This can be explained by the fact that the levels of Aβ1-40 are significantly lower compared with the mutants of the HEK293 cell model [340,341]. Therefore SH-SY5Y APPwt represents a cell model for initial sporadic AD [341]. As a result, the cellular stress level is significantly lower, and ANG continues to be produced at increased levels during the stress response. If one follows the hypothesis that ANG is downregulated or no longer upregulated during chronic stress, a reduction or at least no change in ANG expression should be observed when SH-SY5Y cells are treated with 5 µM rotenone. This is exactly what was found experimentally (Fig. 30). Although ANG expression increases in the control cell line SH-SY5Y Mock, it is significantly lower than the SH-SY5Y APPwt. There is also no increase in the SH-SY5Y mutant treated with rotenone compared to the untreated APPwt. Only a significant increase in the levels of ANG compared with the SH-SY5Y Mock has been determinable, but this also occurred in the cell model without rotenone treatment and is therefore not relevant. This result also supports the hypothesis that the expression of ANG is reduced or unchanged upon chronic exposure to a stressor and that the protective response of the cell is absent, leading to increased apoptosis. Exposure to 5 µM rotenone for 24 h was not performed because initial preliminary experiments showed that a large proportion of the cells were apoptotic after this incubation period, and thus protein extraction was no longer possible.

3.2. Expression of ANG in different tissues of mice.

3.2.1. Age-dependent expression of ANG in aged mice

The biggest risk factor to develop AD is aging itself. The aging process is characterized by various dysfunctions, such as increased ROS or a decrease in synapse number. These changes are likely all triggered by mitochondrial dysfunction, leading to neurodegeneration. A total of 20 wt C57BL/6J mice were recruited to analyze how the expression of ANG behaves in an aging model. Young 3-month-old mice were used as controls, and 12-month-old mice were used as the aged group to be studied. This experiment was used to analyze whether there is a dependence between the age of the animals and the expression of ANG. The animals used are listed again under section *2.1.8. Animals* in Table 7. All animals were euthanized by cervical dislocation. Hippocampus, cerebral cortex, and cerebellum were then immediately dissected and snap-frozen in liquid nitrogen. Proteins were isolated from all tissues, followed by determination of ANG expression by WB.

3.2.1.1. Expression of ANG in mouse brain tissue

First, the expression of ANG in the brains of aged male mice was examined. A total of 12 young 3-months-old animals were used as young controls, and 8 old 12-months-old animals were used as aged cohorts. Using this model, it was possible to obtain an indication of the age dependence of ANG expression during aging itself in male and female individuals. Especially in females, AD development is more frequent in old age than in males of the same age. According to US and European reports, women account for two-thirds of all known clinical AD cases [355]. Various hypotheses try to explain this difference. In addition to the influence of estrogens, the longer lifespan of women also plays a role since aging itself represents one of the greatest risk factors [356].

First, significantly altered levels of ANG were determined in all brain areas (Fig. 31) of male mice. In the hippocampus, expression was reduced to 24.10%, in the cerebral cortex to 39.32%, and in the cerebellum to 45.94%. A clear dependence of ANG levels based on age can be deduced based on the determined changes.

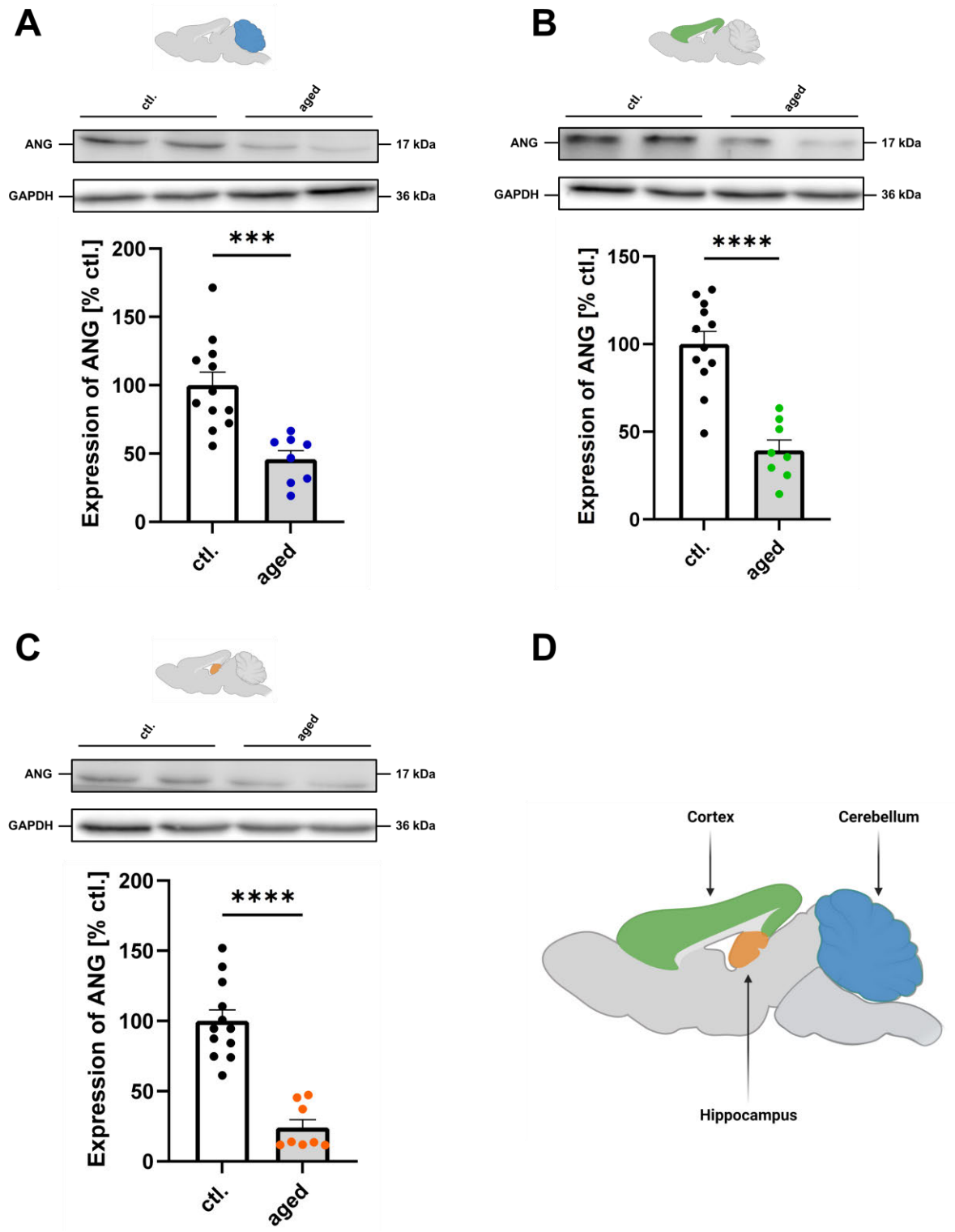

Figure 31. Expression of ANG in mouse male brain tissue. **(A)** Expression of ANG in mouse cerebellum. **(B)** Expression of ANG in mouse cerebral cortex. **(C)** Expression of ANG in mouse hippocampus. **(D)** Dissected brain areas. Data are expressed as mean ± SEM; student's unpaired t-test (*p <0.05; **p <0.01, ***p <0.001, ****p <0.0001). n = 8-12. n = 1 is equivalent to 1 animal.

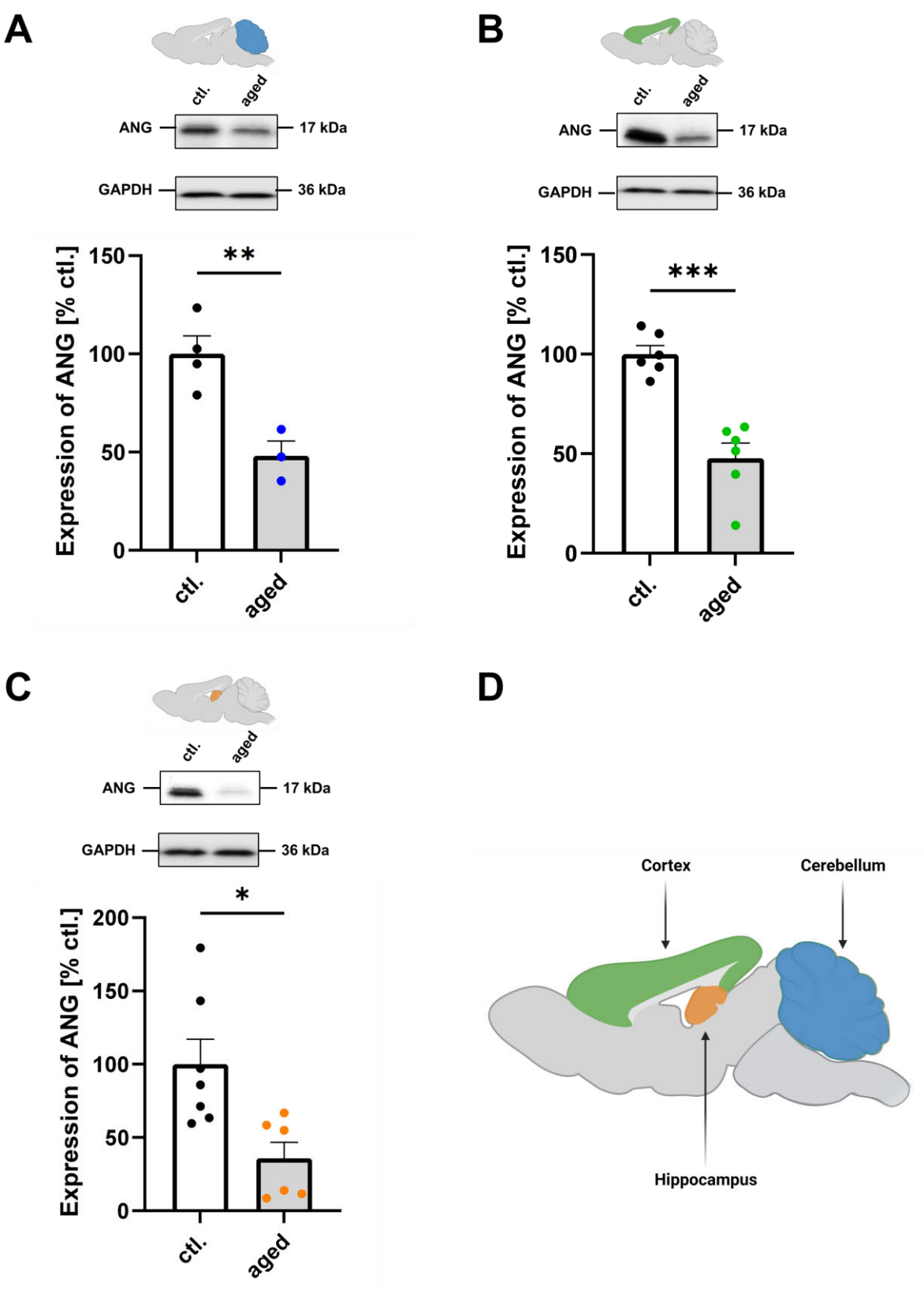

Figure 32. Expression of ANG in mouse female brain tissue. **(A)** Expression of ANG in mouse cerebellum. **(B)** Expression of ANG in mouse cerebral cortex. **(C)** Expression of ANG in mouse hippocampus. **(D)** Dissected brain areas. Data are expressed as mean ± SEM; student's unpaired t-test (*p <0.05; **p <0.01, ***p <0.001). n = 3-7. n = 1 is equivalent to 1 animal.

Second, a significant alteration in ANG expression was determined in the female mice in all dissected brain areas. In the cerebellum, the levels were only 48.12% (Fig. 32 A), in the cerebral cortex, 47.74% (Fig. 32 B), and in the hippocampus, 35.72% (Fig 32 C) compared to the 3-month-old young control. Thus, a reduction of ANG levels in all brain areas used is also seen in the female individuals, just as in the males.

3.2.1.2. Determination of the expression of ANG in additional organs of aged and transgenic mice

From all animals, the organs heart, lung, liver, and kidney were dissected again to verify whether the effects were observed in section *3.2.1.1. Expression of ANG in mouse brain tissue* occurs only centrally in the brain or peripherally. Also, in the following section, transgenic mice have already been studied here to provide a link to the AD dependent effect and to study AD specific effects in central tissues. Again, all animals were euthanized by cervical dislocation, and the corresponding organs were subsequently snap-frozen in liquid nitrogen. Proteins were then extracted from all organs, and WB determined ANG expression.

3.2.1.2.1. Expression of ANG in Liver of male and female mice.

In general, the liver plays an important role for ANG since it is an essential organ, which usually is mainly responsible for the metabolism and detoxification of various substances in the human body. For this reason, it is of particular interest to determine whether the effects previously found can also be observed in the liver periphery.

Initially, the discovery of another band during the evaluation of the WB was striking. This band originates from the presence of the ANG dimer, which could be detected for the first time in the liver compared to the brain samples. As the monomer, the dimer continues to possess ribonuclease activity [[174]]. The expression of ANG in the *m* yWT, *m* yTG, *m* oTG, *f* yWT, *f* yTG, *f* oTG shows no significant alterations compared to the respective control. However, a slight but not significant decrease in ANG levels was observed in the *m* oWT. Such a trend can also be observed in the *f* oWT, but it is insignificant. Looking now at the results of the expression of the ANG dimer, no significant change can be seen in the cohort of *m* yWT, *m* yTG, *m* oWT, *m* oTG, *f* yWT,

and *f* oTG. In contrast, a significant increase in ANG level was observed in *f* yTG and *f* oWT compared with the respective control. Especially in *f* oWT, the increase is again more pronounced than in *f* yTG.

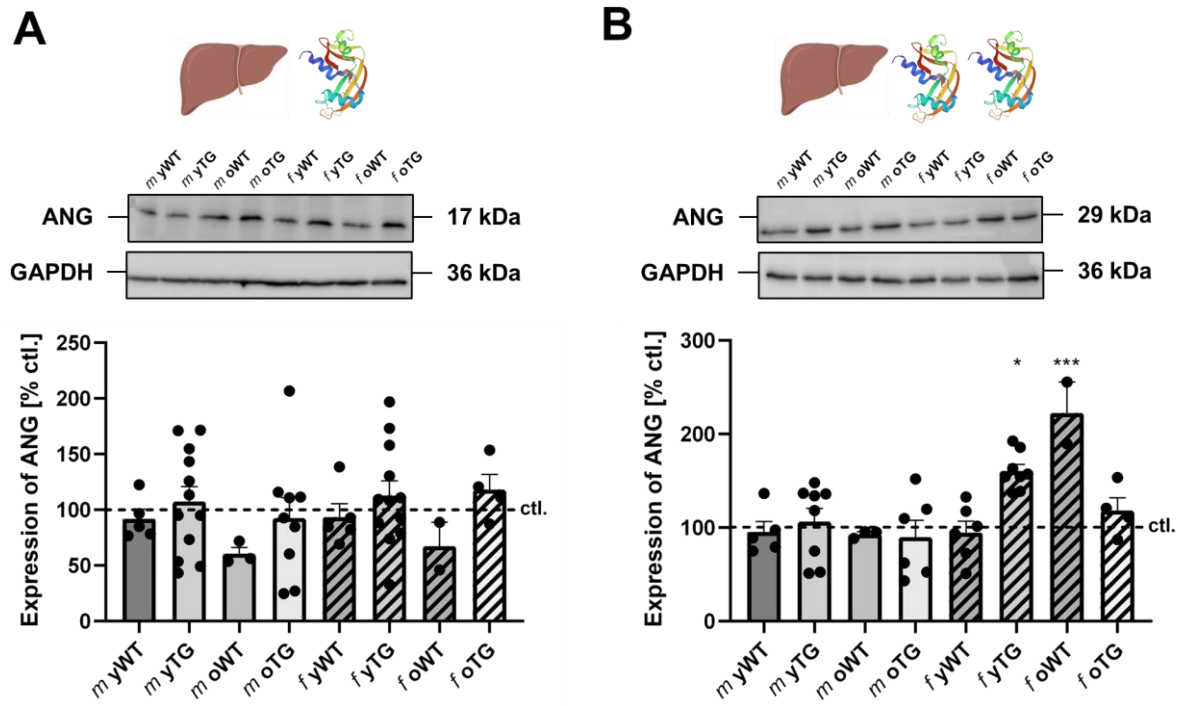

Figure 33. (A) Expression of ANG Monomer and **(B)** ANG Dimer in mouse liver tissue. Data are expressed as mean ± SEM; one-way ANOVA (*p <0.05; **p <0.01, ***p <0.001). n = 2-12. n = 1 is equivalent to 1 animal. Blank bars represent male individuals. Striped bars represent female individuals. **Abbr.:** ctl.: control, *m* yWT: male young wildtype, *m* yTG: male young transgenic, *m* oWT: male old wildtype, *f* yWT: female young wildtype, *f* yTG: female young transgenic, *f* oWT: female old wildtype, *f* oTG: female old transgenic.

3.2.1.2.2. Expression of ANG in heart of male and female mice.

Second, the determination of ANG expression was not possible because no ANG could be detected during the illumination of WB. Different concentrations (20 µg – 80 µg) of protein extract were tested, resulting in no ANG expression in heart tissue. This result also matches broad expression analyses of the human proteome, in which the expression of ANG was determined by RNAseq and was also barely detectable compared to other organs [357].

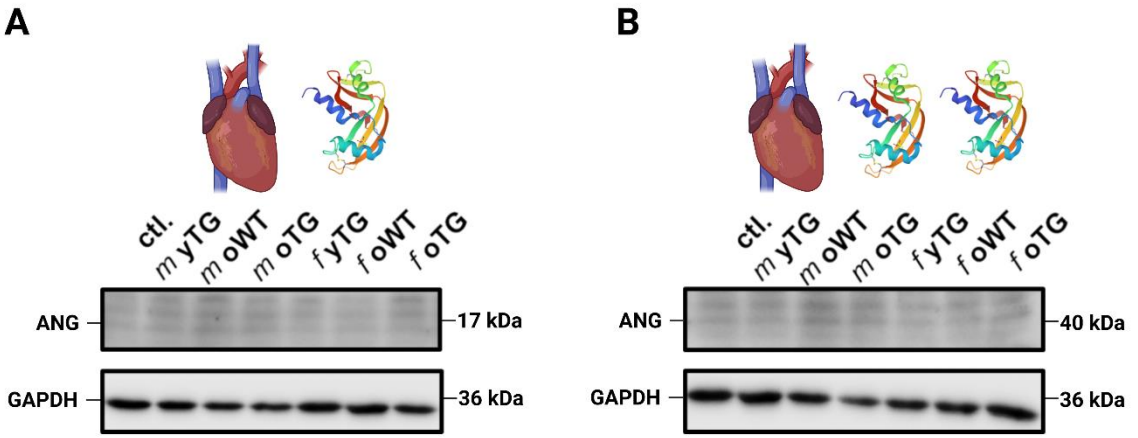

Figure 34. (A) Expression of ANG monomer and **(B)** ANG Dimer in mouse heart tissue. **Abbr.:** ctl.: control, m yTG: male young transgenic, m oWT: male old wildtype, f yTG: female young transgenic, f oWT: female old wildtype, f oTG: female old transgenic.

3.2.1.2.3. Expression of ANG in lung of male and female mice

Third, expression levels of ANG were determined in lung tissue.

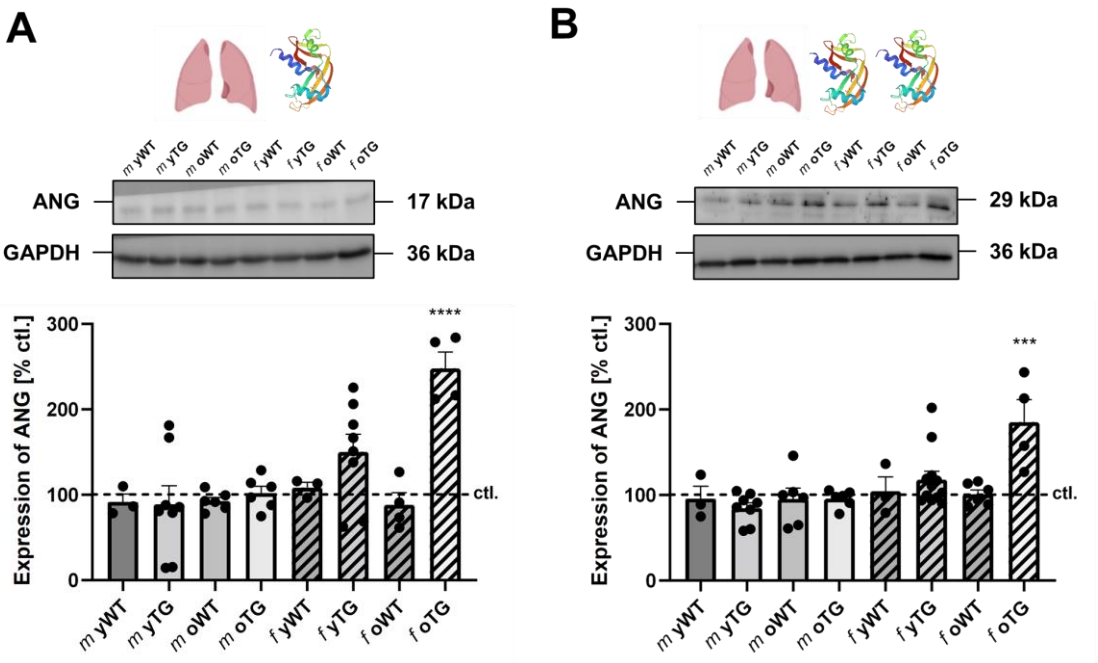

Figure 35. (A) Expression of ANG monomer and **(B)** dimer in mice lung. Data are expressed as mean ± SEM; one-way ANOVA (*p <0.05; **p <0.01, ***p <0.001, ****p <0.0001). n = 2-10. n = 1 is equivalent to 1 animal. Blank bars represent male individuals. Striped bars represent female individuals. **Abbr.:** ctl.: control, *m* yWT: male young wildtype, *m* yTG: male young transgenic, *m* oWT: male old wildtype, *f* yWT: female young wildtype, *f* yTG: female young transgenic, *f* oWT: female old wildtype, *f* oTG: female old transgenic.

No alterations are detected in *m* yWT, *m* yTG, *m* oWT, *m* oTG, *f* yWT and *f* oWT in ANG monomer compared to the respective control. An increased tendency could be detected in *f* yTG. A significant increase could be determined in *f* oTG compared to the respective old control. The same tendency could be determined in ANG dimer. No alterations in ANG expression are determined in *m* yWT, *m* yTG, *m* oWT, *m* oTG, *f* yWT, and *f* oWT. *F* yTG shows a small tendency of increased ANG levels. A significant increase in expression of ANG dimer was detected in *f* oTG.

3.2.1.2.4. Expression of ANG in kidney of male and female mice

Fourth, expression levels of ANG were determined in kidney tissue. No alterations in the ANG monomer were detected in *m* yWT, *m* yTG, *m* oWT, *m* oTG, *f* yWT, and *f* o WT compared to the respective control. A decreased tendency could be detected in *f* yTG, and *f* oTG. No alterations in the ANG dimer could be detected. Only a slight decreased trend in *f* yTG, and *f* oTG can be seen.

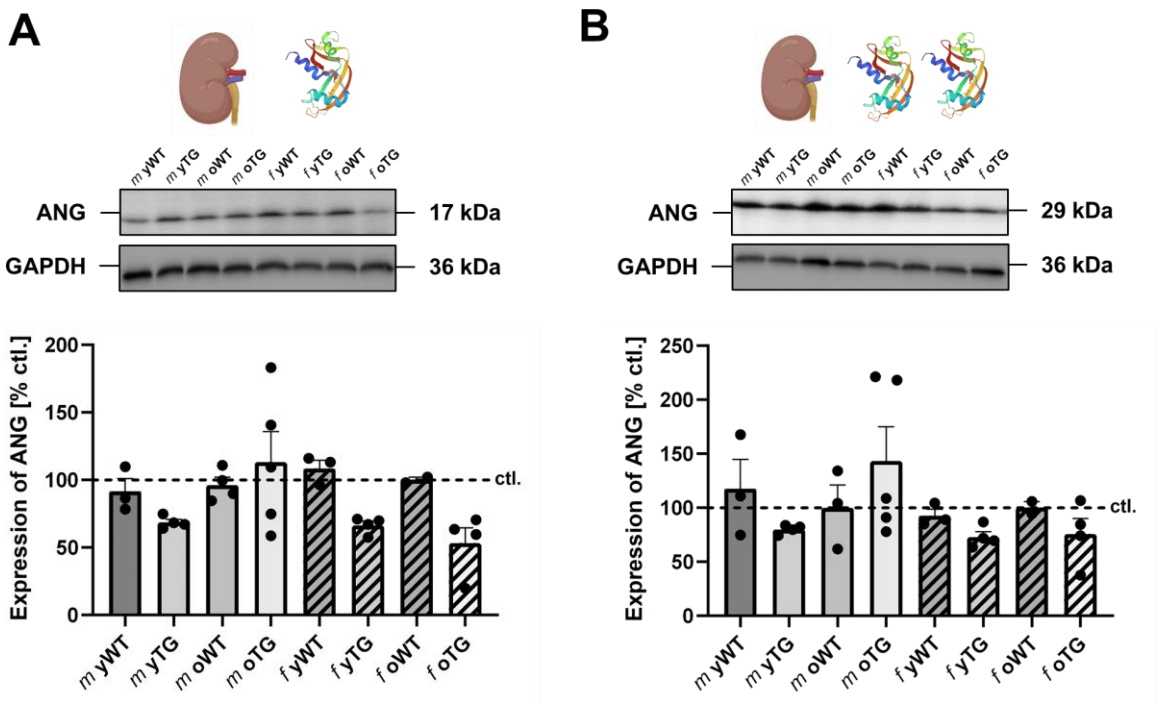

Figure 36. **(A)** Expression of ANG monomer and **(B)** dimer in mice kidney. Data are expressed as mean ± SEM. one-way ANOVA, n = 2-8. n = 1 is equivalent to 1 animal. Blank bars represent male individuals. Striped bars represent female individuals. **Abbr.:** ctl.: control, *m* yWT: male young wildtype, *m* yTG: male young transgenic, *m* oWT: male old wildtype, *f* yWT: female young wildtype, *f* yTG: female young transgenic, *f* oWT: female old wildtype, *f* oTG: female old transgenic.

3.2.1.2.5. Comparison of Expression of ANG in mouse organs

Table 12. Overview of ANG expression in all dissected mouse organs. Arrows show significant changes, arrows in brackets show non-significant trends.

	Organ	*m* yWT	*m* yTG	*m* oWT	*m* oTG	*f* yWT	*f* yTG	*f* oWT	*f* oTG
Monomer	Liver	↔	↔	(↓)	↔	↔	↔	(↓)	↔
	Heart	-	-	-	-	-	-	-	-
	Lung	↔	↔	↔	↔	↔	(↑)	↔	↑
	Kidney	↔	(↓)	↔	↔	↔	(↓)	↔	(↓)
Dimer	Liver	↔	↔	↔	↔	↔	↑	↑	↔
	Heart	-	-	-	-	-	-	-	-
	Lung	↔	↔	↔	↔	↔	↔	↔	↑
	Kidney	↔	↔	↔	(↑)	↔	↔	↔	↔

3.2.2. AD-dependent dysregulation of expression of ANG in transgenic mice

Since the results obtained previously refer only to the process of aging, the next step was to use an AD model, which allowed us to study the impact of AD on the expression of ANG. We obtained transgenic (tg) 5X FAD mice for this experiment, also known as Tg6799 strain. This is a widely used mouse model because it has many AD-related phenotypes and shows the disease's early and aggressive appearance.

The aged animals were also included in all assays to create better comparability for completeness. In all cases, the results are described in *3.2.1.1. Expression of ANG in mouse brain* could be confirmed again. All young transgenic animals (yTG) were referred to the young control (3-month-old animals), the old transgenic animals (oTG) to the respective old control (12-month-old animals). In all transgenic animals, a tendency or, in some cases, a significant effect can be observed for ANG. A tendency toward increasing ANG levels could be observed in the cerebellum of both young males (yTG, Fig. 37 A) and old male transgenic animals (oTG, Fig. 37 A). Interestingly, an exactly opposite effect is observed in the comparable female samples (female yTG and oTG, Fig. 37 B). In the female yTG animals, even a significant decrease in ANG expression is observed compared to the control. In contrast, the old female transgenic

cerebellum samples show no change in ANG expression but only a tendency to decrease.

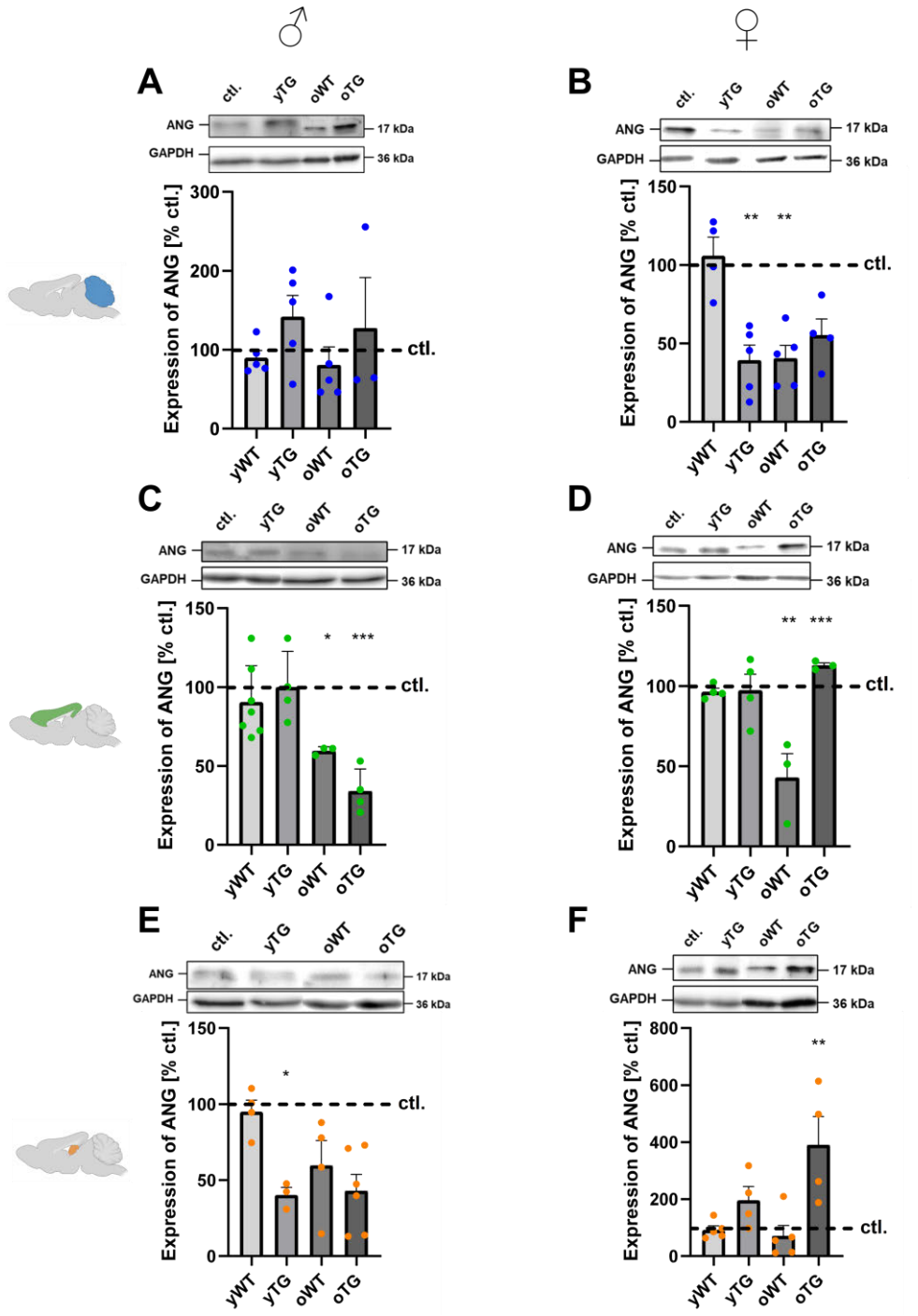

Figure 37. Expression of ANG in murine male and female brain tissue. **(A)** Expression of ANG in male mouse cerebellum. **(B)** Expression of ANG in female mouse cerebellum. **(C)** Expression of ANG in mouse male cerebral cortex. **(D)** Expression of ANG in mouse female cerebral cortex. **(E)** Expression of ANG in mouse male hippocampus. **(F)** Expression of ANG in mouse female hippocampus. Data are expressed as mean ± SEM; one-way ANOVA (*p <0.05; **p <0.01, ***p <0.001). n = 3-7. n = 1 is equivalent to 1 animal. **Abbr.:** ctl.: control, yTG: young transgenic, oWT: old wildtype, oTG: old transgenic.

The cerebellum was chosen as a negative control for the experiment because there is largely no association with AD in this brain area. In contrast, no change in the cerebral cortex is observed in male yTG (Fig. 37 C) and female yTG (Fig. 37 D). Interestingly, however, a significant change is observed in the old animals. A significant decrease in the expression of ANG was observed in the cortex of male oTG. In contrast, the cortex of female oTG surprisingly shows a significant increase in ANG expression levels compared to the respective control. Also, male and female oWT show significantly decreased expression of ANG. In the hippocampal region, a significant decrease in ANG expression is observed in male yTG (Fig. 37 E). An equal but nonsignificant change is also observed in male oTG (Fig. 37 E). In contrast to the male transgenic animals, a significant increase in ANG expression of female mice was observed in oTG (Fig. 37 F). The female yTG only shows a slightly increased tendency, but it is nonsignificant. Thus, it was found that significant effects were observed in the cerebral cortex and hippocampus brain regions relevant to AD. Interestingly, these effects are also exactly opposite in gender in most cases. Such gender-specific effects are particularly interesting.

3.2.3. Sex dependent differences of ANG expression in different brain areas of young and old transgenic mice.

Against the background that the exposure of women to AD is significantly higher, it is worthwhile to compare the expression of ANG values in the different brain areas. Comparing the male and female results, it quickly becomes clear that partly opposite effects can be observed. The expression of ANG is decreased in male yTG but increased in female yTG, looking at the levels in the hippocampus. Surprisingly, the levels in the cerebellum are also exactly opposite, e.g., they were increased in male yTG and decreased in female yTG. In the cerebral cortex, however, the values were the same. Surprisingly, in all aged animals, the differences in males and females are not observed. In aged tg animals, a sex-specific effect is again observed. In male oTG, ANG expression is decreased in both hippocampus and cortex but increased in the cerebellum. In female oTG, just the opposite is observed.

Table 13. Overview of Expression of ANG in different sex. Arrows show significant changes, arrows in brackets show non-significant trends. **Abbr.**: Hip: hippocampus, Cx: cerebral cortex.

	yWT			yTG			oWT			oTG		
	Hip	**Cx**	**Cere**	**Hip**	**Cx**	**Cere**	**Hip**	**Cx**	**Cere**	**Hip**	**Cx**	**Cere**
♂	↔	↔	↔	↓	↔	(↑)	(↓)	↓	↔	(↓)	↓	(↑)
♀	↔	↔	↔	(↑)	↔	↓	(↓)	↓	↓	↑	↑	(↓)

3.2.4. Discussion

After determining ANG expression in aged individuals, a significant decrease in ANG levels was observed in both males and females. In the brain area of the hippocampus, cerebral cortex, and cerebellum, this effect was observed in all animals. All aged animals were 12 months old. A mouse ages about 25 times faster than a human [358]. Concerning the total life span of a laboratory mouse, the total survival curve already decreases dramatically at this stage. For this reason, this model is perfectly suitable as an aging model. The aging process also leads to various cellular changes in mice and generally represents the greatest risk factor for developing neurodegenerative diseases such as AD. Declining cognitive performance, decreased mitochondrial function, increased ROS levels, and generally slowed cellular processes are classic changes associated with aging. These processes also lead to persistent stress in the cells, as the antioxidant system, for example, is significantly less active. Due to these aging processes, it has already been described in the literature that protein biosynthesis is inhibited [359]. This could be an explanation for reduced ANG levels. If one revisits the hypothesis from the beginning of this section, which states that ANG expression is downregulated during chronic stress, this also applies in this case. Persistently elevated ROS levels and altered mitochondrial function up to mitochondrial dysfunction lead to chronic stress response in the body and trigger an increased occurrence of apoptotic processes in the cells of various tissues. In neurons, such a process then leads to the process of neurodegeneration, which in the long term leads to the development of neurodegenerative diseases such as AD. Since the expression of ANG is reduced in the hippocampus and cerebral cortex, which are particularly affected in AD, it can be assumed that the neuroprotective effect of ANG is lost due to reduced ANG levels [329,360]. As a result, pro-apoptotic signaling is no longer inhibited by cleavage of tRNA and the derived fragments but may now be enhanced

by activating caspase 3 and 9. The consequence is an additional pro-neurodegenerative mechanism which, as a consequence of the process of aging, further enhances this progression.

Considering the results of the experiments with brain tissue in the 5X FAD mice, many statements can be made. First of all, the 5X FAD model is one of the most striking AD models of all since the animals show first symptoms already at the age of 3 months, which progress rapidly over time. For this reason, brain samples were taken both at the onset of the first symptoms, at 3 months of age, and 12 months of age. This provides an AD model covering both early and late AD forms. Both young and aged wt C57BL/6J mice served as controls. Among all results, in both yTG and oTG, the cerebellar brain area behaves opposite to the hippocampus and cerebral cortex in all sexes. The cerebellum is used as a negative control, as little to no influence of AD is described here. This makes the resulting significance of the results more important since this affects all samples. In this experiment, however, the complexity of the disease AD became clear once again, as even effects between the individual sexes could be determined. In the yTG animals, it is immediately evident that ANG expression in males is exactly the opposite of that in females. The males show significantly decreased ANG levels in the hippocampus, while the females show an increased tendency. This would imply that the protective effect of ANG in the hippocampus is absent in males, and neurodegeneration is enhanced in this area. On the other hand, females should have increased protection against neurodegeneration, according to these results. The increase could be because more Aβ was present in the individuals than in the corresponding males. However, it is clear that not only this one mechanism is involved in neurodegeneration in the development of AD. The prevalence of AD is generally higher in females than in males. This is mainly due to the influence of estrogens and the overall more extended life expectancy of women [355]. Since aging is one of the most important factors, it could be that the influence of mitochondrial dysfunction and increased ROS levels prevails, and neurodegeneration is triggered over time. This sex-specific effect is also found in the cerebellum, where expression varies within each sex on the one hand but also, on the other hand, differs in comparison. In the 12-month-old oTG animals, this trend is again confirmed. Here, the same results were obtained as in the yTG. Only an effect in the cerebral cortex was added here, also sex-specific. Here, too, the hypothesis established earlier applies. Another point could be that, as in ALS and PD, a loss-of-function mutation is also

present in ANG [179,328,361]. This would mean that ANG no longer has ribonuclease activity, no matter how highly expressed. Since this mechanism has already occurred in other neurodegenerative diseases, likely, this is also the case in AD. Initial studies have already identified ANG mutation in AD patients, but its function or effect remains still unclear [361]. Subsequently, it would be interesting to study 24-month-old animals to determine whether the permanent chronic stress caused by Aβ in TG animals leads to reduced ANG expression, as shown in the cell model. However, this is almost impossible because many mice die naturally before this age. However, this experiment demonstrated an AD-specific effect on ANG expression, especially in females.

Since the previously obtained results were all from central tissues, it is even more interesting to see if these changes also occur in the periphery. Starting with the liver, strikingly, both male oWT and female oWT showed a decrease in ANG expression in the ANG monomer. Just as in the brain areas hippocampus, cerebral cortex, and cerebellum, age-related dysregulation also occurs. A clear trend can be seen in females, but this change is not significant. These results support the earlier hypothesis that age-related cellular changes lead to a significant decrease in ANG expression. This implies that in addition to the lack of neuroprotective effect in old age, the apoptosis inhibitory effect on the liver cells may also be absent. This would also support the aging process in peripheral tissues and further progression induced by mitochondrial dysfunction and increased ROS levels. ANG dimer's expression also shows a significant change, but only in females. However, these results are consistent with those of previous studies, in which the expression of ANG was also frequently upregulated in yTG and oTG. However, further studies are needed here, as the ANG dimer is largely unexplored; only the ribonuclease activity, which remains conserved, is known [174].

Finally, significant peripheral changes in ANG expression were found in the liver and lung. However, no change could be detected in the kidney, and no ANG was detectable at all in the heart. These peripherally found effects show that there are not only central changes in the brain. This is particularly interesting since changes such as mitochondrial dysfunction have already been found in lymphocytes of AD patients [331,332,334,336,362,363]. New possibilities arise from this result, e.g., involvement of ANG in the pathophysiology of AD, and histological tissue analysis of the periphery may allow early determination of a change with disease onset.

The next interesting step for analysis would be the blood analysis, as it has already been described that peripheral changes such as mitochondrial dysfunction and increased ROS levels in AD patients have already been observed in lymphocytes [331,332,334,336,362,363].

3.3. Expression of ANG in rats

3.3.1. ANG Expression in rat hippocampus and cerebral cortex

To investigate the previously observed changes also in a different model, we used the TgF344-AD rat model. The rats show an age-dependent increase in Aβ40 and Aβ42 levels at 6-26 months. An advantage of the model is that the number of neurons in the hippocampus and cerebral cortex is comparable to the number of neurons in wt rats at the same age between 6-26 months [343]. A total of 16 animals were recruited for ANG expression analysis. From each sex, 2 wt and 2 tg animals were used at 6 and 15 months of age, respectively. This ensures that the pathophysiology of AD is just beginning in the young model.

In Fig. 38 A and B, the expression of ANG in the hippocampus of male and female rats is shown. A significant increase in ANG levels was observed in aged male transgenic animals (oTG) compared with the wildtype. No alterations were observed in all other cohorts. In female rats, no change in ANG expression was also detected. A significant increase in ANG levels was detected in the cerebral cortex of male young transgenic rats (yTG) (Fig. 38 C) compared with the control. The increase in oTG in the hippocampus is at least a trend but not significant. In the cortex of female rats, as in the hippocampus, no altered ANG expression is found in all cohorts.

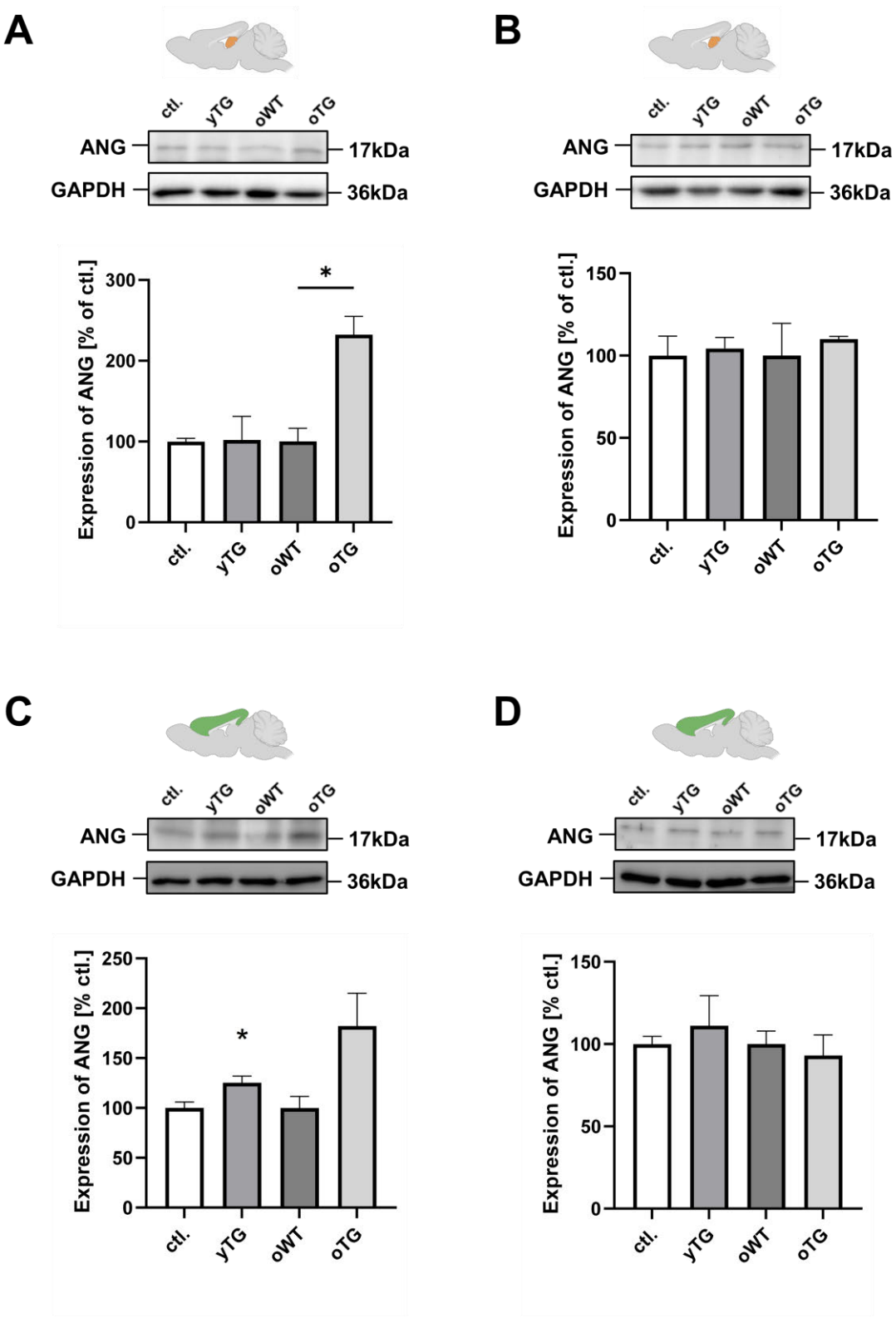

Figure 38. Expression of ANG in rat brains. **(A)** Expression of ANG in hippocampus of male rats **(B)** Expression of ANG in hippocampus of female rats **(C)** Expression of ANG in cerebral cortex of male rats **(D)** Expression of ANG in cerebral cortex of female rats. Data are expressed as mean ± SEM; student's unpaired t-test (*p <0.05). n = 2. n = 1 is equivalent to 1 animal. **Abbr.:** ctl.: control, yTG: young transgenic, oWT: old wildtype, oTG: old transgenic.

Table 14. Expression of ANG in TgF344- and wt rats. Arrows show significant changes, arrows in brackets show non-significant trends. **Abbr.**: Hip: hippocampus, Cx: cerebral cortex.

	yTG		oWT		oTG	
	Hip	**Cx**	**Hip**	**Cx**	**Hip**	**Cx**
♂	↔	↑	↔	↔	↑	(↑)
♀	↔	↔	↔	↔	↔	↔

3.4.2. Discussion

Compared to the 5X FAD mouse model, the TgF344 AD model represents a much weaker relation to the progression of AD because the levels of Aβ 1-40 are much lower. For this reason, the model cannot be directly compared with the very strongly progressive 5X FAD mouse model. Also, only 2 animals per cohort were obtained, which reduces comparability. It is also striking that the previously sex-specific effects found in both the 5X FAD and the human model are not present. This could be because of the different model used for this experiment. No alterations in expression have been determined in both the hippocampus and cerebral cortex in females. In males, a significant increase has been observed in the hippocampus in oTG and the cortex in yTG and a trend in oTG. However, to what extent these results fit into the thesis stated at the beginning is difficult to say because of the small *n* number. Small outliers are also repeatedly observed in the mouse and human samples. In the case of rats, due to the number of only 2 animals, no exact mean value can be calculated and further analyses still have to be performed.

3.5. Human brain tissue samples

3.5.2. Expression of ANG in human cortical brain tissue

To further investigate the previously obtained results, the next logical step was to study human samples from elderly and AD patients. The Netherland Brain Bank (NBB), based in Amsterdam, provided the samples. In total, we received 32 human cerebral cortex samples. We obtained 14 female and 6 male AD cortexes and 6 female and male non-demented control subjects. In this way, we covered a broad cohort of different individuals. In this experiment, the influence of both AD and aging on ANG

expression was investigated. All AD patients were compared with the non-demented control group.

Fig. 39 shows the expression of ANG monomers (region *A* and *C*) and ANG dimers (region *B* and *D*). Surprisingly, for the ANG monomer, the results of the mouse experiments could be confirmed in both male and female patients, especially regarding the sex differences. This refers to the expression of the ANG monomer, as the dimer could not be detected in the mouse model. In the cohort of AD patients, a significant reduction in the expression of the ANG monomer was observed in the cortex (Fig. 39 A*).* In contrast, the ANG dimer (Fig. 39 B) showed only a trend toward decrease compared with the nondemented control. In contrast, the female patients showed a significant increase in the expression of the ANG monomer in the cortex compared with the nondemented control subjects (Fig. 39 C). ANG dimer expression also showed a significant increase in ANG levels (Fig. 39 D). Thus, an exactly opposite effect was observed in the female patients concerning the expression of the ANG monomer and the ANG dimer compared with the male individuals.

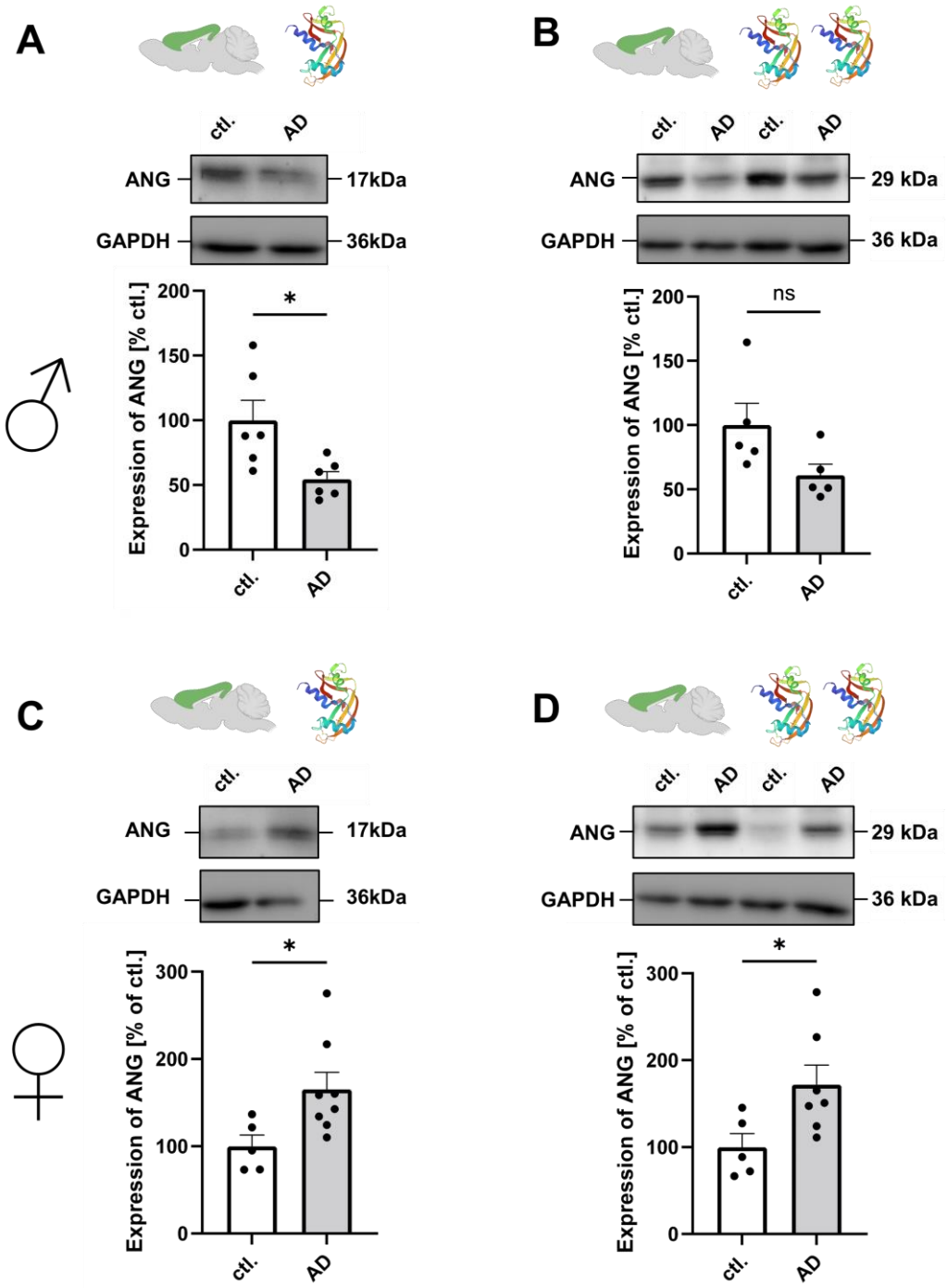

Figure 39. Expression of ANG monomer and ANG dimer in human brain tissue. **(A)** Expression of ANG in cerebral cortex of male and **(B)** female brain tissue. Data are expressed as mean ± SEM; student's unpaired t-test (*p <0.05). n = 5-8. n = 1 is equivalent to 1 human individuum.

To explore the aging effect, "non-demented controls" were used and divided into two groups according to age, each with a difference of about 10 years. The younger control group served as the control, and the older group served as the cohort to be analyzed. Analysis of the ANG monomer and dimer was again performed using WB.

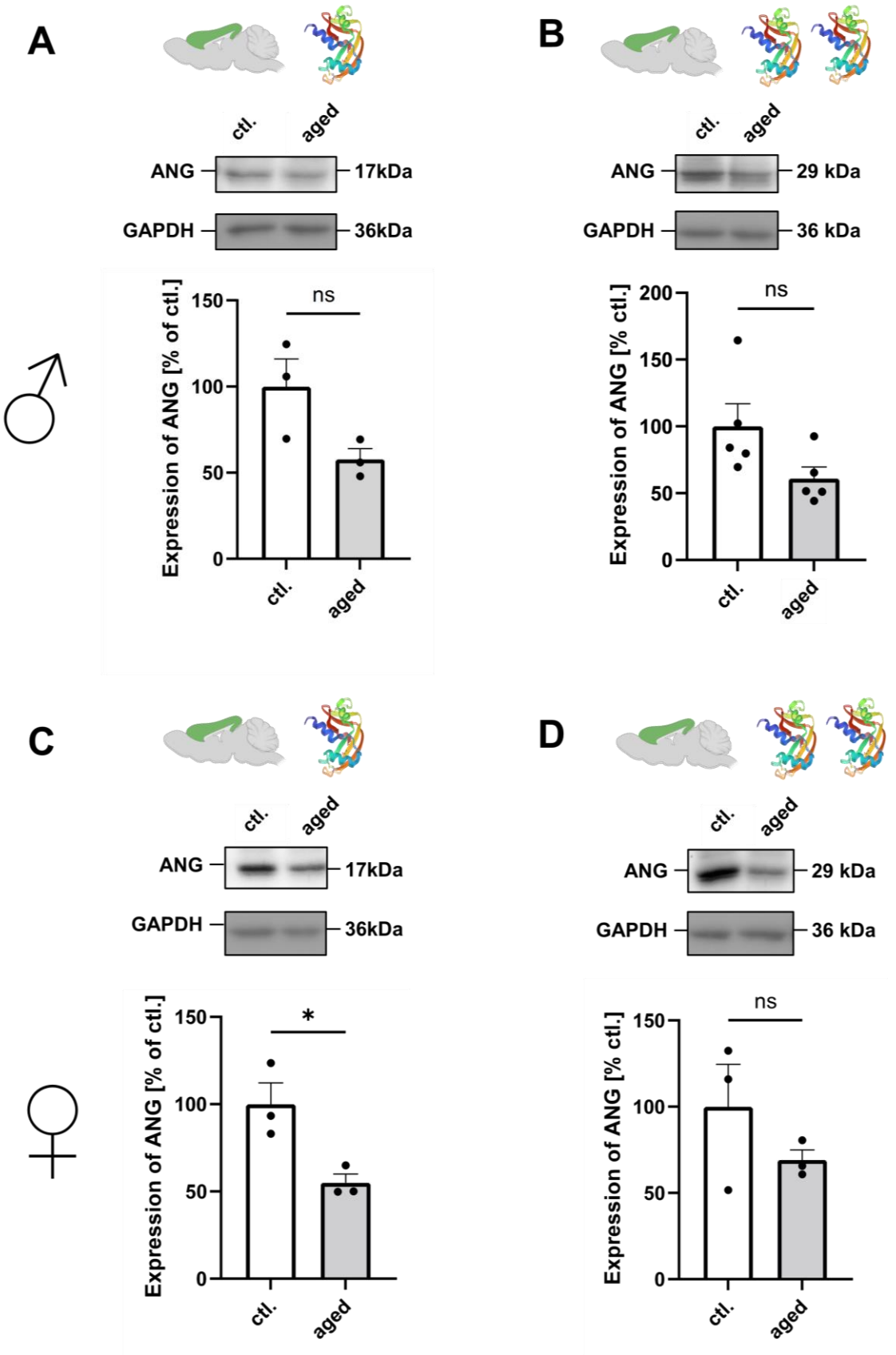

Figure 40. Expression of ANG monomer and ANG dimer in aged human brain tissue. **(A)** Expression of ANG in cerebral cortex of male and **(B)** female brain tissue. Data are expressed as mean ± SEM; student's unpaired t-test (*p <0.05). n = 3-5. n = 1 is equivalent to 1 human individuum.

Fig. 40 shows the analysis of the aged brains. In the cerebral cortex of the male patients, there is no significant change in the expression of the ANG monomer and the dimer, but a decreasing trend (areas A and B) is detectable. This is consistent with the decrease in ANG levels in the older cohort as observed in the mouse model. In contrast, a significant decrease in the expression of the ANG monomer can be observed in female patients (area C). The ANG dimer also shows no significant change but, as in the male individuals, a trend toward reduced ANG levels (area D).

3.5.3. Age-dependent reduced expression of ANG in human hippocampus and cortex brain samples from human Aging, Dementia and TBI study

Last, we analyzed RNA sequencing datasets from 107 brains, including 377 samples from cortical grey (parietal and temporal) and white matter (parietal) and hippocampus, to determine the alteration and expression of ANG in clinical patient datasets from the *Aging, Dementia, and TBI Study*. After the analysis, the RNAseq datasets were divided into the following age groups: 75-80, 81-85, 86-89, 90-94, and 95-99. On this basis, the age dependence of ANG expression can be re-examined.

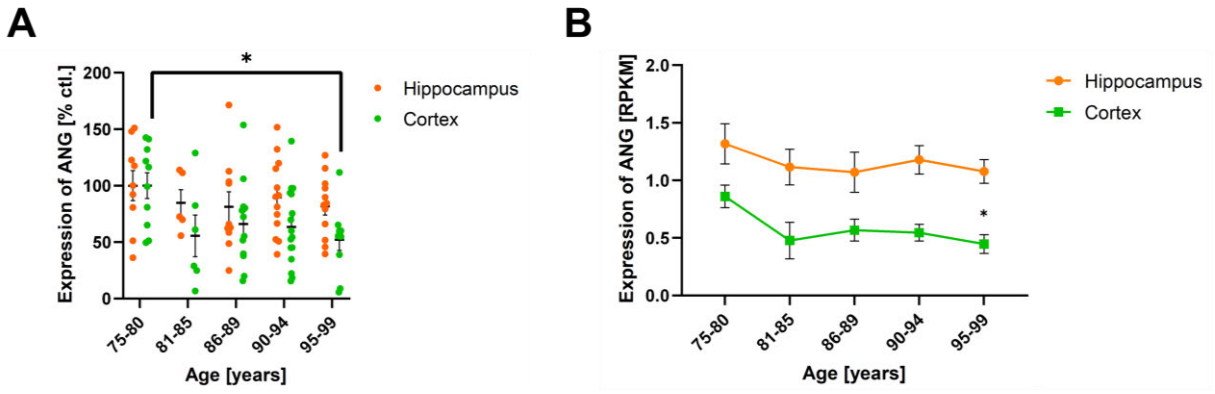

Figure 41. Expression of ANG in different aged cohorts. **(A)** Dysregulation of ANG during aging in the human cerebral cortex and hippocampus. **(B)** Mean values of ANGs expression in cerebal cortex and hippocampus. Data are expressed as mean ± SEM; student's unpaired t-test (*p <0.05). n = 3-5. n = 1 is equivalent to 1 human individuum.

The expression of ANG in the cerebral cortex decreases significantly over time in older groups (Fig. 41). The ANG level in the oldest group of 95-99 years was only 52.04%

compared to the respective control group. A decreasing trend is also observed in the hippocampus, but it is not significant. Again, the results obtained here strengthen the thesis that ANG expression decreases with age.

3.5.4. Discussion

Analysis of human cortical brain samples confirmed the results obtained in the experiments with aged and 5X FAD mice. In the male individuals, as in the 5X FAD animals, a significant reduction was confirmed in the cerebral cortex, whereas in the females, a significant increase in ANG expression was detected (Fig. 39 A, C). Surprisingly, the effect of age-related dysregulation of ANG could also be determined experimentally (Fig. 40 A, C). These results also confirm the hypothesis made at the beginning of this work that the expression of ANG is influenced by aging processes and during the progression of AD. Exactly what these factors are cannot be said at this time. What is clear is that the effect is not only caused by Aβ plaques or hyperphosphorylated tau tangles. This claim can be confirmed because a reduction in ANG expression was observed equally in both male-aged and 5X FAD animals. Since the 5X FAD animals had significantly increased levels of Aβ1-40 compared with naturally aged animals, a sole influence of this stressor is unlikely. The results of the human brain samples confirm this, as there were patients with and without Aβ plaques in the male individuals. Aging itself is an important factor as processes such as mitochondrial dysfunction and increased ROS concentrations continue to progress. An additional stressor such as Aβ could promote this progression but is not solely responsible. The observation that upregulation was found in female 5X-FAD mice, and human individuals confirm this consideration. Therefore, it cannot be excluded that the presence of Aβ plaques further enhances this process. Since the expression behaves differently in the female individuals, it must be assumed that AD influences the expression otherwise, the results here would also have to be similar to those in the older cohort. The results also confirm previous research findings in the literature that Aβ alone is not responsible for AD development but may play a role. The failure of various antibodies to reduce Aβ plaques further confirms this. Thus, other factors must combine with Aβ plaques, hyperphosphorylated tau, and the aging process itself to trigger such a severe progressive disease [364,365].

However, this study highlights the impact of aging on the dysregulation of ANG expression. In both the aged mouse and aged human models, a reduction in expression was observed in all cohorts across sexes. This hypothesis is again clearly supported by the analysis of the *ACT study* results. In this study, RNAseq data were evaluated to analyze the expression of various proteins. When analyzing the expression of ANG throughout different cohorts, which were subdivided by age, a significant decrease in ANG expression can be observed, as in the cortical brain samples we analyzed (Fig. 41). This trend could also be observed in the hippocampus, supporting the hypothesis, as the results were obtained in independent experiments.

The involvement of the ANG dimer should also not be ignored since little is known about its role. Since the formation of an ANG dimer requires the aggregation of two ANG monomers, the possibility of interaction with other proteins should not be ignored. However, further research is needed in this area as no results are known in the literature. Also, the possible increased or decreased interaction of an ANG dimer with tRNA during stress-induced degradation should be further explored. The previously observed sex-specific effects in the AD cohort could also be found again, so that female individuals always behave in the opposite direction to males. This also confirms the sex differences known in the literature, especially the increased expression of AD in females due to, e.g., estrogen-specific effects or longer life expectancy [356].

Thus, cross-model dysregulation of expression was found to be age-specific, on the one hand, and gender- and AD-specific, on the other, in a large-scale cohort of diverse individuals.

Chapter 4

4. Analysis of RNA modifications

It is now known that many diseases are directly related to changes at the RNA level. An emerging area is the study of tRNA and its fragments. These play a major role in translation, among other things, but also in many other regulatory mechanisms at the cellular level. In particular, during stress responses, various RNAs are up- and down-regulated to respond rapidly to the body's response. For example, it is known that tRNA can be cleaved into two halves, known as tiRNAs, when triggered by ANG. These two tiRNAs are thus able to inhibit cytochrome c-induced apoptosis. This leads to a neuroprotective effect. For this mechanism, an equilibrium of tRNA-derived fragments is crucial. If too many tiRNAs are present, this leads to an increased stress response, triggering apoptosis [204]. This example shows how close the body's protective and pathological reaction could be. However, in the case of a stress reaction, the tiRNAs can also form the previously treated SGs and pack them with mRNA. These mRNAs then contain the information for the proteins that are important for the cell's survival [204,255]. In addition to tiRNAs, there are also smaller fragments, the so-called tRFs. These are formed when a tiRNA is further degraded by ANG or Dicer [204]. These small fragments have now been widely linked to cancer because they interact with the tumor suppressor gene p53 [366]. Their role in neurodegenerative diseases is not yet known. Another factor that plays a major role is the formation of various RNA modifications. These can be, for example, modifications in the form of methylations. However, this can lead to the function of the corresponding RNA, in our case a tRNA, being completely lost or becoming a different one. An example of this is the modification m^5C. Methylations within the variable loop of tRNAs at position C48/49/50 mediated by NSUN2 protect tRNAs against the stress-induced cleavage by ANG. Lacking the RNA modification m^5C at position C48/49/50 leads to a tight binding by ANG, resulting in an accumulation of 5'-tRNA-derived small fragments [313]. On this background, we examined tRNAs, tiRNAs, and tRFs for their changes in both cells and animal models and analyzed their patterns. All of this shows that RNA research has played an increasingly important role not only since the onset of the SARS-CoV-2 pandemic. However, it has gained renewed attention as a result of mRNA vaccines.

4.1. Analysis of tRNA modifications in HEK293 cells

4.1.1. tRNA, tiRNA and tRFs

First, the known HEK293 cell model consisting of HEKut, HEK APPwt, and HEK APPsw was analyzed to determine RNA modification changes.

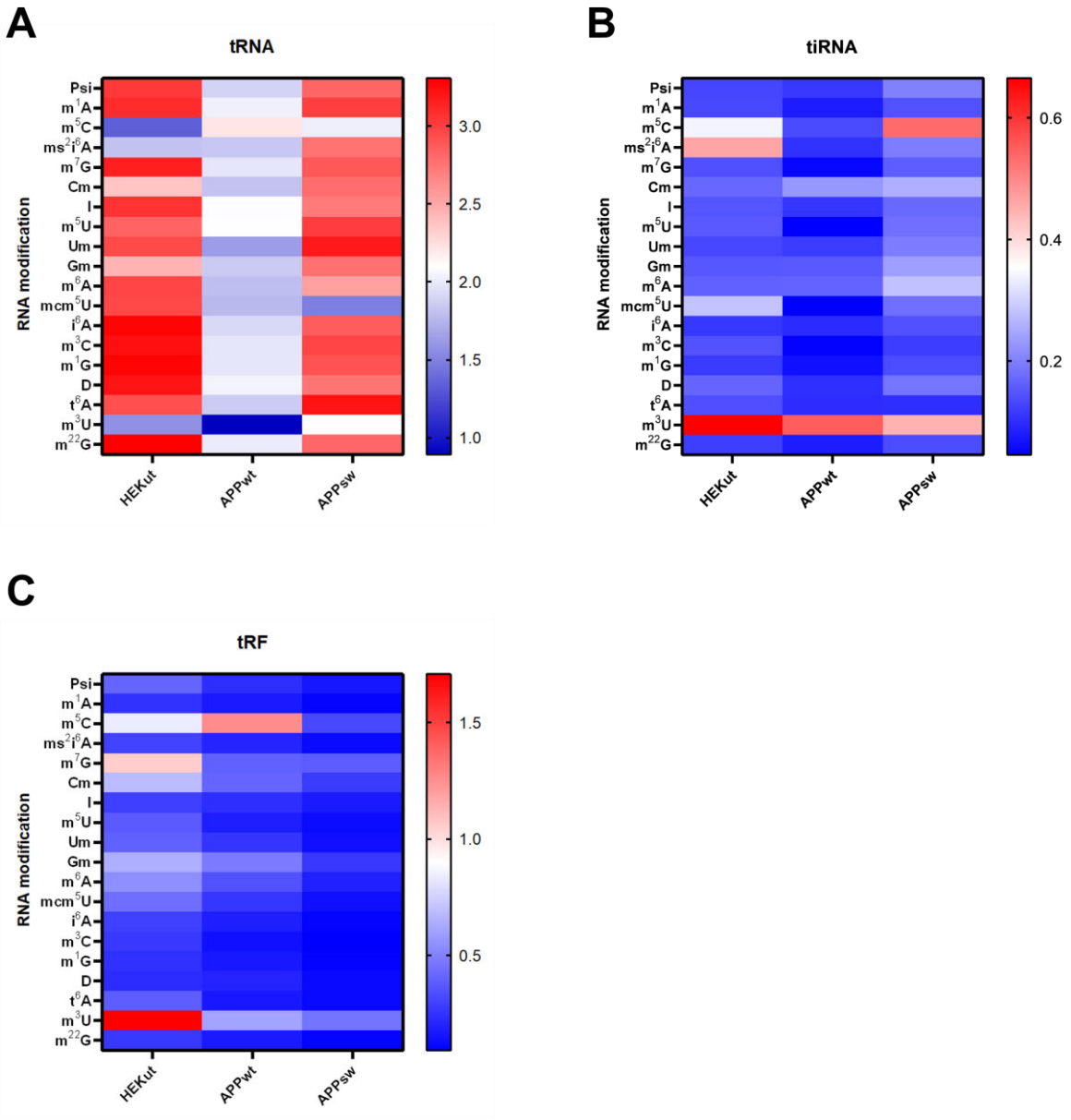

Figure 42. RNA Modifications in different tRNA-derived fragments in HEK293 cells. **(A)** Modification pattern in tRNA. **(B)** Modification pattern in tiRNA. **(C)** Modification pattern in tRF. Data are expressed as mean; n = *3* technical replicates. Each row was normalized by its mean.

A clear pattern becomes apparent in the tRNAs in Fig. 42 A. Both the HEKut control cells and the APPsw mutant show an increased number of tRNA modifications. In contrast, the APPwt cells show a rather low occurrence of modifications. This pattern is also comparable to the expression levels of ANG in the HEK cell model in section *3.1.1. Expression of ANG in HEK293 cells and SH-SY5Y cells*, where a U-shape can also be seen as the APPwt cells express less ANG. Strikingly, the modification m^5C, which normally leads to increased degradation of tRNA by ANG when it is not present, is downregulated mainly in the control cell line. In contrast, this modification tends to be downregulated in both AD models wt and sw. In contrast, the modification pattern of tiRNA is much less pronounced. Depending on the tRNA half-formed, the modification may not be present to explain that finding. Nevertheless, a slight modification pattern can also be seen in the tiRNAs. Again, both the control cell line HEKut and the AD cell line APPsw show more modifications than the MCI model APPwt. In contrast, the modification pattern of the tRFs is different. Most of the modifications are seen in the HEKut cells, decreasing from the APPwt to the APPsw cells. This can be explained by the fact that the tRFs correspond to only the size of a quarter of the tRNAs, which means that some modifications may not be detected at all. Nevertheless, the modification patterns are clearly visible, especially for the tRNAs.

4.1.2. Discussion

A clear pattern is immediately apparent looking at the results of the tRNA modifications. If instead of a heat map, one were to insert a bar graph showing the strength of expression of a modification on the y axis, a "U-shape" would be seen. This pattern was already observed in the analysis of ANG expression in HEK293 cells in section *3.1.1. Expression of ANG in HEK293 cells and SH-SY5Y cells*. There, too, the expression of ANG was significantly lower in the APPwt mutant, whereas the control HEKut and the other mutant APPsw showed stronger expression. To some extent, this pattern is also found in the tRNA modifications. Again, it is striking that the mutant APPwt has significantly fewer tRNA modifications than the other two cell lines. There is hardly any difference between the control and the mutant APPsw, which shows significantly increased levels of Aβ. Because of that, an AD-specific effect can be excluded. However, it is well worth looking at the mutant APP wt. Almost all modifications recorded on the tRNA are more or less slightly pronounced, e.g., they range from 0.0-2.2. For this reason, with one exception, no individual modification can

be singled out and a statement made about the effect of the modification. However, the modification m^5C is interesting. This modification is located at position C48/49/50 and in the literature is said to have the task to prevent the degradation of the tRNA triggered by ANG and thus to prevent a predominant cleavage of the tRNA and is thus used as a prime example for the influence of tRNA modifications on regulatory processes of the RNA. Exactly this modification m^5C is now most pronounced in the mutant APP wt. This would imply that in APPwt cells, the degradation of tRNA by ANG is increasingly prevented. However, if we look at the results obtained, it is precisely in this mutant that ANG expression is at its lowest [169,313]. Compared to the other modifications, m^5C is also less expressed in the APPsw mutant. It is known in the literature that the absence of m^5C leads to an accumulation of 5'-tiRNAs, which in turn inhibit protein translation and lead to enhanced apoptosis [169,313]. Even if the expression of ANG is significantly lower in APP wt, it could be that there is an accumulation of 5'-tiRNAs, especially in the APPsw cells, and thus apoptosis is induced to a greater extent. This would fit with the general observation that it is precisely here that m^5C is poorly expressed, and the mutants are strongly prone to apoptosis. The analysis of the RNA modifications of the tiRNAs fits this hypothesis. Admittedly, no clear pattern is detectable here because not all modifications are present on the respective halves. However, it is striking that the m^5C levels increase, especially in the APPsw mutants. This could, of course, indicate an increased presence of this modification or an accumulation of 5'-tiRNAs. Even if m^5C is theoretically less expressed, an increased presence of tRNA halves would indicate this modification as increased. However, since this is not experimentally testable, this is only an assumption. Therefore, modifications in tRFs are also difficult to evaluate since no statement can be made about which fragment is dominantly present.

4.2. Analysis of tRNA modification in an AD mouse model

After analyzing the cell model, an aged and AD mouse model was used, and the RNA modification changes were determined in young and old mice. The model used is the same as that used for ANG expression analysis. 5XFAD mice were also recruited in this experiment. RNA modifications were analyzed using LC-MS/MS.

4.2.1. RNA Modifications in young mice

To analyze RNA modification changes in young mice, 4 animals were recruited at a time. Again, the cerebellum, cerebral cortex, and hippocampus were used for analyzation of RNA modifications by LC-MS/MS.

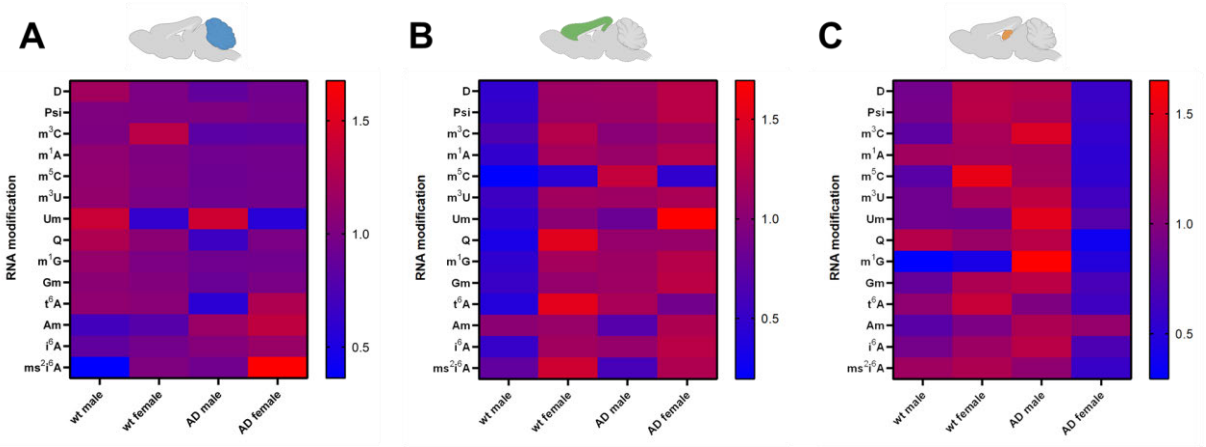

Figure 43. Heatmaps of tRNA fraction in young mice brain. **(A)** Modification pattern in cerebellum. **(B)** Modification pattern in cerebral cortex. **(C)** Modification pattern in hippocampus. n = 3 technical replicates. Each row was normalized by its mean. **Abbr.:** wt: wildtype, AD: Alzheimer's Disease.

Fig. 43 shows the tRNA changes in young mice's cerebellum, cerebral cortex, and hippocampus. It can be seen that the pattern of the cerebellum (Fig. 43 A) is different from that of the cerebral cortex and hippocampus. No clear pattern is seen there; only isolated changes stand out, but the majority are present in a balanced manner. On the other hand, in the cerebral cortex, it is noticeable that almost all modifications are downregulated in the wt males. However, more RNA modifications are present compared with wt females. An AD-specific effect can also be detected between the wt and AD males. No difference could be detected between the wt and AD females. It is striking that the modification m^5C is only extremely weakly expressed in all individuals. Thus, in the cerebral cortex, on the one hand, a sex-specific effect and, on the other hand, an AD-specific effect could be detected in the male individuals. A difference between wt males and wt females is first apparent in the hippocampus. In wt females, most tRNA modifications are significantly more abundant. In particular, the modification m^5C is significantly increased compared to males. An increase is also detectable in the

male AD cohort compared with the wildtype. A decrease in all modifications can be seen in comparing wt and AD females in the AD model.

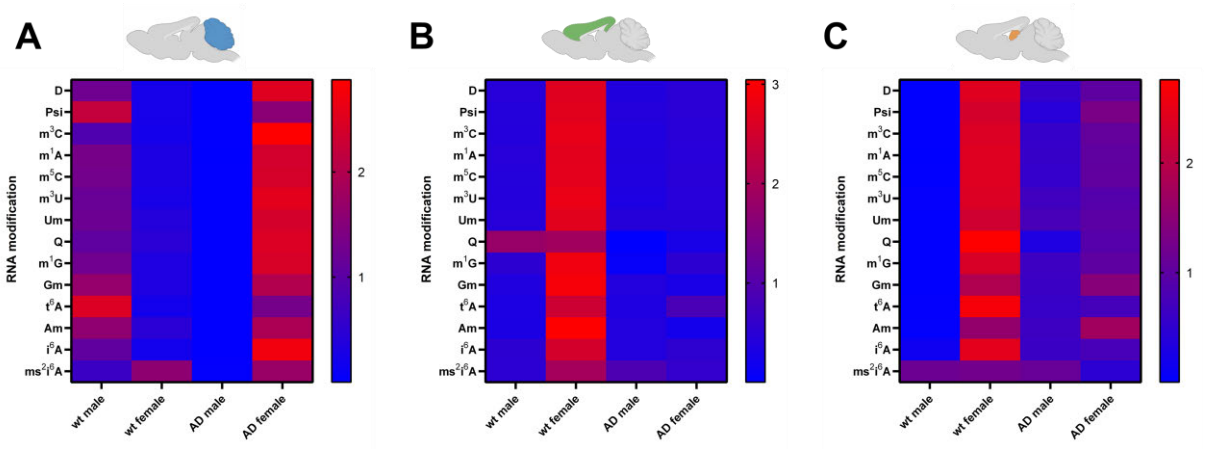

Figure 44. Heatmaps of tiRNA fraction in young mice brain. **(A)** Modification pattern in cerebellum. **(B)** Modification pattern in cerebral cortex. **(C)** Modification pattern in hippocampus. n = 3 technical replicates. Each row was normalized by its mean. **Abbr.:** wt: wildtype, AD: Alzheimer's Disease.

Fig. 44 shows RNA modifications of tiRNAs in 3-months old mice. It can be clearly seen that the pattern in cerebellum tissue is different compared to the cerebral cortex and hippocampus. Comparing wt males with AD males, it is noticeable that in the wt individuals, there are more modifications. In the females, exactly the opposite can be seen. There are fewer modifications in the wt females than in the AD females. In the cerebral cortex, however, the modifications of the wt females are strongly increased. In all other individuals, these are at a relatively equal level. In the hippocampus, too, all modifications are more pronounced in the wt females than in the other individuals. Only in the AD female are the modifications still slightly more present than in the other individuals. There is no real difference between wt and AD males.

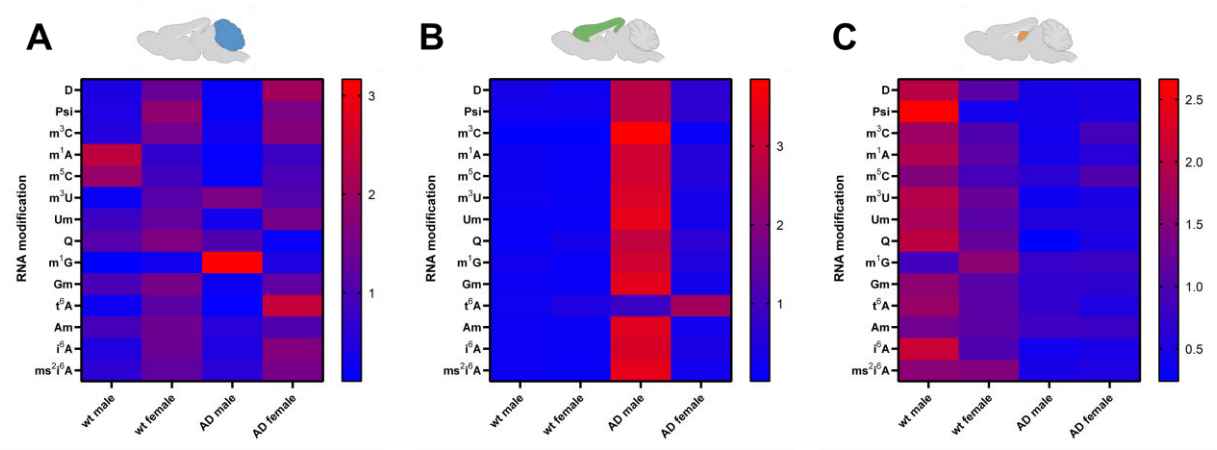

Figure 45: Heatmaps of tRF fractions in young mice brain. **(A)** Modification pattern in cerebellum. **(B)** Modification pattern in cerebral cortex. **(C)** Modification pattern in hippocampus. n = 3 technical replicates. Each row was normalized by its mean. **Abbr.:** wt: wildtype, AD: Alzheimer's Disease.

Fig. 45 shows the RNA modifications in tRFs of young mice in the cerebellum, cerebral cortex, and hippocampus. In the cerebellum, a pattern is noticeable in which the females have more apparent modifications than the other individuals. There are more modifications in the AD females than in the wt females. More modifications can be seen in the wildtype in the male individuals. The strong modification pattern in the AD male specimens in the cerebral cortex is noticeable. In all other individuals, there are hardly any modifications. However, in the hippocampus, the modifications are most pronounced in the wt males. The AD males, on the one hand, show hardly any modifications. A gender-specific effect can also be seen in the wt females, where the modifications are weaker than the wt males. On the other hand, in AD individuals, only a few modifications are present.

4.2.2. RNA Modifications in old mice

To analyze RNA modification changes in old mice, 4 animals were recruited at a time. Again, the cerebellum, cerebral cortex, and hippocampus were used for analyzation of RNA modifications by LC-MS/MS.

When looking at the tRNA modifications, apparent differences become visible here. Different modification patterns between males and females in the cerebellum are

visible. There are fewer modifications in the wt males than in the wt females. The same results can be determined for AD individuals. Again, there are fewer modifications in the AD males than in the AD females. There is also an effect as changes within a group (wt or AD) increase, looking at individuals among themselves.

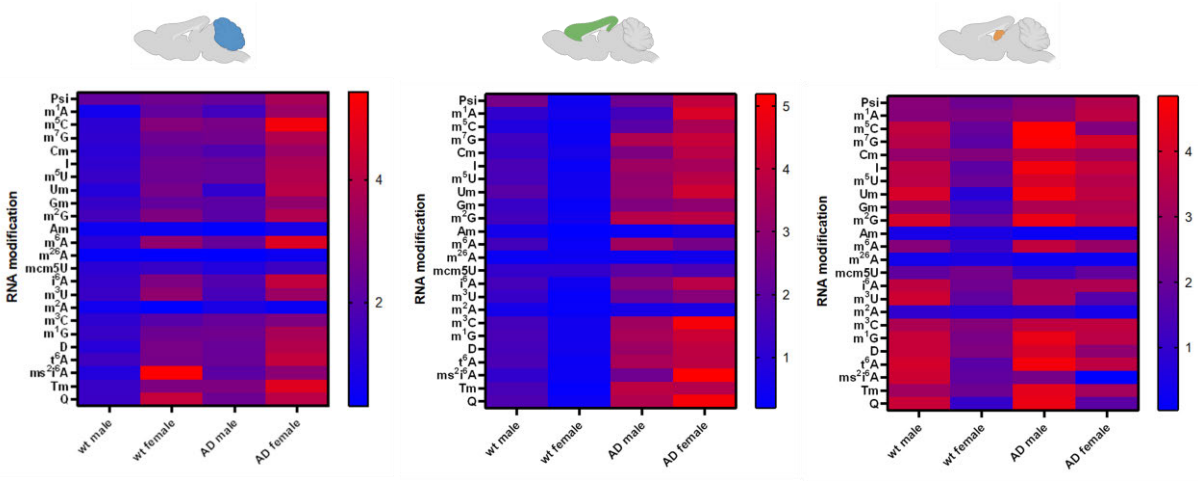

Figure 46. Heatmaps of tRNA fraction in old mice brain. **(A)** Modification pattern in cerebellum. **(B)** Modification pattern in cerebral cortex. **(C)** Modification pattern in hippocampus. n = 3 technical replicates. Each row was normalized by its mean. **Abbr.:** wt: wildtype, AD: Alzheimer's Disease.

Looking at tRNA modifications in the cerebral cortex, it is clear that there is an apparent AD effect. There are comparatively few RNA modifications in both male and female wt. However, this changes in individuals with AD. There, an increase in RNA modifications can be seen. There is a tendency for AD females to have slightly more tRNA modifications comparing both AD males and AD females. In the hippocampus, both sex- and AD-specific effects could be analyzed. The wt males show an increased amount of RNA modifications compared to the wt females. However, an apparent effect is also seen within one sex. Both females and males show more RNA modifications in the respective AD individuals compared to the wt control.

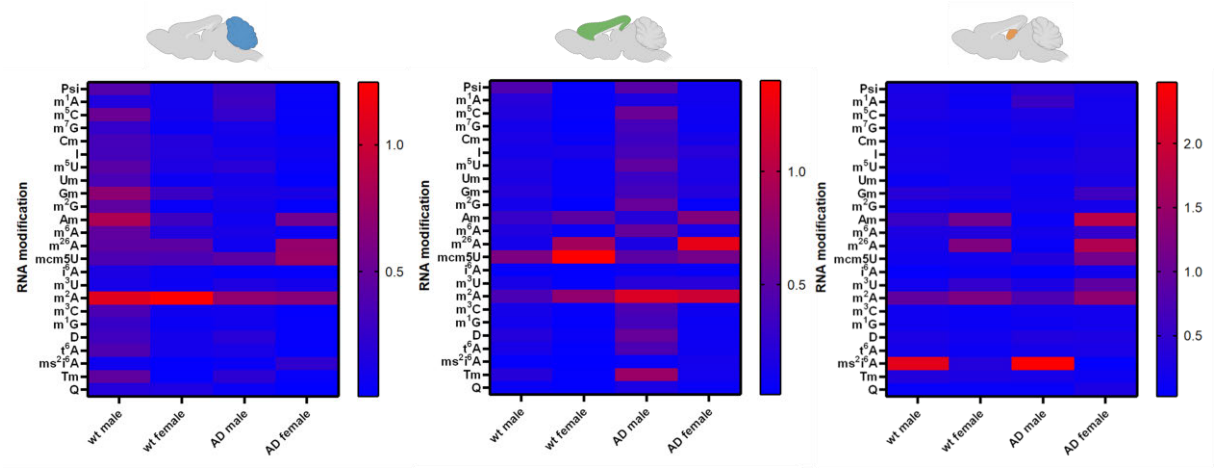

Figure 47. Heatmaps of tiRNA fractions in old mice brain. **(A)** Modification pattern in cerebellum. **(B)** Modification pattern in cerebral cortex. **(C)** Modification pattern in hippocampus. n = 3 technical replicates. Each row was normalized by its mean. **Abbr.:** wt: wildtype, AD: Alzheimer's Disease.

Compared with tRNA modifications, fewer modifications are observed in tiRNAs, but this is due to the bisection of tRNA. In the cerebellum, differences are seen between wildtype and AD animals. Slightly more modifications occur in wt males than in wt females. A decrease in modifications is also detectable between wt males and AD males. In contrast, a slight increase in the number of modifications is seen in wt females compared to AD females. However, there is no difference between the wt and AD females in the cerebral cortex. In contrast, however, there is an effect between the wt and AD males. In the hippocampus, wt and AD females again behave very similarly, and in this case, wt and AD males also behave similarly. Both show similar modification patterns between wt and AD in their respective sexes. However, this highlights a difference between the two sexes when comparing wt males and females and AD males and females. In both cases, there are more modifications in females than in males.

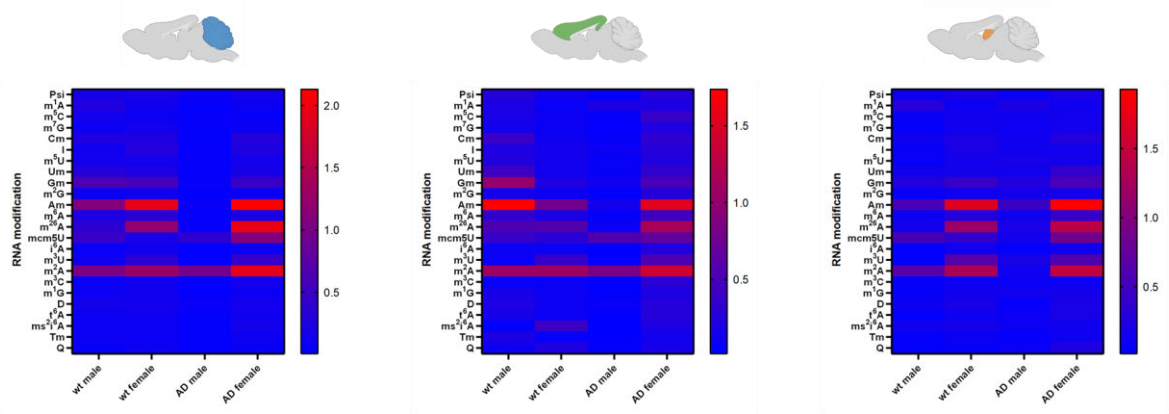

Figure 48. Heatmaps of tRF fractions in old mice brain. **(A)** Modification pattern in cerebellum. **(B)** Modification pattern in cerebral cortex. **(C)** Modification pattern in hippocampus. n = 3 technical replicates. Each row was normalized by its mean. **Abbr.:** wt: wildtype, AD: Alzheimer's Disease.

Fig. 48 shows the results of the analysis of RNA modifications in tRFs. It is striking that, again, as with the tiRNAs, significantly fewer modifications are seen than the tRNAs. Only the Am, and m^2A modifications are partially increased, indicating some degradation of the samples. Otherwise, no clear pattern of RNA modifications can be seen, as almost all modifications are close to 0.

4.2.3. Discussion

The analysis of RNA modification changes in the tRNA of aged mice again allows a variety of conclusions. Looking first at the hippocampus, it is clear that a sex-specific effect can be observed. Comparing both the wt and AD samples, it is clear that females generally have fewer modifications in each case. Thus, again an effect is visible that was already seen with the expression of ANG. Again, special attention is paid to the modification m^5C to establish an ANG connection. As mentioned earlier, lower expression of m^5C leads to increased accumulation of 5'-tiRNAs, which triggers an enhanced stress response, including increased apoptosis, especially in the hippocampus and cerebral cortex [313]. This same modification is reduced in the hippocampus in females in both individuals with and without AD. These observations correlate with the expression of ANG in 5X-FAD mice. There, increased ANG levels were found in female oTG. This suggests that ANG may enhance the degradation of tRNAs and induce enhanced apoptosis by accumulating 5'-tiRNA. This may further explain additionally why significantly more female individuals develop AD. The

enhanced apoptosis triggered in this way would lead to increased neurodegeneration in hippocampal neurons. This observation does not apply directly to the cerebral cortex since this is also a different brain area. There, increased levels of m^5C are found in AD males and females. One could conclude that cortical neurons in m^5C deficiency are better protected against the excessive apoptosis triggered by ANG. However, this mechanism is not the only one leading to neurodegeneration. Surprisingly, m^5C levels are reduced in the corresponding wt animals, e.g., in older animals, ANG might degrade more tRNAs, leading to accumulation of 5'-tiRNAs, resulting in inhibited translation and enhanced apoptosis. This could be a factor that would further drive the aging process even if ANG expression was reduced in the aged model. However, it is also clear that further analysis is needed to support this theory. However, looking at the generality of the changes, an evident AD effect was detected. While only a few changes are strongly pronounced in the cerebral cortex of male and female wt patients, the corresponding changes in RNA modifications are much more pronounced in the AD cohort. The RNA modifications of the tRNAs in the cerebellum were also analyzed. Again, the cerebellum behaves differently than in the experiments before. There, the modifications are more pronounced in females than in males. Since the cerebellum, at least so far, plays no known role in AD, it can be used as a negative control.

The results of the RNA modification analysis of the tiRNAs and the tRFs of young mice are much more difficult. There are some patterns in tiRNA and tRF. Especially the increased amount of wt female tiRNA in cerebral cortex and hippocampus is noticeable, suggesting a sex-specific effect like it is found many times during that study. This could also be the case in hippocampus tRFs while there is a difference between wt male and female. Also, the RNA modification analysis results of the tiRNAs and the tRFs of old mice are much more difficult. A clear statement cannot be made since almost no modification is significantly increased. It can be seen that it is only slightly expressed in all tiRNAs and the tRFs looking at the modification m^5C. This could be partly because the modification is formed so little or partly because the half or fragment containing m^5C is significantly less present. The problem with modifications on tiRNA and tRFs is that it is even impossible to determine which exact fragment is present because of the method. A mixture of 5'- and 3' tiRNAs or one of each fragment could be higher concentrated. Another problem is, especially for tRFs, that it is not possible to cut out only tRFs but only an area in which they occur during the method. These circumstances make it difficult to formulate precise hypotheses. For this reason, the

focus was on tRNA modifications since this methodological problem does not exist here.

4.3. Analysis of RNA modifications in the TgF344-AD rat model

To investigate the previously observed RNA modification changes also in a different model, we used the TgF344-AD rat model. An advantage of the model is that the number of neurons in the hippocampus and cortex is comparable to the number of neurons in wt rats at the same age between 6-26 months [343].

4.3.1. RNA modifications in young and old wildtype and TgF344-AD rats different brain regions

A total of 16 animals were recruited for RNA modification analysis by LC-MS/MS. From each sex, 2 wt and 2 tg animals were used at 6 and 15 months of age, respectively. This ensures that the pathophysiology of AD is just beginning in the young model. In the older model, the manifestations of the disease are already well advanced.

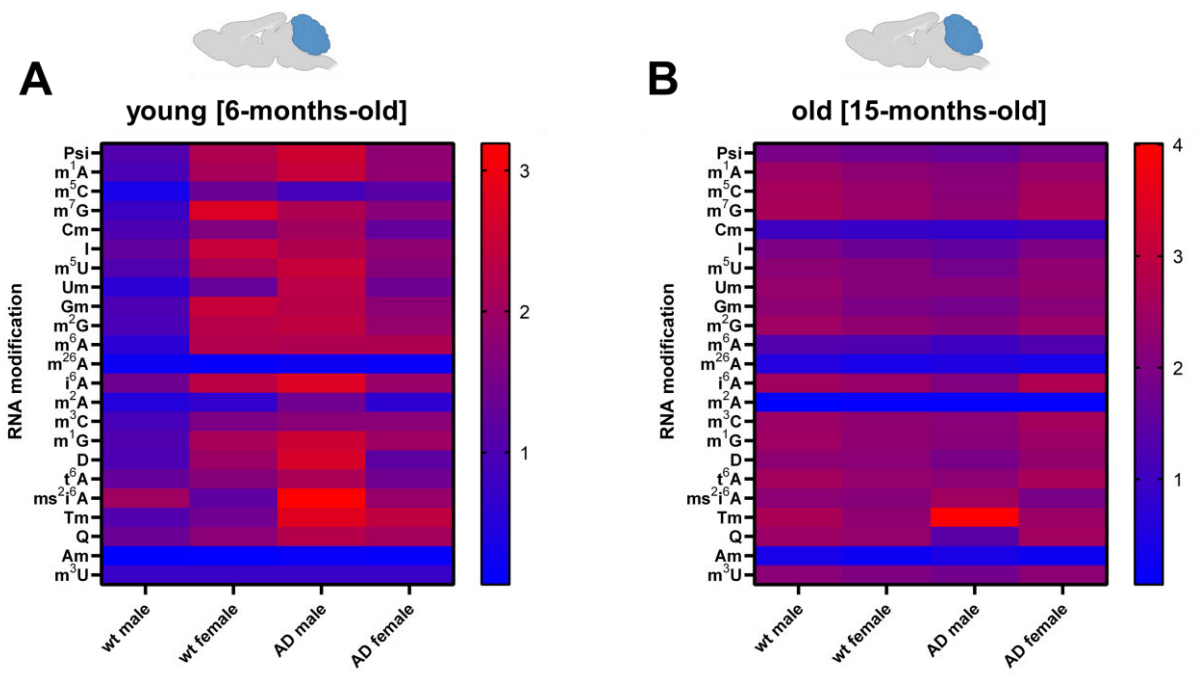

Figure 49. Heatmaps of tRNA fractions in young and old rats brain. **(A)** Modification pattern in cerebellum of young rats. **(B)** Modification pattern in cerebellum of old rats. n = 3 technical replicates. Each row was normalized by its mean.

Fig. 49 A and B show the tRNA modifications of young and old wildtype and TgF344-AD rats in the cerebellum. The difference between young and old animals is striking. In the 15-month-old animals, no differences are seen between wt and AD and male and female. In contrast, a clear pattern of change is evident in the young animals. Between wt males and wt females, an apparent increase of the modification pattern could be detected. An effect within the males can also be seen as the modification pattern in the AD model increases. Within the female sex, only a slight decrease in tRNA modifications can be seen. In contrast, no real difference can be seen in the 15-month-old animals. A more or less identical pattern could be detected in all animals with small variations. The degradation markers Am and m^3U are not very pronounced in both cohorts, which is why one can speak of a good RNA quality.

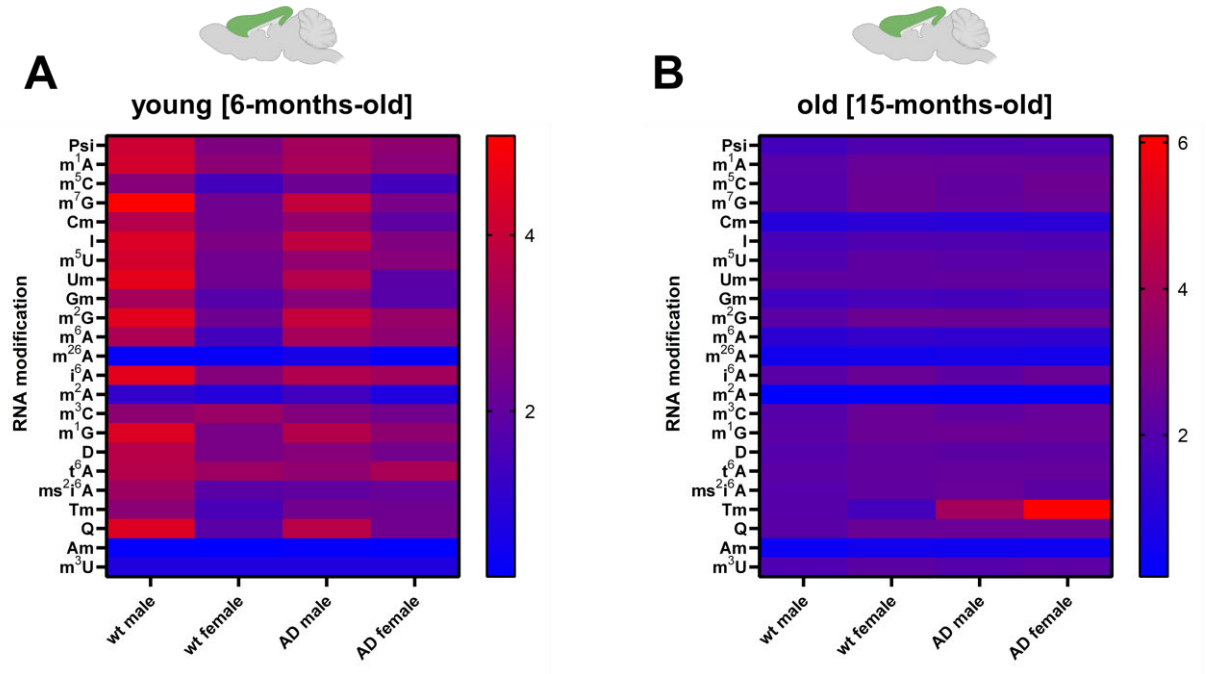

Figure 50. Heatmaps of tRNA fractions in young and old rats brain. **(A)** Modification pattern in cerebral cortex of young rats. **(B)** Modification pattern in cerebral cortex of old rats. n = 3 technical replicates. Each row was normalized by its mean. **Abbr.:** wt: wildtype, AD: Alzheimer's Disease.

Fig. 50 shows the tRNA modification pattern in the cerebral cortex of young and old wildtype and TgF344-AD rats. Again, it is striking that the modification pattern is lost in the aged model, and no difference can be detected between the different groups consisting of wt males/females and AD males/females. Only the wt males show a

minimally reduced modification pattern, but this difference is minimal. In contrast, there are more effects in adolescent rats. The degradation markers Am and m^3U also initially show low values, from which it can be concluded that no degradation of RNA has occurred. A sex-specific difference could also be detected in young animals. Wt males show a significantly higher modification pattern, e.g., the individual changes are more distinctive than wt females. The wt females show a less pronounced pattern for all modifications. The situation is similar for the male and female AD samples. Again, the male AD samples show a stronger modification expression than the female AD samples. A slight reduction was also found in the AD samples comparing the wt male and AD male cohort, but this difference is much less distinctive than the gender variations.

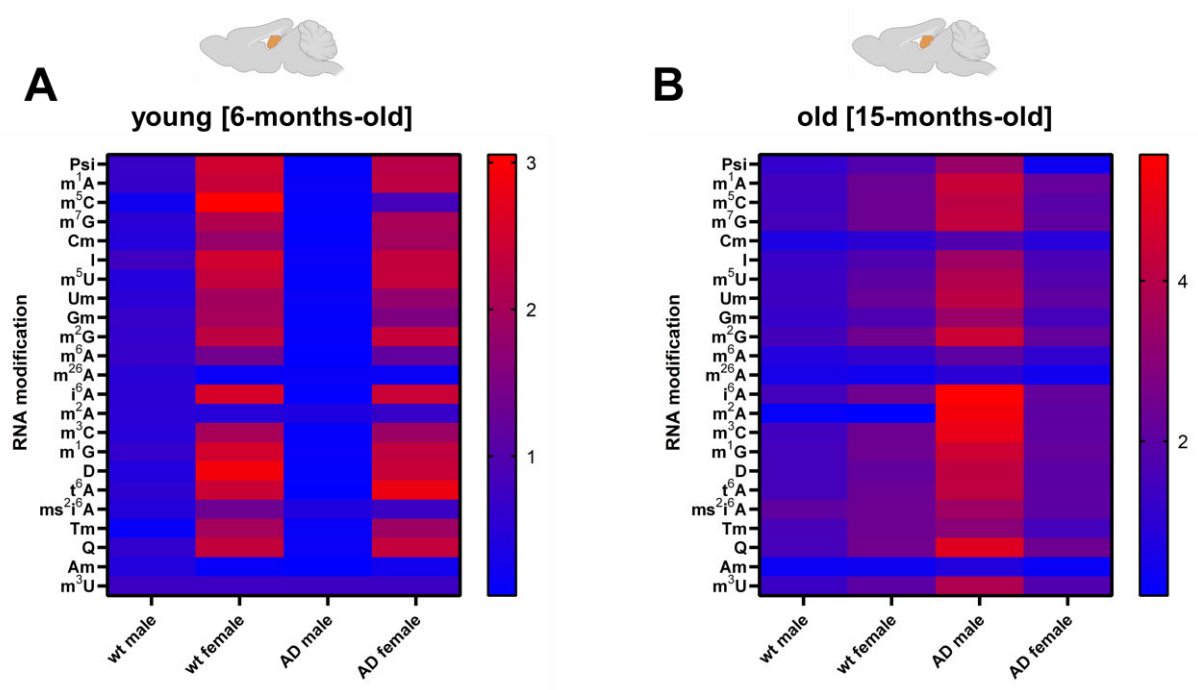

Figure 51. Heatmaps of tRNA fractions in young and old rats brain. **(A)** Modification pattern in hippocampus of young rats. **(B)** Modification pattern in hippocampus of old rats. n = 3 technical replicates. Each row was normalized by its mean. **Abbr.:** wt: wildtype, AD: Alzheimer's Disease.

Fig. 51 shows the tRNA modifications in the hippocampus of young and old wildtype and TgF344-AD rats. In contrast to the cerebellum and cortex, the presence of a modification pattern is directly evident. Comparing wt and AD males, an increase in modifications was found in the AD model. A slight increase in modifications is observed

in the female wt animals, even within the male cohort. A much clearer pattern is seen in the young 6-month-old rats. A clear sex-specific effect was observed. Compared to the males, the females always show a significantly increased occurrence of all mutations. A difference within the cohort of females is also striking. In the female wt samples, m^5C is more pronounced than in the AD model. m^5C is normally present to protect tRNA from degradation by ANG. In both young and old animals, the degradation markers Am and m^3U are again low to moderately expressed, indicating no degradation in the samples.

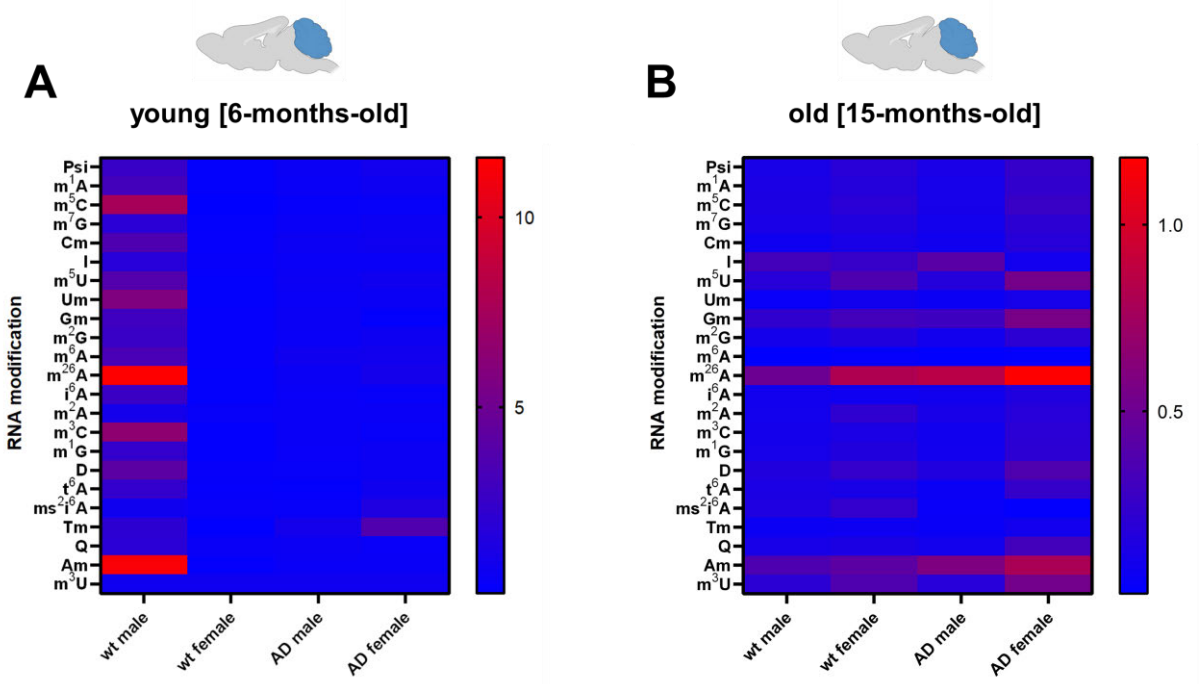

Figure 52. Heatmaps of tiRNA fractions in young and old rats brain. **(A)** Modification pattern in cerebellum of young rats. **(B)** Modification pattern in cerebellum of old rats. n = 3 technical replicates. Each row was normalized by its mean. **Abbr.:** wt: wildtype, AD: Alzheimer's Disease.

After the tRNA modifications, the modifications were determined on the obtained tRNA fragments. First, the tiRNAs were analyzed for their RNA modifications. No clear pattern can be identified in the cerebellum of old animals after analyzing the RNA modifications. The modifications are slightly more distinctive in the female samples than in the corresponding male cohort, but these differences are small and only affect single modifications. No difference could be found between the male wt and the male AD cohorts. Similarly, only a minimal increase in the expression of the modifications is

observed in the female wt and AD samples. However, in the young, 6-month-old animals, a significantly increased number of RNA modifications is observed in the male wt samples. Again, it is striking that m^5C is upregulated and downregulated in all other cohorts. The degradation markers are largely downregulated in all samples. Only in the wt male is Am strongly upregulated, but since m^3U is not increased, it can be assumed that little or no degradation has occurred.

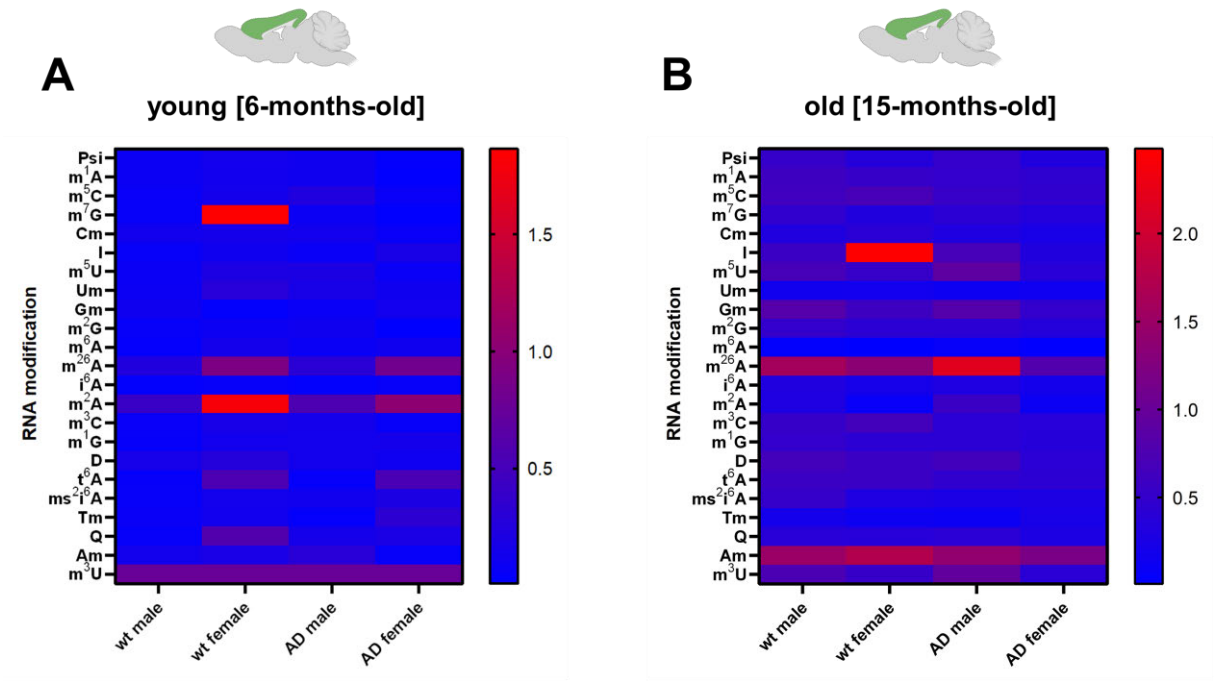

Figure 53. Heatmaps of tiRNA fractions in young and old rats brain. **(A)** Modification pattern in cerebral cortex of young rats. **(B)** Modification pattern in cerebral cortex of old rats. n = 3 technical replicates. Each row was normalized by its mean. **Abbr.:** wt: wildtype, AD: Alzheimer's Disease.

The changes in tiRNA in the cortex do not show a consistent pattern in the aged 15-month-old rats. I is clearly upregulated in the wt female samples. In addition to these two stronger modifications, only one basic pattern is evident between AD males and AD females, with AD females showing lower modification levels than males, but none of the modifications stands out here. There is no apparent difference between wt males and wt females; only minor differences could be detected. For example, m^3C and m^5C are minimally more prominent in females, while Gm and Am are more prominent in males. A slight sex-specific difference was observed in the young 6-month-old rats. Expression of the modifications was stronger in the female wt samples than in the male

wt samples. In addition, two modifications, m^7G and m^2A, stood out clearly in the female wt samples. In contrast, there is no difference between the male and female AD samples, except for the increase in m^2A in the female AD samples. One of the young animals' degradation markers (m^3U) is slightly increased, whereas Am is not. However, Am is slightly increased in the older animals, whereas m^3U is not.

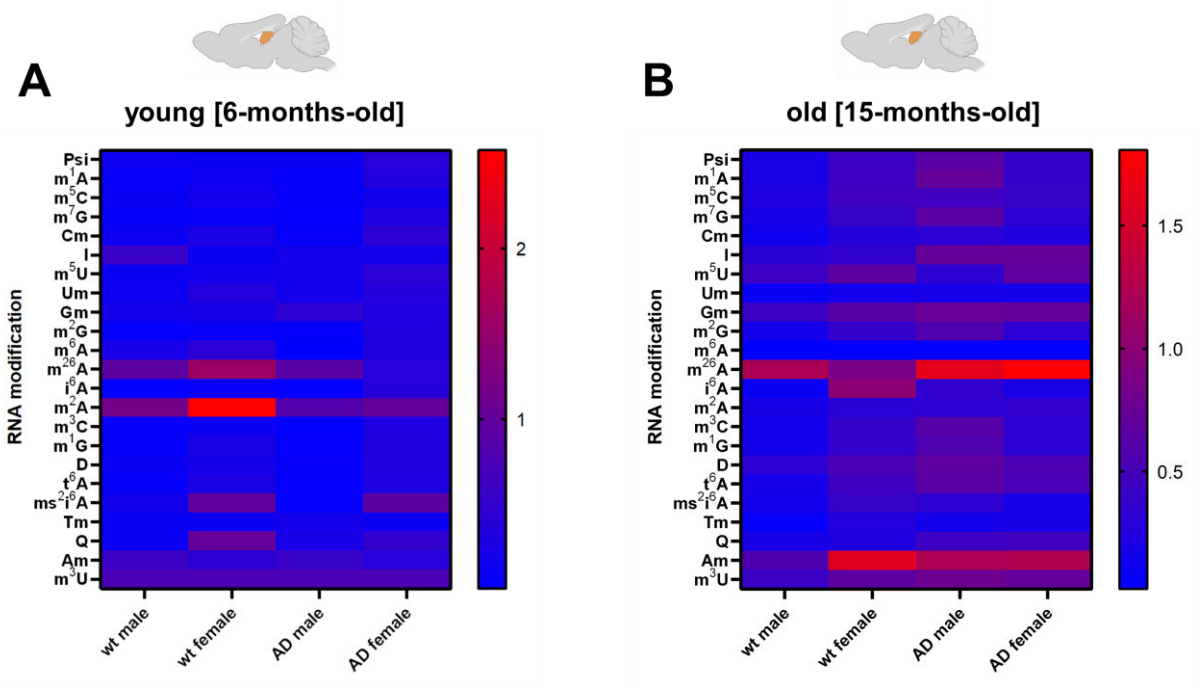

Figure 54. Heatmaps of tiRNA fractions in young and old rats brain. **(A)** Modification pattern in hippocampus of young rats. **(B)** Modification pattern in hippocampus of old rats. n = 3 technical replicates. Each row was normalized by its mean. **Abbr.:** wt: wildtype, AD: Alzheimer's Disease.

The tiRNA modifications in the hippocampus of 15-month-old rats show a modification pattern. This is not as distinctive as for tRNA, which is also due to its cleavage, but it can be seen. There is an increase in modifications from wt males to AD males. There is little difference between wt males and wt females and between wt females and AD females. There is also a slight decrease in the magnitude of the changes while comparing AD males to AD females. In contrast, a slight pattern of RNA changes is again seen in the young, 6-month-old mice. It can be seen that the female samples have more RNA modifications than the corresponding male samples during the comparison of male and female wt samples. Queuosine (Q) is also more distinctive in

the female wt samples than in all other samples. In contrast, the m^2A modifications are highly expressed in all samples except the female AD sample.

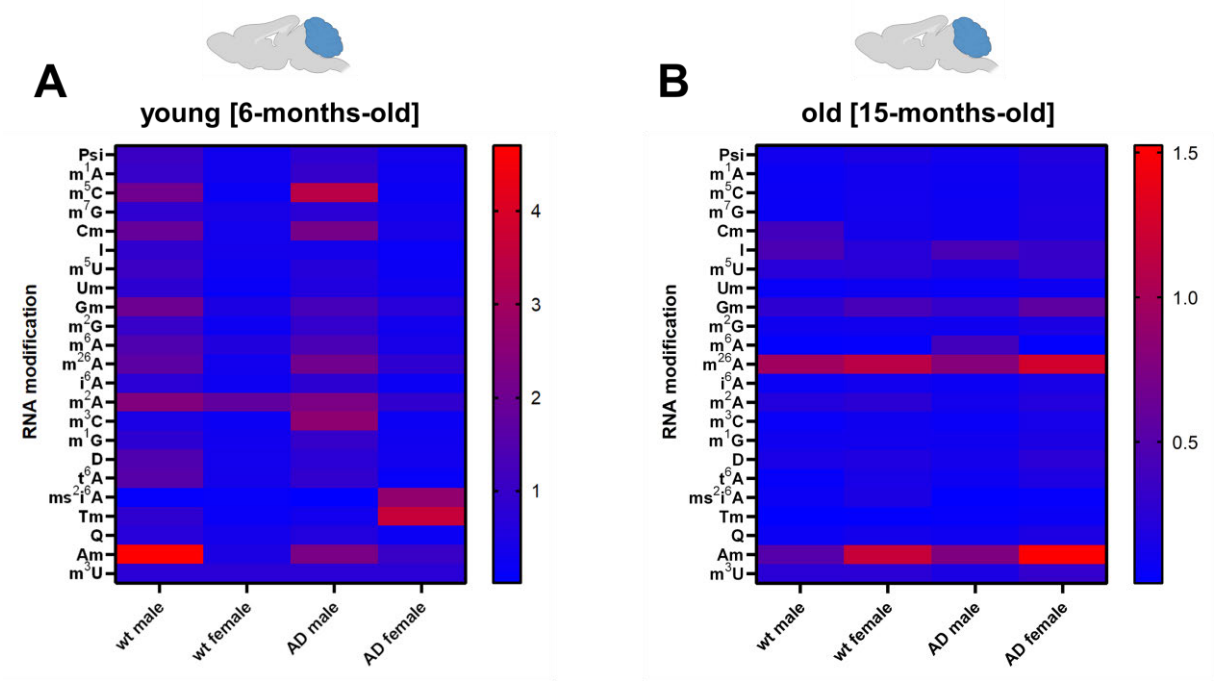

Figure 55. Heatmaps of tRF fractions in young and old rats brain. **(A)** Modification pattern in cerebellum of young rats. **(B)** Modification pattern in cerebellum of old rats. n = 3 technical replicates. Each row was normalized by its mean. **Abbr.:** wt: wildtype, AD: Alzheimer's Disease.

Fig. 55 shows the RNA modifications of the smallest tRNA-dependent fragments. In 15-month-old rats, no real difference between cohorts is evident. Only in isolated cases are modifications upregulated, such as in AD male I, AD female Gm, wt female Gm, and wt males Cm and I. Am, one of the degradation markers is also increased in almost all samples except the male control group. A pattern of modifications is evident in the 6-month-old young rats. A clear sex-specific effect was observed. RNA modifications are more distinctive in the male wt and male AD cohorts than in the corresponding female cohort. Again, the m^5C modification is more present in the wt males and AD males than in the female samples. Am, one of the degradation markers is increased in the male samples in the young cohort.

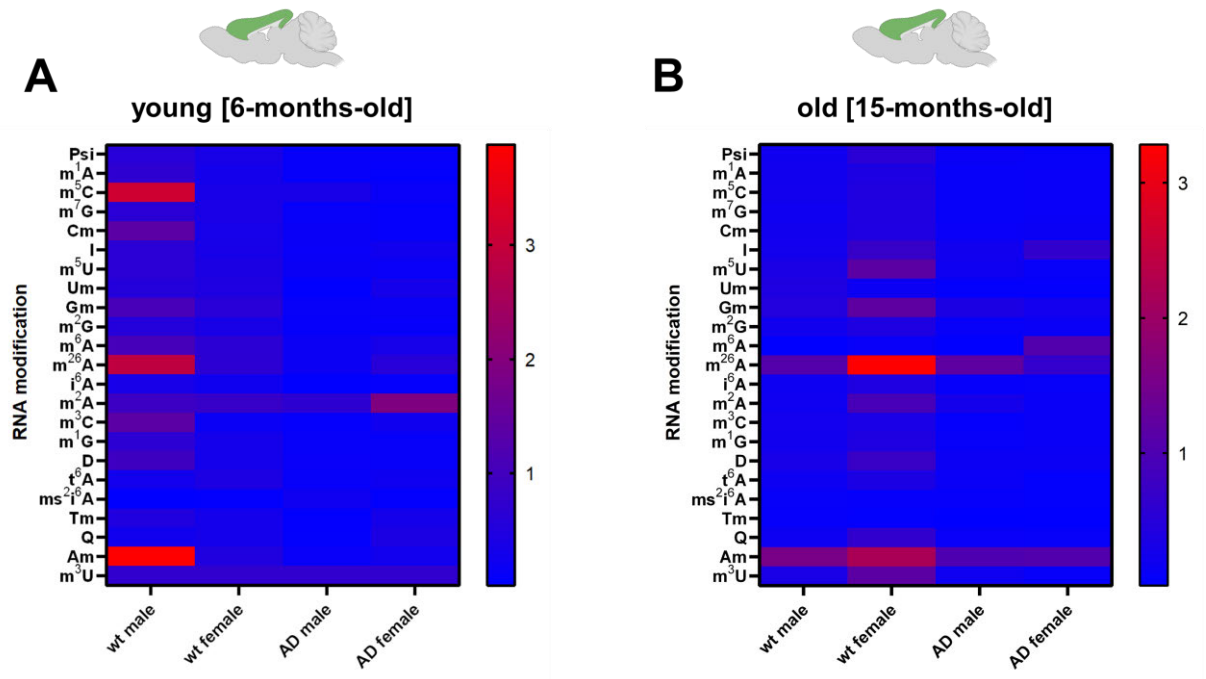

Figure 56. Heatmaps of tRF fractions in young and old rats brain. **(A)** Modification pattern in cerebral cortex of young rats. **(B)** Modification pattern in cerebral cortex of old rats. n = 3 technical replicates. Each row was normalized by its mean. **Abbr.:** wt: wildtype, AD: Alzheimer's Disease.

In the cerebral cortex Fig. 56 of old 15-month-old rats, most RNA modifications are detected in cohort wt female. In all other cohorts, only isolated modifications occur that do not show a specific pattern. The modifications decrease while comparing wt females with AD females. Only m^6A and I are still detectable. There is no difference between wt males and AD males. The RNA modifications are most distinctive in the young, 6-month-old animals, especially in the wt males. Again, the m^5C modification is the most distinctive. In the remaining cohorts (female wt animals, male AD animals, and female AD animals), few modifications are detectable, except m^2A in the samples from female AD animals. In the old animals, one degradation marker (Am) is slightly increased in all samples. In young animals, this is the case only in the wt males. The other degradation marker, m^3U, is not increased in all samples.

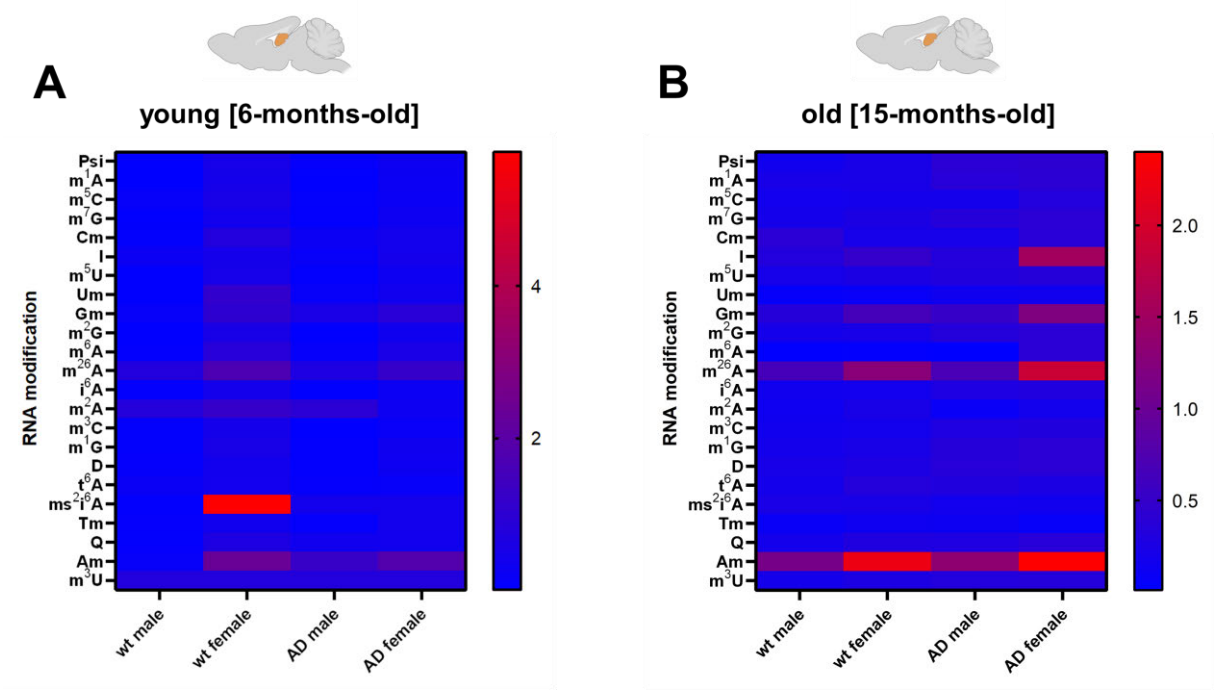

Figure 57. Heatmaps of tRF fractions in young and old rats brain tissue. **(A)** Modification pattern in hippocampus of young rats. **(B)** Modification pattern in hippocampus of old rats. n = 3 technical replicates. Each row was normalized by its mean. **Abbr.:** wt: wildtype, AD: Alzheimer's Disease.

In the hippocampus of 15-month-old rats, $m^{62}A$ was mainly detectable in the female samples. There, too, $m^{62}A$ is increased and, in the female AD samples, additionally I and Gm. Within the male cohort, there is no difference in the modification pattern. In all samples, the modification Am is present. In the young, 6-month-old rats, ms^2i^6A is increased in the female wt samples, and all other modifications are at approximately the same level. There is a slight increase from male to female, but this effect is minimal. No difference is observed between all other cohorts. Degradation markers are also low in young animals.

4.3.2. Quality control of all samples using RNA integrity (RIN^e values)

The samples were again applied to the Agilent TapeStation system to check the quality of the RNA. The values determined there are referred to as RIN^e values. In the range of 7.0-9.0, the RNA is said to be of excellent quality. A small amount of each sample was applied to a TapeStation gel and analyzed with the system. The RIN^e values obtained were then evaluated.

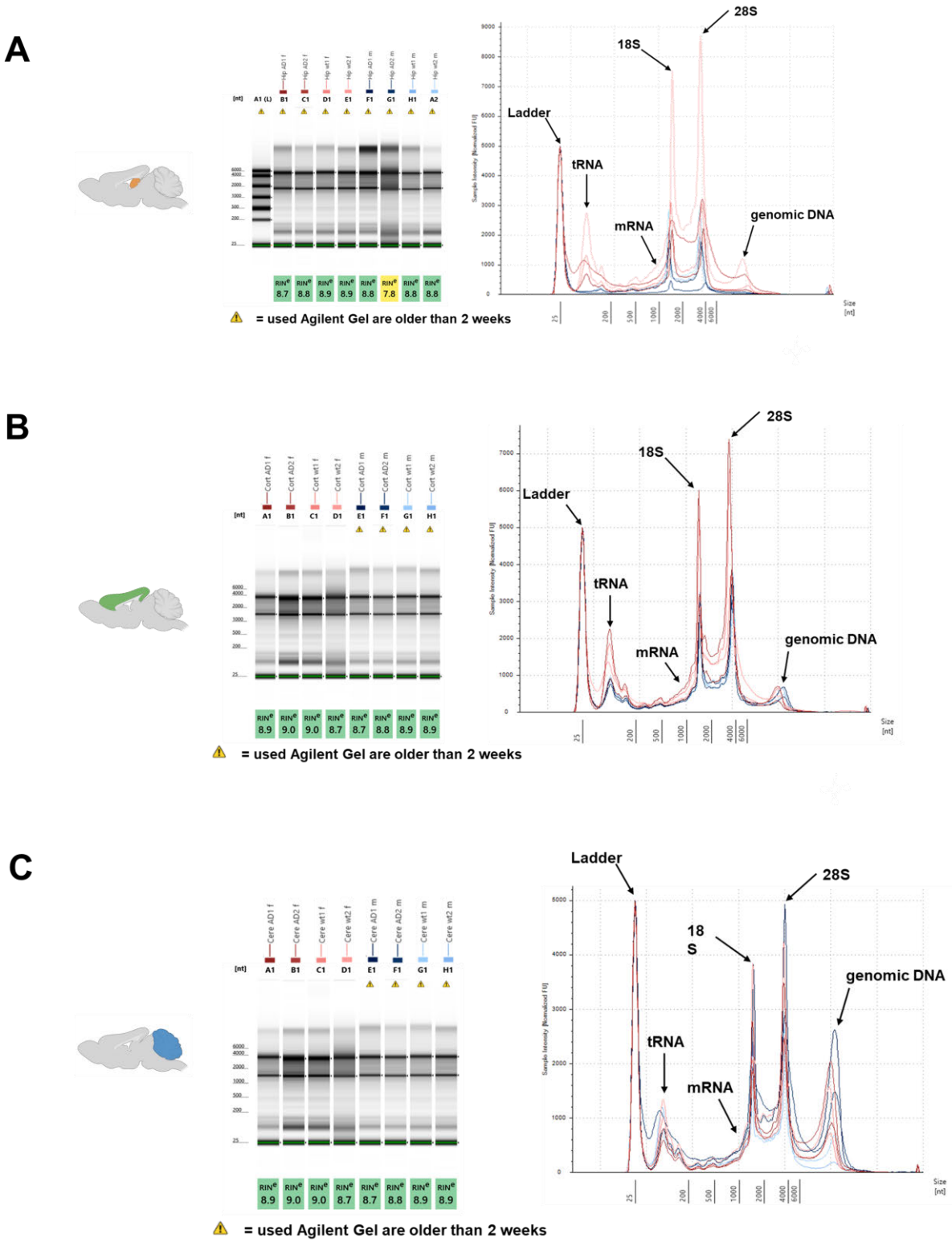

Figure 58. Representative TapeStation Profiles of total RNA from **(A)** hippocampus, **(B)** cerebral cortex, and **(C)** cerebellum.

Fig. 58 A-C shows all RIN^e values obtained, including gel images and chromatograms. The quality of the RNA can be checked using these two variables. Any deviation toward

the poor quality of the sample would be evident in both the chromatogram and the gel image. In all cases, the RIN^e value is between 7.8-9.0 and thus in the excellent range. It can therefore be assumed that the RNA is of very good quality.

4.3.3. Discussion

When analyzing the tRNA modifications of rat brains, a pattern in the hippocampus of young 6-month-old rats is directly apparent. Thus, a sex-specific effect is evident. Again, the m^{5}C modification is conspicuous. Here, the expression of this modification is very low in both male and female AD subjects. This again supports the hypothesis that the absence of m^{5}C leads to enhanced inhibition of protein translation and apoptosis induced by the accumulation of 5'-tiRNAs in hippocampal neurons. This observation was compared with the old 15-month-old rats. As observed previously, m^{5}C levels are reduced in AD females. These observations are also found in the cerebral cortex of young 6-month-old rats. Again, m^{5}C is less pronounced in males and females, but this effect is stronger in females. This effect is also seen in the old rats, but almost all modifications are reduced. These results complement each other and support this hypothesis mentioned above. For completeness, the modifications of cerebellar tRNAs were also determined. As in the previous analyses, the modification pattern was different. However, it must be said that also in the cerebellum, especially in the young rats, the levels of m^{5}C are significantly lower compared to the other modifications. The most interesting brain area in these results is certainly the hippocampus.

The analysis of the modifications of the tiRNAs and tRFs is, as already before with the mice, clearly more difficult, since again it cannot be said exactly which fragment is present in which quantity, possibly influencing the results. However, in these samples it is evident that the modification m^{5}C is reduced in both young and old rats in both the hippocampus and the cortex in the tiRNAs. Since this modification occurs on the 5'-tiRNA half, it can be assumed that at least the detection of this modification is correct since it is also consistent with the results of the analysis of the modifications of the tRNAs. The same applies to the m^{5}C values for the tRFs. However, it must be added here that the group of tRFs is very heterogeneous, and no statement can be made based on the heat maps alone about the extent to which fragment is present or the cellular consequences of the absence of this modification. If we focus on the RNA

modifications of the tRNAs, since we can assume that only tRNAs are analyzed due to the methodology used, it can be stated that various RNA modifications change in the course of the aging process. Thus, the pattern of modifications present in young animals is lost with age in the cerebellum and the cerebral cortex. Only in the hippocampus, an evident change was detected. This change mainly affects the AD male cohort; all other cohorts behave as in the other brain areas where the modifications equalize in strength. The quality of the samples is confirmed by the RIN^e values obtained, which were all determined during quality control. In order to be able to make a clear statement about the changes in the tiRNAs and tRFs, further experiments and analyses must be performed.

Chapter 5

5. Conclusion and future perspective

In this thesis, we investigated how the expression of ANG changes during aging and under the influence of AD and how these processes affect RNA modifications of tRNAs and tRNA-dependent fragments. Different cell and animal models and human brain samples were used to investigate this hypothesis. Initially, the changes in the expression of ANG were analyzed. As discussed in Chapter 3, specific dysregulations of ANG expression could be determined regarding both age-dependence and sex-specific AD effects. Most significant is the age-specific reduction of ANG during the process of aging, which could be detected in both animal and human models. This dysregulation suggests that ANG-induced inhibition of apoptosis, triggered by cleavage of tRNA, may no longer usually proceed, and increased apoptosis may occur. If this process occurs in neurons, the process of neurodegeneration is inevitable. Since this process could be determined in male and female individuals, it was even more surprising to find sex-specific effects in animal and human AD models. In all brain areas strongly affected by AD, such as the hippocampus and cortex, significant increases in ANG expression could be determined in both female yTG and oTG. This shows a clearly common effect compared to the male individuals and reveals the unique impact of gender in AD. As described in Chapter 3, females are significantly more frequently affected by AD. Since the expression of ANG significantly influences the degradation of tRNA and thus the synthesis of tRNA-dependent fragments, the following point was the analysis of RNA. Here, particular attention was paid to modifications of the tRNA, since changes can lead to altered binding of ANG, which can affect the synthesis of the tRNA-dependent fragments. Here it becomes evident what mass of data and thus also perspectives the analysis of RNA modifications provides. This thesis mainly focused on the m^5C modification, as it is directly related to ANG binding to different tRNAs. The analysis of m^5C revealed some partly sex- but also AD-specific modifications, which may lead to altered binding of ANG to the affected tRNA and, consequently, the apoptosis inhibitory effect. This process is localized in neuronal cells, leading to progressive neurodegeneration. This fact once again highlights the importance of changes at the RNA level, especially RNA modifications, in the development of diseases in general and neurodegenerative diseases in particular AD.

However, more fundamental research is needed to gain further important insights. However, the results obtained in this thesis represent an entirely new starting point in the search for the cause of AD. This opens up various possibilities for the future, such as using RNA modifications as biological markers in AD development. In particular, the development of mRNA-based Covid-19 vaccines has shown that therapies using this molecule are possible and successful. Especially due to the diversity of RNA, it is exciting as a target and as a therapeutic agent. Especially from the point of view of individualized therapy, RNA can make a huge step towards curing various currently still incurable diseases, such as AD. With the progress of research, more and more RNA-based therapies and causes of diseases will be discovered in the future. Also, the changes in the expression of ANG, both age- and sex-specific, contribute to advancing the search for AD's cause since it is the process of aging itself that represents the greatest risk factor for the development of AD. Hopefully, the results obtained in this thesis will reveal new targets for AD treatment and gain new insights into the complex pathomechanism involved in aging, neurodegeneration, and AD.

Chapter 6

6. Bibliography

1. Ageing. Available at: https://www.who.int/health-topics/ageing#tab=tab_1. (Accessed: 7th February 2022)
2. Life expectancy at birth (years). Available at: https://www.who.int/data/gho/data/indicators/indicator-details/GHO/life-expectancy-at-birth-(years). (Accessed: 7th February 2022)
3. Livingston, G. *et al.* Dementia prevention, intervention, and care: 2020 report of the Lancet Commission. *Lancet* **396**, 413–446 (2020).
4. World Alzheimer report 2018. (2018).
5. Dementia. Available at: https://www.who.int/news-room/fact-sheets/detail/dementia. (Accessed: 7th February 2022)
6. Niu, H., Álvarez-Álvarez, I., Guillén-Grima, F. & Aguinaga-Ontoso, I. Prevalencia e incidencia de la enfermedad de Alzheimer en Europa: metaanálisis. *Neurología* **32**, 523–532 (2017).
7. Knopman, D. S. *et al.* Alzheimer disease. *Nat. Rev. Dis. Prim.* **7**, 33 (2021).
8. 2021 Alzheimer's disease facts and figures. *Alzheimer's Dement.* **17**, 327–406 (2021).
9. World Health Organization (WHO). Global action plan on the public health response to dementia 2017 - 2025. *Geneva World Heal. Organ.* 27 (2017).
10. ICD-11 for Mortality and Morbidity Statistics. Available at: https://icd.who.int/browse11/l-m/en. (Accessed: 7th February 2022)
11. Arbeitsgemeinschaft der Wissenschaftlichen Medizinischen Fachgesellschaften (AWMF)- & Ständige Kommission Leitlinien. S3-Leitlinie 'Demenzen'. Available at: https://www.awmf.org/uploads/tx_szleitlinien/038-013l_S3-Demenzen-2016-07.pdf. (Accessed: 7th February 2022)

12. Masters, C. L. *et al.* Alzheimers disease. *Nat. Rev. Dis. Prim.* **1**, 15056 (2015).

13. Giau, V. Van *et al.* Genetic analyses of early-onset Alzheimer's disease using next generation sequencing. *Sci. Rep.* **9**, 8368 (2019).

14. Van Giau, V. *et al.* Identification of a novel mutation in APP gene in a Thai subject with early-onset Alzheimer's disease. *Neuropsychiatr. Dis. Treat.* **14**, 3015–3023 (2018).

15. Giau, V. Van *et al.* Novel PSEN1 p.Gly417Ala mutation in a Korean patient with early-onset Alzheimer's disease with parkinsonism. *Neurobiol. Aging* **72**, 188.e13-188.e17 (2018).

16. Bagyinszky, E. *et al.* PSEN1 p.Thr116Ile Variant in Two Korean Families with Young Onset Alzheimer's Disease. *International Journal of Molecular Sciences* **19**, (2018).

17. Park, J. *et al.* Identification of a novel PSEN1 mutation (Leu232Pro) in a Korean patient with early-onset Alzheimer's disease and a family history of dementia. *Neurobiol. Aging* **56**, 212.e11-212.e17 (2017).

18. Goate, A. *et al.* Segregation of a missense mutation in the amyloid precursor protein gene with familial Alzheimer's disease. *Nature* **349**, 704–706 (1991).

19. Rogaev, E. I. *et al.* Familial Alzheimer's disease in kindreds with missense mutations in a gene on chromosome 1 related to the Alzheimer's disease type 3 gene. *Nature* **376**, 775–778 (1995).

20. Giau, V. Van, Pyun, J.-M., Bagyinszky, E., An, S. S. A. & Kim, S. A pathogenic PSEN2 p.His169Asn mutation associated with early-onset Alzheimer's disease. *Clin. Interv. Aging* **13**, 1321–1329 (2018).

21. Cacace, R., Sleegers, K. & Van Broeckhoven, C. Molecular genetics of early-onset Alzheimer's disease revisited. *Alzheimer's Dement.* **12**, 733–748 (2016).

22. Wingo, T. S., Lah, J. J., Levey, A. I. & Cutler, D. J. Autosomal Recessive Causes Likely in Early-Onset Alzheimer Disease. *Arch. Neurol.* **69**, 59–64 (2012).

23. Brouwers, N., Sleegers, K. & Van Broeckhoven, C. Molecular genetics of Alzheimer's disease: An update. *Ann. Med.* **40**, 562–583 (2008).

24. Giau, V. Van, Bagyinszky, E., An, S. S. A. & Kim, S. Clinical genetic strategies for early onset neurodegenerative diseases. *Mol. Cell. Toxicol.* **14**, 123–142 (2018).

25. Van Giau, V., An, S. S. A., Bagyinszky, E. & Kim, S. Gene panels and primers for next generation sequencing studies on neurodegenerative disorders. *Mol. Cell. Toxicol.* **11**, 89–143 (2015).

26. Karch, C. M. & Goate, A. M. Alzheimers Disease Risk Genes and Mechanisms of Disease Pathogenesis. *Biol. Psychiatry* **77**, 43–51 (2015).

27. Giau, V. Van, Bagyinszky, E., An, S. S. A. & Kim, S. Y. Role of apolipoprotein E in neurodegenerative diseases. *Neuropsychiatr. Dis. Treat.* **11**, 1723–1737 (2015).

28. A. Armstrong, R. Risk factors for Alzheimer's disease. *Folia Neuropathol.* **57**, 87–105 (2019).

29. van der Flier, W. M. *et al.* Vascular cognitive impairment. *Nat. Rev. Dis. Prim.* **4**, 18003 (2018).

30. Hachinski, V. C., Bowler, J. V & Loeb, C. Vascular dementia. *Neurology* **43**, 2159 (1993).

31. Hachinski, V. Vascular Dementia: A Radical Redefinition. *Dement. Geriatr. Cogn. Disord.* **5**, 130–132 (1994).

32. O'Brien, J. T. *et al.* Vascular cognitive impairment. *Lancet Neurol.* **2**, 89–98 (2003).

33. International, A. D. & University, M. World Alzheimer Report 2021: Journey through the diagnosis of dementia. (2021).

34. Eisner, V., Picard, M. & Hajnóczky, G. Mitochondrial dynamics in adaptive and maladaptive cellular stress responses. *Nat. Cell Biol.* **20**, 755–765 (2018).

35. Fontanesi, F. Mitochondria: Structure and Role in Respiration. *eLS* 1–13 (2015).

36. Krauss, S. Mitochondria: Structure and Role in Respiration. *eLS* (2001).

37. Schenkel, L. C. & Bakovic, M. Formation and regulation of mitochondrial membranes. *Int. J. Cell Biol.* **2014**, 709828 (2014).

38. Pakendorf, B. & Stoneking, M. Mitochondrial DNA and human Evolution. *Annu. Rev. Genomics Hum. Genet.* **6**, 165–183 (2005).

39. Bogenhagen, D. F. Mitochondrial DNA nucleoid structure. *Biochim. Biophys. Acta - Gene Regul. Mech.* **1819**, 914–920 (2012).

40. Smeitink, J., van den Heuvel, L. & DiMauro, S. The genetics and pathology of oxidative phosphorylation. *Nat. Rev. Genet.* **2**, 342–352 (2001).

41. Cogliati, S., Cabrera-Alarcón, J. L. & Enriquez, J. A. Regulation and functional role of the electron transport chain supercomplexes. *Biochem. Soc. Trans.* **49**, 2655–2668 (2021).

42. Chaban, Y., Boekema, E. J. & Dudkina, N. V. Structures of mitochondrial oxidative phosphorylation supercomplexes and mechanisms for their stabilisation. *Biochim. Biophys. Acta - Bioenerg.* **1837**, 418–426 (2014).

43. Berg, J. M., Tymoczko, J. L., Gatto, G. J. & Stryer, L. Stryer Biochemie. *Stryer Biochem.* (2018).

44. Nolfi-Donegan, D., Braganza, A. & Shiva, S. Mitochondrial electron transport chain: Oxidative phosphorylation, oxidant production, and methods of measurement. *Redox Biol.* **37**, 101674 (2020).

45. Nicholls, D. G. Fluorescence Measurement of Mitochondrial Membrane Potential Changes in Cultured Cells BT - Mitochondrial Bioenergetics: Methods and Protocols. in (eds. Palmeira, C. M. & Moreno, A. J.) 119–133 (Humana Press, 2012).

46. Burtscher, J., Cappellano, G., Omori, A., Koshiba, T. & Millet, G. P. Mitochondria: In the Cross Fire of SARS-CoV-2 and Immunity. *iScience* **23**, 101631 (2020).

47. Mills, E. L., Kelly, B. & O'Neill, L. A. J. Mitochondria are the powerhouses of immunity. *Nat. Immunol.* **18**, 488–498 (2017).

48. Tilokani, L., Nagashima, S., Paupe, V. & Prudent, J. Mitochondrial dynamics: overview of molecular mechanisms. *Essays Biochem.* **62**, 341–360 (2018).

49. Wai, T. & Langer, T. Mitochondrial Dynamics and Metabolic Regulation. *Trends Endocrinol. Metab.* **27**, 105–117 (2016).

50. Gatti, P., Ilamathi, H. S., Todkar, K. & Germain, M. Mitochondria Targeted Viral Replication and Survival Strategies—Prospective on SARS-CoV-2 . *Frontiers in Pharmacology* **11**, (2020).

51. Pfeffer, C. M. & Singh, A. T. K. Apoptosis: A Target for Anticancer Therapy. *Int. J. Mol. Sci.* **19**, 448 (2018).

52. Galluzzi, L. *et al.* Molecular mechanisms of cell death: recommendations of the Nomenclature Committee on Cell Death 2018. *Cell Death Differ.* **25**, 486–541 (2018).

53. Saxton, W. M. & Hollenbeck, P. J. The axonal transport of mitochondria. *J. Cell Sci.* **125**, 2095–2104 (2012).

54. Lovas, J. R. & Wang, X. The meaning of mitochondrial movement to a neuron's life. *Biochim. Biophys. Acta* **1833**, 184–194 (2013).

55. Barnhart, E. L. Mechanics of mitochondrial motility in neurons. *Curr. Opin. Cell Biol.* **38**, 90–99 (2016).

56. Yankner, B. A., Lu, T. & Loerch, P. The Aging Brain. *Annu. Rev. Pathol. Mech. Dis.* **3**, 41–66 (2008).

57. Albert, M., Duffy, F. H. & Naeser, M. Nonlinear changes in cognition with age and their neurophysiologic correlates. *Can. J. Psychol.* **41**, 141 (1987).

58. Craik, F. I. M., Moscovitch, M. & McDowd, J. M. Contributions of surface and conceptual information to performance on implicit and explicit memory tasks. *Journal of Experimental Psychology: Learning, Memory, and Cognition* **20**, 864–875 (1994).

59. Petersen, R. C., Smith, G., Kokmen, E., Ivnik, R. J. & Tangalos, E. G. Memory function in normal aging. *Neurology* **42**, 396–401 (1992).

60. Zelinski, E. M. & Burnight, K. P. Sixteen-year longitudinal and time lag changes in memory and cognition in older adults. *Psychology and Aging* **12**, 503–513 (1997).

61. Persson, J. *et al.* Selection requirements during verb generation: differential recruitment in older and younger adults. *Neuroimage* **23**, 1382–1390 (2004).

62. Logan, J. M., Sanders, A. L., Snyder, A. Z., Morris, J. C. & Buckner, R. L. Under-Recruitment and Nonselective Recruitment: Dissociable Neural Mechanisms Associated with Aging. *Neuron* **33**, 827–840 (2002).

63. A., S. S., K., C. M., Michael, B., R., R. P. & A., B. C. Imaging correlates of brain function in monkeys and rats isolates a hippocampal subregion differentially vulnerable to aging. *Proc. Natl. Acad. Sci.* **101**, 7181–7186 (2004).

64. Hedden, T. & Gabrieli, J. D. E. Insights into the ageing mind: a view from cognitive neuroscience. *Nat. Rev. Neurosci.* **5**, 87–96 (2004).

65. Burke, S. N. & Barnes, C. A. Neural plasticity in the ageing brain. *Nat. Rev. Neurosci.* **7**, 30–40 (2006).

66. Bartzokis, G. *et al.* White Matter Structural Integrity in Healthy Aging Adults and Patients With Alzheimer Disease: A Magnetic Resonance Imaging Study. *Arch. Neurol.* **60**, 393–398 (2003).

67. Liu, X., Erikson, C. & Brun, A. Cortical Synaptic Changes and Gliosis in Normal Aging, Alzheimer's Disease and Frontal Lobe Degeneration. *Dement. Geriatr. Cogn. Disord.* **7**, 128–134 (1996).

68. Bourgeois, J.-P. & Rakic, P. Synaptogenesis in the Occipital Cortex of Macaque Monkey Devoid of Retinal Input From Early Embryonic Stages. *Eur. J. Neurosci.* **8**, 942–950 (1996).

69. Barnes, C. A. Memory deficits associated with senescence: A neurophysiological and behavioral study in the rat. *Journal of Comparative and Physiological Psychology* **93**, 74–104 (1979).

70. Landfield, P. W. & Lynch, G. Impaired monosynaptic potentiation in in vitro hippocampal slices from aged, memory-deficient rats. *Journal of Gerontology* **32**, 523–533 (1977).

71. Barnes, C. A., Rao, G. & Houston, F. P. LTP induction threshold change in old rats at the perforant path-granule cell synapse. *Neurobiology of Aging* **21**, 613–620 (2000).

72. Norris, C. M., Korol, D. L. & Foster, T. C. Increased Susceptibility to Induction of Long-Term Depression and Long-Term Potentiation Reversal during Aging. *J. Neurosci.* **16**, 5382–5392 (1996).

73. Olivier, T. & W., L. P. Increase in Single L-Type Calcium Channels in Hippocampal Neurons During Aging. *Science (80-.).* **272**, 1017–1020 (1996).

74. Geula, C. *et al.* Loss of calbindin-D28k from aging human cholinergic basal forebrain: Relation to neuronal loss. *J. Comp. Neurol.* **455**, 249–259 (2003).

75. Lu, T. *et al.* Gene regulation and DNA damage in the ageing human brain. *Nature* **429**, 883–891 (2004).

76. Mecocci, P., MacGarvey, U. & Beal, M. F. Oxidative damage to mitochondrial DNA is increased in Alzheimer's disease. *Ann. Neurol.* (1994).

77. L., H. M. *et al.* Does oxidative damage to DNA increase with age? *Proc. Natl. Acad. Sci.* **98**, 10469–10474 (2001).

78. Jiankang, L. *et al.* Memory loss in old rats is associated with brain mitochondrial decay and RNA/DNA oxidation: Partial reversal by feeding acetyl-l-carnitine and/or R-α-lipoic acid. *Proc. Natl. Acad. Sci.* **99**, 2356–2361 (2002).

79. Wallace, D. C. A Mitochondrial Paradigm of Metabolic and Degenerative Diseases, Aging, and Cancer: A Dawn for Evolutionary Medicine. *Annu. Rev. Genet.* **39**, 359–407 (2005).

80. Holt, I. J., Harding, A. E. & Morgan-Hughes, J. A. Deletions of muscle mitochondrial DNA in patients with mitochondrial myopathies. *Nature* **331**, 717–719 (1988).

81. Wallace, D. C. *et al.* Familial mitochondrial encephalomyopathy (MERRF): Genetic, pathophysiological, and biochemical characterization of a mitochondrial DNA disease. *Cell* **55**, 601–610 (1988).

82. Richter, C., Park, J. W. & Ames, B. N. Normal oxidative damage to mitochondrial and nuclear DNA is extensive. *Proc. Natl. Acad. Sci.* **85**, 6465–6467 (1988).

83. Lin, M. T., Simon, D. K., Ahn, C. H., Kim, L. M. & Beal, M. F. High aggregate burden of somatic mtDNA point mutations in aging and Alzheimer's disease brain. *Hum. Mol. Genet.* **11**, 133–145 (2002).

84. E., C. P., Flint, B. M. & C., W. D. Alzheimer's brains harbor somatic mtDNA control-region mutations that suppress mitochondrial transcription and replication. *Proc. Natl. Acad. Sci.* **101**, 10726–10731 (2004).

85. E., S. S. *et al.* Extension of Murine Life Span by Overexpression of Catalase Targeted to Mitochondria. *Science (80-.).* **308**, 1909–1911 (2005).

86. Alzheimer, A. über eigenartige Krankheitsfälle des späteren Alters. *Zeitschrift für die gesamte Neurol. und Psychiatr.* **4**, 356 (1911).

87. Chow, V. W., Mattson, M. P., Wong, P. C. & Gleichmann, M. An overview of APP processing enzymes and products. *Neuromolecular Med.* **12**, 1–12 (2010).

88. Zhang, Y., Thompson, R., Zhang, H. & Xu, H. APP processing in Alzheimer's disease. *Mol. Brain* **4**, 3 (2011).

89. Haass, C., Kaether, C., Thinakaran, G. & Sisodia, S. Trafficking and proteolytic processing of APP. *Cold Spring Harb. Perspect. Med.* **2**, a006270–a006270 (2012).

90. Leuner, K., Müller, W. E. & Reichert, A. S. From Mitochondrial Dysfunction to Amyloid Beta Formation: Novel Insights into the Pathogenesis of Alzheimer's Disease. *Mol. Neurobiol.* **46**, 186–193 (2012).

91. Shankar, G. M. *et al.* Amyloid-β protein dimers isolated directly from Alzheimer's brains impair synaptic plasticity and memory. *Nat. Med.* **14**, 837–842 (2008).

92. Wang, H.-W. *et al.* Soluble oligomers of β amyloid (1-42) inhibit long-term potentiation but not long-term depression in rat dentate gyrus. *Brain Res.* **924**, 133–140 (2002).

93. Reddy, P. H. & Beal, M. F. Amyloid beta, mitochondrial dysfunction and synaptic damage: implications for cognitive decline in aging and Alzheimer's disease. *Trends Mol. Med.* **14**, 45–53 (2008).

94. Leuner, K. *et al.* Mitochondrion-derived reactive oxygen species lead to enhanced amyloid beta formation. *Antioxid. Redox Signal.* **16**, 1421–1433 (2012).

95. Cheignon, C. *et al.* Oxidative stress and the amyloid beta peptide in Alzheimer's disease. *Redox Biol.* **14**, 450–464 (2018).

96. Schilling, T. & Eder, C. Amyloid-β-induced reactive oxygen species production and priming are differentially regulated by ion channels in microglia. *J. Cell. Physiol.* **226**, 3295–3302 (2011).

97. De Felice, F. G. *et al.* Alzheimer's disease-type neuronal tau hyperphosphorylation induced by A beta oligomers. *Neurobiol. Aging* **29**, 1334–1347 (2008).

98. Pooler, A. M. *et al.* Amyloid accelerates tau propagation and toxicity in a model of early Alzheimer's disease. *Acta Neuropathol. Commun.* **3**, 14 (2015).

99. Bloom, G. S. Amyloid-β and Tau: The Trigger and Bullet in Alzheimer Disease Pathogenesis. *JAMA Neurol.* **71**, 505–508 (2014).

100. Hauptmann, S. *et al.* Mitochondrial dysfunction: An early event in Alzheimer pathology accumulates with age in AD transgenic mice. *Neurobiol. Aging* (2009).

101. Kinney, J. W. *et al.* Inflammation as a central mechanism in Alzheimer's disease. *Alzheimer's Dement. (New York, N. Y.)* **4**, 575–590 (2018).

102. Ismail, R. *et al.* The relationships between neuroinflammation, beta-amyloid and tau deposition in Alzheimer's disease: a longitudinal PET study. *J. Neuroinflammation* **17**, 151 (2020).

103. Lee, Y.-J., Han, S. B., Nam, S.-Y., Oh, K.-W. & Hong, J. T. Inflammation and Alzheimer's disease. *Arch. Pharm. Res.* **33**, 1539–1556 (2010).

104. Lott, I. T. & Head, E. Dementia in Down syndrome: unique insights for Alzheimer disease research. *Nat. Rev. Neurol.* **15**, 135–147 (2019).

105. Jörg, M., Plehn, E. J., Friedland, K. & Müller, E. W. Mitochondrial Dysfunction as a Causative Factor in Alzheimer's Disease-Spectrum Disorders: Lymphocytes as a Window to the Brain. *Current Alzheimer Research* **18**, 733–752 (2021).

106. Pagano, G. & Castello, G. Oxidative stress and mitochondrial dysfunction in down syndrome. *Adv. Exp. Med. Biol.* (2012).

107. Hardy, J. & Selkoe, D. J. The amyloid hypothesis of Alzheimer's disease: Progress and problems on the road to therapeutics. *Science* (2002).

108. Pozueta, J., Lefort, R. & Shelanski, M. L. Synaptic changes in Alzheimer's disease and its models. *Neuroscience* (2013).

109. Terry, R. D. *et al.* Physical basis of cognitive alterations in alzheimer's disease: Synapse loss is the major correlate of cognitive impairment. *Ann. Neurol.* (1991).

110. Swerdlow, R. H., Burns, J. M. & Khan, S. M. The Alzheimer's disease mitochondrial cascade hypothesis: Progress and perspectives. *Biochimica et Biophysica Acta - Molecular Basis of Disease* (2014).

111. Heneka, M. T. *et al.* Neuroinflammation in Alzheimer's disease. *The Lancet Neurology* (2015).

112. Jack, C. R. *et al.* Tracking pathophysiological processes in Alzheimer's disease: An updated hypothetical model of dynamic biomarkers. *The Lancet Neurology* (2013).

113. Putcha, D. *et al.* Hippocampal hyperactivation associated with cortical thinning in Alzheimer's disease signature regions in non-demented elderly adults. *J. Neurosci.* (2011).

114. Schreiber, S. *et al.* Alzheimer disease signature neurodegeneration and APOE genotype in mild cognitive impairment with suspected non-Alzheimer disease pathophysiology. *JAMA Neurol.* (2017).

115. Dani, M., Brooks, D. J. & Edison, P. Suspected non Alzheimer's pathology – Is it non-Alzheimer's or non-amyloid? *Ageing Res. Rev.* **36**, 20–31 (2017).

116. Müller, W. E., Eckert, A., Kurz, C., Eckert, G. P. & Leuner, K. Mitochondrial dysfunction: Common final pathway in brain aging and alzheimer's disease-therapeutic aspects. in *Molecular Neurobiology* (2010).

117. Cai, Q. & Tammineni, P. Mitochondrial Aspects of Synaptic Dysfunction in Alzheimer's Disease. *Journal of Alzheimer's Disease* (2017).

118. Castello, M. A. & Soriano, S. On the origin of Alzheimer's disease. Trials and tribulations of the amyloid hypothesis. *Ageing Research Reviews* (2014).

119. Morris, G. *et al.* The Glutathione System: A New Drug Target in Neuroimmune Disorders. *Molecular Neurobiology* (2014).

120. Stockburger, C., Eckert, S., Eckert, G. P., Friedland, K. & Müller, W. E. Mitochondrial Function, Dynamics, and Permeability Transition: A Complex Love Triangle as A Possible Target for the Treatment of Brain Aging and Alzheimer's Disease. *Journal of Alzheimer's Disease* (2018).

121. Reddy, P. H. Mitochondrial dysfunction in aging and Alzheimer's disease: Strategies to protect neurons. *Antioxidants and Redox Signaling* (2007).

122. Kolarova, M., García-Sierra, F., Bartos, A., Ricny, J. & Ripova, D. Structure and pathology of tau protein in Alzheimer disease. *Int. J. Alzheimers. Dis.* **2012**, 731526 (2012).

123. Naseri, N. N., Wang, H., Guo, J., Sharma, M. & Luo, W. The complexity of tau in Alzheimer's disease. *Neurosci. Lett.* **705**, 183–194 (2019).

124. Muralidar, S., Ambi, S. V., Sekaran, S., Thirumalai, D. & Palaniappan, B. Role of tau protein in Alzheimer's disease: The prime pathological player. *Int. J. Biol. Macromol.* **163**, 1599–1617 (2020).

125. Stamer, K., Vogel, R., Thies, E., Mandelkow, E. & Mandelkow, E.-M. Tau blocks traffic of organelles, neurofilaments, and APP vesicles in neurons and enhances oxidative stress. *J. Cell Biol.* **156**, 1051–1063 (2002).

126. DuBoff, B., Götz, J. & Feany, M. B. Tau promotes neurodegeneration via DRP1 mislocalization in vivo. *Neuron* **75**, 618–632 (2012).

127. Li, X.-C. *et al.* Human wild-type full-length tau accumulation disrupts mitochondrial dynamics and the functions via increasing mitofusins. *Sci. Rep.* **6**, 24756 (2016).

128. Cummins, N., Tweedie, A., Zuryn, S., Bertran-Gonzalez, J. & Götz, J. Disease-associated tau impairs mitophagy by inhibiting Parkin translocation to mitochondria. *EMBO J.* **38**, e99360 (2019).

129. Swerdlow, R. H. & Khan, S. M. A 'mitochondrial cascade hypothesis' for sporadic Alzheimer's disease. *Med. Hypotheses* (2004).

130. Swerdlow, R. H., Burns, J. M. & Khan, S. M. The Alzheimer's disease mitochondrial cascade hypothesis. *Journal of Alzheimer's Disease* (2010).

131. Mattson, M. P. & Magnus, T. Ageing and neuronal vulnerability. *Nature Reviews Neuroscience* (2006).

132. Hou, Y. *et al.* NAD+ supplementation normalizes key Alzheimer's features and DNA damage responses in a new AD mouse model with introduced DNA repair deficiency. *Proc. Natl. Acad. Sci. U. S. A.* (2018).

133. Sevigny, J. *et al.* The antibody aducanumab reduces Aβ plaques in Alzheimer's disease. *Nature* (2016)

134. Cunnane, S. C. *et al.* Brain energy rescue: an emerging therapeutic concept for neurodegenerative disorders of ageing. *Nat. Rev. Drug Discov.* (2020).

135. Friedland-Leuner, K., Stockburger, C., Denzer, I., Eckert, G. P. & Müller, W. E. Mitochondrial dysfunction: Cause and consequence of alzheimer's disease. in *Progress in Molecular Biology and Translational Science* (2014).

136. Leuner, K. *et al.* Peripheral mitochondrial dysfunction in Alzheimer's disease: Focus on lymphocytes. *Mol. Neurobiol.* (2012).

137. Müller, W. E. *et al.* Therapeutic efficacy of the Ginkgo special extract EGb761® within the framework of the mitochondrial cascade hypothesis of Alzheimer's disease. *World Journal of Biological Psychiatry* (2017).

138. Grimm, A., Friedland, K. & Eckert, A. Mitochondrial dysfunction: the missing link between aging and sporadic Alzheimer's disease. *Biogerontology* (2016).

139. Tambini, M. D. *et al.* ApoE4 upregulates the activity of mitochondria-associated ER membranes. *EMBO Rep.* (2016).

140. Chen, H. K. *et al.* Apolipoprotein E4 domain interaction mediates detrimental effects on mitochondria and is a potential therapeutic target for alzheimer disease. *J. Biol. Chem.* (2011).

141. Telenti, A., Perkins, B. A. & Venter, J. C. Dynamics of an Aging Genome. *Cell Metabolism* (2016).

142. Valla, J. *et al.* Reduced posterior cingulate mitochondrial activity in expired young adult carriers of the APOE ε4 Allele, the major late-onset Alzheimer's susceptibility gene. *J. Alzheimer's Dis.* (2010).

143. Cho, S. & Zhang, J. Ancient expansion of the ribonuclease A superfamily revealed by genomic analysis of placental and marsupial mammals. *Gene* **373**, 116–125 (2006).

144. Li, S. & Hu, G.-F. Emerging role of angiogenin in stress response and cell survival under adverse conditions. *J. Cell. Physiol.* **227**, 2822–2826 (2012).

145. Zhang, J., Dyer, K. D. & Rosenberg, H. F. RNase 8, a novel RNase A superfamily ribonuclease expressed uniquely in placenta. *Nucleic Acids Res.* **30**, 1169–1175 (2002).

146. Prehn, J. H. M. & Jirström, E. Angiogenin and tRNA fragments in Parkinson's disease and neurodegeneration. *Acta Pharmacologica Sinica* (2020).

147. Fett, J. W. *et al.* Isolation and characterization of angiogenin, an angiogenic protein from human carcinoma cells. *Biochemistry* **24**, 5480–5486 (1985).

148. Strydom, D. J. *et al.* Amino acid sequence of human tumor derived angiogenin. *Biochemistry* **24**, 5486–5494 (1985).

149. Kishimoto, K., Liu, S., Tsuji, T., Olson, K. A. & Hu, G. Endogenous angiogenin in endothelial cells is a general requirement for cell proliferation and angiogenesis. *Oncogene* **24**, 445–456 (2005).

150. Xu, Z. ping, Tsuji, T., Riordan, J. F. & Hu, G. fu. The nuclear function of angiogenin in endothelial cells is related to rRNA production. *Biochem. Biophys. Res. Commun.* (2002).

151. Kim, H.-M., Kang, D.-K., Kim, H. Y., Kang, S. S. & Chang, S.-I. Angiogenin-induced protein kinase B/Akt activation is necessary for angiogenesis but is independent of nuclear translocation of angiogenin in HUVE cells. *Biochem. Biophys. Res. Commun.* **352**, 509–513 (2007).

152. Trouillon, R., Kang, D.-K., Park, H., Chang, S.-I. & O'Hare, D. Angiogenin Induces Nitric Oxide Synthesis in Endothelial Cells through PI-3 and Akt Kinases. *Biochemistry* **49**, 3282–3288 (2010).

153. Peng, Y. *et al.* Angiogenin interacts with ribonuclease inhibitor regulating PI3K/AKT/mTOR signaling pathway in bladder cancer cells. *Cell. Signal.* **26**, 2782–2792 (2014).

154. Harper, J. W. & Vallee, B. L. A covalent angiogenin/ribonuclease hybrid with a fourth disulfide bond generated by regional mutagenesis. *Biochemistry* **28**, 1875–1884 (1989).

155. Shapiro, R., Riordan, J. F. & Vallee, B. L. Characteristic ribonucleolytic activity of human angiogenin. *Biochemistry* **25**, 3527–3532 (1986).

156. Thiyagarajan, N., Ferguson, R., Subramanian, V. & Acharya, K. R. Structural and molecular insights into the mechanism of action of human angiogenin-ALS variants in neurons. *Nat. Commun.* (2012).

157. Acharya, K. R., Shapiro, R., Allen, S. C., Riordan, J. F. & Vallee, B. L. Crystal structure of human angiogenin reveals the structural basis for its functional divergence from ribonuclease. *Proc. Natl. Acad. Sci.* **91**, 2915–2919 (1994).

158. Hallahan, T. W., Shapiro, R. & Vallee, B. L. Dual site model for the organogenic activity of angiogenin. *Proc. Natl. Acad. Sci.* **88**, 2222–2226 (1991).

159. Moroianu, J. & Riordan, J. F. Identification of the Nucleolar Targeting Signal of Human Angiogenin. *Biochem. Biophys. Res. Commun.* **203**, 1765–1772 (1994).

160. Moroianu, J. & Riordan, J. F. Nuclear translocation of angiogenin in proliferating endothelial cells is essential to its angiogenic activity. *Proc. Natl. Acad. Sci.* **91**, 1677–1681 (1994).

161. Shapiro, R. & Vallee, B. L. Site-directed mutagenesis of histidine-13 and histidine-114 of human angiogenin. Alanine derivatives inhibit angiogenin-induced angiogenesis. *Biochemistry* **28**, 7401–7408 (1989).

162. Chatzileontiadou, D. S. M. *et al.* The ammonium sulfate inhibition of human angiogenin. *FEBS Lett.* **590**, 3005–3018 (2016).

163. Papageorgiou, A. C., Shapiro, R. & Acharya, K. R. Molecular recognition of human angiogenin by placental ribonuclease inhibitor—an X-ray crystallographic study at 2.0 Å resolution. *EMBO J.* **16**, 5162–5177 (1997).

164. Sarangdhar, M. A. & Allam, R. Angiogenin (ANG)—Ribonuclease Inhibitor (RNH1) System in Protein Synthesis and Disease. *International Journal of Molecular Sciences* **22**, (2021).

165. Dickson, K. A. *et al.* Ribonuclease Inhibitor Regulates Neovascularization by Human Angiogenin. *Biochemistry* **48**, 3804–3806 (2009).

166. Dickson, K. A., Haigis, M. C. & Raines, R. T. B. T.-P. in N. A. R. and M. B. Ribonuclease Inhibitor: Structure and Function. in **80**, 349–374 (Academic Press, 2005).

167. Kobe, B. & Deisenhofer, J. A structural basis of the interactions between leucine-rich repeats and protein ligands. *Nature* **374**, 183–186 (1995).

168. Mridusmita, S. *et al.* Angiogenin-Cleaved tRNA Halves Interact with Cytochrome c, Protecting Cells from Apoptosis during Osmotic Stress. *Mol. Cell. Biol.* **34**, 2450–2463 (2014).

169. Schaefer, M. *et al.* RNA methylation by Dnmt2 protects transfer RNAs against stress-induced cleavage. *Genes Dev.* **24**, 1590–1595 (2010).

170. EFI - Enzyme Similarity Tool. Available at: https://efi.igb.illinois.edu/efi-est/tutorial.php. (Accessed: 1st March 2022)

171. LIBONATI, M. & GOTTE, G. Oligomerization of bovine ribonuclease A: structural and functional features of its multimers. *Biochem. J.* **380**, 311–327 (2004).

172. Gotte, G. *et al.* Double Domain Swapping in Bovine Seminal RNase: Formation of Distinct N- and C-swapped Tetramers and Multimers with Increasing Biological Activities. *PLoS One* **7**, e46804 (2012).

173. Fagagnini, A. *et al.* Onconase dimerization through 3D domain swapping: structural investigations and increase in the apoptotic effect in cancer cells*. *Biochem. J.* **474**, 3767–3781 (2017).

174. Fasoli, S. *et al.* Dimerization of Human Angiogenin and of Variants Involved in Neurodegenerative Diseases. *International Journal of Molecular Sciences* **22**, (2021).

175. Bennett, M. J., Schlunegger, M. P. & Eisenberg, D. 3D domain swapping: A mechanism for oligomer assembly. *Protein Sci.* **4**, 2455–2468 (1995).

176. Gotte, G. & Menegazzi, M. Biological Activities of Secretory RNases: Focus on Their Oligomerization to Design Antitumor Drugs . *Frontiers in Immunology* **10**, (2019).

177. Greenway, M. J. *et al.* ANG mutations segregate with familial and sporadic amyotrophic lateral sclerosis. *Nat. Genet.* **38**, 411 (2006).

178. Crabtree, B. *et al.* Characterization of Human Angiogenin Variants Implicated in Amyotrophic Lateral Sclerosis. *Biochemistry* **46**, 11810–11818 (2007).

179. Wu, D. *et al.* Angiogenin loss-of-function mutations in amyotrophic lateral sclerosis. *Ann. Neurol.* **62**, 609–617 (2007).

180. Van Es, M. A. *et al.* Angiogenin variants in Parkinson disease and amyotrophic lateral sclerosis. *Annals of Neurology* (2011).

181. Gagliardi, S. *et al.* A Novel Nonsense Angiogenin Mutation is Associated with Alzheimer Disease. *Alzheimer Disease and Associated Disorders* (2019).

182. Goncalves, K. A. *et al.* Angiogenin Promotes Hematopoietic Regeneration by Dichotomously Regulating Quiescence of Stem and Progenitor Cells. *Cell* **166**, 894–906 (2016).

183. Walter, N. G. & Maquat, L. E. Introduction—RNA: From Single Molecules to Medicine. *Chem. Rev.* **118**, 4117–4119 (2018).

184. Wang, D. & Farhana, A. Biochemistry, RNA Structure. *StatPearls* (2021).

185. Kornberg, R. D. The molecular basis of eukaryotic transcription. *Proc. Natl. Acad. Sci.* **104**, 12955–12961 (2007).

186. Artsimovitch, I. RNA synthesis is a team effort. *Nat. Microbiol.* **4**, 1776–1777 (2019).

187. Zawel, L., Kumar, K. P. & Reinberg, D. Recycling of the general transcription factors during RNA polymerase II transcription. *Genes Dev.* **9**, 1479–1490 (1995).

188. F., K. J. & A., G. J. Translocation after Synthesis of a Four-Nucleotide RNA Commits RNA Polymerase II to Promoter Escape. *Mol. Cell. Biol.* **22**, 762–773 (2002).

189. Holstege, F. C. P., Fiedler, U. & Timmers, H. T. M. Three transitions in the RNA polymerase II transcription complex during initiation. *EMBO J.* **16**, 7468–7480 (1997).

190. Clancy, S. RNA Splicing: Introns, Exons and Spliceosome. in (2008).

191. Setten, R. L., Rossi, J. J. & Han, S. The current state and future directions of RNAi-based therapeutics. *Nat. Rev. Drug Discov.* **18**, 421–446 (2019).

192. Early, P. *et al.* Two mRNAs can be produced from a single immunoglobulin μ gene by alternative RNA processing pathways. *Cell* **20**, 313–319 (1980).

193. Saberi, F., Kamali, M., Najafi, A., Yazdanparast, A. & Moghaddam, M. M. Natural antisense RNAs as mRNA regulatory elements in bacteria: a review on function and applications. *Cell. Mol. Biol. Lett.* **21**, 6 (2016).

194. Memczak, S. *et al.* Circular RNAs are a large class of animal RNAs with regulatory potency. *Nature* **495**, 333–338 (2013).

195. Williamson, B. Is HnRNA really pre-mRNA? *Nature* **264**, 397–398 (1976).

196. Gebert, L. F. R. & MacRae, I. J. Regulation of microRNA function in animals. *Nat. Rev. Mol. Cell Biol.* **20**, 21–37 (2019).

197. Shin, Y. *et al.* Structural basis of ribosomal RNA transcription regulation. *Nat. Commun.* **12**, 528 (2021).

198. Statello, L., Guo, C.-J., Chen, L.-L. & Huarte, M. Gene regulation by long non-coding RNAs and its biological functions. *Nat. Rev. Mol. Cell Biol.* **22**, 96–118 (2021).

199. Schimmel, P. The emerging complexity of the tRNA world: mammalian tRNAs beyond protein synthesis. *Nat. Rev. Mol. Cell Biol.* **19**, 45–58 (2018).

200. Houseley, J. & Tollervey, D. The Many Pathways of RNA Degradation. *Cell* **136**, 763–776 (2009).

201. Giegé, R. *et al.* Structure of transfer RNAs: similarity and variability. *WIREs RNA* **3**, 37–61 (2012).

202. W., H. R. *et al.* Structure of a Ribonucleic Acid. *Science (80-.).* **147**, 1462–1465 (1965).

203. Shi, H. & Moore, P. B. The crystal structure of yeast phenylalanine tRNA at 1.93 Å resolution: A classic structure revisited. *RNA* **6**, 1091–1105 (2000).

204. Fagan, S. G., Helm, M. & Prehn, J. H. M. tRNA-derived fragments: A new class of non-coding RNA with key roles in nervous system function and dysfunction. *Prog. Neurobiol.* **205**, 102118 (2021).

205. Kirchner, S. & Ignatova, Z. Emerging roles of tRNA in adaptive translation, signalling dynamics and disease. *Nat. Rev. Genet.* **16**, 98–112 (2015).

206. Giegé, R. The early history of tRNA recognition by aminoacyl-tRNA synthetases. *J. Biosci.* **31**, 477–488 (2006).

207. Giegé, R. & Frugier, M. Transfer RNA Structure and Identity. (2013).

208. Giegé, R. Toward a more complete view of tRNA biology. *Nat. Struct. Mol. Biol.* **15**, 1007–1014 (2008).

209. Staehelin, M. Isoacceptor tRNA's BT - Regulation of Transcription and Translation in Eukaryotes. in (eds. Bautz, E. K. F., Karlson, P. & Kersten, H.) 313–321 (Springer Berlin Heidelberg, 1973).

210. Giegé, R., Sissler, M. & Florentz, C. Universal rules and idiosyncratic features in tRNA identity. *Nucleic Acids Res.* **26**, 5017–5035 (1998).

211. Laguesse, S. *et al.* A Dynamic Unfolded Protein Response Contributes to the Control of Cortical Neurogenesis. *Dev. Cell* **35**, 553–567 (2015).

212. Nedialkova, D. D. & Leidel, S. A. Optimization of Codon Translation Rates via tRNA Modifications Maintains Proteome Integrity. *Cell* **161**, 1606–1618 (2015).

213. Chan, P. P. & Lowe, T. M. GtRNAdb 2.0: an expanded database of transfer RNA genes identified in complete and draft genomes. *Nucleic Acids Res.* **44**, D184–D189 (2016).

214. Phizicky, E. M. & Hopper, A. K. tRNA biology charges to the front. *Genes Dev.* **24**, 1832–1860 (2010).

215. Phizicky, E. M. & Hopper, A. K. tRNA processing, modification, and subcellular dynamics: past, present, and future. *RNA* **21**, 483–485 (2015).

216. Andrew, J. *et al.* The stoned Locus of Drosophila melanogaster Produces a Dicistronic Transcript and Encodes Two Distinct Polypeptides. *Genetics* **143**, 1699–1711 (1996).

217. Walker, S. C. & Engelke, D. R. Ribonuclease P: The Evolution of an Ancient RNA Enzyme. *Crit. Rev. Biochem. Mol. Biol.* **41**, 77–102 (2006).

218. Wellner, K., Betat, H. & Mörl, M. A tRNA's fate is decided at its 3′ end: Collaborative actions of CCA-adding enzyme and RNases involved in tRNA processing and degradation. *Biochim. Biophys. Acta - Gene Regul. Mech.* **1861**, 433–441 (2018).

219. E., W. J., M., W. J., M., P. E. & A., S. P. tRNAs Marked with CCACCA Are Targeted for Degradation. *Science (80-.).* **334**, 817–821 (2011).

220. Schmidt, C. A. & Matera, A. G. tRNA introns: Presence, processing, and purpose. *WIREs RNA* **11**, e1583 (2020).

221. Torres, A. G. Enjoy the Silence: Nearly Half of Human tRNA Genes Are Silent. *Bioinform. Biol. Insights* **13**, 1177932219868454 (2019).

222. Torres, A. G., Reina, O., Stephan-Otto Attolini, C. & Ribas de Pouplana, L. Differential expression of human tRNA genes drives the abundance of tRNA-derived fragments. *Proc. Natl. Acad. Sci.* **116**, 8451–8456 (2019).

223. Kumar, P., Kuscu, C. & Dutta, A. Biogenesis and Function of Transfer RNA-Related Fragments (tRFs). *Trends Biochem. Sci.* **41**, 679–689 (2016).

224. Qi, C. *et al.* Sperm tsRNAs contribute to intergenerational inheritance of an acquired metabolic disorder. *Science (80-.).* **351**, 397–400 (2016).

225. Elkordy, A. *et al.* Stress-induced tRNA cleavage and tiRNA generation in rat neuronal PC12 cells. *J. Neurochem.* **146**, 560–569 (2018).

226. Elkordy, A. *et al.* tiRNAs as a novel biomarker for cell damage assessment in in vitro ischemia-reperfusion model in rat neuronal PC12 cells. *Brain Res.* **1714**, 8–17 (2019).

227. Emara, M. M. *et al.* Angiogenin-induced tRNA-derived stress-induced RNAs promote stress-induced stress granule assembly. *J. Biol. Chem.* (2010).

228. Maute, R. L. *et al.* tRNA-derived microRNA modulates proliferation and the DNA damage response and is down-regulated in B cell lymphoma. *Proc. Natl. Acad. Sci.* **110**, 1404–1409 (2013).

229. Yamasaki, S., Ivanov, P., Hu, G. F. & Anderson, P. Angiogenin cleaves tRNA and promotes stress-induced translational repression. *J. Cell Biol.* (2009).

230. Song, M.-S. & Rossi, J. J. Molecular mechanisms of Dicer: endonuclease and enzymatic activity. *Biochem. J.* **474**, 1603–1618 (2017).

231. Lee, Y. S., Shibata, Y., Malhotra, A. & Dutta, A. A novel class of small RNAs: tRNA-derived RNA fragments (tRFs). *Genes Dev.* **23**, 2639–2649 (2009).

232. Cole, C. *et al.* Filtering of deep sequencing data reveals the existence of abundant Dicer-dependent small RNAs derived from tRNAs. *RNA* **15**, 2147–2160 (2009).

233. Babiarz, J. E., Ruby, J. G., Wang, Y., Bartel, D. P. & Blelloch, R. Mouse ES cells express endogenous shRNAs, siRNAs, and other Microprocessor-independent, Dicer-dependent small RNAs. *Genes Dev.* **22**, 2773–2785 (2008).

234. Schopman, N. C. T., Heynen, S., Haasnoot, J. & Berkhout, B. A miRNA-tRNA mix-up: tRNA origin of proposed miRNA. *RNA Biol.* **7**, 573–576 (2010).

235. Langenberger, D., Çakir, M. V., Hoffmann, S. & Stadler, P. F. Dicer-Processed Small RNAs: Rules and Exceptions. *J. Exp. Zool. Part B Mol. Dev. Evol.* **320**, 35–46 (2013).

236. Gebetsberger, J., Wyss, L., Mleczko, A. M., Reuther, J. & Polacek, N. A tRNA-derived fragment competes with mRNA for ribosome binding and regulates translation during stress. *RNA Biol.* **14**, 1364–1373 (2017).

237. Gebetsberger, J., Zywicki, M., Künzi, A. & Polacek, N. tRNA-Derived Fragments Target the Ribosome and Function as Regulatory Non-Coding RNA in *Haloferax volcanii*. *Archaea* **2012**, 260909 (2012).

238. Kumar, P., Anaya, J., Mudunuri, S. B. & Dutta, A. Meta-analysis of tRNA derived RNA fragments reveals that they are evolutionarily conserved and associate with AGO proteins to recognize specific RNA targets. *BMC Biol.* **12**, 78 (2014).

239. Jehn, J. *et al.* 5' tRNA halves are highly expressed in the primate hippocampus and might sequence-specifically regulate gene expression. *RNA* **26**, 694–707 (2020).

240. Li, H., Wu, C., Aramayo, R., Sachs, M. S. & Harlow, M. L. Synaptic vesicles contain small ribonucleic acids (sRNAs) including transfer RNA fragments (trfRNA) and microRNAs (miRNA). *Sci. Rep.* **5**, 14918 (2015).

241. Wei, Z. *et al.* Coding and noncoding landscape of extracellular RNA released by human glioma stem cells. *Nat. Commun.* **8**, 1145 (2017).

242. Hogg, M. C. *et al.* 5'ValCAC tRNA fragment generated as part of a protective angiogenin response provides prognostic value in amyotrophic lateral sclerosis. *Brain Commun.* **2**, fcaa138–fcaa138 (2020).

243. Ivanov, P., Emara, M. M., Villen, J., Gygi, S. P. & Anderson, P. Angiogenin-Induced tRNA Fragments Inhibit Translation Initiation. *Mol. Cell* (2011).

244. Anderson, P. & Ivanov, P. tRNA fragments in human health and disease. *FEBS Lett.* **588**, 4297–4304 (2014).

245. Ivanov, P. *et al.* G-quadruplex structures contribute to the neuroprotective effects of angiogenin-induced tRNA fragments. *Proc. Natl. Acad. Sci.* **111**, 18201–18206 (2014).

246. Lyons, S. M. *et al.* eIF4G has intrinsic G-quadruplex binding activity that is required for tiRNA function. *Nucleic Acids Res.* **48**, 6223–6233 (2020).

247. Lyons, S. M., Achorn, C., Kedersha, N. L., Anderson, P. J. & Ivanov, P. YB-1 regulates tiRNA-induced Stress Granule formation but not translational repression. *Nucleic Acids Res.* **44**, 6949–6960 (2016).

248. Bartel, D. P. Metazoan MicroRNAs. *Cell* **173**, 20–51 (2018).

249. Jidong, L. *et al.* Argonaute2 Is the Catalytic Engine of Mammalian RNAi. *Science (80-.).* **305**, 1437–1441 (2004).

250. Meister, G. *et al.* Human Argonaute2 Mediates RNA Cleavage Targeted by miRNAs and siRNAs. *Mol. Cell* **15**, 185–197 (2004).

251. Skorupa, A. *et al.* Motoneurons secrete angiogenin to induce RNA cleavage in astroglia. *J. Neurosci.* **32**, 5024–5038 (2012).

252. Skorupa, A. *et al.* Angiogenin induces modifications in the astrocyte secretome: Relevance to amyotrophic lateral sclerosis. *J. Proteomics* **91**, 274–285 (2013).

253. Zhang, X. *et al.* IL-4 Inhibits the Biogenesis of an Epigenetically Suppressive PIWI-Interacting RNA To Upregulate CD1a Molecules on Monocytes/Dendritic Cells. *J. Immunol.* **196**, 1591–1603 (2016).

254. Zhijun, W., Li, X., Junjie, S. & Zhenghong, Y. The 3′ CCACCA Sequence of tRNAAla(UGC) Is the Motif That Is Important in Inducing Th1-Like Immune Response, and This Motif Can Be Recognized by Toll-Like Receptor 3. *Clin. Vaccine Immunol.* **13**, 733–739 (2006).

255. Wolozin, B. & Ivanov, P. Stress granules and neurodegeneration. *Nat. Rev. Neurosci.* **20**, 649–666 (2019).

256. Liu-Yesucevitz, L. *et al.* Tar DNA Binding Protein-43 (TDP-43) Associates with Stress Granules: Analysis of Cultured Cells and Pathological Brain Tissue. *PLoS One* **5**, e13250 (2010).

257. Gupta, N. *et al.* Stress granule-associated protein G3BP2 regulates breast tumor initiation. *Proc. Natl. Acad. Sci.* **114**, 1033–1038 (2017).

258. Valentin-Vega, Y. A. *et al.* Cancer-associated DDX3X mutations drive stress granule assembly and impair global translation. *Sci. Rep.* **6**, 25996 (2016).

259. Anderson, P., Kedersha, N. & Ivanov, P. Stress granules, P-bodies and cancer. *Biochim. Biophys. Acta - Gene Regul. Mech.* **1849**, 861–870 (2015).

260. Kedersha, N. *et al.* Dynamic shuttling of TIA-1 accompanies the recruitment of mRNA to mammalian stress granules. *J. Cell Biol.* (2000).

261. Kedersha, N. L., Gupta, M., Li, W., Miller, I. & Anderson, P. RNA-binding proteins TIA-1 and TIAR link the phosphorylation of eIF-2α to the assembly of mammalian stress granules. *J. Cell Biol.* (1999).

262. Kedersha, N. *et al.* Evidence That Ternary Complex (eIF2-GTP-tRNAi Met)–Deficient Preinitiation Complexes Are Core Constituents of Mammalian Stress Granules. *Mol. Biol. Cell* **13**, 195–210 (2001).

263. Markmiller, S. *et al.* Context-Dependent and Disease-Specific Diversity in Protein Interactions within Stress Granules. *Cell* **172**, 590-604.e13 (2018).

264. Wheeler, J. R., Matheny, T., Jain, S., Abrisch, R. & Parker, R. Distinct stages in stress granule assembly and disassembly. *Elife* **5**, e18413 (2016).

265. Fujimura, K., Sasaki, A. T. & Anderson, P. Selenite targets eIF4E-binding protein-1 to inhibit translation initiation and induce the assembly of non-canonical stress granules. *Nucleic Acids Res.* **40**, 8099–8110 (2012).

266. Emara, M. M. *et al.* Hydrogen peroxide induces stress granule formation independent of eIF2α phosphorylation. *Biochem. Biophys. Res. Commun.* **423**, 763–769 (2012).

267. Szaflarski, W. *et al.* Vinca alkaloid drugs promote stress-induced translational repression and stress granule formation. *Oncotarget* **7**, 30307–30322 (2016).

268. Thoreen, C. C. *et al.* A unifying model for mTORC1-mediated regulation of mRNA translation. *Nature* **485**, 109–113 (2012).

269. Jackson, R. J., Hellen, C. U. T. & Pestova, T. V. The mechanism of eukaryotic translation initiation and principles of its regulation. *Nat. Rev. Mol. Cell Biol.* **11**, 113–127 (2010).

270. Wek, R. C. Role of eIF2α Kinases in Translational Control and Adaptation to Cellular Stress. *Cold Spring Harb. Perspect. Biol.* **10**, a032870 (2018).

271. Wek, S. A., Zhu, S. & Wek, R. C. The histidyl-tRNA synthetase-related sequence in the eIF-2 alpha protein kinase GCN2 interacts with tRNA and is required for activation in response to starvation for different amino acids. *Mol. Cell. Biol.* **15**, 4497–4506 (1995).

272. Harding, H. P., Zhang, Y., Bertolotti, A., Zeng, H. & Ron, D. Perk Is Essential for Translational Regulation and Cell Survival during the Unfolded Protein Response. *Mol. Cell* **5**, 897–904 (2000).

273. Srivastava, S. P., Kumar, K. U. & Kaufman, R. J. Phosphorylation of Eukaryotic Translation Initiation Factor 2 Mediates Apoptosis in Response to Activation of the Double-stranded RNA-dependent Protein Kinase*. *J. Biol. Chem.* **273**, 2416–2423 (1998).

274. McEwen, E. *et al.* Heme-regulated Inhibitor Kinase-mediated Phosphorylation of Eukaryotic Translation Initiation Factor 2 Inhibits Translation, Induces Stress Granule Formation, and Mediates Survival upon Arsenite Exposure*. *J. Biol. Chem.* **280**, 16925–16933 (2005).

275. Kedersha, N. & Anderson, P. Stress granules: sites of mRNA triage that regulate mRNA stability and translatability. *Biochem. Soc. Trans.* **30**, 963–969 (2002).

276. Maziuk, B. F. *et al.* RNA binding proteins co-localize with small tau inclusions in tauopathy. *Acta Neuropathol. Commun.* **6**, 71 (2018).

277. Li, Y. *et al.* Immunoprecipitation and mass spectrometry defines an extensive RBM45 protein-protein interaction network. *Brain Res.* **1647**, 79–93 (2016).

278. Umoh, M. E. *et al.* A proteomic network approach across the ALS-FTD disease spectrum resolves clinical phenotypes and genetic vulnerability in human brain. *EMBO Mol. Med.* **10**, 48–62 (2018).

279. Gunawardana, C. G. *et al.* The Human Tau Interactome: Binding to the Ribonucleoproteome, and Impaired Binding of the Proline-to-Leucine Mutant at Position 301 (P301L) to Chaperones and the Proteasome. *Mol. Cell. Proteomics* **14**, 3000–3014 (2015).

280. Gilks, N. *et al.* Stress granule assembly is mediated by prion-like aggregation of TIA-1. *Mol. Biol. Cell* **15**, 5383–5398 (2004).

281. Bounedjah, O. *et al.* Free mRNA in excess upon polysome dissociation is a scaffold for protein multimerization to form stress granules. *Nucleic Acids Res.* **42**, 8678–8691 (2014).

282. Bley, N. *et al.* Stress granules are dispensable for mRNA stabilization during cellular stress. *Nucleic Acids Res.* **43**, e26–e26 (2015).

283. Vogler, T. O. *et al.* TDP-43 and RNA form amyloid-like myo-granules in regenerating muscle. *Nature* **563**, 508–513 (2018).

284. Gasset-Rosa, F. *et al.* Cytoplasmic TDP-43 De-mixing Independent of Stress Granules Drives Inhibition of Nuclear Import, Loss of Nuclear TDP-43, and Cell Death. *Neuron* **102**, 339-357.e7 (2019).

285. Mann, J. R. *et al.* RNA Binding Antagonizes Neurotoxic Phase Transitions of TDP-43. *Neuron* **102**, 321-338.e8 (2019).

286. Afroz, T. *et al.* Functional and dynamic polymerization of the ALS-linked protein TDP-43 antagonizes its pathologic aggregation. *Nat. Commun.* **8**, 45 (2017).

287. Vanderweyde, T. *et al.* Interaction of tau with the RNA-Binding Protein TIA1 Regulates tau Pathophysiology and Toxicity. *Cell Rep.* **15**, 1455–1466 (2016).

288. Kampers, T., Friedhoff, P., Biernat, J., Mandelkow, E.-M. & Mandelkow, E. RNA stimulates aggregation of microtubule-associated protein tau into Alzheimer-like paired helical filaments. *FEBS Lett.* **399**, 344–349 (1996).

289. Friedhoff, P., Schneider, A., Mandelkow, E.-M. & Mandelkow, E. Rapid Assembly of Alzheimer-like Paired Helical Filaments from Microtubule-Associated Protein Tau Monitored by Fluorescence in Solution. *Biochemistry* **37**, 10223–10230 (1998).

290. Wilson, D. M. & Binder, L. I. Free fatty acids stimulate the polymerization of tau and amyloid beta peptides. In vitro evidence for a common effector of pathogenesis in Alzheimer's disease. *Am. J. Pathol.* **150**, 2181–2195 (1997).

291. Zhang, X. *et al.* RNA stores tau reversibly in complex coacervates. *PLoS Biol.* **15**, e2002183–e2002183 (2017).

292. Vanderweyde, T. *et al.* Contrasting pathology of the stress granule proteins TIA-1 and G3BP in tauopathies. *J. Neurosci.* **32**, 8270–8283 (2012).

293. Silva, J. M. *et al.* Dysregulation of autophagy and stress granule-related proteins in stress-driven Tau pathology. *Cell Death Differ.* (2019).

294. Phillips, K., Kedersha, N., Shen, L., Blackshear, P. J. & Anderson, P. Arthritis suppressor genes TIA-1 and TTP dampen the expression of tumor necrosis factor alpha, cyclooxygenase 2, and inflammatory arthritis. *Proc. Natl. Acad. Sci. U. S. A.* **101**, 2011–2016 (2004).

295. Ghosh, S. & Geahlen, R. L. Stress Granules Modulate SYK to Cause Microglial Cell Dysfunction in Alzheimer's Disease. *EBioMedicine* **2**, 1785–1798 (2015).

296. Guerreiro, R. *et al.* TREM2 variants in Alzheimer's disease. *N. Engl. J. Med.* **368**, 117–127 (2013).

297. Pimenova, A. A., Raj, T. & Goate, A. M. Untangling Genetic Risk for Alzheimer's Disease. *Biol. Psychiatry* **83**, 300–310 (2018).

298. D., R. E. *et al.* Reducing Endogenous Tau Ameliorates Amyloid ß-Induced Deficits in an Alzheimer's Disease Mouse Model. *Science (80-.).* **316**, 750–754 (2007).

299. Vossel, K. A. *et al.* Tau reduction prevents Abeta-induced defects in axonal transport. *Science* **330**, 198 (2010).

300. Cruts, M. *et al.* Null mutations in progranulin cause ubiquitin-positive frontotemporal dementia linked to chromosome 17q21. *Nature* **442**, 920–924 (2006).

301. Melamed, Z. *et al.* Premature polyadenylation-mediated loss of stathmin-2 is a hallmark of TDP-43-dependent neurodegeneration. *Nat. Neurosci.* **22**, 180–190 (2019).

302. Klim, J. R. *et al.* ALS-implicated protein TDP-43 sustains levels of STMN2, a mediator of motor neuron growth and repair. *Nat. Neurosci.* **22**, 167–179 (2019).

303. Baker, D. J. & Petersen, R. C. Cellular senescence in brain aging and neurodegenerative diseases: evidence and perspectives. *J. Clin. Invest.* **128**, 1208–1216 (2018).

304. Dhahbi, J. M. *et al.* 5' tRNA halves are present as abundant complexes in serum, concentrated in blood cells, and modulated by aging and calorie restriction. *BMC Genomics* **14**, 298 (2013).

305. Boccaletto, P. *et al.* MODOMICS: A database of RNA modification pathways. 2017 update. *Nucleic Acids Res.* (2018).

306. Motorin, Y. & Helm, M. RNA nucleotide methylation. *WIREs RNA* **2**, 611–631 (2011).

307. Helm, M. Post-transcriptional nucleotide modification and alternative folding of RNA. *Nucleic Acids Res.* **34**, 721–733 (2006).

308. Motorin, Y. & Helm, M. tRNA Stabilization by Modified Nucleotides. *Biochemistry* **49**, 4934–4944 (2010).

309. Chernyakov, I., Whipple, J. M., Kotelawala, L., Grayhack, E. J. & Phizicky, E. M. Degradation of several hypomodified mature tRNA species in Saccharomyces cerevisiae is mediated by Met22 and the 5′–3′ exonucleases Rat1 and Xrn1. *Genes Dev.* **22**, 1369–1380 (2008).

310. Dewe, J. M., Whipple, J. M., Chernyakov, I., Jaramillo, L. N. & Phizicky, E. M. The yeast rapid tRNA decay pathway competes with elongation factor 1A for substrate tRNAs and acts on tRNAs lacking one or more of several modifications. *RNA* **18**, 1886–1896 (2012).

311. Payea, M. J. *et al.* Widespread temperature sensitivity and tRNA decay due to mutations in a yeast tRNA. *RNA* **24**, 410–422 (2018).

312. Oberbauer, V. & Schaefer, M. R. tRNA-Derived Small RNAs: Biogenesis, Modification, Function and Potential Impact on Human Disease Development. *Genes (Basel).* **9**, 607 (2018).

313. Blanco, S. *et al.* Aberrant methylation of tRNAs links cellular stress to neuro-developmental disorders. *EMBO J.* **33**, 2020–2039 (2014).

314. de Crécy-Lagard, V. *et al.* Matching tRNA modifications in humans to their known and predicted enzymes. *Nucleic Acids Res.* **47**, 2143–2159 (2019).

315. Schaffrath, R. & Leidel, S. A. Wobble uridine modifications-a reason to live, a reason to die?! *RNA Biol.* **14**, 1209–1222 (2017).

316. Alazami, A. M. *et al.* Mutation in ADAT3, encoding adenosine deaminase acting on transfer RNA, causes intellectual disability and strabismus. *J. Med. Genet.* **50**, 425 LP – 430 (2013).

317. Guy, M. P. *et al.* Defects in tRNA Anticodon Loop 2'-O-Methylation Are Implicated in Nonsyndromic X-Linked Intellectual Disability due to Mutations in FTSJ1. *Hum. Mutat.* **36**, 1176–1187 (2015).

318. Hawer, H. *et al.* Roles of Elongator Dependent tRNA Modification Pathways in Neurodegeneration and Cancer. *Genes (Basel).* **10**, 19 (2018).

319. Ramos, J. *et al.* Formation of tRNA Wobble Inosine in Humans Is Disrupted by a Millennia-Old Mutation Causing Intellectual Disability. *Mol. Cell. Biol.* **39**, e00203-19 (2019).

320. Shaheen, R. *et al.* Mutation in WDR4 impairs tRNA m(7)G46 methylation and causes a distinct form of microcephalic primordial dwarfism. *Genome Biol.* **16**, 210 (2015).

321. Shaheen, R. *et al.* A homozygous truncating mutation in PUS3 expands the role of tRNA modification in normal cognition. *Hum. Genet.* **135**, 707–713 (2016).

322. Shaheen, R. *et al.* PUS7 mutations impair pseudouridylation in humans and cause intellectual disability and microcephaly. *Hum. Genet.* **138**, 231–239 (2019).

323. Esteve-Puig, R., Bueno-Costa, A. & Esteller, M. Writers, readers and erasers of RNA modifications in cancer. *Cancer Lett.* **474**, 127–137 (2020).

324. Knopman, D. S., Jones, D. T. & Greicius, M. D. Failure to demonstrate efficacy of aducanumab: An analysis of the EMERGE and ENGAGE trials as reported by Biogen, December 2019. *Alzheimer's Dement.* **17**, 696–701 (2021).

325. European Medicines Agency. Refusal of the marketing authorisation for Aduhelm (aducanumab). *Eur. Med. Agency Sci. Med. Heal.* (2021).

326. Greenway, M. J. *et al.* ANG mutations segregate with familial and 'sporadic' amyotrophic lateral sclerosis. *Nat. Genet.* (2006).

327. Rayaprolu, S. *et al.* Angiogenin variation and Parkinson disease. *Annals of Neurology* (2012).

328. Aluri, K. C., Salisbury, J. P., Prehn, J. H. M. & Agar, J. N. Loss of angiogenin function is related to earlier ALS onset and a paradoxical increase in ALS duration. *Sci. Rep.* **10**, 3715 (2020).

329. Steidinger, T. U., Standaert, D. G. & Yacoubian, T. A. A neuroprotective role for angiogenin in models of Parkinson's disease. *J. Neurochem.* **116**, 334–341 (2011).

330. Eckert, A., Förstl, H., Zerfass, R., Hennerici, M. & Müller, W. E. Free intracellular calcium in peripheral cells in Alzheimer's disease. *Neurobiol. Aging* **18**, 281–284 (1997).

331. Schindowski, K. *et al.* Impact of Aging: Sporadic, and Genetic Risk Factors on Vulnerability to Apoptosis in Alzheimer's Disease. *NeuroMolecular Med.* (2003).

332. Schindowski, K., Leutner, S., Kressmann, S., Eckert, A. & Müller, W. E. Age-related increase of oxidative stress-induced apoptosis in mice prevention by Ginkgo biloba extract (EGb761). *J. Neurol.* (2001).

333. Hartmann, H., Velbinger, K., Eckert, A. & Müller, W. E. Region-specific downregulation of free intracellular calcium in the aged rat brain. *Neurobiol. Aging* **17**, 557–563 (1996).

334. Schindowski, K. *et al.* Increased T-cell reactivity and elevated levels of CD8+ memory T-cells in Alzheimer's disease-patients and T-cell hyporeactivity in an Alzheimer's disease-mouse model: Implications for immunotherapy. *NeuroMolecular Med.* (2007).

335. Schuessel, K. *et al.* Aging sensitizes toward ROS formation and lipid peroxidation in PS1M146L transgenic mice. *Free Radic. Biol. Med.* (2006).

336. Eckert, A. *et al.* Alzheimer's disease-like alterations in peripheral cells from presenilin-1 transgenic mice. *Neurobiol. Dis.* (2001).

337. Leutner, S., Eckert, A. & Müller, W. E. ROS generation, lipid peroxidation and antioxidant enzyme activities in the aging brain. *J. Neurol.* (2001).

338. Russell, W. C., Graham, F. L., Smiley, J. & Nairn, R. Characteristics of a Human Cell Line Transformed by DNA from Human Adenovirus Type 5. *J. Gen. Virol.* **36**, 59–72 (1977).

339. Keil, U. *et al.* Amyloid-induced Changes in Nitric Oxide Production and Mitochondrial Activity Lead to Apoptosis. *J. Biol. Chem.* **279**, 50310–50320 (2004).

340. JL Biedler. SH-SY5Y | ATCC. (1970). Available at: https://www.atcc.org/products/crl-2266?matchtype=&network=g&device=c&adposition=&keyword=&gclid=EAIaIQobChMI1YWMgrf79QIVxbKGCh2RhAt-EAAYAiAAEgKHEfD_BwE. (Accessed: 13th February 2022)

341. Stockburger, C. *et al.* A cell model for the initial phase of sporadic Alzheimer's disease. *J. Alzheimer's Dis.* (2014).

342. Oakley, H. *et al.* Intraneuronal β-Amyloid Aggregates, Neurodegeneration, and Neuron Loss in Transgenic Mice with Five Familial Alzheimers Disease Mutations: Potential Factors in Amyloid Plaque Formation. *J. Neurosci.* **26**, 10129–10140 (2006).

343. Cohen, R. M. *et al.* A transgenic Alzheimer rat with plaques, tau pathology, behavioral impairment, oligomeric aβ, and frank neuronal loss. *J. Neurosci.* **33**, 6245–6256 (2013).

344. Bakkour, A., Morris, J. C., Wolk, D. A. & Dickerson, B. C. The effects of aging and Alzheimer's disease on cerebral cortical anatomy: specificity and differential relationships with cognition. *Neuroimage* **76**, 332–344 (2013).

345. DeTure, M. A. & Dickson, D. W. The neuropathological diagnosis of Alzheimer's disease. *Mol. Neurodegener.* **14**, 32 (2019).

346. Montine, T. J., Sonnen, J. A., Montine, K. S., Crane, P. K. & Larson, E. B. Adult Changes in Thought study: dementia is an individually varying convergent syndrome with prevalent clinically silent diseases that may be modified by some commonly used therapeutics. *Curr. Alzheimer Res.* **9**, 718–723 (2012).

347. Rhein, V. *et al.* Amyloid-beta leads to impaired cellular respiration, energy production and mitochondrial electron chain complex activities in human neuroblastoma cells. *Cell. Mol. Neurobiol.* (2009).

348. Scheuermann, S. *et al.* Homodimerization of Amyloid Precursor Protein and Its Implication in the Amyloidogenic Pathway of Alzheimer's Disease *. *J. Biol. Chem.* **276**, 33923–33929 (2001).

349. Stockburger, C. *et al.* A Mitochondrial Role of SV2a Protein in Aging and Alzheimer's Disease: Studies with Levetiracetam. *J. Alzheimer's Dis.* **50**, 201–215 (2016).

350. Suzanne Clancy & William Brown. Translation: DNA to mRNA to Protein | Learn Science at Scitable. Available at: https://www.nature.com/scitable/topicpage/translation-dna-to-mrna-to-protein-393/. (Accessed: 12th February 2022)

351. Sheikh, M. S. & Fornace, A. J. Regulation of translation initiation following stress. *Oncogene* **18**, 6121–6128 (1999).

352. Rousakis, A. *et al.* Diverse functions of mRNA metabolism factors in stress defense and aging of Caenorhabditis elegans. *PLoS One* (2014).

353. Alzahrani, E., Alghamdi, W., Ullah, M. Z. & Khan, Y. D. Identification of stress response proteins through fusion of machine learning models and statistical paradigms. *Sci. Rep.* **11**, 21767 (2021).

354. Chu, Q. *et al.* Regulation of the ER stress response by a mitochondrial microprotein. *Nat. Commun.* **10**, 4883 (2019).

355. 2013 Alzheimer's disease facts and figures. *Alzheimer's Dement.* **9**, 208–245 (2013).

356. Mielke, M. M., Vemuri, P. & Rocca, W. A. Clinical epidemiology of Alzheimer's disease: assessing sex and gender differences. *Clin. Epidemiol.* **6**, 37–48 (2014).

357. Uhlén, M. *et al.* Tissue-based map of the human proteome. *Science (80-.).* **347**, (2015).

358. When are mice considered old? Available at: https://www.jax.org/news-and-insights/jax-blog/2017/november/when-are-mice-considered-old#. (Accessed: 13th February 2022)

359. Anisimova, A. S., Alexandrov, A. I., Makarova, N. E., Gladyshev, V. N. & Dmitriev, S. E. Protein synthesis and quality control in aging. *Aging (Albany. NY).* **10**, 4269–4288 (2018).

360. Subramanian, V., Crabtree, B. & Acharya, K. R. Human angiogenin is a neuroprotective factor and amyotrophic lateral sclerosis associated angiogenin variants affect neurite extension/pathfinding and survival of motor neurons. *Hum. Mol. Genet.* **17**, 130–149 (2008).

361. Patel, D. *et al.* Association of Rare Coding Mutations With Alzheimer Disease and Other Dementias Among Adults of European Ancestry. *JAMA Netw. open* **2**, e191350–e191350 (2019).

362. Eckert, A., Förstl, H., Zerfass, R., Hennerici, M. & Müller, W. E. Free Intracellular Calcium in Peripheral Cells in Alzheimer's Disease. *Neurobiol. Aging* **18**, 281–284 (1997).

363. Leuner, K. *et al.* Enhanced apoptosis, oxidative stress and mitochondrial dysfunction in lymphocytes as potential biomarkers for Alzheimer's disease. *Journal of Neural Transmission, Supplementa* (2007).

364. van Dyck, C. H. Anti-Amyloid-β Monoclonal Antibodies for Alzheimer's Disease: Pitfalls and Promise. *Biol. Psychiatry* **83**, 311–319 (2018).

365. Mullard, A. Anti-amyloid failures stack up as Alzheimer antibody flops. *Nat. Rev. Drug Discov.* (2019).

366. Inoue, M. *et al.* Tyrosine pre-transfer RNA fragments are linked to p53-dependent neuronal cell death via PKM2. *Biochem. Biophys. Res. Commun.* **525**, 726–732 (2020).

Chapter 7

7. Figures and Tables

7.1. Figures

All figures were created using BioRender.com.

7.2. Tables

[redacted]

[redacted]

[redacted]

[redacted]

[redacted]

[redacted]

[redacted]